POLITECNICO DI TORINO
Repository ISTITUZIONALE

A Simulation-Based Study on Driver Behavior when Negotiating Curves with Sight Limitations

(Article begins on next page)

04 August 2020

Doctoral Dissertation
Doctoral Program in Civil and Environmental Engineering (31st Cycle)

A Simulation-Based Study on Driver Behavior when Negotiating Curves with Sight Limitations

Lorenzo Catani

* * * * * *

Supervisor
Prof. M. Bassani

Doctoral Examination Committee:
Prof. F. Bella, Referee, Roma TRE University
Prof. S. D. Cafiso, University of Catania
Prof. J. Lee, University of Central Florida
Prof. M. Piras, Politecnico di Torino
Prof. A. Spoto, Referee, University of Padua

Politecnico di Torino
March 2019

I hereby declare that, the contents and organization of this dissertation constitute my own original work and does not compromise in any way the rights of third parties, including those relating to the security of personal data.

Lorenzo Catani
Turin, March 7th, 2019

This page intentionally left blank.

Summary

In the field of road design and road safety, well designed and executed experimental activities using a driving simulator can support the evaluation of operational and behavioral effects of road geometrics.

This work aimed to analyze the effects of sight limitations on driver performance when negotiating horizontal curves. Although the effects of road design parameters, such as the radius or lane/shoulder width, have been the subject of investigation in the past, the influence of the available sight distance (ASD) over driver behavior has remained largely unexplored. The ASD is a fundamental parameter in road design and its assessment is fundamental for safe driving operations.

To begin with, the fixed base driving simulator at the *Politecnico di Torino* was validated. Behavioral parameters relating to speeds and trajectories of thirty-three volunteers were collected both in the field (by means of an instrumented vehicle with a Mobile Mapping System) and in a simulated environment. Comparative and statistical approaches were used to compare free-flow speeds and unconditioned traveled paths. Participants adopted greater speeds and were more inclined to anticipate steering maneuvers in simulated drives than on the real track. The analyses revealed a relative validity with respect to operating speed, anticipatory distance, and mean trajectory curvatures along bends. Simulator sickness phenomena were monitored during the experiments, and some countermeasures were adopted in advance to try to prevent it.

Afterwards, the main study focused on an analysis of operational effects (i.e., speed, trajectory, and vision mechanisms) of drivers when negotiating curves with sight limitations at the driving simulator. Different ASDs were obtained by combining the radius of curvature and the distance of lateral sight obstructions from the lane centerline. Seventy-seven drivers were involved in two separate and consecutive experiments carried out on selected road tracks. In the first investigation, only driving speeds and vehicle trajectories were observed; in the

second, eye-tracking glasses were used to monitor driver eye movements and fixations. Results showed that the greater the ASD, the higher the speeds, while the dispersion of trajectory decreased. Speeds were not influenced by ASD along sharp bends, and the presence of lateral sight obstructions was a significant factor in curve guidance. Driver fixations evidenced that the preferred visual strategy in relation to road curvature involved the use of tangential points with longitudinal road elements (i.e., horizontal markings, road edges, sight obstruction). For higher values of ASD, fixations moved towards more distant points of the future path or of the roadway, in accordance with more complex visual strategies. Different attitudes were also observed between the steering strategies adopted by novice and experienced drivers, and between the driving styles adopted by aggressive and cautious drivers. Driver behavior adjustments in response to different sight conditions are presented here and discussed.

Acknowledgements

I would like to acknowledge prof. Marco Bassani for the care and support that constantly provided me during the entire Doctoral Program. He offered me the opportunity to start a new research topic in the field of transportation infrastructures design at the *Politecnico di Torino*, that is the driving simulation. His experience and research attitudes have been very precious for the development of the experimental activities and to outline the contents of this document.

I would like to thank also the professors who reviewed this thesis: their comments and observations were very useful to improve the quality of the document, and the knowledge in the field.

Thanks to Luca, my colleagues, and the staff at the Department of Environment, Land, and Infrastructure Engineering for their interest on my work, and for the time dedicated to my research activities.

Finally, thanks to Claudia who lighten my life.

To my parents,

who always trusted in me

List of Contents

List of Figures

List of Tables

Introduction

For decades, road engineers have designed the radius (R) of a horizontal curve with the equation:

$$\frac{v^2}{R} = g \cdot \left(\tan \alpha + f_t \right) \qquad\qquad\qquad \text{(eq. 1)}$$

to guarantee the stability of a vehicle travelling at a design speed (v) benefiting from a cross slope ($\tan \alpha$) and a transversal friction (f_t) between tires and road surface (g is the gravitational acceleration). In Italy, this equation was accepted without question until 2001.

According to rules introduced with the current Italian policy for road design and construction (MIT, 2001), in addition to the vehicle stability principles, the designer must insure an available sight distance (ASD) from the driver point of view that is greater than the distance necessary to perform emergency stopping, overtaking, and lane changing maneuvers (which can be all identified as required sight distances, RSD). On specific road sites where ASD $\geq$ RSD, emergency stopping, overtaking, or lane changing maneuvers are deemed to be safe.

Although technical standards impose these requirements, the same do not consider the effects that the ASD may have on driver behavior. From an engineering point of view, preferred speeds and driven trajectory reflect the driver behavior. Another important factor to be assessed includes her/his visual attention while traveling. Unfortunately, neither the standards nor the scientific literature in the field provided the designer with adequate tools for the estimation of the influence of actual sight conditions along the curve. This knowledge would be of fundamental importance for the full assessment of the operational and behavioral effects produced by road geometric decisions, which the designer adopts in compliance with technical standards.

In Italy in 2016, 21.7% of road crashes occurred on rural roads and highways took place along curves [1]. The statistics also reveal that the most frequent contributory behaviors are distracted driving and speeding. Speed is unquestionably a major contributing factor to the rate of accidents and to their level of severity in terms of fatalities and/or injuries. Similarly, the adoption of inadequate trajectories or hazardous maneuvers can also increase the risk of accident occurrence. Therefore, any action on geometric factors that influence driver's choices would be strategic for the implementation of safety management policies.

These forewords are the motivations for this work. It is not yet necessary to have a qualitative relationship between driving behavior and sight conditions, but a quantitative estimation leads to predictive models, which are essential in the development of new design rules and supporting better design decisions.

In this framework, the driving simulation is a novel approach that helps researchers to investigate a multitude of driving scenarios. A high volume of work has been carried out with this approach, yielding knowledge useful for the improvement of design standards and decisions. Operational and behavioral effects of road geometrics, intersection configuration assessment, safety countermeasures implementation, are examples of possible applications of driving simulation studies in the field of road design and road safety. With experiments at a driving simulator, a set of independent variables (i.e., road geometrics, traffic and weather conditions, drivers' characteristics) are controlled, as well as a series of events that the driver has to deal with. Dependent variables depicting driver behavior are continuously monitored and then used to understand phenomena and, in case, to build predictive models for practical applications.

Prior to any simulation research, however, a validation study must be performed. Specifically, the behavioral validity is required to understand if the experimental results can, in fact, be used to correctly predict driver behavior in real driving conditions (Kaptein et al, 1996).

The activities presented in Part A of this document concern the validation of the fixed-base driving simulator at the *Politecnico di Torino*. The investigation involved the comparison of driving speeds and adopted trajectories collected on two-lane rural road segments by means of a Mobile Mapping System (MMS) mounted on a passenger car, and on the same segments replicated at the driving simulator. The actual environment was accurately reproduced in the virtual model to reflect road geometrics, traffic conditions, and roadside elements.

Thirty-three drivers were involved in real and simulated drives. To preclude random effects due to traffic, only unconditioned data (free-flow speeds and undisturbed trajectories) were selected for analysis. Accordingly, data collected at intersections were ignored.

The originality of this initial work derives from the specific experimental design, the configuration of investigated infrastructure, and the structure of gathered data which, unlike most previous contributions, was continuous rather than spot. Furthermore, the steering behavior was analyzed by means of geometric parameters to describe vehicle trajectory. Instead of evaluating the effects of road

geometrics on spot lateral positions in the lane, in this investigation the analyses of the anticipatory distance (d_a), the average curvature (c) along the curve, and the curvature change rate (c_r) were performed to validate the driving simulator.

It is worth noting that free-flow conditions are more critical for driving simulator validation studies, since geometrical and operational conditions favor the free choice of speeds, which in turn are influenced by the risk perception of drivers. Hence, such testing conditions are of great interest in Road Engineering studies since they are consistent with the basic hypotheses and assumptions adopted to design roads.

The second part of this document (Part B) presents an investigation on driver behavior when subjected to different sight limitations along curves. In particular, the effects of the ASD on driver behavior and performance were carefully evaluated. The research focuses on horizontal curves since these specific road sections are the most critical in terms of safety.

To address the research questions, two experiments were carried out by involving a total of seventy-seven volunteers. Different tracks of a two-lane rural highway were designed so as to provide a range of ASD values along horizontal curves from 120 to 430 m in radius (R). The sight distance was limited by means of a lateral obstruction (in the form of a stone wall), placed at different distances from the carriageway.

Driver behavior in terms of driving speed, adopted trajectory (curvature, lane position, dispersion of trajectory), and visual strategies (gaze direction and fixations) used in curve negotiation, was observed. In fact, visual information and dynamic parameters are perceived and elaborated by drivers who then act on driving controls, mainly steering wheel, gearshift, gas and brake pedals (AASHTO, 2011).

Some vision mechanisms already presented in the literature (Wann and Land, 2000; Boer, 1996; Land and Lee, 1994) were used to detect the visual strategies while negotiating curves. Sub-classes of vision mechanisms were distinguished on the basis of the fixated roadway element used to drive (horizontal markings, roadside elements, margin delineators, sight obstructions).

Collected data on driver's choices were systematically related to the geometric elements in the roadway (radius and distance of the obstruction from the carriageway), and with the actual ASD. Fixation times adopted by participants were also used to characterize the difference in attitudes between experienced and novice as well as between aggressive and prudent drivers. The relationships linking driver performance and vision mechanisms will be crucial to improve the knowledge of the operational effects of road design.

This thesis has been organized into two main parts: Part A illustrates the initial activities performed at the driving simulator, including the validation study; Part B describes the two experiments developed to understand the effects of ASD. Both parts define the fundamental glossary and present a review of existing literature in the field. Thereafter, the document indicates the research variables, the experimental design, and the protocols that were followed during the

experiments. The data gathered were processed and analyzed to provide evidence for the main results of this experimental work, with dedicated conclusions. Attachments are provided at the end of this manuscript.

Part A:

First Steps with Driving Simulator[1]

Abstract. A driving simulator needs to be validated prior to specific investigations to generalize the achieved results. Although the driving simulation offers several advantages (control, repeatability, costs, safety), one of the main drawbacks is the simulator sickness experienced by test drivers, that leads to time and data loss. For this reason, specific countermeasures must be implemented in the experimental design and laboratory settings. This Part presents the activities performed for the behavioral validation of the fixed-base driving simulator of the *Politecnico di Torino*. The variables of interest were the driving speed and those related to the vehicle trajectory (anticipatory distance, average curvature, and curvature change rate), that were associated to each geometric elements of the test track. Results evidenced that a relative validity was achieved for driving speed along low curvature elements, for anticipatory distance, and mean curvatures of trajectories along bends; absolute validity was achieved for speeds on more demanding elements (curves of small radius), and for curve exiting maneuvers.

---

[1] The activities described in this Part were partly presented in:

1. Bassani, M., Catani, L., Ignazzi, A. A., and Piras, M. (2018, September). Validation of a Fixed-Base Driving Simulator to Assess Behavioural Effects of Road Geometrics. In *Proceedings of the DSC 2018 EUROPE VR Driving Simulation Conference & Exhibition* (pp. 101-108). Antibes, France; and

2. Catani, L., and Bassani, M. (2019, January). Anticipatory Distance, Curvature, and Curvature Change Rate in Compound Curve Negotiation: A Comparison between Real and Simulated Driving. In *98th TRB Annual Meeting*. Washington, D.C.

1. Definitions and Background

This Section introduces the main glossary that recurs in this manuscript, the variables observed during the experiments, and the essential literature that was used to acquire knowledge, to find inspirations for this study, and to support the results interpretation.

1.1 Definitions

The *driving simulator* is a research equipment used in several fields, e.g. automotive, ergonomics, human factors, and road safety. In road design, it is employed to test a new road layout and intersections configuration, to monitor operating behavior of drivers, to evaluate the effectiveness of a safety intervention, etc.

Its main advantages consist in the possibility of controlling research variables and reproducing identical scenarios for several test drivers who are not exposed to hazardous real traffic operations. In addition, an experiment with a driving simulator requires the motivation of participants (to operate like a real driving) and an accurate representation of the road. Hence, the virtual environment should simulate a real driving scenario on the one hand, and reduce as much as possible the unavoidable *simulator sickness* on the other one (see §2).

Before conducting any experiment, a driving simulator requires its prior *validation*. This activity establishes that the same parameters (variables or outputs) are observed both in the real and in the simulated world, and then compared. According to literature, it is distinguished in *physical* or *behavioral* (Blaauw, 1982). The former, also called *fidelity*, considers the sole equipment and the degree of functionality of components; the second focuses on factors that impact on driver decisions in terms of adopted speed, position in the lane, brake action, etc. The comparison between the two environments may reveal an *absolute* or a *relative* validity. It is absolute if observed outcomes and effects are identical both in the real world and at the simulator; it is relative when results differ for the same/similar magnitude, and in the same direction.

A review of different validation approaches and methodologies was widely discussed by Blana (1996). The validity achieved by a driving simulator is strictly related to the specific conditions in which drivers operate; furthermore, each validation activity is task-dependent, thus it is not adequate to cover different variables and contexts. For research purposes, Törnros (1998) observed that a driving simulator should reach at least a relative validity, whereas the absolute one is not compulsory. This is supported by the principle that researchers do not always look for numerical values; instead they may be interested on the effects of independent variables, and the correspondent difference between treatment and control samples. The gathered findings from several simulator types and driving

task give robustness to the research in simulator validity (Mullen et al., 2011; Godley et al., 2002).

During simulations, drivers are exposed to the occurrence of *sickness*, which consists in perceiving discomfort symptoms caused by the simulator itself. This phenomenon is mainly due to the mismatch between expectations and feelings, and may be distinguished in motion and simulator sickness. In the years, its occurrence has been manifested both on low-cost and advanced driving simulators. Such tricky condition may lead to several symptoms (e.g., eyestrain, sweating, nausea, headache, vomiting, etc.) that do not usually occur while driving a real car.

One of the main causes that contribute to sickness is the *optic flow*. It is a visual flow produced by the translatory movement of objects in the field of view (Goldstein, 2008). The optic flow is interpreted by the peripheral vision, and provides information about turning maneuvers and speed perception. This motion may produce *vection*, that is the perception of the observer's movement in the space without sufficient cues applied to itself. For these reasons, larger field of view provided by multiple screens (or projectors) of a simulator guarantees a greater immersion, but it may generate more stimulation of peripheral vision, and consequently an increase in conflicts between visual, kinesthetic, and vestibular information.

1.2 Literature Review

Firsts driving simulators were developed in 1960s in United States and Europe. The main uses were aimed to understanding driver behavior, and to study vehicle components and aerodynamics. Their growth increased in last decades with the technological advances in electronic, computer graphics, and hardware components. Currently, driving simulators are distributed worldwide for various purposes, such as training, assessment, demonstration, and research.

1.2.1 Simulator Validity

In a validation study, responses from vehicle and drivers when observed in the field and on a simulator for the same driving experience are compared. Most common behavioral responses are operating speed, vehicle trajectory, effects of risky driving conditions, etc. Each validation study is specific for the road environment and apparatus where it was carried out. Hence, a research activity carried out on a rural road is worth if a validation study in the same context has been performed in advance (Mullen et al., 2011).

On the other hand, the type of simulator may drastically affect the validity. Fixed-base simulators do not reproduce any motion of the simulated vehicle, whereas motion platforms with 1 to 9 degrees of freedom return displacements, accelerations, and rotations in some or all the three directions. These characteristics could influence the research activity in terms of speed perception, driver adaptation, simulator sickness, etc. (Kaptein et al., 1996).

Simulator validity experiments have not been yet standardized. For this reason, literature studies differ for a series of experimental conditions and simulator devices. As mentioned, the use of a static driving simulator allows to

perceive speed mainly from visual information. This can be provided from a single screen (Lee et al., 2003), multiple screens (e.g., Llopis-Castelló et al., 2016), or projected images on flat (e.g., Bella, 2008) or cylindrical surface (e.g., Branzi et al., 2017), to reproduce different fields of view. Other ways to perceive speed are provided by the sound system and/or through vibration pads mounted on the device. Conversely, motion on driving simulator can be supplied by means of a Stewart platform (e.g., Kemeny and Panerai, 2003) or a displacement system (e.g., Salaani et al., 2001) connected to a cabin. Figure 1.1 shows the mentioned devices of increasing complexity and cost, while a complete review and classification of driving simulators was provided by Eryilmaz et al. (2014).

The validation of these equipment involves the calibration of the entire system. All driver's operations must generate a reply in terms of vehicle control and visual, kinesthetic, and auditory cues, like in real driving conditions. For this reason, the calibration process gradually increases in complexity with the class and cost of the simulator.

Researchers were interested in investigating several experimental conditions, like urban (e.g., Klee et al., 1999) and rural roads like highways (e.g., Blaauw, 1982), freeways (e.g., Engström et al., 2005), and road tunnels (Törnros, 1998). These tests were performed on car (e.g., Losa et al., 2013) or truck (Panerai et al., 2001), and in different visibility conditions: during daytime, night-time (e.g., Hallvig et al., 2013), or in presence of fog (e.g., Pretto et al., 2008). Eventually, Bella (2005a) and McAvoy et al. (2007) performed studies to validate the driving simulator along work zones.

Operating speed

Driver speed is one of the most studied variables for the behavioral validation of driving simulators (Branzi et al., 2017; Llopis-Castelló et al., 2016; Losa et al., 2013; Bella, 2008; Bella, 2005a; Bittner et al., 2002; Godley et al., 2002; Panerai et al., 2001; Törnros, 1998; Blaauw, 1982).
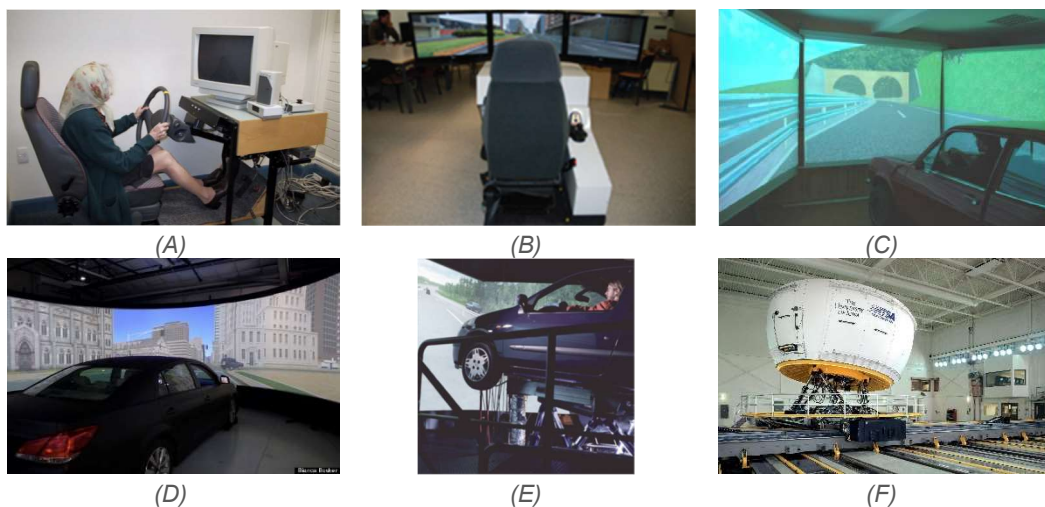
Figure 1.1. Examples of simulator devices: fixed-base with single screen (A), multiple screens (B), flat projected image (C), cylindrical screen (at Stanford University, D); motion-base with Stewart platform (E), and with displacement system (F)

Every simulator records continuous data at a specific acquisition frequency or sampling rate (e.g., 10 Hz means ten data per second). Conversely, field data may be collected in two main ways: through spot speed surveys or by means of instrumented vehicles. In the first case, video cameras (Bella, 2005a) or laser speed meters (Bella, 2008) collect measures of a sample of drivers who traveled in the observed sections, taking implicitly part to the research. Thus, the spot speed survey provides discrete information on actual speeds that occurred at predefined measurement sites. In the second case, participants are directly involved in the experiments, thus they know the aim and the task to perform (e.g., Bittner et al., 2002). This last operation is usually carried out by implementing an integrated system of an Inertial Measurement Unit (IMU) and/or a Global Positioning System (GPS) antenna, that allows to measure the position of the vehicle at a pre-set frequency (normally in the range 1-100 Hz). In this way, a speed profile along the observed test track can be derived, avoiding deficiencies of data collection, and allowing the computation of acceleration/deceleration and speed differentials (e.g., Montella et al., 2014). This distinction results also in considering different or identical drivers' samples for field and simulated experiments.

For instance, Godley et al. (2002) evaluated the effectiveness of perceptual countermeasures both with real and simulated driving, with the aim of validating the Monash University Accident Research Centre (MUARC) driving simulator for speed research. They compared drivers' speed in two road configurations (control and treatment), along left- and right-hand curves, and approaching to a stop sign. The authors observed that participants drove slower in simulated environment than in real vehicle. Similar results were obtained by Klee et al. (1999) and Bella (2005a). The first dealt with the validation of the static simulator at the University of Central Florida. The same participants drove an instrumented car in a campus road and in the reproduced virtual scenario; speeds were collected and compared in 16 locations along the test track. The absolute validity was excluded since in 10 of 16 stations the observed speeds on-road were greater than in the simulator of about 5-10 km/h. Bella used the CRISS (Inter-University Research Center for Road Safety) driving simulator to investigate the speed adopted along a work zone in a two-lane highway. Field data were collected through a laser speed meter on ten measurement sites, whereas simulated ones were recorded every 5 m and statistically treated to estimate the significance of speed differentials.

Shinar and Ronen (2007) performed the validation of the STISIM driving simulator following a different approach. They observed the ability of the participants to estimate or to produce a defined driving speed on the basis of their perception of motion in the simulated environment. The capability of a driving simulator to reproduce the experimental scenario and an authentic sensation of speed is a fundamental criterion for its validity (Colombet et al., 2010; Kemeny, 2009; Pretto et al., 2008; Pretto and Chatziastros, 2006).

From the analysis of literature on simulator validation activities, the following main points may be argued:

- the use of motion-base driving simulator which returns longitudinal and lateral acceleration increases its fidelity and the possibility of reaching the absolute validation (Blaauw, 1982);

- the motion system requires a complex calibration of the equipment; a lack in settings may increase sickness effects on drivers (Törnros, 1998);
- the graphical quality of the virtual scenario influences driver performance; the presence and the position of elements in the road environment affect the optic flow and speed perception, that may be different from real world (Klee et al., 1999);
- the accuracy of speed and distance perception changes on the basis of the field of view (FOV) provided by visual devices; the larger the FOV the better is the feeling of the driver to perceive her/his self-motion in the virtual environment (Kemeny and Panerai, 2003);
- the relative validity of a driving simulator is a fundamental requirement for speed research, whereas the absolute validity is better but not necessary (Törnros, 1998);
- only the absolute validity allows to calibrate speed models; relative validity permits to evaluate the effects of experimental treatments with respect to the control conditions (Bittner et al., 2002).

Adopted trajectory

Although robust outcomes were attained with kinematic variables, contrasting results have been documented for the validation activities based on vehicle position in the travelled lane (Blana and Golias, 2002; Törnros, 1998; Wade and Hammond, 1998).

As observed variable, Törnros (1998) considered the distance between the car center of gravity and the right line close to the nearest side wall of tunnels; Wade and Hammond (1998) referred to the distance from the front-left tire to the road centerline marking; while Blana and Golias (2002) employed the distance between the front-right tire and the lane lateral marking. The VTI driving simulator in Törnros (1998), and the WAS driving simulator in Wade and Hammond (1998) obtained a relative validity, while for the Leeds Advanced Driving Simulator of Blana and Golias (2002) neither absolute nor relative validity was reached.

Specifically, Törnros (1998) evaluated the driver behavior along road tunnels. Participants positioned the vehicle much distant from the wall when it was on the left than on the right. Such results occurred both for straight and curved sections. Eventually, the distance to the side line was, in general, greater in the real tunnel than on simulated one.

Wade and Hammond (1998) demonstrated that the mean deviation from the road axis was higher in the virtual than in real scenarios. This was observed along four different road configurations (baseline, C1, C2, C3), that provided similar patterns in the two environments. It is worth noting that drivers have to maintain a constant speed along the track.

Blana and Golias (2002) found that the difference between the lateral displacements measured in real and simulated driving environments had the same sign (i.e., always greater) for any speed value. The mean lateral displacement in real driving conditions was always greater than in the simulated one, while on-road standard deviation of lateral displacement was always lower than the same in simulated conditions. Nevertheless, differences between real and

simulated driving were found to be dependent on speed. According to Törnros (1998), they concluded that in simulated conditions drivers underestimated the risks associated with the roadside environment, losing the sense of the correct lane position.

However, differences in roadside layout between real and virtual environments, and the difference in perception of vehicle occupancy in the lane between the two environments may explain the differences in lateral displacement magnitude and trend. Furthermore, it should be pointed out that the lateral distance may fail to explain behavioral validity of a driving simulator since, at a single location, the same position could belong to different trajectories. In fact, drivers may behave differently in the two environments as a result of their perception and interpretation of the road scenario. When negotiating a curve, they decide where to start the turning maneuver, and the angular speed of the steering wheel to keep the vehicle in the lane. Furthermore, in case of simple curve design, drivers need to anticipate the steering operation due to the sudden change of curvature (direct connection between the tangent and the circular curve); it is not necessary when a transition curve is interposed between the two elements (Bonneson, 2000).

Nevertheless, such hypotheses must be verified. The comparison between the steering behavior of the same driver in field and in simulated environment provides a novel approach in assessing the verisimilitude of a driving simulator.

Simulator-driver interaction

In driving simulation drivers operate safely and should behave as in the real world. Aside from speed and vehicle position, the correct perception of the information provided by the simulation is fundamental to perform experiments and extrapolate results to the real world.

Jamson (2000) used the Leeds Driving Simulator to investigate the effects of image resolution and field of view on driver performance (speed and lateral position). He noticed that the settings of the simulator are task-dependent: simulations with high resolution and reduced field of view produced speed closer to real world; conversely, similar lane positions were observed for lower resolution and greater field of view. He concluded that simulators should be set up on the basis of the research aims.

Other studies evaluated the interaction between human and simulation by considering the perception of the surrounding space. In particular, the egocentric distance is the one measured from the observer to the target placed in the same environment. There is wide literature related to the comparison between perceived egocentric distance on real and simulated scenario, and to computer graphic solutions to increase fidelity (Thompson et al., 2004; Willemsen and Gooch, 2002). Although those referred to the driving task are limited, most of all highlighted the tendency of underestimating the actual distance on virtual environments due to the compression of the image and motion parallax.

While driving, the distance estimation is a crucial and constant function that helps the user in steering maneuvers, or to keep the safe distance (headway) from the vehicle ahead (Kemeny and Panerai, 2003). Risto and Martens (2014) validated

the Lumo Drive v2.5 simulator with respect to the driver headway choice. Participants were instructed to maintain a distance-based and a time-based headways, both in the virtual environment and in an instrumented vehicle. Headways adopted by following time instructions were lower than those adopted on the basis of distance; between the two driving contexts, there was no significant difference of headway choice produced by the different instructions.

In the field of road safety, simulators are useful tools to test hazardous events by controlling parameters and avoiding risks for drivers and operators. Hence, the hazard detection is one of the main feature that a driving simulator must tickle to the driver. For instance, this can be analyzed by monitoring drivers' operations in different environmental conditions (e.g., day, night, rainy, foggy; Wood et al., 2014; Mueller and Trick, 2012). Underwood et al. (2011) tested the capabilities of the Faros GB3 driving simulator (Konstantopoulos et al., 2010) by comparing the eye scan and the fixation durations of novice and experienced drivers that traveled in the field, through a virtual urban environment, and while watching a movie of a vehicle moving in the traffic. The observation of similar patterns in both drivers' categories suggested a relative validity of their equipment. Specifically, experienced drivers monitored the roadway more than unexperienced ones, with shorter eye fixation durations.

This branch of research has been developed in recent years due to the greater fidelity of new equipment, improvements in computer graphics, and advances in the manufacture of add-on tools (e.g., eye-trackers). The investigation of driver behavior in both environments reveals the capability of the simulator to faithfully reproduce real and risky scenarios. For instance, this kind of validity is required in research activities that want to develop road safety improvements (e.g. to determine the most efficient speed mitigation strategy on an existent road segment characterized by high accident rate).

Moreover, the behavioral analysis may evidence psychological and physiological effects that influence driver's risk perception. Indeed, operations performed into a laboratory may provide a limited sense of exposure to hazards, vehicle damages, traffic controls, etc. that may occur in real driving conditions. Finally, motivation, involvement, and correct training of test drivers must be ensured to collect reliable data.

1.2.2 Simulator Sickness

As well documented in Stoner et al. (2011), reports of ill feelings linked to the use of driving simulator are widely known but not exhaustively understood. This enduring task started from the firsts flight simulators in 1957, and nowadays people are still trying to solve this critical issue.

Experienced sickness may be caused by two elements: the physical motion and the simulator itself (Casali, 1986). In motion-base simulators, the vestibular system is totally involved in the simulation; thus, the body motion could be different, unexpected, or distorted with respect to actual cues in real driving. On the other hand, sickness may be produced by visual stimuli, as vection or perceived motion, even without any physical interaction with the driver (Kennedy et al., 1988). Hettinger and Riccio (1992) asserted that sickness symptoms principally

occur in novice drivers that approach with simulators, during the firsts exposures, and where scenarios are characterized by intense optic flow or recurrent acceleration changes.

Three are the most known theories that explain the concept of simulator sickness: cue conflict theory, postural instability, and poison theory (Stoner et al., 2011).

The former states that illness is caused by the mismatch between the expectation of the sensory system founded on own experience and the actually happening in the simulator. This experience may occur in motion-base simulators for a delay between the onset of visual or motion cues (transport delay, §2.1), in fixed-base simulators where the driver is not moving but visual cues are presented through the displays without stimulate the vestibular system, and in head-mounted display, e.g. caused by low update rate of the device with respect to the actual head movements. Although cue conflict theory is widely accepted, some issues arose from research community on its utility as a justification for simulator sickness (Kolasinski, 1995). Stoffregen and Riccio (1991) synthetized them in few points:

- there is not a reliable formula that allows to predict simulator sickness;
- even if motion cues are determinant factors to feel sickness, it is not defined the reason why car chase video does not produce sickness like driving simulation;
- it is not clear why some drivers manifest sickness at first exposures, and symptoms disappear in following experiences;
- there is not a physiological justification of nauseogenic responses generated by the cue conflict.

Nevertheless, cue conflict theory is supported by available experimental data, confirming its approval by scientists. Main findings to lower sickness rate referred to virtual scenario design, where expectation from the vestibular system should be weakened (i.e., by reducing sharp maneuvers or lowering acceleration forces) or optic flow in the peripheral field of vision reduced (i.e., by containing the number of elements of the landscape, and placing them at an adequate distance from the road).

The postural instability is the lack consequence of driver's attempt to find a (postural) stability in a new environment like the simulation (Stoffregen and Riccio, 1991). Human sensory systems continuously work to find and maintain a postural stability in the actual environment. Thus, sickness occurs when the driver is not able to find strategies that accomplish the new stability in a reasonable time. Because of this, a gradually exposure to simulation may reduce sickness symptoms over time.

The poison theory (Treisman, 1977) hold up that illness symptoms occur during driving simulation are comparable with those associated with the assumption of poison, e.g. vomiting. In other words, the human body reacts to this discomfort throwing out automatically the stomach contents. Also in this case, no predicting solutions and unforeseeable effect on drivers are relevant limitations of this theory.

Obviously, any driving experience affected by sickness should be rejected, otherwise the validity of collected data results unsatisfied. This because driver psychology and performance change in terms of motivation, concentration, attention, or also with physical actions (e.g., closing eyes, yawning). In addition, participants might adjust their behavior to avoid sickness, influencing experimental results and research learning.

For these reasons, some sickness measurement techniques have been developed in the last decades. The most used is the Simulator Sickness Questionnaire (SSQ, in Kennedy et al., 1993). It contains a list of symptoms that the simulation can generate, and drivers should indicate the rate (none, slight, moderate, or severe) of each one. Through explained and precise classification rules and weighted means, the total score is the numeric quantification of the perceived simulator sickness. Other authors (Bertin et al., 2004) tried to understand and quantify simulator sickness by means of physiological measures, as heart frequency, and skin temperature and resistance. Although prior works (e.g., Espié, 1999; Mullen et al., 1998) did not rose up any relevant result, they found a strong correlation between such measurements and drivers' feedback during the simulation. Recently, Young et al. (2007) addressed that a potential factor that increases sickness onset is the time of administration. Specifically, drivers conscious of the possible symptoms generated by the simulation showed a higher score at SSQ than those which are uninformed of such effects. In that study, the importance of the experimental protocol on drivers' psychological attitudes was also evidenced.

2. Simulator Sickness Countermeasures

Data collected in a research activity are reliable if no error occurred during the planning and acquisition phases, including the possibility of manifesting sickness on drivers. As a matter of fact, some countermeasures that prevent its occurrence may be planned in advance, in the design of the virtual scenario, in setting the simulator components, or adopting adequate experimental protocols.

This Section provides a brief description of activities performed in this thesis, focusing on the actions introduced to avoid simulator sickness, and the resulting effects.

2.1 Preventive Measures

Factors that are associated with simulator sickness may be grouped into three categories: individual, simulator, and experimental assignment (Kolasinski, 1995).

From the individual viewpoint, the literature suggests to discard people who have fatigue, disturbed sleep, a hangover, head colds, ear or respiratory problems, pregnancy, or those who are recently subjected to medical care (Kennedy et al., 1987). As well, drivers who experienced sickness in previous occasions, must not participate in further experiments, since they are more inclined to show sickness again (Allen and Reimer, 2006).

However, Kennedy et al. (2000) declared that simulator sickness decreases over subsequent exposures, and grows with time during a driving session. Johnson (2005) stated that the simulation exposure should not exceed two hours in total, but it is a general practice in the field to design driving sessions between 5 and 25 minutes. The more demanding is the scenario and the task, the shorter should be the simulation. Furthermore, it is suggested to separate consecutive drives with 10 minutes of break (Philip et al., 2005).

Subjective characteristics of individuals, like age, gender, perceptual style, ethnicity, etc., are also relevant factors to sickness occurrence. Literature provides several experiences that highlighted the effects of individual differences (Stoner et al., 2011).

As aforementioned, the type of simulator plays a role on sickness. The key note is that there is no one simulator which may fulfill all research tasks, but each type works well for certain scenarios and demands.

One of the leading factors is the field of view (FOV) provided by the screens/projectors. The wider is the FOV, the greater is the optic flow and vection stimulated by the peripheral vision (Kennedy et al., 1988). As already said, the FOV should be compatible to the experimental task: e.g., it is not reliable to test driver behavior at intersections with a single screen, since at least 180° of FOV is required. When there are multiple screens, they must be adequately aligned to provide a correct visualization of the 3d world. Otherwise, distortions of the scenery may affect the perception of self-motion while traveling.

On the hardware side, the visual equipment is characterized by the image resolution and the graphics update rate. High resolution leads to reduce eyestrain and difficulty in focusing as per the accurate definition of the elements in the virtual world. On the other hand, an update rate of 60 Hz is the minimum requirement for driving simulators to prevent dropped frames and lags between the control input and the its presentation in the visual system. This type of lag is just an example of the transport delay. It generally refers to the time that the calculator needs to receive an input, to elaborate it, and to return the new state of the simulation. The occurrence of transport delays both for visual and dynamic systems may result in conflicts between the vestibular and visual systems, thus influencing driver performance.

Finally, the design of the virtual scenario requires to:

- limit the cues in the FOV that improve the perception of optic flow;
- minimize sharp maneuvers or direction changes;
- reduce the number of abrupt decelerations.

Thus, there is the need to balance the presence of trees, street furniture and buildings that supply a similarity to the real world, with the interest of reducing hints that stress human vision (Stoner et al., 2011). By contrast, the relative movement (or flow) of such elements in the surrounding environment provides a beneficial optical flow that helps the driver to adequately perceive her/his traveling speed. Such feeling of motion could be also detected through markings, joints, or sporadic defects on the road pavement that scrolled under the vehicle (Andersen, 2011). These strategies, combined with a correct tuning of the engine sound and proportional vibrations of the equipment, have less impact on sensory conflicts, and contribute to increase the simulator fidelity.

Some of these preventive measures to reduce simulator sickness have been employed in this research activity, and discussed in the following Section.

2.2 Activities and Effects

The driving simulator was delivered to the *Politecnico di Torino* in March 2015. It was located in the new Road Safety and Driving Simulation Laboratory of the Department of Environment, Land and Infrastructure Engineering (Figure 2.1).

It was immediately clear that the coral paint of the walls (Figure 2.1A) was not suitable for simulation testing. Indeed, wide literature supports the use of dark rooms, that mitigates the occurrence of simulator sickness if the subject is able to see only few reference points in the peripheral view (Casali and Wierwille, 1980). To fulfill such solution, walls were painted in black and a black roller curtain was installed close to windows to obstruct the sunlight.

(A)   *(B)*

Figure 2.1. (A) First picture of the driving simulator in the Road Safety and Driving Simulation Laboratory; (B) picture of a simulation in the new dark room

Secondly, the optic flow produced on the lateral screens of the simulator, associated to the inability of perceiving accelerations and vibrations of the vehicle, may produce a conflict in the vestibular system, resulting in sickness.

This was tested through a specific experiment in which the virtual scenario was designed by placing different elements in the road surrounding (e.g., cones, trees, advertising panels, buildings, etc.), and increasing their frequency from the initial to the end of the test track. Thus, the driver was subjected to a gradually growth of the optic flow in the peripheral field of view. It was quantified by means of a MATLAB® toolbox (Computer Vision System) that computes motion vectors of the pixels that significantly change their color from a snap-shot to the consecutive (Optic Flow in base conditions, OF_{bc}) (Figure 2.2). The produced optic flow ($OF_{p,i}$) was calculated by scaling the OF_{bc} for the adopted speed of the i-th test driver (TD).

During the experiment, the subjective evaluation of the health state was associated with biometric parameters (heart rate, galvanic skin response, and skin temperature). The effects of optic flow variation were observed in terms of difference of the actual physiological measure (stress condition) from the initial one (rest condition). Where abrupt changes of optic flow occurred, such difference raised to 4 bpm (beats per minute), and 2 S (siemens, measure of conductance). The skin temperature of TDs who manifested intense effects increased on average of 0.2°C. Results revealed the correlation between the optic flow and sickness, associated with the influence of visual stresses on physiological state (Carle, 2016).

(A)   *(B)*
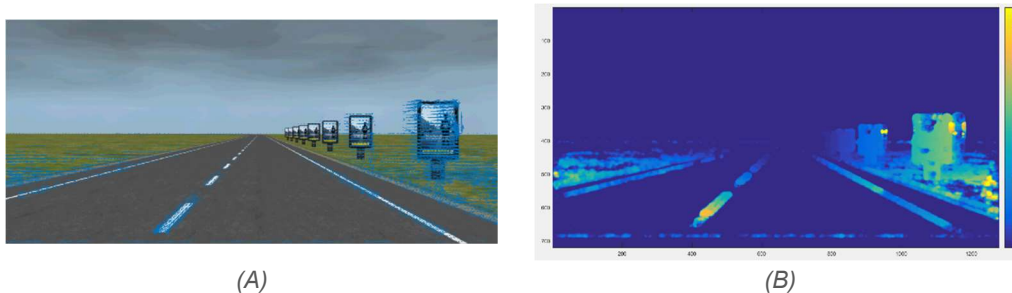
Figure 2.2. Analysis of the section at station 3+300 m, with (A) motion vectors, and with (B) the chromatic matrix of displacement intensity

The design of the virtual environment of experimental tracks (described in Part B of this document) was carried out on the basis of the suggestions provided by the previous work. Objects, vegetation, and buildings were arranged at a sufficient distance from the roadway, and strewn in the surrounding terrain. Their placement along the track was balanced, (i) to limit the database memory size, and (ii) to conceal the visible path after a curve with a sight limitation.

The number of objects (with a memory size from 1 to 7 MB) was restricted in order to avoid lags during the simulation. The dimension of the whole database amount to 230 MB. Therefore, objects position was concentrated in the internal side of curves, as to narrow the future (and visible) path, and to induce the driver to focus on the road ahead.

The experimental protocol may also influence the occurrence of sickness. As mentioned (§1.2.2), training sessions before the experiment at the simulator gradually enhance the confidence with the equipment and improve the adaptation in the virtual world. For comparison purposes, Figure 2.3 shows the percentage of drivers that manifested main sickness effects (eyestrain, nausea, vertigo, headache, fatigue, sweating) during the experimental driving, with and without the prior training sessions. These consisted on two scenarios submitted in two different days: the first one was a simple circuit, with four-lane carriageway, and low traffic flow; the second was a track with similar geometric and environmental characteristics with respect to the experimental scenario. Five drivers (63%) of eight that carried out the experimental driving without the training experienced simulator sickness. The introduction of the training within the experimental protocol reduced this percentage to 17% (four of twenty-three participants).

Specifically, drivers declared the level of each symptom with a score from 0 to 3 (none, low, moderate, high, respectively). For the eight drivers that did not carried out the training, the main suffered effects were nausea and vertigo. On the other hand, those who manifested sickness also after the training, declared eyestrain (1) and sweating (2).
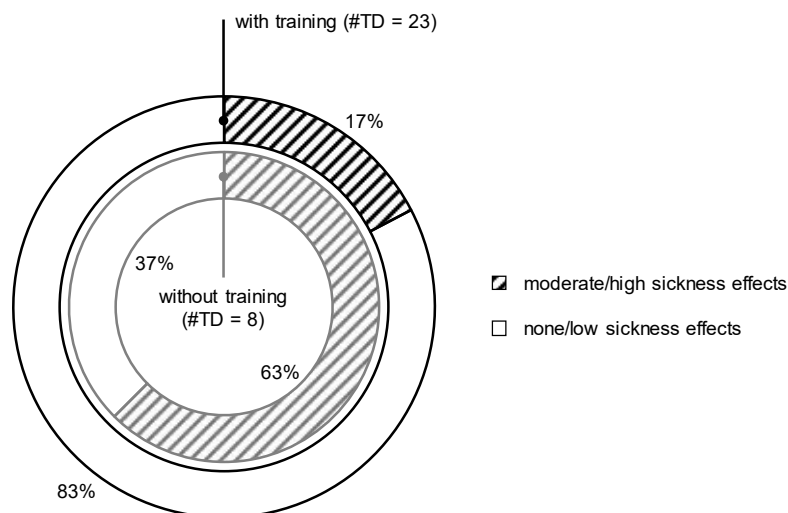
Figure 2.3. Effects of the experimental protocol (with/without training) on perceived sickness

Furthermore, the training phase allows also to discard drivers that are not able to compensate the difference between real and virtual environment. In fact, Kalteniece and Krumina (2014) evidenced that 5-20% of people cannot see 3d, because of vision problems (strabismus, stereo blindness, etc.). In addition, Bos (2018) observed that there is a reduced transfer of training in people who are sick but continue to drive. Thus, the operator must communicate to participants, that any feeling different from normal driving conditions are useless for the experimental purposes.

Figure 2.4 shows the answers to simulator sickness questionnaires submitted to drivers after the three experiments carried out in this thesis work, and presented later in this document. It is worth noting the high level of some symptoms (sweating, nausea, vertigo) for the reasons already explained. In the further experiments, the number of participants who manifested sickness reduced, less for eyestrain. In the Experiment #2 it could be justified because of the use of eye-tracking glasses, that slightly overheat while recording. On the other hand, the number of drivers who reported sweating symptoms increased from the Experiment #1 to the Experiment #2 probably due to the different season in which the drives were carried out (winter and summer, respectively).

The simulation duration is an additional factor that may affect both drivers' motivation and induced sickness. According to Philip et al. (2003), simulations of all three experiments were designed in order to complete the driving tasks in less than twenty minutes. Such conditions allowed to maintain high heedful level of drivers, minimizing fatigue, boredom, and lack of interest.
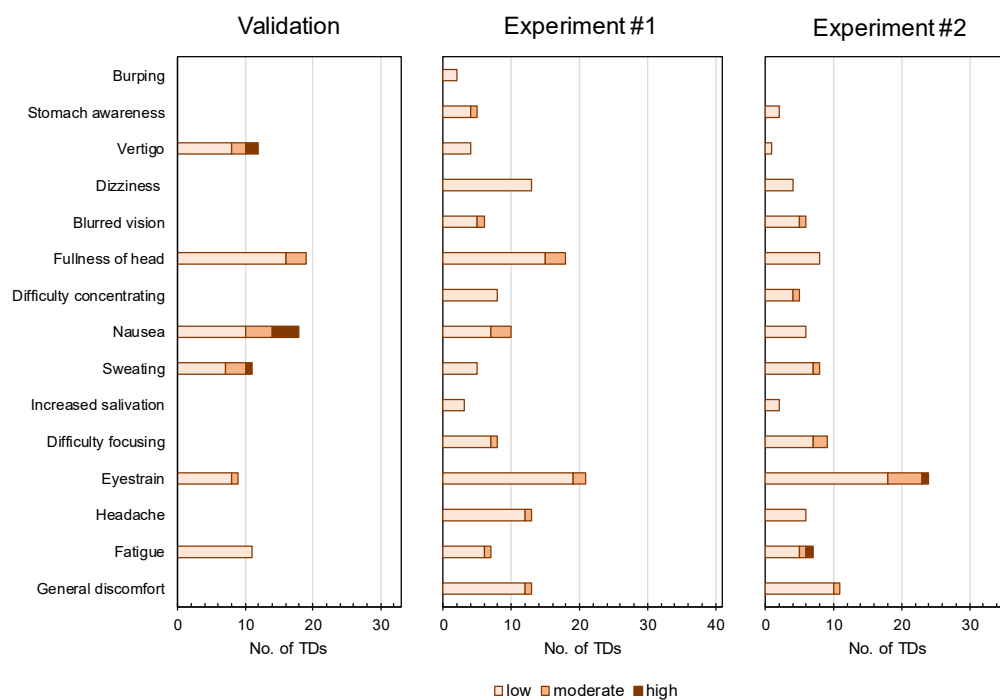
Figure 2.4. Number of Test Drivers (TDs) that experienced simulator sickness symptoms after the three experiments presented in this manuscript

In conclusion, the lesson learned for the mitigation of simulator sickness is summarized as follows:

- the use of a dark room helps in simulator sickness mitigation, but few reference points must remain visible to the driver;
- the road environment should be reproduced in the simulation to accommodate the driver in a context similar to reality, but at the same time it should be not extremely faithful since the effects of moving objects is perceived differently. Thus, participants may focus more on the road characteristics (independent variables for road engineers/designers) without confounding effects in the surrounding;
- the simulator sickness occurrence cannot be totally excluded or prevented; a number of other factors could potentially influence the driver susceptibility to sickness, such as driver motivation, medical conditions, etc.;
- the involvement of TDs in the research activity and the shared objectives allow also to gather reliable data, free from outliers (driving style as in a video game).

3. Experimental Activities

The design of the present work started from the existing literature and the knowledge in the field of road design and management. Its characters of originality are related to the methodology of data acquisition in the field, and the analysis of results in function of the road track geometrics.

3.1 Equipment

The fixed-base driving simulator at the *Politecnico di Torino* was manufactured by Oktal (now called AV Simulation, France). The simulator is composed of two computers, three screens that reproduce the virtual environment, a complete cockpit with a real steering wheel, manual gearbox, dashboard, pedals, and seat. Table 3.1 lists the whole components with technical specifications, and Figure 3.1 shows the driving simulator inside the dark room of the laboratory.

Table 3.1. Simulator components and characteristics

Function	Devices	Features
Computation	Master PC	Processor: Intel Xeon E5-1620 v2, 3.70 GHz
		Video card: NVIDIA GeForce® GTX 780 Ti
		RAM: 8 Gb
		Memory: 512 Gb
	Visual PC	Processor: Intel Xeon E5-1620 v3, 3.50 GHz
		Video card: NVIDIA GeForce® GTX 780 Ti
		RAM: 8 Gb
		Memory: 512 Gb
Visual	No. 3 screens	32-inch Full High-Definition (1080p)
		Graphics update rate: 50/60 Hz
		Field of view: ≈ 130°
	Dashboard	20 × 15 cm display
		Speedometer and rev counter
Sound	Dolby Surround Pro Logic II	No. 5 speakers + No. 1 subwoofer
Operation	Steering wheel	Actual from factory
		Force-feedback system
		No limitation of rotation
	Gearbox	No. 6 gears + reverse
		Driver owner: Fanatech
	Pedals	Accelerator, brake and clutch
		Driver owner: Fanatech
	Buttons	Engine start, handbrake, klaxon, and emergency stop
	Seat	Actual from factory
		Seat belt

Figure 3.1. Current layout of the fixed-base driving simulator in the Road Safety and Driving Simulation Laboratory at the Politecnico di Torino

The two calculators have different functions: one is the "master" and is linked to the control station, where the operator can interface with the software for scenario design, simulation control, and data export; the second is the "visual" computer and it is committed to the generation and visualization of the virtual environment on screens by means of dedicated graphic cards.

The force-feedback steering wheel allows the driver to perceive pavement roughness, wheels' rolling, and shocks during the simulation. The dashboard shows the speedometer and the rev counter, and is placed behind the steering wheel, like real car displays. The FOV is approximately 130°, adequate for a correct perception of speed on fixed-base driving simulators (Kemeny and Panerai, 2003).

SCANeR^{TM}studio (v. 1.4) is the software developed by AV Simulation and used to design the experimental tracks, generate the 3d model of the environment, manage vehicle settings, create the scenario, control the simulation, collect and export data.

Naturalistic drives were performed with an instrumented family car that was set as a Mobile Mapping System (MMS). The vehicle was equipped with a front video camera, and an integrated device with Inertial Measurement Unit and Global Positioning System sensors (IMU-enabled GPS).

The Garmin action camera (Figure 3.2A) records video in 1080p at 30 fps, and is equipped with a GPS sensor that collects spatial information at a frequency of 1 Hz. The camera was used to survey traffic conditions during the naturalistic drives without obstructing the driver's field of vision.

The Xsens IMU-GPS device (Figure 3.2B) is a compact sensor, adequate for automotive survey, with acceptable accuracy. The IMU uses the strapdown configuration, which means that the reference system is integrated with the vehicle (or body). The GPS gathers spatial positions in the geographical coordinate system (ϕ, λ) at 1 Hz, and the IMU measures accelerations (a_x, a_y, a_z) and rotations (roll, pitch, and yaw) in the three directions during the motion. A proprietary software generates an output file containing position, speed, accelerations, and rotations, for every sampling time (10 Hz in this study). For its characteristics, the device is considered a low-cost product. The specifications of the two devices are shown in Table 3.2.

Figure 3.3 shows the positions of the equipment on the MMS, as well as the position of the test driver (TD) and the Assistant. He instructed the TD during the driving and controlled the equipment linked to the laptop.

(A)   (B)

Figure 3.2. (A) Action cam Garmin VIRB® Elite; and (B) Xsens Mti-G IMU sensor with GPS antenna

Table 3.2. Specifications of devices installed on the MMS

Devices	Features	Values
Video camera	Image sensor	16 MP
	Resolution	1080p @ 30 fps
	Temperature range	-15 to 60°C
GPS-IMU	Angular Rate:	
	Range Roll, Pitch, Yaw	± 300°/s
	Bias: Roll, Pitch	± 0.5°/s
	Bias: Yaw	± 1.0°/s
	Resolution	0.05°
	Acceleration:	
	Range X/Y/Z	± 50 m/s^2
	Bias: X/Y/Z	± 0.02 m/s^2
	Resolution	0.0098 m/s^2
	Update Rate	512 Hz
	Internal GPS:	
	Raw Measurements	L1 frequency, C/A code
	No. Channels	50
	Max. update rate	4 Hz
	Operating temperature	-40 to 85°C
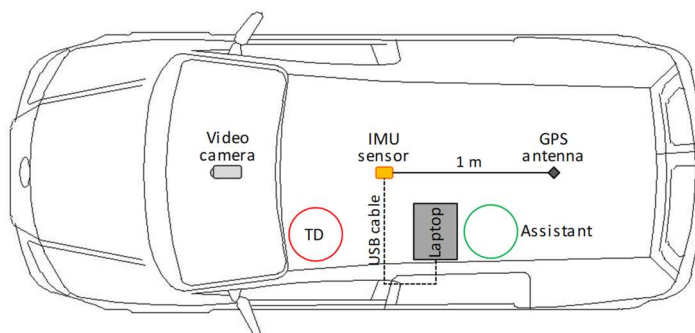
Figure 3.3. Equipment mounted on the vehicle used for real driving

3.2 Test Track

A validation study requires that the actual road geometrics and environment are faithfully reproduced in the virtual scenario.

The selected road track is located in the suburb of Turin (Italy), and is composed of the segments that surround the National Park of Stupinigi (Figure 3.4). Specifically, the design information of Segment #3 was known from a previous work of Bassani et al. (2012). Its location close to the *Politecnico di Torino*, the low traffic volume, and the possibility of completing the circuit in less than 20 minutes, were features that contributed to its selection. It is 15.8 km long, and composed of a sequence of two-lane rural roads separated by roundabout and crossing intersections.

The segments notation goes from 1 to 7, by considering each stretch with the right-of-way. The one indicated with the star (*) was not considered in the analysis due to the reduced carriageway width (5.0 m), and for the presence of two speed bumps that influence driver speed. The circuit was driven only in the clockwise direction.

The reconstruction of the road axis in *SCANeR^TMstudio* was accomplished by knowing the horizontal alignment of the Segment #3 (Bassani et al., 2012), and high resolution aerial images and orthophotos (*GeoPortale Piemonte*, 2017) of the entire area (extended about 20 km^2), accurately imported as background (Figure 3.5A). The geometric elements of the remaining part of the circuit were reproduced by adopting the centerline marking as reference for the regression of the road alignment, and ensuring the best correspondence of the road platform with the background images. Figure 3.6 shows the curvature diagrams of the seven segments, and Table 3.3 synthetized the main characteristics of the test track.
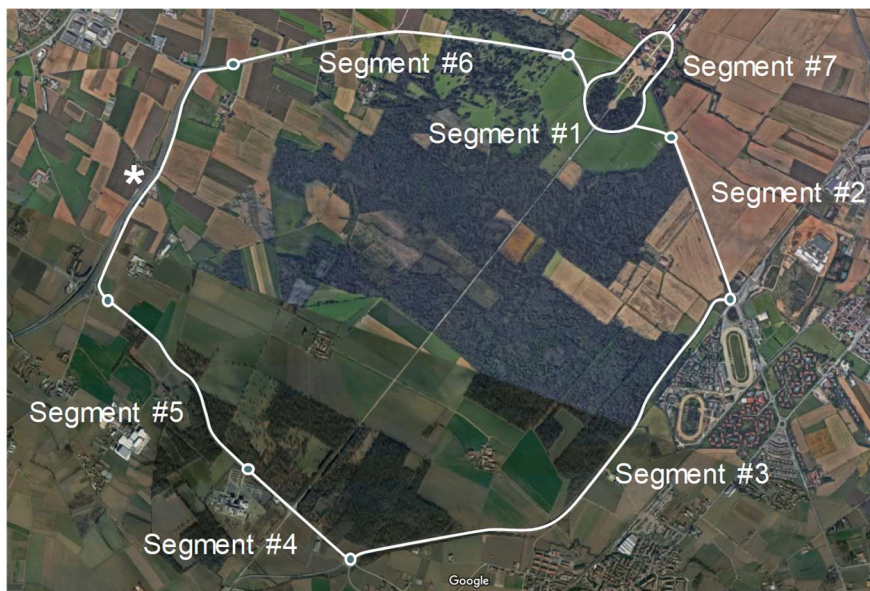
*Figure 3.4. Test track around the National Park of Stupinigi, Turin (Italy) with segment notation. The symbol * indicates the segment that was neglected in the data analysis*
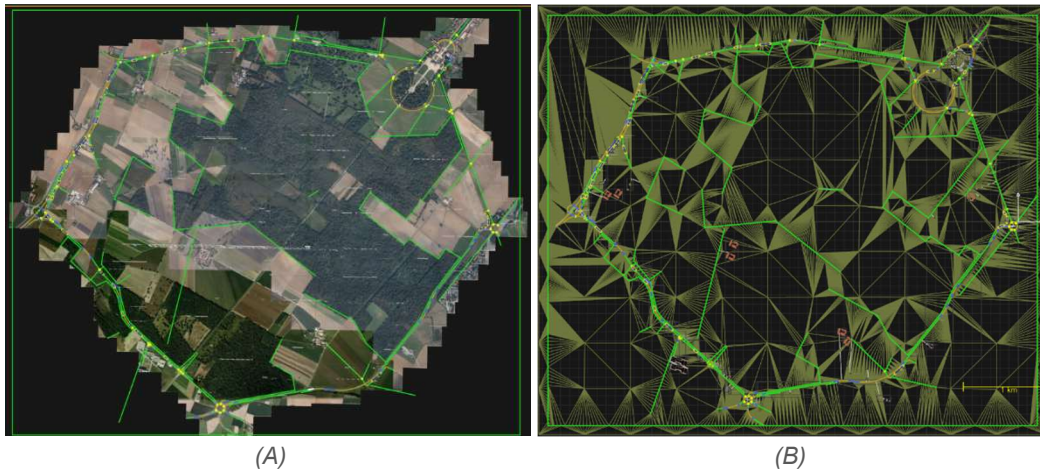
Figure 3.5. Test track reproduced in SCANeR^{TM}studio with (A) background 3d aerial images, and (B) the terrain triangulation
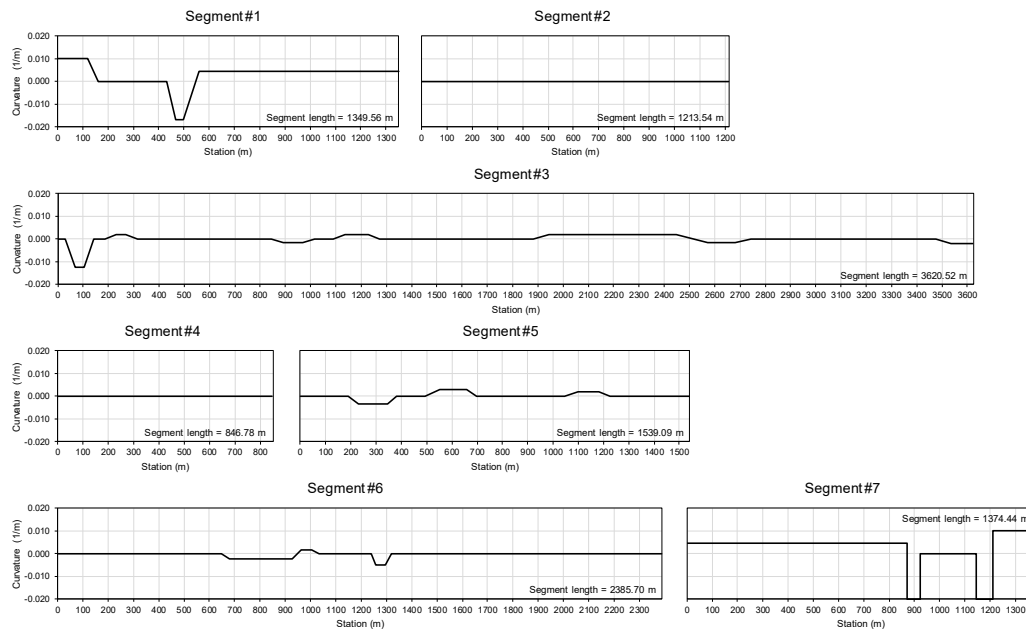
Figure 3.6. Curvature diagrams of the seven observed segments

Table 3.3. Geometric characteristics of the road segments considered for simulator validation

Total length	15,800	m
Carriageway width (min-max)	7.0 - 7.5	m
Shoulder width (min-max)	0 - 1.5	m
Posted speed limit (min-max)	50 - 90	km/h
Number of:		
short tangents ($L \leq 200$ m)	4	
long tangents ($L > 200$ m)	12	
curves with $R \leq 300$ m	10	
curves with $R > 300$ m	10	

Ninety-five 3d aerial images were used to evaluate the vertical alignment of the test track. The design profile was adapted as much as possible to the terrain elevation. In general, the track is developed in an almost flat terrain. The length of the circuit in the 3d model was successfully compared with the actual length of the road (see the pilot study, §3.3).

A preliminary video-survey was carried out to collect information of the road environment, in terms of markings, street furniture, vertical signs, vegetation, trees, and buildings, in order to build an accurate virtual model. This was accomplished through the use of objects included in the software database or by importing 3d items from the software *SketchUp* (*.dae* file format). For instance, Figure 3.7 shows the 3d model of the hunting residence of Stupinigi included in the virtual scenario.

The end of the "Terrain" design in *SCANeR^{TM}studio* consisted in computing the Delaunay triangulation among the elements of the database (Figure 3.5B), and generating the terrain 3d model. This is a controversial operation with respect to usual road design, where the Digital Terrain Model (DTM) is one of the input for the designer.

After the realization of the 3d model, the "Scenario" mode allowed to introduce events, traffic, other users (e.g., bicyclists, pedestrians, etc.), and to manage vehicle and environmental parameters. Events can be coded in *python* language with simply "if-then" rules. For instance, such functions were employed to show driving instructions on the central screen in correspondence to intersections. Autonomous vehicles were placed only in the opposite travel direction, simulating the presence of other users on the network, without influencing the drivers' preferred speed.

Figure 3.7. Virtual environment view from the starting point of the simulation

3.3 Drivers Sample, Naturalistic Observations, and Driving Simulations

Drivers' recruiting started in November 2015. Some faculty and staff of the *Politecnico di Torino* and other volunteers involved in this activity were informed about the purpose of the research. The recruiting form gathered personal information (gender, year of birth, contacts, year of acquisition of the driving license, vehicle use and experience), as well as number of crashes in which he/she has been involved, and level of education. Furthermore, people had to declare their confidence with video games; this attitude may influence the approach with driving simulation, reducing the motivation and the risk perception.

Drivers were also involved in training sessions to increase confidence with the equipment (as discussed in §2.2). These drives were performed firstly in a simple test circuit, and successively in a scenario with similar characteristics of the test track (e.g., curve radii, intersections, vegetation, etc.). The simulations lasted respectively 5 and 10 minutes to avoid fatigue effects on drivers. Those drivers who did not complete the training scenarios were excluded.

Thirty-three participants (25 males and 8 females) ranging from 26 to 69 years old were involved in field and simulated experiments. All of them were volunteers that approached to the driving simulator for the very first time. Main personal information are reported in Table 3.4.

The same experimental protocol was followed both in field and virtual environments. It consisted of:

- administration of a questionnaire on the health state;
- performing cognitive tests;
- driving experiment;
- performing cognitive tests;
- administration of a post-drive questionnaire.

In the initial questionnaire, TDs had to declare its health state, in terms of general wellness, recent assumption of drugs or alcohol, and the time of last meal. This information was useful to identify the general conditions of the driver before carrying out the experiment.

Visual and auditory cognitive tests were provided by an on-line website [2]. These tests measured the reaction times of TDs subjected to visual and auditory stimuli. The former was provided by the appearance of a green dot on the screen, the second by the hearing of a sound. Participants must click as soon as possible when the stimuli were provided by the platform. Each test was composed by seventeen repetitions. Reaction times gave an indication of the cognitive state of TDs, before and after the driving experiment. Specifically, discrepancies of such measures may be associated with mental workload or carsick.

Table 3.4. Characteristics of the drivers' sample

	No.	Age			Driving experience		Vehicle use
		min	mean	max	mean	st.dev.	mean
	(-)	(years)	(years)	(years)	(years)	(years)	(km/year)
Male	25	26	46.4	69	26.8	11.2	19,596
Female	8	26	39.4	57	21.5	12.0	8,143
Total	33	26	44.7	69	25.5	11.5	17,010

The naturalistic driving was performed first. TDs had the time to keep confidence with the vehicle inside the parking area that included the starting/ending point of the circuit (Figure 3.8). The car was the same for all participants. After the regulation of the seat, steering-wheel, and rear-view mirrors positions, all TDs were instructed to adopt their usual driving behavior, and to follow the indications of the Assistant during the track (Figure 3.3). The IMU-GPS sensor was set to collect data at a frequency of 10 Hz.

The simulated driving was performed at least two weeks after the real one. It was preceded by a trial driving (10 min) and a rest period (10 min). These allowed to re-establish the confidence with the equipment and to recover the ordinary psycho-physical conditions of the driver. Approaching to the experimental test, they were invited to follow the instructions on the screen and to stop the simulation in case of sickness. Also in this case the acquisition frequency was set to 10 Hz. Although the indications of the path to follow were provided in two different ways (through speech in the field, and by means of text messages at the simulator), they have not compromised the reliability of data collected along segments. In fact, it is worth noting that instructions were given approaching the intersections, and/or inside the roundabouts, elements that were not included in the analyses.

44.998131 N
7.607357 E
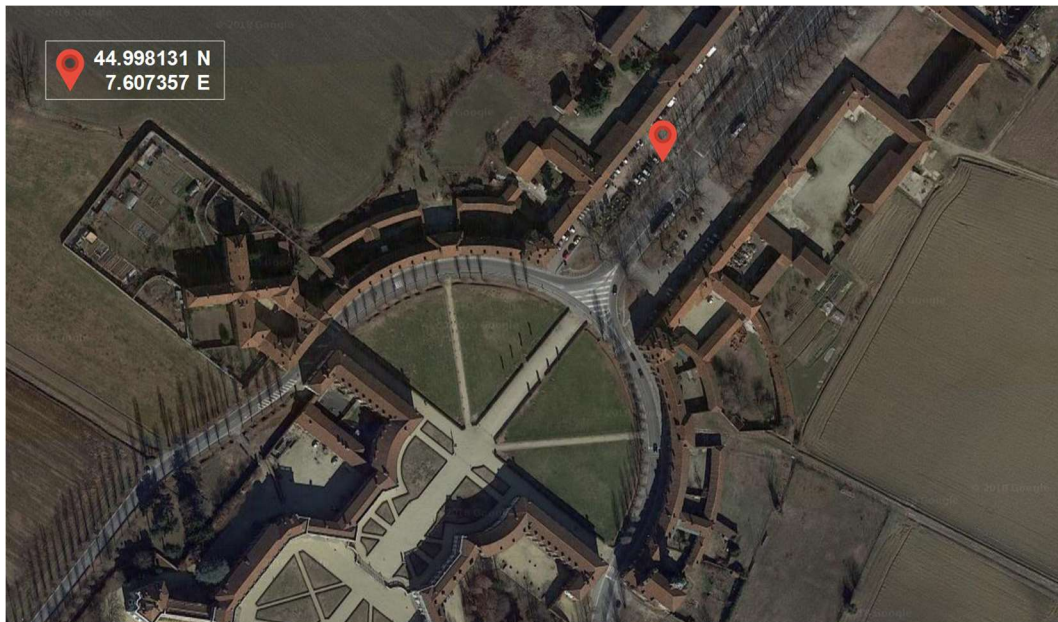
Figure 3.8. Indication and localization of the starting/ending point of the real circuit

The post-drive questionnaires were different for the two experiences. After the field driving, participants had to declare the knowledge of the track (travel frequency), their confidence with the vehicle, and if they were influenced by the measuring equipment and the video camera. It is worth noting that most of them (94%) were not familiar with the driven road segments, and anyone reported an influence of the surveying devices. On the other hand, the post-simulation questionnaire asked information about the fidelity of the road scenario, of the on-board devices, and the perceived level of sickness. This was quantified according to the Simulator Sickness Questionnaire (SSQ) suggested by Kennedy et al. (1993). Specifically, TDs reported the level (none, low, moderate, high) of occurrence of main symptoms (fatigue, sweating, headache, nausea, eyestrain, vertigo).

The experimental protocol, the timing of sequential operations, data collection, and preparatory analysis were tested through a pilot study. This was carried out by means of a reduced sample of four TDs that were not involved in the experiment. This preliminary and fundamental activity ensured the procedure effectiveness, limiting errors, and solving timing issues during surveys. As mentioned, the comparison of the traveled distance in both environments ensured the consistency between the two tracks (virtual and real). In this stage, a drive was also performed by maintaining the vehicle as much as possible centrally to the lane in order to define a "reference" trajectory. This was useful during data manipulation to attribute speed and trajectory data on a unique reference system (curvilinear abscissa, s – see §4.1.1). Another solved issue was the setting of the simulator brake pedal. The software provides three types of regulation: default, tourism, and race. The four involved TDs had to stop the vehicle at a stop/yield line in the scenario. The most reliable and manageable solution was the response supplied by the default regulation, since the others elicited mistakes in force modulation to fulfil the task (also related to the limitation of the static driving simulator).

3.4 Drivers' Performance and Feedback

All thirty-three TDs performed without problems the driving in the field, whereas two of them (TD#11 and TD#12) did not complete the driving experiment at the simulator for sickness occurrence.

Reaction times data collected through cognitive tests revealed that 64% of TDs increased visual cognitive performance after the naturalistic driving; this percentage reduced to 61% for the simulated driving. In both environments, the 45% of TDs reduced their auditory cognitive performance.

Figure 3.9 shows the mean (M) and the standard deviation (SD) of reaction times collected on visual/auditory cognitive tests for the rest of the sample. Average reaction time decreased slightly after driving, both for visual and auditory stimuli; the same occurred for the standard deviation. Mean values of simulated driving were lower than those in the field. These data revealed a general slight improvement in the drivers' sample of cognitive performance after driving.
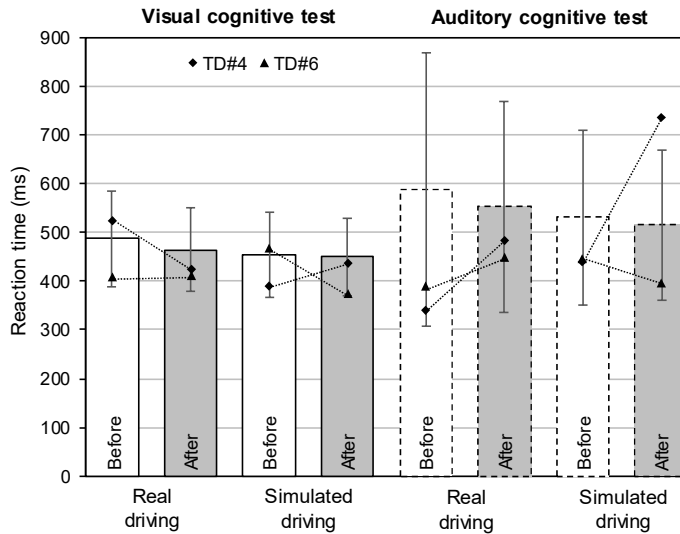
Figure 3.9. Results of cognitive tests in terms of mean and standard deviation (vertical bars). Single values are reported for TD#4 and TD#6 who experienced sickness

Nevertheless, the single discrepancies between before (T_B) and after (T_A) reaction times may reveal an increased level of concentration ($\Delta = T_A - T_B < 0$) on the one hand, or even an induced fatigue ($\Delta > 0$) produced by the driving experience. The variation (Δ) in reaction times among the TDs who did not manifest sickness (27) was negligible (< 100 ms).

However, four drivers suffered moderate or high level of sickness symptoms, that conditioned their performance on cognitive tests. Figure 3.9 reports the average reaction times for two of them (TD#4 and TD#6). In the case of TD#4, data shows decreasing cognitive performance after the driving simulations; the TD#6 behaved in the opposite way. Other two TDs (TD#13 and TD#17) showed average visual/auditory reaction times after simulation outside the interval (M + SD); for these reasons, these four TDs were removed from the data domain of Figure 3.9, and from the sample.

Post-drive questionnaires provided feedbacks on the fidelity of the virtual scenario and on the simulator equipment, with answers synthetized in Figure 3.10A. TDs found a realistic reproduction of the road environment, the horizontal markings and the vertical signs, as well as the presence of vehicles on the roadway. These evidences confirm the verisimilitude of the virtual environment.

TDs were also satisfied about the on-board equipment, acceleration pedal, gearbox, and engine sound. However, some complains were done on the lateral rear-view mirrors placed in the bottom-corners of the lateral screens. Their position did not correspond with the actual one (unfortunately the position cannot be set by the operator). In addition, the perception of the brake pedal obtained a negative feedback. Surely, more training allows to get better confidence with the pedal setting. A summary of feedbacks is reported in Figure 3.10B.
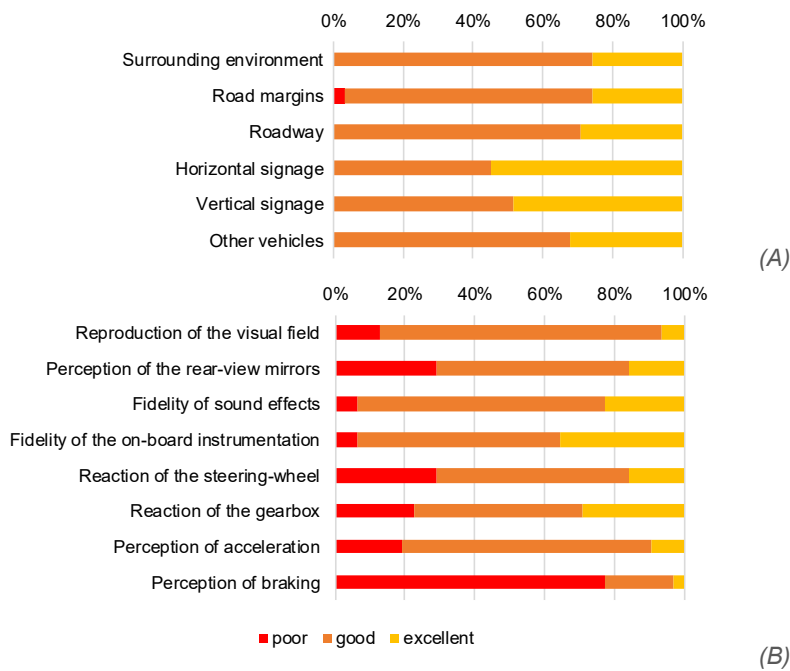
Figure 3.10. Answers of post-drive questionnaires regarding (A) the fidelity of the road scenario, and (B) the interaction with devices

Nevertheless, the negative feedbacks were not impactful on operating speed: TDs were alone in the traveled lane and would not control behind vehicles through rear-view mirrors; moreover, each stretch had the right-of-way, thus limiting the use of brake only approaching the intersections.

Questionnaires collected also information about the speed perception: 52% of TDs estimated speed by looking at the speed gauge, 17% by hearing the engine sound and surrounding effects, 12% through flowing images in the lateral screens, and others referred also to shift position (6%), scrolling of pavement surface and road signs (6%).

A preliminary speed analysis was performed on speed profiles to verify the presence of outliers (speed data conditioned by the vehicle ahead or overtaking maneuvers were removed yet, §4.1.1). For each segment, a confidence interval equal to three times the standard deviation was considered around the mean speed profile. Despite TDs were aware of the activity aim, the speed profile of TD#21 fell outside (above) this interval. For this reason, data associated to TD#21 were excluded from analyses due to the unrealistic behavior (excessive aggressiveness) at the simulator.

4. Behavioral Validity of the Driving Simulator

The behavioral validity of the driving simulator at the *Politecnico di Torino* was assessed for the driving speed, and for quantities related to the vehicle trajectory. The first type is a well-known procedure, that in the present work was determined as a function of the different geometrics of road elements. On the other side, driving trajectory was described in terms of anticipatory distance, average curvature along bends, and curvature change rate (along transitions).

4.1 Operating Speed

4.1.1 Data Processing

Speed comparison required that collected data were reported in the same reference system. For this reason, vehicle positions expressed in geographical coordinates in the field, and in local coordinates in the simulator, were converted into cartographical ones, without considering the elevation (hypothesis of flat terrain). The destination coordinate system was the Universal Transverse Mercator (UTM), that is expressed by East and North distances (in m) from the zone's central meridian and the Equator, respectively. Italy is included in 3 zones: 32, 33, and 34, whereas Turin is placed in the 32N zone.

The transformation of geographic to cartographic coordinates was computed through the Hirvonen's formulas (Cina, 2014), by considering the false origin[2] $(x_0, y_0) = (500, 0)$ km, and the scale factor along the central meridian, $m_c = 0.9996$.

The conversion of local in cartographic coordinates implies the use a flat roto-translation with isotropic scale variation. It needs four parameters: two translations of the origin, a rotation ϕ, and a scale factor λ. The knowledge of the coordinates of a sufficient number of points (at least 2) in both reference systems, and the linearization of the problem ($a = \lambda \cdot cos\phi$, $b = \lambda \cdot sin\phi$), allowed to estimate the four variables as follows (Cina, 2014):

$$
\begin{aligned}
E_0 + ax + by - E = 0 \\
N_0 - ay - bx - N = 0
\end{aligned}
\qquad \text{(eq. 2)}
$$

where (x, y) are the known local coordinates, (E, N) the known cartographic coordinates, (E_0, N_0) the unknown origin position, and a, b the unknown parameters for conversion. The solution of the equations system through Ordinary Least Square (OLS) method provided the values listed in Table 4.1.

---

[2] The false origin is a computational solution to avoid coordinates with negative numbers. Indeed, the central meridian of each zone (y axis) coincides with 500,000 m East.

Table 4.1. Solution of the system through OLS method

Variable	U. M.	Value
E_0	m	390,706.71
N_0	m	4,981,681.50
a	-	0.9999763
b	-	0.0000258

To simplify the analysis, points that constitute driver trajectory were split in seven subsets, by determining the initial and final points of each segment, both in the field and in the simulator. In particular, the final point of each segment was set as to exclude the sections preceding the intersections, that were more influenced by the intersection itself than by the road geometrics.

Subsets of different drivers were not yet comparable since each was composed by a different number of points, as a function of the adopted speed. For this reason, the "reference" trajectories in the real and in the virtual environment were established during the pilot study in order to associate speed data to the same station (or curvilinear abscissa). These trajectories were sampled with a frequency of 10 Hz, and were adopted to define the list of measurement points for each segment. A dedicated algorithm in MATLAB® (§A.1) was developed to refer speed values of *i*-th adopted trajectory with the closest point of the corresponding reference one.

Furthermore, speeds of drivers influenced by the vehicle ahead or who carried out overtaking maneuvers were removed from the subsets. This operation was accomplished by means of the video recordings collected in the field. Only free-flow speeds were considered in following analyses, as those of drivers that were unaffected by simulator sickness.

Data resulted from this operation were used to generate all graphs and to perform comparative and statistical analyses reported in the following Sections.

4.1.2 Comparative Analysis

Data processing allowed to get free-flow speed samples at every measurement site in the field (S_F) and at the simulator (S_S); their size ranged between 16 and 27. For comparison purposes, the 15th, 50th, and 85th percentiles of speed were computed from the set of speed data associated to each measurement point.

Figure 4.1 shows the trends of those pertaining on field and simulated environment, by means of square plots. Points close to the equality line evidence the equivalence between the two scenarios. Each variation indicates the tendency of driving faster in one scenario with respect to the other. In the bottom of the figure, the summary of the number of measurement points, the number of TDs, and the number of analyzed speed values (for percentiles computation) for both environment is reported. It is worth noting that along some segments the speed profile of TDs influenced by vehicles ahead was truncated to consider free-flow conditions only.
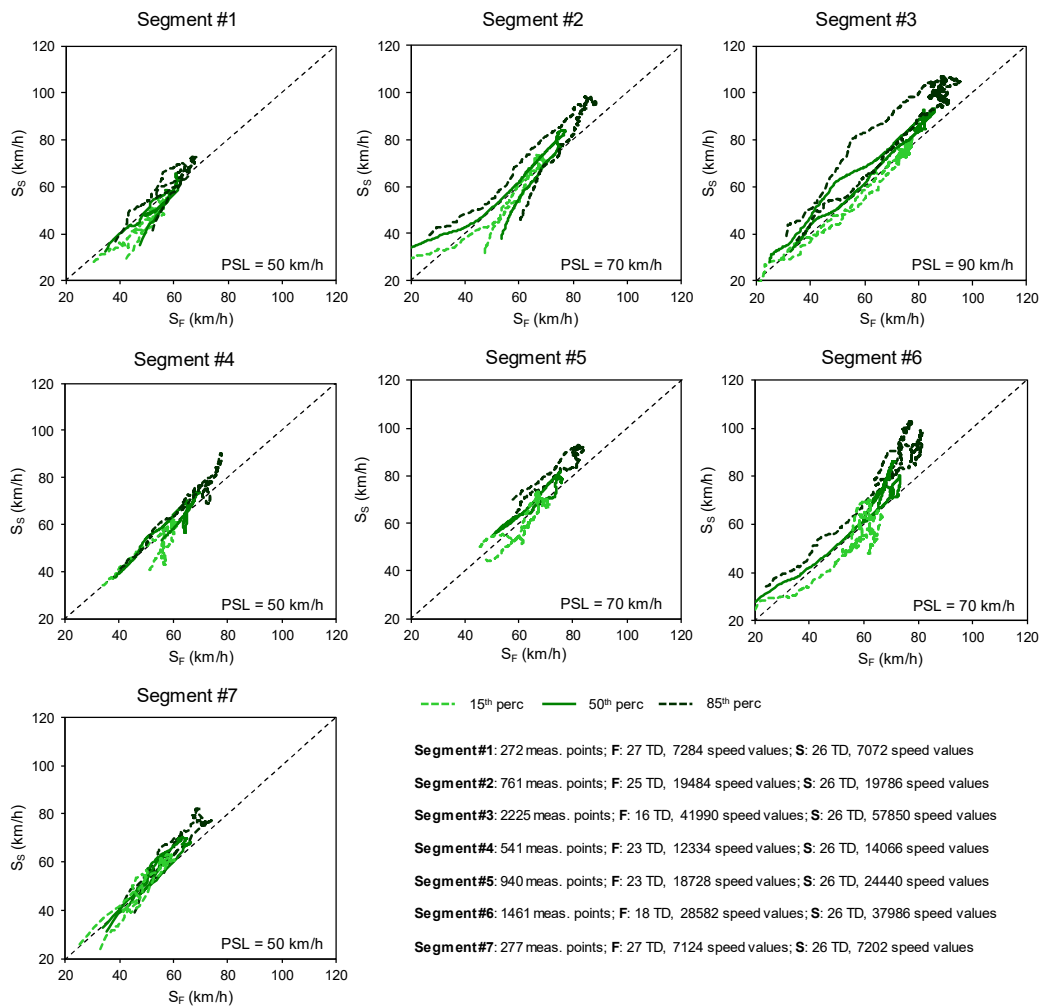
Figure 4.1. Plots of the comparison between mean speed profiles in the field (S_F) and in simulated (S_S) environment, for the seven road segments (PSL = Posted Speed Limit, F = field, S = simulator)

Plots show that S_S was generally higher than S_F for the majority of road segments (e.g., Segments #3 and #6). Conversely, Segments #1 and #7 include a long curve ($R = 228$ m) that strongly conditioned the adopted speed in both contexts. Figure 4.1 also shows that the 15th and 50th percentile curves tend to be less dispersed than 85th ones: this observation indicates that the more aggressive participants maintained their driving habits, adopting higher speeds in the simulated drives, whereas the rest of the sample drove with similar speeds in both environments. This supports the observation of Wade and Hammond (1998) in which aggressive drivers on real world showed a similar behavior also in the simulated context.

Figure 4.2 shows the average profile of speeds collected in the field (red line) and in the simulator (blue line), together with the curvature diagram of the road alignment (black line), in order to evidence the relationship between the speed differentials and the road element (i.e., circular curve, tangent, transition). Standard deviations in the sample were computed every 100 m, and showed with vertical bars.
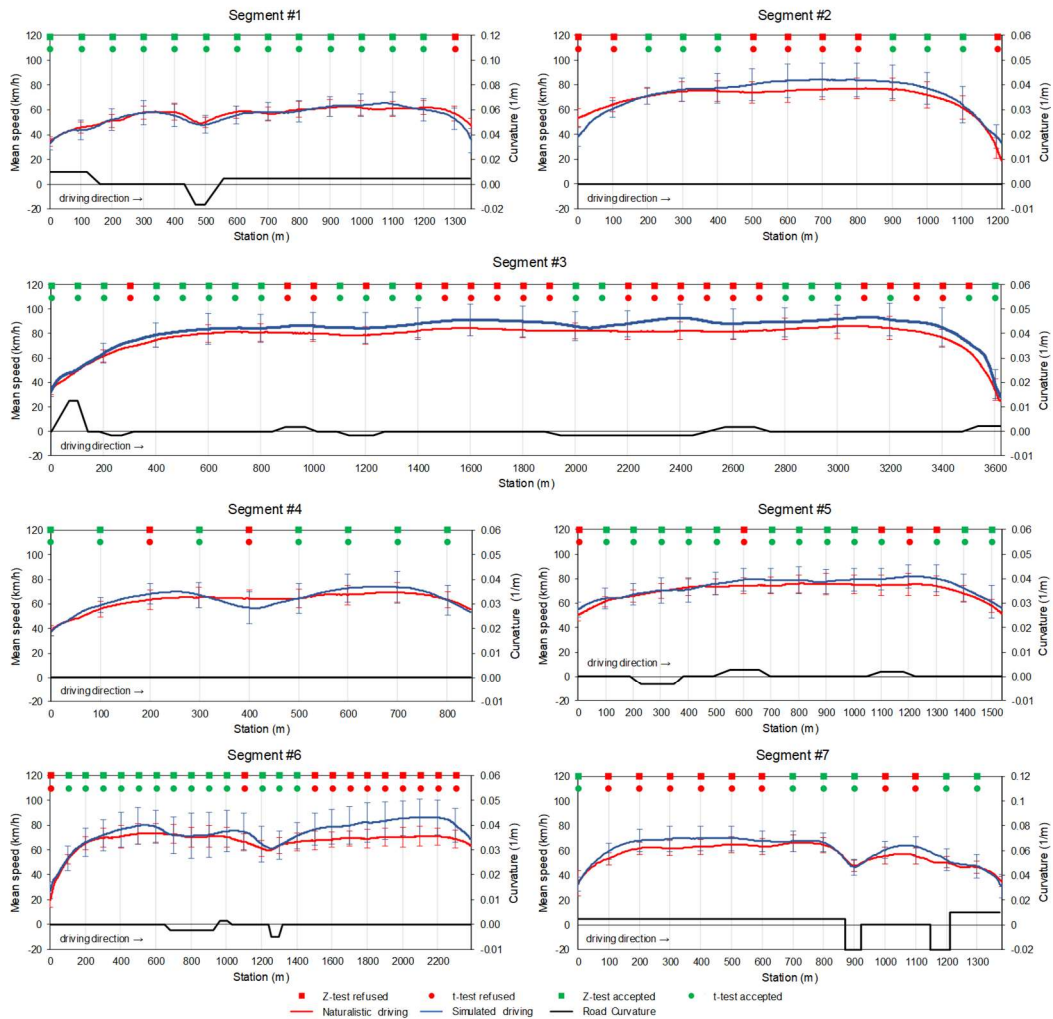
Figure 4.2. Mean speed profiles and statistical test results along observed segments (blue and red vertical bars indicate the values of the standard deviation of speeds for simulated and real driving conditions, respectively)

As mentioned, speeds at simulator on Segments #1 and #7 are very comparable to those measured in the field. The greater speed difference (ΔS = 3.8 km/h) occurred at station 1,100 m on Segment #1, while in Segment #7 the maximum ΔS is 7.4 km/h. This segment contains also two sharp curves, where ΔS is equal to 1.5 and 2.1 km/h.

In the other segments, S_S was usually greater than S_F, with the sole exception of acceleration stretches, and at station 400 m of Segment #4. In that section there was an abandoned intersection, that in the virtual model created some difficulties on TDs in interpreting the roadway. Drivers reacted to this misjudgment by lowering the adopted speed. Moreover, speed profiles show that ΔS varies with curvature: specifically, larger values were observed in sections characterized by null or low curvature (tangents and shallow curves).

Differently from literature, SDs in real driving conditions were always lower than those measured at the driving simulator. However, Bella (2008) and Branzi et al. (2017) collected field data by considered a random drivers' sample that traversed specific road sections, while in this study the same group of TDs was

surveyed in both environments. A validation of such analysis will be discussed in the next Section.

4.1.3 Statistical Analysis

Speed data extracted every 100 m along the circuit were statistically compared by means of the *Z*-test and a sequence of *F*- and *t*-tests. The first compares the mean of data distributions in the field and in the simulator, assuming known variances. Conversely, the *t*-test compares samples of unknown variances, by preliminary asses the ratio between the variances of the two samples through the *F*-test. The choice of using both procedures derived from the reduced sample size (ranging between 16 and 27 data): it is at the lower limit to run the *Z*-test but sufficient for the coupled *F*- and *t*-tests. The assumptions of the statistical tests were checked with a non-parametric test (Kolmogorov-Smirnov test). It revealed that all speed samples (127 measurement sites × 2 environments) were normally distributed. For the four tests, a level of significance (α) equal to 5% was adopted.

The outcomes of the *Z*- and *t*-tests are presented in Figure 4.2. Green indicators show that the null hypothesis (H_0) is accepted, meaning that the two speed distributions are part of the same population, thus an absolute validity is plausible. On the contrary, red symbols indicate that H_0 is rejected. The Hedges's effect size (*g*) and the power[3] of the *Z*-test were also computed to support the results. The first was determined through the combined variance (σ^2_{comb}):

$$\sigma^2_{comb} = \frac{(N_F - 1) \cdot \sigma_F^2 + (N_S - 1) \cdot \sigma_S^2}{(N_F + N_S - 2)}$$

(eq. 3)

Thus, the effect size (*g*) proposed by Hedges is equal to:

$$g = \frac{\overline{S}_F - \overline{S}_S}{\sqrt{\sigma^2_{comb}}}$$

(eq. 4)

where N_F and σ_F is the sample size and the standard deviation of speed observations in the field, N_S and σ_S the corresponding in simulator environment, $\overline{S}_F$ and $\overline{S}_S$ are the mean speed values for each measurement site respectively in the field and at the simulator (Hedges, 1981).

The test power was calculated by means of a post hoc analysis, following the procedure explained in detail in Bella (2005a). Specifically, the difference Δ was assumed to be equal to 10% of the average S_F value, meaning that a discrepancy lower than 10% between field and simulator data does not nullify the analysis of driver behavior. All results of statistical tests were reported in §A.2.

All points of Segment #1 satisfied the tests (*g* range = .03-.54; 1−β range = .73-.93), except for station 1,300 m. This was not confirmed in Segment #2

---

[3] The power of a statistical test is the probability of correctly refusing the H_0 when it is false; it is the complement to 1 of the β-value, named "type II error" (Cohen, 1988).

(completely straight) on the initial, central and final parts (when H_0 was accepted, g range = .03-.52; 1–β range = .44-.97). Along the Segment #3, the H_0 was accepted only in 16 points (g range = .04-.56; 1–β range = .18-.92). At stations where H_0 was rejected, S_S was higher than S_F, with an average ΔS of 6.5 km/h. The results for Segment #4 revealed that only two points did not satisfy H_0 (refer to the considerations of station 400 m, §4.1.2). In the others, the range of g was equal to .003-.53, and the corresponding power was between .60-.94. In Segment #5, statistical tests were accepted in all stations (g range = .03-.48; 1–β range = .53-.92), with the exception for the entry point and those in correspondence of the two curves with $R > 300$ m. In both cases the average ΔS was 5.7 km/h. Thirteen of 24 stations (54%) of Segment #6 accepted H_0: in the first tangent, in the shallow left-hand curve, and in proximity of the sharp leftward curves (g range = .03-.53; 1–β range = .40-.74). In the last segment, tests were rejected in the initial long rightward curve ($\Delta S = 5.8$ km/h), and in the tangent ($\Delta S = 5.8$ km/h). When the H_0 was accepted, the Hedges's g ranged between .10-.26, and the power of the Z-test was equal to .32-.93. It is worth noting that the maximum effect size that led to accepted H_0 was equal to .56, which means that at least 78% of the two groups are overlapped.

Table 4.2 summarizes the results for each road element. Specifically, measurement sites were grouped into six sets, by considering their location on short ($L \leq 200$ m) and long ($L > 200$ m) straights, sharp ($R \leq 300$ m) and shallow ($R > 300$ m) bends, initial and final analyzed sections of the segments. It can be appreciated that in more demanding geometric elements (sharp curves and short tangents) the speed distributions were more comparable than in the other parts of the track. This also occurred at the initial and final portions of long tangent (see Segment #2), and starting of long curves (see curve #3 of Segment #1, and curve #5 of Segment #3). The table reveals that the H_0 was accepted in 57% of measurement sites, mainly along the intersection approaches and departures, where drivers decelerated to stop the vehicle or accelerated to reach their preferred speed, as well as along sharp curves ($R \leq 300$ m) and short tangents. In 40% of cases, the driving simulator reached a relative validity for shallow curves ($R > 300$ m), where the mean speeds in the field were always lower than those observed at the simulator, with a mean $\Delta S = 5.1$ km/h. The same value (5.1 km/h) was obtained for tangents longer than 200 m. Only in 3% of cases the speed collected in field was higher than that at the driving simulator.

Table 4.2. Validation results

Road element	No. of sections	Null hypothesis accepted (absolute validity)	Null hypothesis rejected (relative validity)	
			$S_S > S_F$	$S_S \leq S_F$
Short tangents ($L \leq 200$ m)	2	2 (100%)	0 (0%)	0 (0%)
Long tangents ($L > 200$ m)	64	36 (56%)	26 (41%)	2 (3%)
Curves ($R \leq 300$ m)	23	17 (74%)	6 (26%)	0 (0%)
Curves ($R > 300$ m)	24	9 (38%)	15 (62%)	0 (0%)
Intersection approaches	7	4 (57%)	2 (29%)	1 (14%)
Intersection departures	7	4 (57%)	2 (29%)	1 (14%)
Total	127	72 (57%)	51 (40%)	4 (3%)

However, Cohen (1988) suggested that acceptable results must be associated to a strength $(1–\beta)$ equal or higher or than 0.80. It is worth noting from computations (§A.2) that such condition is not satisfied on 1 measurement point along short tangents, 20 sites along long tangents, 3 along sharp curves, 4 on shallow curves, 4 at intersection approaches, and 1 at intersection departures. Therefore, the absolute validity can be confirmed only for tight bends (in 61% of measurement sites the H_0 was accepted), and not for the other elements, where a prevalence of points with a relative validity occurred.

Validation of the sample of field speeds

A speed survey was carried out in four sites along the experimental track to check the characteristics of the observed sample with respect to a different drivers sample that traveled on the same road network (Figure 4.3A). For this purpose, a cross-sectional video survey was performed by means of a video camera mounted in a vehicle parked along the roadside, as to be hidden from oncoming vehicles (Figure 4.3B). Two sections were located along Segment #3 in two lay-by areas, one along Segment #4 in a driveway, and one along Segment #6 in a parking area adjacent to the roadway.

The methodology to collect speed data is based on the principle of triangulation. It requires the presence of two references in the frame, and the knowledge of:

- the distance from the camera to the lane marking;
- the carriageway and shoulders width; and
- the distance (baseline) between the two references.

From these measures, it is possible to evaluate the distance traveled by vehicles within the lanes (assumed along the centerline), and consequently the speed of the vehicles. This was computed through the ratio of traveled distance and the time employed to travel the stretch of road included in the "virtual" triangle. The latter was estimated by means of an accurate analysis of videos (recorded at 30 fps), by observing the times in which the vehicle obscured the first and second references.

(A)   (B)

Figure 4.3. (A) Position of the control sections along the test track, and (B) picture from the trunk of the parked vehicle during recordings

Surveys were carried out during the same hours of field driving experiments, as to consider the same circulation conditions. Recordings lasted between 15 and 18 minutes, and only passenger cars that travelled in the same direction (inner lane of the circuit) were observed for speed estimation (Table 4.3).

Free-flow speeds were selected for the comparison with previous speed data. Those were identified on the basis of the time interval between following vehicles: as suggested by Misaghi and Hassan (2005), a headway of 5 seconds was considered to distinguish conditioned from free-flow (unconditioned) vehicles. Table 4.4 reports the summary of estimates computed for the speed samples in the field, collected with the two methodologies.

Once again, Z- and t-tests were employed for speed validation (Table 4.5). The statistical tests compared the mean values of the two speed distributions (the one derived from survey and the one deduced from Figure 4.2), and led to identical results. Specifically, the tests accepted the null hypothesis H_0 (equal mean), with a significance level of 5%, with the sole exception of Site #2. Hedges's g value and power of the Z-test were also computed and reported in the table. The probability of a Type II error was lower than 40% for Sites #1 and #4, but it increased to 52% in the Site #3, presumably due to the reduced sample sizes and the greater variance. In fact, the correspondent effect size ($g = .50$) is medium, indicating that the distance between the two samples is about half standard deviation.

Table 4.3. Details of cross-sectional video surveys

Site #	Segment #	Station	Video duration	# observed vehicles	# vehicles in free-flow
1	3	2+500 m	18' 32"	113	38
2	3	1+800 m	18' 02"	108	43
3	4	0+240 m	15' 08"	97	27
4	6	1+660 m	18' 20"	107	41

Table 4.4. Summary of estimates (Mean and Standard Deviation) and size (n) for the speed samples. ΔM represents the difference between mean values

Site #	Field experimental driving			Cross-sectional survey			ΔM
	M	SD	n	M	SD	n	
1	81.28	6.74	17	85.81	16.18	38	4.53
2	83.35	6.28	20	100.35	18.36	43	17.00
3	65.23	8.20	23	71.56	15.37	27	6.32
4	69.16	6.41	16	73.98	16.74	41	4.82

Table 4.5. Results of statistical tests (g = Hedges's effect size; 1–β = power)

Site #	t-test			Z-test			1–β	g
	$p(T \leq t_{crit})$	T	t_{crit}	$p(Z \leq Z_{crit})$	Z	Z_{crit}		
1	.273	1.11	2.01	.143	1.46	1.96	.75	.32
2	$1.63 \cdot 10^{-4}$	4.02	2.00	$5.71 \cdot 10^{-8}$	5.43	1.96	.76	1.09
3	.083	1.77	2.01	.064	1.85	1.96	.48	.50
4	.270	1.11	2.00	.116	1.57	1.96	.62	.33

Sites #1, #3, and #4 were the most demanding in terms of road geometry; they compelled drivers belonging to the two samples (those unknown individuals who traversed the section, and the group of volunteers involved in field survey) to adopt similar speeds. In contrast, the Site #2 was positioned at the end of a very long tangent and less demanding segment. In this case, the rejection of null hypothesis is attributed to the conditioning of the volunteer drivers, that were reasonably influenced since involved in the validation study.

4.2 Anticipatory Distance and Trajectory Curvature

The analysis of the drivers steering behavior was performed only along Segment #3 (Figure 3.4). It was selected among the others since geometrics of the track are known from previous investigation (Bassani et al., 2012). Detailed data of this Segment are included in Figure 4.4.

From considerations discussed in §1.2.1, a behavioral validation of the driving simulator was conducted by taking the trajectory geometry (driver action on the steering wheel) into account. Vehicles' tracking data were collected in real and simulated environments. Specifically, geometric parameters able to describe the longitudinal characteristics of the vehicle trajectory (anticipatory distance, the average curvature along the curve, and the curvature change rate) were evaluated. This approach had never previously been considered in other driving simulator validity study, which mainly had referred to the evaluation of the lateral displacement of vehicles in specific road sections.

The anticipatory distance (d_a) measures the difference between the position where the driver initiates the steering maneuver and the tangent to spiral (TS) point. Similarly, d_a measures the distance between the position where the driver starts steering before the curve to spiral (CS) point. The point where drivers nullified the steering angle with respect to the reverse (R) point along a reverse spiral was also considered (Figure 4.5).

C1	C2		C3	C4		C5		C6		C7
R=80m	R=550m		R=550m	R=550m		R=550m		R=550m		R=500m
A=55m	A=160m		A=160m	A=160m		A=185m		A=185m		A=170m
L_C=36m	L_C=36m		L_C=77m	L_C=90m		L_C=504m		L_C=108m		L_C=112m
L_S=38m	L_S=47m		L_S=47m	L_S=47m		L_S=62m		L_S=62m		L_S=58m
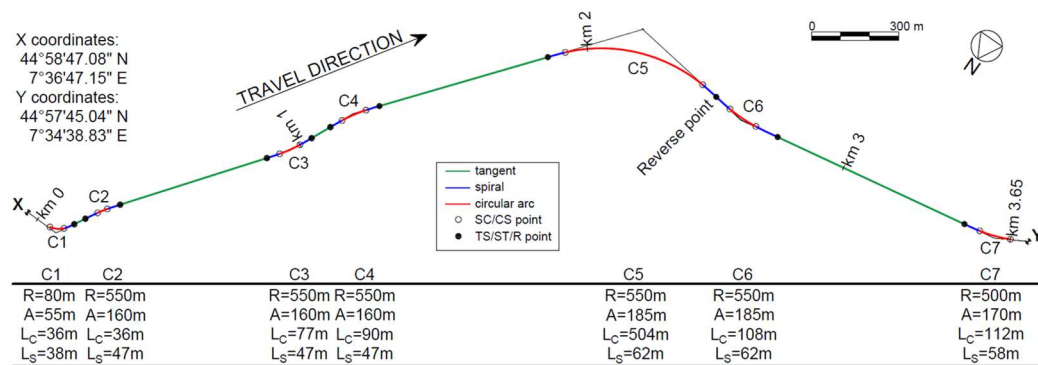
Figure 4.4. Road layout of the Segment #3 considered in the study (R = curve radius, A = spiral scale factor, L_C = length of circular arc, L_S = length of spiral)
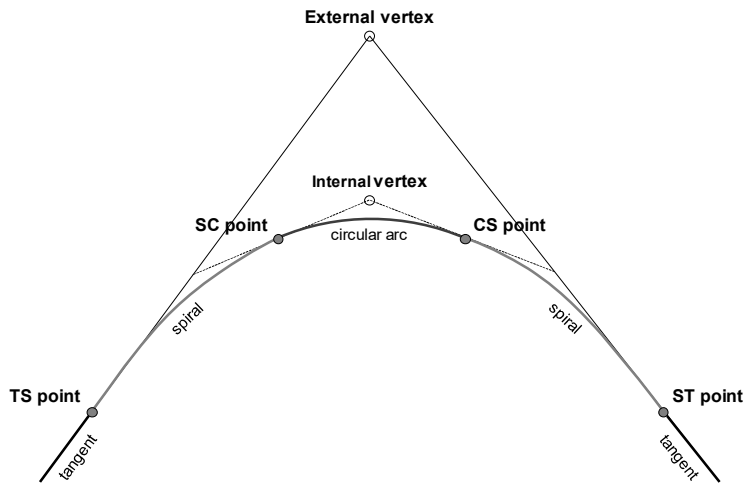
Figure 4.5. Scheme of a curve alignment with the indication of TS, SC, CS, and ST points

TS and CS points indicate the station at which the steering maneuver should start to maintain the correct position in the lane. d_a reflects the anticipatory behavior postulated by Donges (1978) that depends on the perceived oncoming curvature gained from a forward view of the road.

In contrast, the c_r is the curvature variation along the vehicle trajectory; it is computed as the ratio between the curvature variation and the distance along which this change occurs. Differently from d_a, c_r reflects the compensatory mechanisms (Donges, 1978) that driver assumes to correct errors made when anticipating the steering maneuver with respect to the curvature change points, and to bring the vehicle back on to the correct path in the lane.

The curvature (c) of the vehicle trajectory in the circular arc portion of a compound curve (composed in order of spiral, circular arc, and spiral) reflects the ability of a driver to read and adopt the designed radius assumed by the designer. The three measures (d_a, c, and c_r) reflect the longitudinal behavior of drivers when negotiating the road alignment along curves.

4.2.1 Data Processing

Figure 4.6 depicts the spatial data collected during naturalistic and simulated driving in the cartographic reference system (§4.1.1).

The as-built alignment was used as a reference element to define the curvilinear abscissa for comparing data collected in the two environments. This was necessary since each trajectory had its own length, and a direct comparison between positions measured on different trajectories was not possible without the use of a reference line. This operation was accomplished by means of a dedicated MATLAB® algorithm (§A.1).
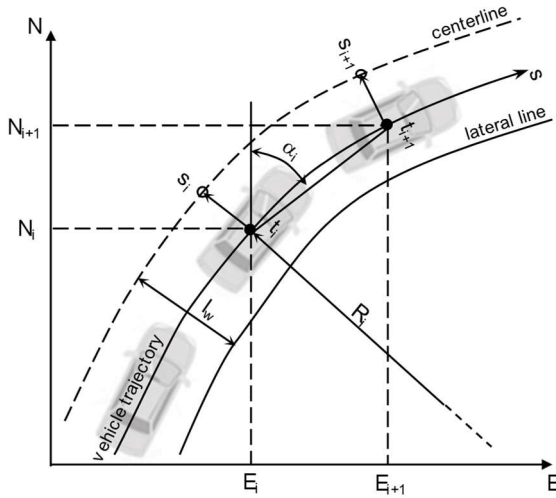
Figure 4.6. Description of positioning data collected in the field and at the driving simulator

Positions of the vehicle barycenter (E_i, N_i) were used to derive vehicle orientation (heading, α_i):

$$\alpha_i = \tan^{-1}\left(\frac{E_{i+1} - E_i}{N_{i+1} - N_i}\right) \qquad \text{(eq. 5)}$$

The first and second derivatives of the heading angle are the curvature (c) and the curvature change rate (c_r) of the driving trajectory respectively. When available at small station differences (i.e., at high sampling frequency), c and c_r reported in the example of Figure 4.7 derive from the following two equations:

$$c_i = \left(\frac{d\alpha}{ds}\right)_i = \frac{\alpha_{i+1} - \alpha_i}{s_{i+1} - s_i} \qquad \text{(eq. 6)}$$

$$c_{r,i} = \left(\frac{dc}{ds}\right)_i = \left|\frac{c_{i+1} - c_i}{s_{i+1} - s_i}\right| \qquad \text{(eq. 7)}$$

In the three equations, E and N represent the East and North coordinates of the two points i and $i+1$; the curvilinear abscissa (s) for the real and simulated environments was determined by discretizing the as-built alignment every 12 cm. Curvature was assumed positive in the case of a rightward curve, while c_r was considered in absolute value.

The heading obtained from eq. 5 suffered from usual Gaussian noise affecting positioning systems. Hence, headings were filtered to remove the noise as per the "semivariogram method" (Murato and Saito, 1999). In accordance with Gikas and Stratakos (2012), the heading data was estimated as the moving average of an interval whose width was set to reduce the local noise component in the data without affecting the actual information content of the trajectory geometry.
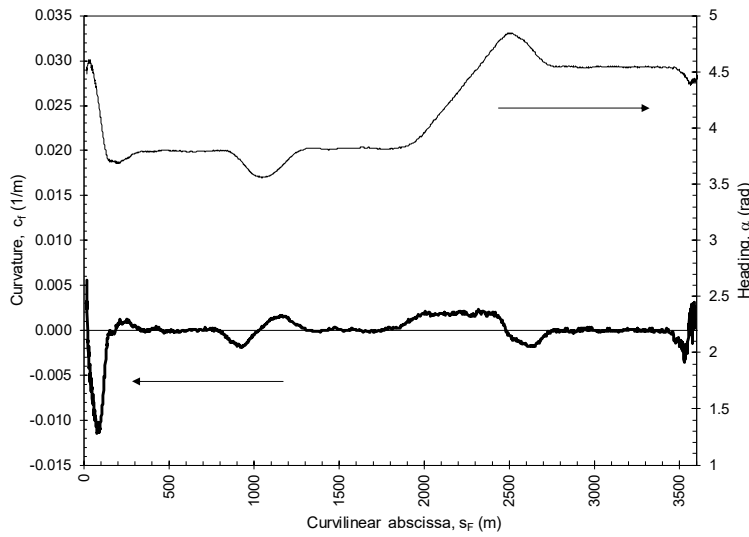
Figure 4.7. Example of field heading and curvature data as a function of the curvilinear abscissa (s_F)

This operation was possible by an estimation of the semivariogram variable γ_α for the entire set of N heading data (α) available:

$$\gamma_\alpha = \frac{\sum_{i=1}^{N} [\alpha(s_i) - \alpha(s_i + h)]^2}{2 \cdot N \cdot \sigma_\alpha} \qquad \text{(eq. 8)}$$

where the correlation lag h represents the width of the data interval averaged to remove the Gaussian noise (Delay and de Marsily, 1994), and σ_α is the standard deviation of the entire heading dataset. The graph of Figure 4.8 shows the points where γ_α changes its initial linearity.
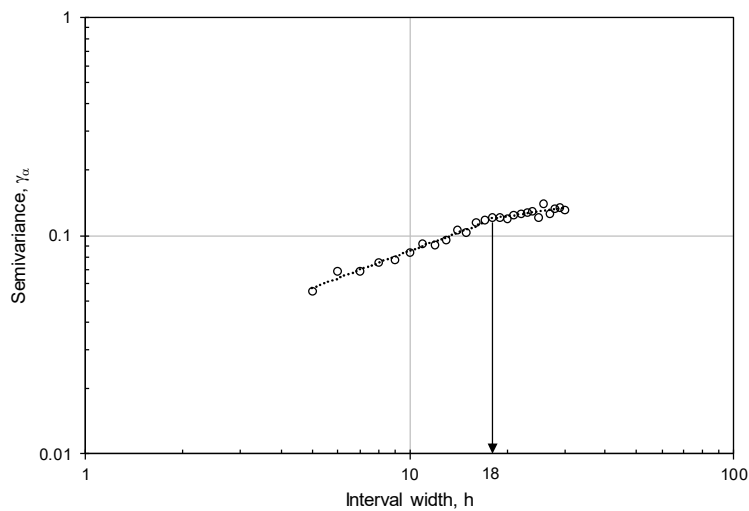
Figure 4.8. Semivariogram analysis (γ_α) of heading data for TD#1 in field observations (N = 1502, σ_α = 0.16037)

The graph indicates that eighteen heading data across the central (*i*) point were necessary for a filtering action able to remove the Gaussian noise from the dataset of this test driver. Similar analyses were carried out for the other drivers involved with a specific filter being applied to each dataset. As mentioned in §4.1.1, only unconditioned data was considered in the analysis. In the Segment #3, 49 trajectories were analyzed: 26 were collected on the driving simulator, and 23 in the field.

4.2.2 Comparative and Statistical Analyses

Curvature data for the two environments were elaborated to derive:

- the distance d_a between the positions where drivers started the steering maneuver before the TS/CS points;
- the average curvature (*c*) along the circular arc; and
- the average curvature change rate (c_r) along transitions and reverse spirals.

Figure 4.9 illustrates the recurrent trend observed in the data: most of drivers anticipate the action on the steering wheel before the point where the curvature actually changes (TS/CS points); this results in different *c* and c_r values of the adopted trajectory.

Figure 4.9 also shows the three geometric cases considered in the data analysis: the road sections across the TS point (Figure 4.9A), the sections across the CS point (Figure 4.9B), and the section around the reverse (R) point (Figure 4.9C). Each case includes two graphs: the first depicts the curvature observed in the field (red line) in comparison with the field road alignment curvature (black line); while the second shows differences between the trajectory curvature (green line) and the road curvature in the virtual model (black line).
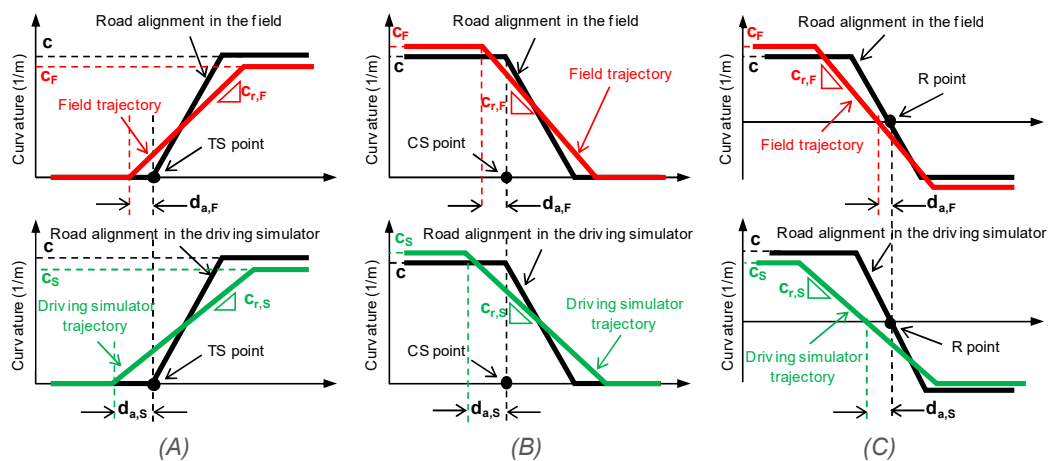
Figure 4.9. Schematic representation of curvature profiles used to elaborate the anticipatory distance (d_a) and the average curvature change rate (c_r) at straight to transition (A), curve to transition (B), and reverse (C) points (subscript "S" stands for "simulation", subscript "F" stands for "field")

Anticipatory distance (d_a)

Observations of d_a are shown in Figure 4.10 and Figure 4.11. Here, and in further analyses, collected data were depicted with box-plots, showing the median value, the 95% confidence interval for the difference in two medians (notches of the box[4]), the 1st and 3rd quartiles, and outliers. The t- and Z-test were performed to verify the null hypothesis H_0, which determines whether the compared datasets belong to the same population (i.e., the means and standard deviations of the two datasets are comparable, thus demonstrating the absolute validity of the driving simulator). Otherwise, in case of H_0 hypothesis rejection, data were analyzed to evaluate the direction and the magnitude of the difference between samples (i.e. assessing the relative validity). Here and in further sections, the outcomes of the t-tests were displayed in the figures; they consist of field and simulated sample sizes (N_F and N_S, respectively), degrees of freedom (dof), statistic t or t^*, p-value, and t critical (t_{crit}). Specifically, t refers to the t-value obtained assuming equal variances, whereas t^* is the computed t-value assuming different variances between samples. These assumptions were verified *a priori* with the F-test. All the other results (i.e., Z-test, power, effect size g) were reported in §A.2. A level of significance of 5% was assumed for all statistical tests.

The Kolmogorov-Smirnov (K-S) test revealed that d_a data were normally distributed (field data: $D_{n,max}$ = .250, $D_{n,crit}$ = .276 for 23 values; simulator data: $D_{n,max}$ = .150, $D_{n,crit}$ = .264 for 26 values; level of significance = 5%).

Figure 4.10 shows that median values of d_a in the simulated scenario were always higher than those in the field. These differences are always combined with huge values of Hedges's effect size (> 1), less for the cases of approaching C2 and C5, where large effect sizes occur (≈ .80).

The tendency to anticipate the steering action when negotiating the transition was always verified in the simulated environment. In the field only a few drivers tended to start the steering after the TS point: this was the case for curve C2 for entering maneuvers (Case A of Figure 4.9), and C2, C4, and C5 for exiting maneuver (Case B). The observations of Willemsen and Gooch (2002) supported these results. They sustained that perceived egocentric distances in the virtual environment are consistently underestimated when compared to the assessment of the same in the real world.

This finding may be attributed to two factors: the less detailed nature of the virtual environment with respect to the real one, and the limited quality of the visual hardware employed. These two aspects curb the sense of depth perceived by a driver looking at the simulator screens. The fact that drivers involved in experiments at the driving simulator underestimated distances, implies an accentuation of the drivers' anticipatory behavior with respect to the same event in real driving (Kemeny and Panerai, 2003; Loomis and Knapp, 2003).

---

[4] The notches of box-plots extend to +/−1.58·IQR/$\sqrt{n}$, where IQR is the interquartile range (difference between the 3rd and 1st quartiles), and n the sample size (R Core Team, 2016).

Case A (of Figure 4.9)

Case B (of Figure 4.9)

Case C (of Figure 4.9)
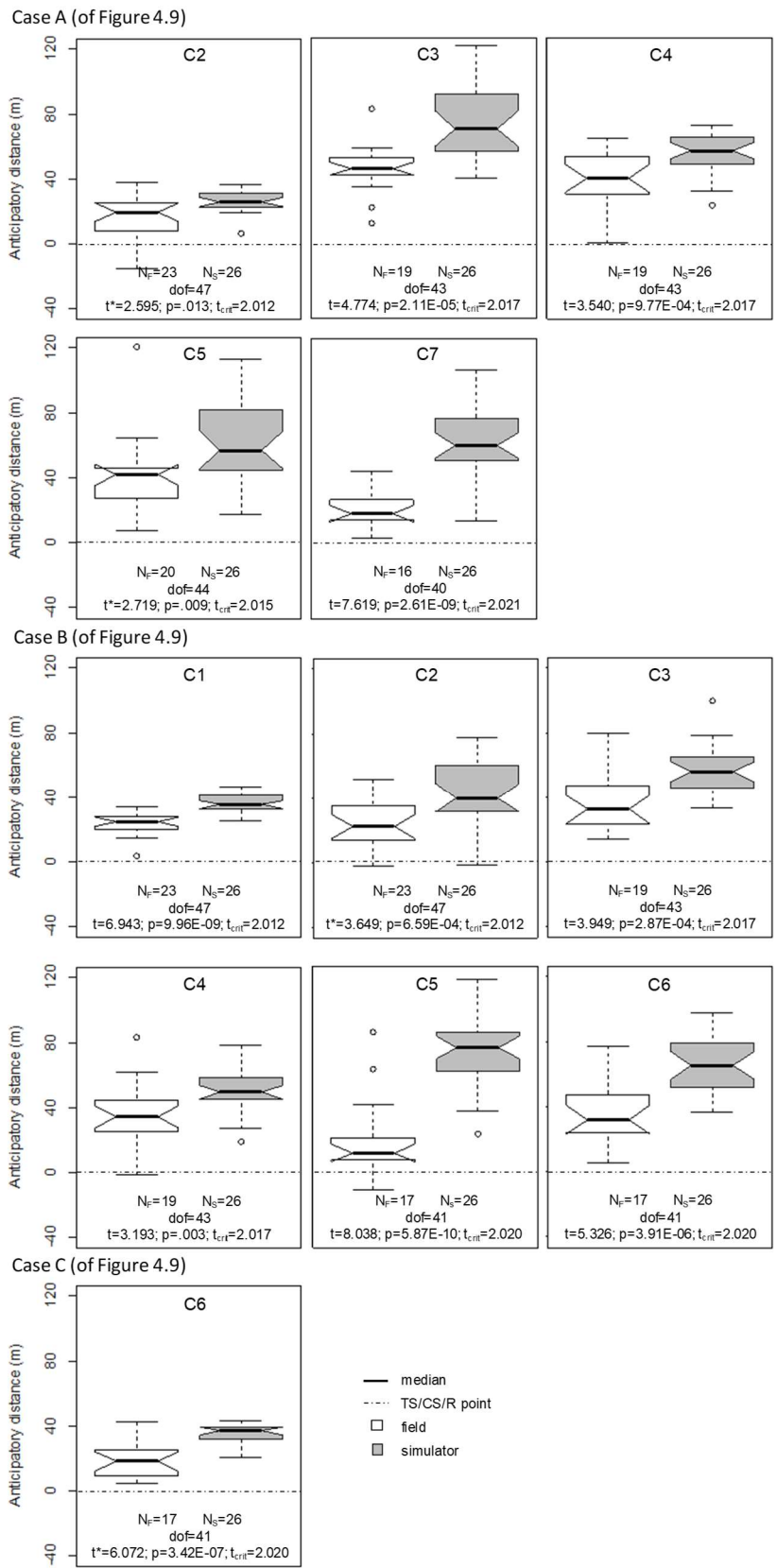
Figure 4.10. Box-plots for comparison of curvature anticipatory distance between field and simulated driving
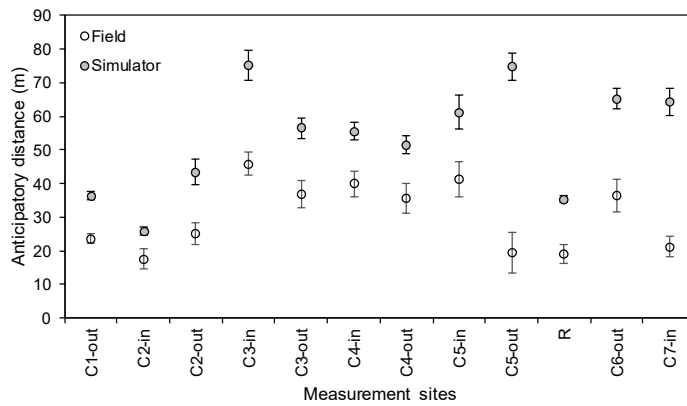
Figure 4.11. Overview of the comparison between average anticipatory distances collected in the field and at the simulator (vertical bars represent the standard error). "In" means curve approach, "out" means curve exiting

Statistical tests revealed that the H_0 was always rejected for both entering and exiting maneuvers ($t_{C,i} > t_{crit}$; $Z_{C,i} > Z_{crit}$). This result led to the relative validity of the driving simulator for these specific conditions. A detailed examination revealed that observational data values collected on the simulator are consistently higher than those from real driving scenarios.

In Figure 4.12, d_a values were grouped as a function of the two spiral lengths, ($L_S = 46.55$ m in C2, C3, C4; $L_S = 62.23$ m in C5, C6), which differ as a result of the different scale factor (*A*) adopted by the road designer. Also in this case, the comparison between data collected in field and at the simulator led to reject the null hypothesis (equality of anticipatory distance). In the four evaluations, large effect size *g* was observed (> .80), representing significant differences between real and simulated data.
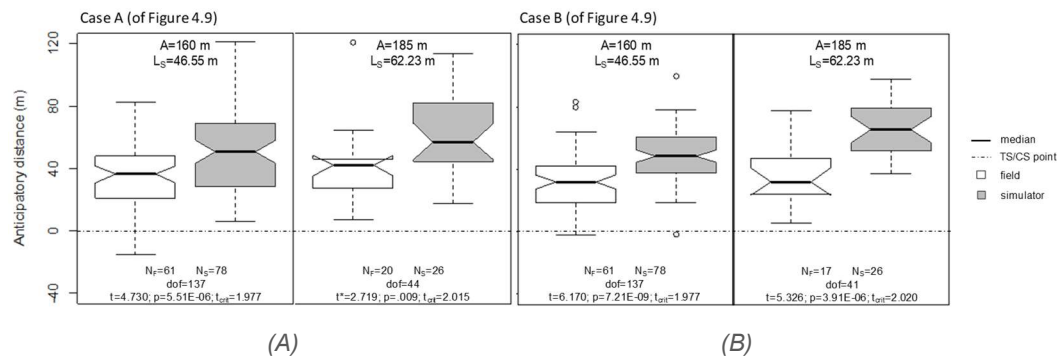
Figure 4.12. Values of anticipatory distances for entering (A) and exiting (B) curves for different lengths of spirals (A = scale factor of spirals, L_S = length of spiral)

It is worth noting that as the spiral length increased, the d_a in the simulated scenario increased too, while no significant variation in d_a was evident for data collected in real driving conditions (Case A: $t(79) = 1.522$, $p = .13$; Case B: $t(76) = .905$, $p = .37$). Results can be explained, once again, by the fact that the distances of TS (Case A) and CS (Case B) from the driver point of view were altered due to a limited perception of depth in the simulated environment.

Average curvature along circular arc

Results for mean curvature (c) are reported in Figure 4.13 and Figure 4.14 (the results for C7 are omitted since drivers were mostly affected by the presence of a roundabout at the end of the curve). Rightward curves are at the top of the figure, and leftward curves at the bottom. The K-S test revealed all curvature data to be normally distributed with a level of significance of 5% (field data: $D_{n,max}$ = .220, $D_{n,crit}$ = .276 for 23 values; simulator data: $D_{n,max}$ = .150, $D_{n,crit}$ = .264 for 26 values).

The absolute average c values observed in the field were lower than the correspondent at the simulator, less for the case of C5 ($c_F–c_S$ = –2·10^{-5} m^{-1}). However, these differences led to accept H_0 for C2 ($t^*(47)$ = 1.006, p = .32, g = .29, 1–β = .75), and C6 ($t^*(41)$ = 1.559, p = .13, g = .49, 1–β = .98), while it was rejected in the others (C1: $t(47)$ = 4.343, $p < 2·10^{-4}$, g = 1.24; C3: $t(43)$ = 2.085, p = .04, g = .63; C4: $t^*(43)$ = 2.266, p = .03, g = .68; and C5: $t^*(41)$ = 2.290, p = .03, g = .71). Medium effect size values (< .50) imply that at least 80% of the two groups (along C2 and C5) are overlapped. When the H_0 was accepted, the strength of the Z-test suggests the acceptability of results (assuming a Δ equal to 15% of the c_F).

The observations from real driving scenarios were closer to the reference values than those from the simulated driving scenarios, but the dispersion of the former is always greater than the latter (notice the extension of whiskers of box-plots, and see §A.2). As expected, the longest curve C5 (L_C equal to 504 m) reduced the dispersion of c values around the medians, in both environments. Thus, a relative validity was achieved for this trajectory characteristic: differences between field and simulator curvatures are in the same direction (positive considering absolute values), and of the same magnitude (1·10^{-4} m^{-1}), with the exception of the sharpest (C1) and longest (C5) curves.
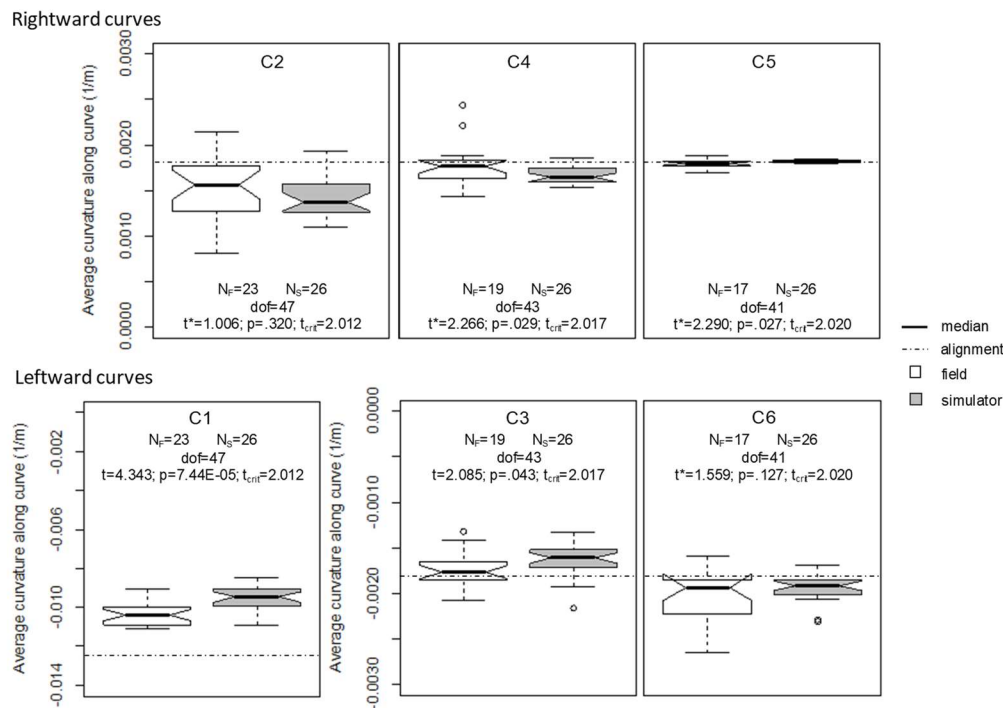
Figure 4.13. Box-plots for comparison of average curvature values (c) along the curve in real and simulated driving observations
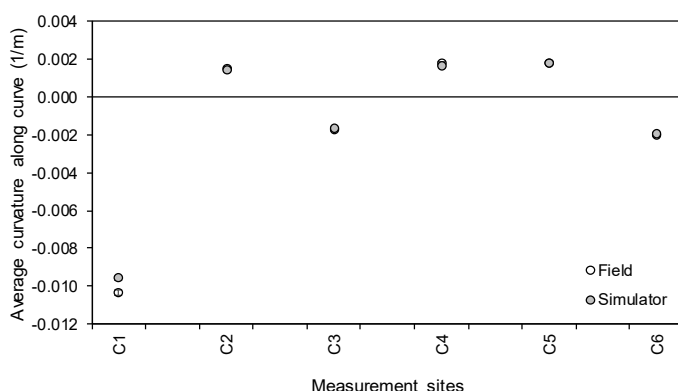
Figure 4.14. Overview of the comparison between average curvature along bends collected in the field and at the simulator (vertical bars represent the standard error)

Furthermore, the absolute median values of *c* were generally lower than the designed curvature, apart from curve C6, which is located after the R (reverse) point. Observations in both environments suggest that most drivers adopted trajectories with a lower radius to compensate for errors made when traversing the reverse curve between C5 and C6, as well evidenced by the anticipation of the R point documented in Figure 4.10 (case C).

Average curvature change rate (c_r) along spirals

Figure 4.15 and Figure 4.16 show the results for c_r when approaching and exiting the curves. Mean values and dispersions of the sample were compared with the curvature change rate of spirals (according to eq. 7, it is the ratio between *c* and L_S). Again, the K-S test revealed that collected data were normally distributed (field data: $D_{n,max}$ = .240, $D_{n,crit}$ = .276 for 23 values; simulator data: $D_{n,max}$ = .230, $D_{n,crit}$ = .264 for 26 values; level of significance = 5%).

For Case A (curve entry), the comparison between collected data revealed that median values in field were higher than the corresponding at the simulator, less for C2. In this case ($t(47)$ = .078, p = .94, g = .02, 1–β = .78) and for C5 ($t(44)$ = 1.263, p = .21, g = .38, 1–β = .82; assuming a Δ equal to 30% the $c_{r,F}$) the difference between mean values is not statistically significant. On the other hand, the H_0 was always accepted for the samples of Case B (curve exiting), which showed low effect size and reduced probability to run into the Type II error (C1: $t(47)$ = .454, p = .65, g = .13, 1–β = 1.00; C2: $t(47)$ = 1.314, p = .20, g = .38, 1-β = .57; C3: $t(43)$ = .625, p = .54, g = .19, 1–β = .72; C4: $t(43)$ = 1.355, p = .18, g = .41, 1-β = .72; and C6: $t(41)$ = 1.150, p = .26, g = .36, 1–β = .66). In correspondence of the reverse point (between C5 and C6) the difference between field and simulator curvature change rate is statistically significant ($t^*(41)$ = 7.005, $p < 2 \cdot 10^{-8}$, g = 2.18).

These outcomes determine a relative validation of the driving simulator for curvature change rate when approaching curves (average $\Delta c_r = 8 \cdot 10^{-6}$ m^{-2}), with field data greater than laboratory ones. The absolute validity is determined for driving maneuvers when exiting from curves.
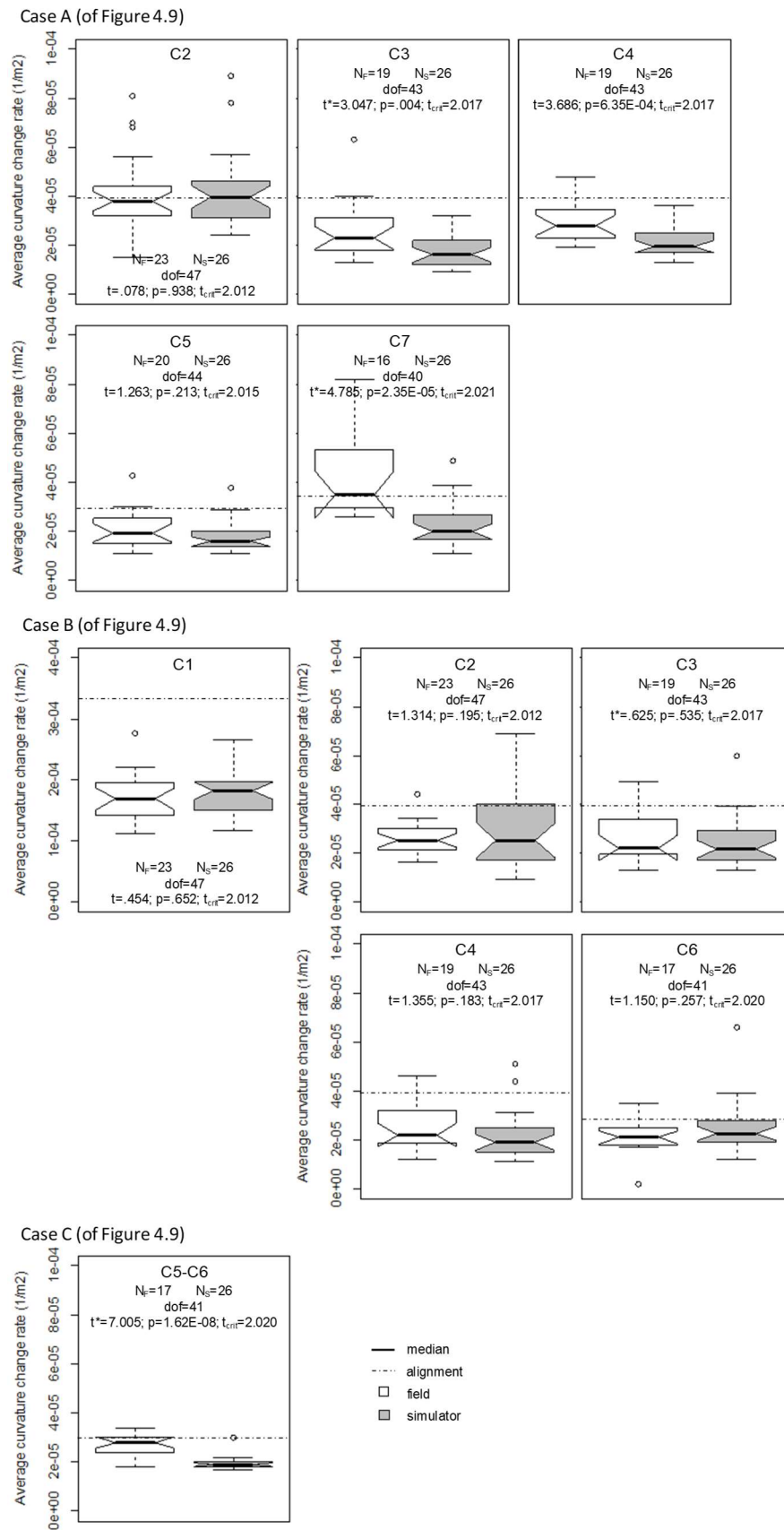
Figure 4.15. Box-plots for comparison of average curvature change rate between straights and curves in real and simulated driving

For most drivers c_r was lower than the designed value in both environments thus confirming their need to compensate for errors made when anticipating the curvature change at TS and CS points. This result was also confirmed for C1, C2, C3, C4, and C6 curves (case B), and in the reverse point (Case C). The differences in this last case may also be imputed to the difficulty of drivers in perceiving the egocentric distance with the R point in the simulated environment. Furthermore, the steering action in the simulated condition was heavily anticipated, as shown in Figure 4.10 (case B), resulting in a lower c_r value.

It is worth noting that data for the entry section of C2 curve were distributed across the reference value of the designed alignment. These observations were different from the others, since C2 was located immediately after the sharpest curve in the track (C1), where speeds were lower than in the rest of the investigated road segment (refer to Figure 4.2). Thus, higher speeds adopted in the virtual environment resulted in a smoother trajectory characterized by longer anticipatory distances and reduced curvature change rates, with respect to observations in the field.
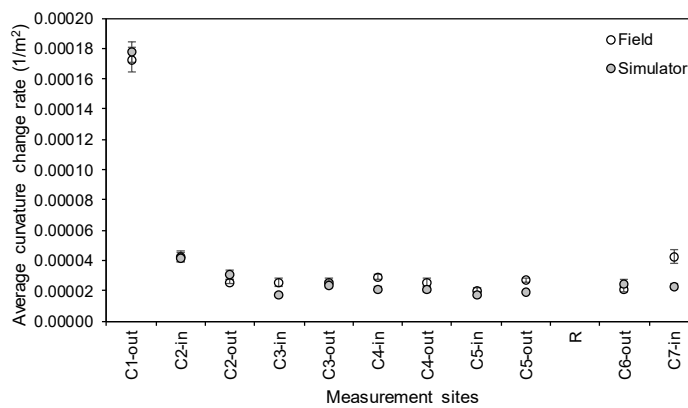
Figure 4.16. Overview of the comparison between average curvature change rate collected in the field and at the simulator (vertical bars represent the standard error). "In" means curve approach, "out" means curve exiting

5. Conclusions

The first part of this investigation dealt with the validation of the fixed-base driving simulator in the Road Safety and Driving Simulation Laboratory at the *Politecnico di Torino*.

Issues associated with simulator sickness were accurately evaluated. According to literature, data collected from participants who are disturbed by the simulation conditions are not reliable and should be carefully removed from the dataset. Therefore, in this study specific countermeasures were adopted to prevent its occurrence:

- the setting of a dark room to reduce any background side-effects;
- the design of the virtual environment, by limiting the optic flow and vection;
- the preliminary training of participants to improve their confidence and motivation; and
- the planning of an adequate experimental protocol that alternates driving sessions with rest periods.

The validity study involved the comparison of driving speed, trajectory, and steering data collected in real and virtual environments, capturing the differences as a function of the road geometry. The selected test track was 16 km long and located in the suburb of Turin (Italy). To reach a more robust conclusion, the behavior of a selected group of volunteers (thirty-three) was monitored, and associated with cognitive performance, and response feedback to a questionnaire on simulator fidelity and induced sickness.

Good results were achieved for the realistic nature of the simulator components, such as the visual and sound systems, the gas pedal and the gearbox reactions. Test drivers found the virtual scenario to be faithful to the real one. However, they affirmed that the interaction with the brake pedal was an issue. According to literature, this is typical for all fixed-base driving simulators where drivers cannot modulate the action on the pedal as a function of the perceived deceleration. However, this setting did not significantly affect free-flow speeds and adopted trajectories in deceleration sections.

Driver behavior data in terms of operating speeds and spatial data points of the traveled paths were gathered from an instrumented vehicle and the simulator, with a sampling frequency of 10 Hz. In particular, headings, curvature and curvature change rate were computed from collected spatial points. A filtering algorithm as per the semivariogram method was used to remove noise captured with the GPS-IMU positioning system used to track the vehicle in the field.

Any data relating to participants who manifested simulator sickness or assumed inappropriate behavior (too aggressive), were discarded from the database. The rest of the data was configured to associate collected measurements with the curvilinear abscissa (station) of each road Segment.

Speed data were compared by means of the 15th, 50th, and 85th percentiles among the whole sample. Square plots evidenced that the 15th and 50th percentile curves tend to be less dispersed than 85th ones, indicating that the speed differentials (ΔS) increase for greater speed values. The significance of speed differences between field and simulated drives was also assessed by means of statistical tests. They revealed that comparable behavior occurred along short tangents and tight curves ($R \leq 300$ m), even if a small part of measurement sites was affected by a low tests' power; the equivalence of speeds is less frequent but more significant on long tangents and shallow curves.

The results for operating speeds are consistent with previous works (Llopis-Castelló et al., 2016; Bella, 2008; Bittner et al., 2002) regarding the effects of more demanding road elements (i.e., sharp curves) that induce drivers to limit speeds in both real and virtual scenarios. Along less demanding sections, the speed differential between real and simulated contexts increases as the speed increases, thus leading to a relative validity rather than an absolute one. This difference in speed behavior is attributable to a difference between the levels of risk perception in the two contexts, thus leading to conclusions similar to those of Bella (2008).

The methodology proposed for the analysis of trajectories represents an alternative to current practice which is limited to the transversal position in the lane and which has generated controversial results in scientific literature.

In this study, most drivers anticipated the point of change in curvature despite the presence of spiral curves. In both driving environments, the anticipatory distance (d_a) also interests the approaching tangent even if the segment was designed according to modern Italian standards which impose the use of clothoids (MIT, 2001). With a spiral between a tangent and a circular arc, drivers do not need to anticipate the steering action for curve negotiation. The magnitude of the anticipatory distance was higher in the simulated scenario than in the real one. This finding is attributable to the variable nature of driver perception of the egocentric distance with respect to the point of curvature change (i.e., tangent to spiral - TS, curve to spiral - CS, reverse point - R). For these reasons, the driving simulator achieved a relative validity.

The absolute curvature (c) values of investigated bends were greater in the field than in the laboratory. The statistical tests revealed that a relative validity was achieved for four of the six curves in the segment, except for the cases of the sharpest (C1) and the longest (C5) bends.

Greater anticipatory distance led drivers to compensate for any errors made when approaching the TS/CS/R points by reducing the angular speed of the steering wheel (i.e., the c_r values of vehicle trajectory) along transition and reverse spirals. This behavior was observed in both environments. The observed average curvature change rates (c_r) along spirals were lower than those estimated from the as-built alignment information. Comparing the c_r values in both contexts, an absolute validity was assessed along exiting spiral (from curve to tangent); in the other two cases (entering transition and reverse point), the c_r adopted at the simulator is lower than the one used in the field (relative validity).

The behavioral validity of the fixed-base driving simulator at the *Politecnico di Torino* was assessed under specific roadway (two-lane highway) and environmental (rural) conditions. Behavioral analyses in different contexts (e.g., urban roads or freeways) require a new validation study of the variables of interest.

Future research will be based on the experience gained in the field. The same road category was considered in the successive studies documented in Part B, as well as the tips that the validation study provided in terms of experimental design and protocol.

In conclusion, the driving simulator reaches an overall relative validity for the investigated variables. This characteristic of the outcomes has to be accounted for in the interpretation of simulation outputs for field applications.

References

AASHTO (2011). *A Policy on Geometric Design of Highways and Streets, 6th edition*. American Association of State Highway, and Transportation Officials, Washington, D.C. ISBN: 978-1-56051-508-1

Allen, R. W., and Reimer, B. (2006). New approaches to simulation and the older operator. *Advances in Transportation Studies: An International Journal*, SI, 3-8.

Andersen, G. J. (2011). Sensory and perceptual factors in the design of driving simulation displays. In *Handbook of driving simulation for engineering, medicine, and psychology* (pp. 8:1-12). Boca Raton, FL: CRC Press.

Bassani, M., Lingua, A., Piras, M., De Agostino, M., Marinelli, G., and Petrini, G. (2012, January). Alignment data collection of highways using mobile mapping and image analysis techniques. In *Proceedings of 91st Annual Meeting of the Transportation Research Board*. Washington, D.C.

Bella, F. (2005a). Validation of a driving simulator for work zone design. *Transportation Research Record: Journal of the Transportation Research Board, No. 1937*, 136-144.

Bella, F. (2008). Driving simulator for speed research on two-lane rural roads. *Accident Analysis and Prevention, 40*(3), 1078-1087.

Bertin, R. J. V., Guillot, A., Collet, C., Vienne, F., Espié, S., and Graf, W. (2004, October). Objective measurement of simulator sickness and the role of visual-vestibular conflict situations: a study with vestibular-loss (a-reflexive) subjects (poster). In *Proceedings of the Society for Neurosciences 34th Annual Meeting*. San Diego (CA), USA.

Bittner, A., Simsek Jr, O., Levison, W., and Campbell, J. (2002). On-road versus simulator data in driver model development driver performance model experience. *Transportation Research Record, No. 1803*, 38-44.

Blaauw, G. J. (1982). Driving experience and task demands in simulator and instrumented car: a validation study. *Human Factors, 24*(4), 473-486.

Blana, E. (1996). Driving simulator validation studies: A literature review. *Working Paper 480*, Institute of Transport Studies, University of Leeds, Leeds, UK.

Blana, E., and Golias, J. (2002). Differences between vehicle lateral displacement on the road and in a fixed-base simulator. *Human Factors*, *44*(2), 303-313.

Boer, E. R. (1996, September). Tangent point oriented curve negotiation. In *Proceedings of the Intelligent Vehicles Symposium* (pp. 7-12). IEEE.

Bonneson, J. A. (2000). Kinematic approach to horizontal curve transition design. *Transportation Research Record, No. 1737*, 1-8.

Bos, J. E. (2018, September). Motion sickness, simulator sickness, and automated vehicles. In *DSC 2018 EUROPE VR Driving Simulation Conference & Exhibition*. Antibes, France.

Branzi, V., Domenichini, L., and La Torre, F. (2017). Drivers' speed behaviour in real and simulated urban roads - A validation study. *Transportation Research Part F: Traffic Psychology and Behaviour*, *49*, 1-17.

Carle, A. (2016). *Indagine sperimentale sulla valutazione degli effetti di disagio percepiti nella guida simulata*. Master's Thesis. Politecnico di Torino, Torino, Italy.

Casali, J. G., and Wierwille, W. W. (1980). The effects of various design alternatives on moving-base driving simulator discomfort. *Human Factors*, *22*(6), 741-756.

Casali, J. G. (1986). *Vehicular simulation-induced sickness, Volume I: An overview* (No. IEOR-8501). Virginia Polytechnic Institute and State University, VA.

Cina, A. (2014). *Dal GPS al GNSS (Global Navigation Satellite System). Per la Geomatica* (in Italian). Torino, Italy: Celid.

Cohen, J. (1988). *Statistical power analysis for the behavioral sciences*, *2nd edition*. Hillsdale, NJ: Erlbaum.

Colombet F., Paillot D., Mérienne F. and Kemeny A. (2010, September). Impact of geometric field of view on speed perception. In *Proceedings of the Driving Simulation Conference* (pp. 69-79). Chalon-sur-Saône, France.

Delay, F., and de Marsily, G. (1994). The integral of the semivariogram: A powerful method for adjusting the semivariogram in geostatistics. *Mathematical Geology*, *26*(3), 301-321.

Donges, E. (1978). A two-level model of driver steering behavior. *Human Factors*, *20*(6), 691-707.

Engström, J., Johansson, E., and Östlund, J. (2005). Effects of visual and cognitive load in real and simulated motorway driving. *Transportation Research Part F: Traffic Psychology and Behaviour*, *8*(2), 97-120.

Eryilmaz, U., Tokmak, H. S., Cagiltay, K., Isler, V., and Eryilmaz, N. O. (2014). A novel classification method for driving simulators based on existing flight simulator classification standards. *Transportation Research Part C: Emerging Technologies*, *42*, 132-146.

Espié, S. (1999). Vehicle-driven simulator versus traffic-driven simulator: the INRETS approach. In *Proceedings of the Driving Simulation Conference* (pp. 367-376). Paris, France.

Gikas, V., and Stratakos, J. (2012). A novel geodetic engineering method for accurate and automated road/railway centerline geometry extraction based on the bearing diagram and fractal behavior. *IEEE Transactions on Intelligent Transportation Systems*, *13*(1), 115-126.

Godley, S. T., Triggs, T. J., and Fildes, B. N. (2002). Driving simulator validation for speed research. *Accident Analysis and Prevention*, *34*(5), 589-600.

Goldstein, E. B. (2008). *Blackwell handbook of sensation and perception*. Malden, MA: John Wiley & Sons.

Hallvig, D., Anund, A., Fors, C., Kecklund, G., Karlsson, J. G., Wahde, M., and Åkerstedt, T. (2013). Sleepy driving on the real road and in the simulator—A comparison. *Accident Analysis and Prevention*, *50*, 44-50.

Hedges, L. V. (1981). Distribution theory for Glass' estimator of effect size and related estimators. *Journal of Educational Statistics*, *6*(2), 107-128.

Hettinger, L. J., and Riccio, G. E. (1992). Visually-induced motion sickness in virtual environments. *Presence: Teleoperators and Virtual Environments*, *1*(3), 306-310.

Jamson, H. (2000, September). Driving simulation validity: issues of field of view and resolution. In *Proceedings of the Driving Simulation Conference* (pp. 57-64). Paris, France.

Johnson, D. M. (2005). *Introduction to and review of simulator sickness research* (No. ARI-RR-1832). U.S. Army Research Institute for the Behavioral and Social Sciences. Arlington, VA.

Kalteniece, A., and Krumina, G. (2014). 3D Cinema and human stereovision. *Advances in Ophthalmology & Visual System*, *1*(4): 00022.

Kaptein, N., Theeuwes, J., and Van Der Horst, R. (1996). Driving simulator validity: Some considerations. *Transportation Research Record, No. 1550*, 30-36.

Kemeny, A., and Panerai, F. (2003). Evaluating perception in driving simulation experiments. *TRENDS in Cognitive Sciences*, *7*(1), 31-37.

Kemeny A. (2009, February). Driving simulation for virtual testing and perception studies. In *Proceedings of the Driving Simulation Conference* (pp. 15-23). Monte Carlo, Monaco.

Kennedy, R. S., Berbaum, K. S., Lilienthal, M. G., Dunlap, W. P., Mulligan, B. E., and Funaro, J. F. (1987). *Guidelines for alleviation of simulator sickness symptomatology* (No. NAVTRASYSCEN-TR-87-007). Naval Training Systems Center. Orlando, FL.

Kennedy, R. S., Hettinger, L., and Lilienthal, M. (1988). Simulator sickness. In *Motion and space sickness* (pp. 317-341). Boca Raton, FL: CRC Press.

Kennedy, R. S., Lane, N. E., Berbaum, K. S., and Lilienthal, M. G. (1993). Simulator sickness questionnaire: An enhanced method for quantifying simulator sickness. *The International Journal of Aviation Psychology*, *3*(3), 203-220.

Kennedy, R. S., Stanney, K. M., and Dunlap, W. P. (2000). Duration and exposure to virtual environments: sickness curves during and across sessions. *Presence: Teleoperators and Virtual Environments*, *9*(5), 463-472.

Klee, H., Bauer, C., Radwan, E., and Al-Deek, H. (1999). Preliminary validation of driving simulator based on forward speed. *Transportation Research Record, No. 1689*, 33-39.

Kolasinski, E. M. (1995). *Simulator sickness in virtual environments*. (No. ARI-TR-1027). U.S. Army Research Institute for the Behavioral and Social Sciences. Alexandria, VA.

Konstantopoulos, P., Crundall, D., and Chapman, P. (2010). Driver's visual attention as a function of driving experience and visibility. Using a driving simulator to explore visual search in day, night and rain driving. *Accident Analysis and Prevention, 42*, 827-834.

Land, M. F., and Lee, D. N. (1994). Where we look when steer, *Nature, 369*(6483), 742-744.

Lee, H. C., Cameron, D., and Lee, A. H. (2003). Assessing the driving performance of older adult drivers: on-road versus simulated driving. *Accident Analysis and Prevention, 35*, 797-803.

Llopis-Castelló, D., Camacho-Torregrosa, F. J., Marín-Morales, J., Pérez-Zuriaga, A. M., García, A., and Dols, J. F. (2016). Validation of a low-cost driving simulator based on continuous speed profiles. *Transportation Research Record: Journal of the Transportation Research Board, No. 2602*, 104-114.

Loomis, J. M., and Knapp, J. M. (2003). Visual perception of egocentric distance in real and virtual environments. In *Virtual and adaptive environments* (pp. 21-46). Mahwah, NJ: Erlbaum.

Losa, M., Frendo, F., Cofrancesco, A., and Bartolozzi, R. (2013). A procedure for validating fixed-base driving simulators. *Transport, 28*(4), 420-430.

McAvoy, D., Schattler, K., and Datta, T. (2007). Driving simulator validation for nighttime construction work zone devices. *Transportation Research Record: Journal of the Transportation Research Board, No. 2015*, 55-63.

Misaghi, P. and Hassan, Y. (2005). Modeling operating speed and speed differential on two-lane rural roads. *Journal of Transportation Engineering, 131*(6), 408-418.

MIT (2001). *Norme funzionali e geometriche per la costruzione delle strade* (in Italian). Ministero delle Infrastrutture e dei Trasporti, D.M. no. 6792 of November 5th.

Montella, A., Galante, F., Imbriani, L. L., Mauriello, F., and Pernetti, M. (2014). Simulator evaluation of drivers' behaviour on horizontal curves of two-lane rural highways. *Advances in Transportation Studies: An International Journal, 34*, 91-104.

Mueller, A. S., and Trick, L. M. (2012). Driving in fog: The effects of driving experience and visibility on speed compensation and hazard avoidance. *Accident Analysis and Prevention, 48*, 472-479.

Mullen, T. J., Berger, R. D., Oman, C. M., and Cohen, R. J. (1998). Human heart rate variability relation is unchanged during motion sickness. *Journal of Vestibular Research, 8*(1), 95-105.

Mullen, N. W., Weaver, B., Riendeau, J. A., Morrison, L. E., and Bédard, M. (2010). Driving performance and susceptibility to simulator sickness: Are they related? *American Journal of Occupational Therapy, 64*(2), 288-295.

Mullen, N. W., Charlton, J., Devlin, A., and Bédard, M. (2011) Simulator validity: behaviors observed on the simulator and on the road. In *Handbook of driving simulation for engineering, medicine, and psychology* (pp. 13:1-18). Boca Raton, FL: CRC Press.

Murato, S., and Saito, T. (1999). The variogram method for a fractal model of a rock joint surface. *Geotechnical and Geological Engineering*, *17*(3-4), 197-210.

Panerai, F., Droulez, J., Kelada, J.-M., Kemeny, A., Balligand, E., and Favre, B. (2001, September). Speed and safety distance control in truck driving: comparison of simulation and a real-world environment. In *Proceedings of the Driving Simulation Conference* (pp. 91-108). Sophia Antipolis (Nice), France.

Philip, P., Sagaspe, P., Taillard, J., Valtat, C., Moore, N., Åkerstedt, T., Charles, A., and Bioulac, B. (2005). Fatigue, sleepiness, and performance in simulated versus real driving conditions. *Sleep*, *28*(12), 1511-1516.

Philip, P., Taillard, J., Klein, E., Sagaspe, P., Charles, A., Davies, W. L., Guilleminault, C., and Bioulac, B. (2003). Effect of fatigue on performance measured by a driving simulator in automobile drivers. *Journal of Psychosomatic Research*, *55*(3), 197-200.

Pretto P. and Chatziastros A. (2006, October). Changes in optic flow and scene contrast affect the driving speed. In *Proceedings of the Driving Simulation Conference* (pp. 263-272). Paris, France.

Pretto, P., Vidal, M., and Chatziastros, A. (2008, February). Why fog increases the perceived speed. In *Proceedings of the Driving Simulation Conference* (pp. 223-235), Monte Carlo, Monaco.

R Core Team (2016). *R: A language and environment for statistical computing*. R Foundation for Statistical Computing, Vienna, Austria. http://www.R-project.org/

Risto, M., and Martens, M. H. (2014). Driver headway choice: A comparison between driving simulator and real-road driving. *Transportation Research Part F: Traffic Psychology and Behaviour*, *25*, 1-9.

Salaani, M. K., Grygier, P. A., and Heydinger, G. J. (2001). *Model Validation of the 1998 Chevrolet Malibu for the National Advanced Driving Simulator* (No. 2001-01-0141). SAE Technical Paper.

Shinar, D., and Ronen, A. (2007). Validation of speed perception and production in a single screen simulator. *Advances in Transportation Studies: An International Journal*, *SI 1*, 51-56.

Stoffregen, T., and Riccio, G. (1991). An ecological critique of the sensory conflict theory of motion sickness. *Ecological Psychology*, *3*(3), 159-194.

Stoner, H. A., Fisher, D. L., and Mollenhauer, Jr. M. (2011). Simulator and scenario factors influencing simulator sickness. In *Handbook of driving simulation for engineering, medicine, and psychology* (pp. 14:1-24). Boca Raton, FL: CRC Press.

Thompson, W. B., Willemsen, P., Gooch, A. A., Creem-Regehr, S. H., Loomis, J. M., and Beall, A. C. (2004). Does the quality of the computer graphics matter when judging distances in visually immersive environments? *Presence: Teleoperators and Virtual Environments*, *13*(5), 560-571.

Törnros, J. (1998). Driving behaviour in a real and a simulated road tunnel - A validation study. *Accident Analysis and Prevention*, *30*(4), 497-503.

Treisman, M. (1977). Motion sickness: An evolutionary hypothesis. *Science, 197*, 493-495.

Underwood, G., Crundall, D., and Chapman, P. (2011). Driving simulator validation with hazard perception. *Transportation Research Part F: Traffic Psychology and Behaviour, 14*, 435-446.

Wade, M. G., and Hammond, C. (1998). *Simulation validation: Evaluating driver performance in simulation and the real world. Final report* (No. MN/RC-1998-28). Minnesota Department of Transportation. Minneapolis, MN.

Wann, J. P., and Land, M. F. (2000). Steering with or without the flow: Is the retrieval of heading necessary?. *Trends in Cognitive Sciences*, *4*(8), 319-324.

Willemsen, P., and Gooch, A. A. (2002). Perceived egocentric distances in real, image-based, and traditional virtual environments. In *Proceedings IEEE Virtual Reality 2002* (pp. 275-276).

Wood, J. M., Lacherez, P., and Tyrrell, R. A. (2014). Seeing pedestrians at night: effect of driver age and visual abilities. *Ophthalmic and physiological optics*, *34*(4), 452-458.

Young, S. D., Adelstein, B. D., and Ellis, S. R. (2007). Demand characteristics in assessing motion sickness in a virtual environment: or does taking a motion sickness questionnaire make you sick? *IEEE Transactions on Visualization and Computer Graphics*, *13*(3), 422-428.

Webography

[1] Istituto Nazionale di Statistica (ISTAT), Incidenti Stradali. Anno 2016: https://www.istat.it/it/files//2017/07/Incidenti-stradali-1.pdf.

[2] Cognitivefun website for cognitive tests: cognitivefun.net

Part B:

Operational Effects of Sight Limitations along Curves

Abstract. A sufficient sight distance in front of the driver is required to perform safe operations (i.e., stopping in front of unexpected obstacles, overtaking, change lane), and to correctly perceive the road geometry. These operations are more critical along curves both for sight conditions and for collision risk. In this work, two driving simulation experiments were designed and executed to investigate the behavioral effect due to the presence of sight limitations. Test tracks were designed to include a series of horizontal curves, of different radii and lengths. Continuous sight limitations were disposed on the roadside, at different distances from the carriageway, to provide a set of different available sight distances. Performance of seventy-seven drivers were observed in the two experiments, by collecting speeds, vehicle trajectories data (curvature and lateral displacement), eye movements and fixations. Results showed that the speed increased when the sight distance became longer, whereas the dispersion of trajectory decreased. Tight curves induced lower speeds and a greater variability in vehicle trajectories. The lateral sight obstruction was used by some as a guidance element. Eye-tracking data showed that tangent point model was the most preferred vision mechanism along curves; as the radius of curvature increased, fixations moved towards more distant points of the future path. These steering strategies induced drivers to adopt more correct trajectories for similar speed values.

6. Background

Driving involves a continuous interaction between driver, vehicle, road and environment. The attitude and the experience are traits that influence driver behavior, as well as the travel purpose and vehicle performance. The vehicle interacts with other vehicles in the road network, which is characterized by specific geometry and road elements (Shinar, 2017). The interaction of these factors plays a fundament role while driving, that becomes a dynamic control task where the driver elaborates decisions on the basis of the significant information sourced from the roadway and the environment, and acts appropriate decisions in order to complete his transport objective (Bella, 2013). Hence, cues provided by the road are necessary to manage driver operations, which continuously adapt to the actual driving conditions, control the perceived risk, and avoid risky situations.

6.1 Definitions

Operational effects consist of all the measurable or observable behaviors of an individual or a series of them as a response to actual conditions. More in general, they are the consequences of such behaviors in a larger context such as crashes, traffic densities and speeds, lag and gap between vehicles, etc. In operational analysis, measurements are typically carried out on operating speeds, trajectories, driving errors that may be then used to model several field conditions related to the conducts of road users. The final aim is to get knowledge on the effects of geometric design decisions on operations and safety [3].

One of the parameter that designers must considered in the geometric design of a roads is the *Available Sight Distance* (ASD). The Italian law (MIT, 2001) defines the ASD as "the length of the road stretch that the driver can see in front of her/him regardless the traffic, weather, and lighting conditions". Figure 6.1 depicts the general method used to estimate the ASD from the horizontal radius and the position of sight obstruction(s). Along horizontal curves, the ASD may be limited by the presence of road furniture (i.e., traffic barriers), vegetation, escarpments, and buildings which encroach on the carriageway. According to common road design policies (i.e., AASHTO, 2011; MIT, 2001), the driver's point of view is conventionally positioned in the center of the travelled lane, and the ASD is calculated as the distance between the driver and the most distant point visible along the future vehicle trajectory (black dot in Figure 6.1). Drivers who travel along the rightward curve following a circular curved trajectory of radius r_t with a sight obstruction placed at a constant distance D from the same trajectory, benefit from an ASD equal to:

$$ASD = 2r_t \cdot \arccos\left(1 - \frac{D}{r_t}\right)$$

(eq. 9)
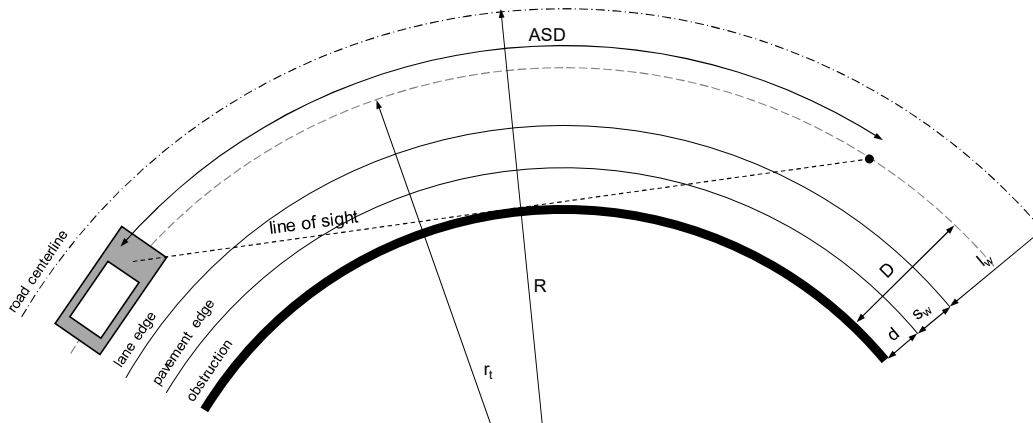
Figure 6.1. Scheme of Available Sigh Distance definition for rightward curves

where *D* is:

$$D = d + s_w + \frac{1}{2} \cdot l_w \qquad \text{(eq. 10)}$$

and *d* is the distance of the sight obstruction from the shoulder, s_w is the shoulder width, and l_w is the lane width.

The road geometric standards (AASHTO, 2011; MIT, 2001) establish also that the ASD must be greater than the *Required Sight Distance* (RSD), useful to perform safe driving maneuvers: the *Stopping Sight Distance* (SSD), the *Passing Sight Distance* (PSD), and the *Decision Sight Distance* (DSD). SSD is the distance required to stop the vehicle before reaching an obstacle along its trajectory. PSD is the distance that the driver needs to overtake a slower vehicle ahead. Lastly, DSD is the distance at which the individual can detect a hazard on the roadway, identify it or its potential risk, and adopt an appropriate speed and path (Campbell et al., 2012). Their estimation depends on the design speed, which in turn can be estimated on the basis of the geometry of road alignment. According to design policies, ASD ≥ RSD is a necessary condition for safe driving operations.

Operational effects are the result of the information that driver perceived from the road environment, the majority of which come from vision. Hence, the *eye-tracking* is certainly one reference methodology to understand what elements the driver is looking at. The eye-tracking is the technique used to capture and record eye movements, which find application in a variety of fields (e.g., cognitive linguistics, psychology, marketing, etc.).

It represents one of the two activities of the so-called *gaze-tracking*, which is the set of hardware and software technologies designed to investigate the interaction between environment and user through the acquisition and processing of observed points. The gaze-tracking is distinguished in eye-tracking, which involves the identification of gaze and fixation positions within the individual field of vision, and head-tracking that considers head movements only.

6.2 Literature Review on Curve Negotiation

Observing and understanding driving behavior as a function of the road and environment characteristics is a challenge for engineers and scientists to improve road safety, or rather reduce fatalities. These activities allow to collect subjective information and performance, that are useful to place the driver in the center of the road design process. In this way, design standards and policies will not be established arbitrarily but consistently with experiences and observations.

It is well accepted that more than 90% of road accidents are caused by human errors. The rest are due to factors associated with the vehicle, the environment, and unknown causes (Singh, 2015). For this reason, human behavior requires deeper investigation as to observe habits and performance that characterize driving activity, in order to prevent dangerous and risky situations.

The following analysis of technical literature highlights the link between driver operations and sight distance. Factors influencing driver's visibility (e.g., alignment, cross-section, environmental, lighting conditions, and sight obstruction along the roadside) are listed and discussed (Choueiri et al., 1994).

6.2.1 Effects of road geometry

Driver behavior and decision change significantly along different road elements like tangents, curves, and transitions. Such changes were monitored in several naturalistic and simulator investigations, performed in rural or urban road contexts.

Roadway curvature controls driving speed, but it may induce errors. For example, driver has to maintain a correct vehicle position along sharp curves, and this is a demanding task for drivers. Bella (2013) and Ben-Bassat and Shinar (2011) observed a reduced deviation of lateral displacement along straights and shallow curves (low curvature) with respect to tight turns. Curves of reduced radius (high curvature) require a specific control of the vehicle; but the vehicle control task becomes easier as the speed decreases (Calvi, 2015b; Ben-Bassat and Shinar, 2011; Van Winsum and Gosthelp, 1996). In contrast, less demanding geometric elements (low curvature) allow drivers to adopt greater speeds. This explains why vehicles tend to move towards the shoulder along rightward turns, and towards the road centerline along leftward turns (Bella, 2013; Felipe and Navin, 1998; Gawron and Ranney, 1990; Glennon et al., 1983).

Coutton-Jean et al. (2009) observed a direct relationship between speed profiles and radius of curvature. Along sharp curves, speeds decrease in the initial part of the element and subsequently increase from the midpoint of the curve; as the radius becomes larger, speeds grow progressively within the curve. This attitude confirms the adaptation of driver behavior to the road curvature, that operates as a constraint for driver preferred speeds.

In addition, driver behavior is influenced by the presence of transitions between tangents and circular arc. Calvi (2015b) found that curves without clothoid are traveled at a lower speed compared to curves with same radius but including clothoids. The gradual curvature change provides a benefit to drivers, who have more time to estimate and adapt to the actual road curvature. This

favorable effect is more pronounced in sharp curves, but it is not significant in shallow ones. Montella et al. (2014) observed the speed profiles and acceleration/deceleration rates along a sequence of curves of the same radius (400 m). They also noticed that speeds along circular arcs were not constant, and acceleration change rates were greater than those used to define the operating speed profiles (MIT, 2001).

Eventually, the difference between the vehicle lateral displacement and the lane centerline may be used as an indicator of the trajectory accuracy with respect to the ideal trajectory. A reduced variability of lateral position results in a more stable trajectory, which ensures to the driver more time to anticipate hazardous events (Rosey and Auberlet, 2012). Kanellaidis et al. (2000) employed a sizeable drivers sample to investigate the role of alignment characteristics on risk perception, identifying that straight roads were perceived as less dangerous than curved segments. On the contrary, Rushton and Salvucci (2001) argued that drivers do not need to extract complex geometric road features (e.g., curvature), but can safely rely on continuous visual information, as lane markings or road edges.

6.2.2 Effects of cross section layout

Transversal elements of the road include lanes, shoulders, and road margins. According to Bella (2013), drivers are more influenced by the cross-section characteristics than the roadside environment (i.e., safety barriers, vegetation, signals, etc.).

Driving in narrow lanes is a demanding task that induces users in reducing speed, because a more precise steering control is necessary to maintain the vehicle in the lane (De Waard et al., 1995). Thus, lane narrowing may be an effective countermeasure to limit speeding, but an increase in accident rate is observed if lane width tends to be similar to the vehicle size (Martens et al., 1997). Calvi (2015b) observed that, for the same radius, the wider the lanes, the higher the speed. Also the presence of lateral lane markings induces higher speeds (Zador et al., 1987; Shinar et al., 1980), and reduces accidents at the same time (Taylor et al., 1972).

The shoulder width, in the presence of sight obstructions along the roadside, also influences the available sight distance (Figure 6.1). Ben-Bassat and Shinar (2011) concluded that the shoulder width significantly affects the actual speed and the position in the lane only when combined with a guardrail. Its presence contributes to expand the conspicuity of the shoulder, producing a favorable sense of security on drivers. When safety barriers are absent, the shoulder width loses its influence. Small shoulders may create dangerous situations when the driver needs to recover the correct vehicle trajectory after an error and, consequently, it may increase the accident probability due to roadway departures (Kraus et al., 1993). On the other hand, large shoulders ensure space for trajectory recover and increase the sense of safety on drivers (Abele and Møller, 2011; Stamatiadis et al, 2009; Godley et al., 2004), but conversely lead to higher speeds along rightward turns (Bella, 2005b; Godley et al., 2004). Larger shoulders also influence drivers to

stay closer to the lateral right margin (Ben-Bassat and Shinar, 2011; Rosey et al., 2009; Van der Horst and De Ridder, 2007).

Therefore, the shoulder width and the distance to the lateral barrier/obstacle provide a different perception of safety on drivers. Greater speeds were observed along tangents and rightward curves with the guardrail, in comparison to leftward curves. In the former conditions, most drivers prefer to control the clearance to the obstacle and his position within the lane, whereas on left-hand curves the gaze and attention are directed towards the curve, reducing the influence of roadside elements (Ben-Bassat and Shinar, 2011; Shinar et al., 1977).

6.2.3 Effects of surrounding elements and sight obstructions

Elements along the roadside, such as vegetation, trees, walls, fences, buildings, may are sight obstructions and limit the driver sight distance.

Xiao et al. (2007) found that accidents on long and flat tangents are mainly caused by a tedious scenario and the absence of reference points from which drivers could perceive the adopted speed. Other studies revealed that speed is more influenced by the heterogeneity of surrounding areas than by the capability of driver to estimate the sight distance ahead (Antonson et al., 2009). Accordingly, a road scenario characterized by a regular geometry and monotonous surrounding may increase the risk of accidents with respect to a wooded environment.

Driving simulation studies demonstrated that driver behavior is potentially affected by the type and density of vegetation along the roadside. Stamatiadis et al. (2010) detected their influence on driver behavior by means of a Casewise Visual Evaluation (CAVE), but also an increasing perceived discomfort. Jamson et al. (2010) analyzed the influence of trees on the roadside as possible speed reducing treatments. Results showed that their presence does not represent an imminent hazard, so they do not affect speed. More specifically, trees do not affect speeds unless placed near the lane edge (2 m), while there is no influence on speed and lateral position if they are farer than 4.5 m from the lane edge (Van der Horst and De Ridder, 2007). Calvi (2015a) confirmed previous results, identifying a significant reduction of drivers speed when the trees are close to the roadside, associated with vehicle movements towards the road axis. Conversely, when their distance increases, drivers opt for higher speeds associated with a lower lateral movement (Fitzpatrick et al., 2016). Changes of transversal position is critical for head-on crashes, that may occur along tight leftward turns, where also drivers move close to the road centerline, and tend to invade the opposing lane.

Driving speed may be estimated from the available information in the peripheral FOV (surrounding landscape). Road users usually select their speed and trajectory in order to limit the angular speed of objects scrolling in the peripheral view below 2 rad/s. Higher values create annoying effects on drivers (Martens et al., 1997). The presence of vegetation, street furniture, and buildings may attract driver attention and increase her/his perceptive capacity; conversely, an elevate density may cause fatigue (Nelson, 1997). Ideally, the virtual scenario should be designed as to produce an angular speed greater than 2 rad/s when the longitudinal speed of drivers exceeds the posted limit (PSL). In this condition, the maximum driving speed that drivers can adopt would be lower than the PSL, above

which sickness symptoms may occur. However, procedures to comply this principle are not simply feasible.

6.2.4 Behavior analysis and risk compensation theory

Recent studies indicated that accidents are more inclined to occur along horizontal curves than on tangents, since vehicles may violate the stability limits resulting from an incorrect choice of speed and trajectory (Hummer et al., 2010; Charlton, 2007). Therefore, the correct estimation of road curvature and driver behavior when negotiating curves are crucial topics that elicit attention in road design and safety fields (Zakowska, 2010).

Zhao et al. (2013) stated that the driver performance is strongly influenced by the visual information provided by the road context. According to the cognitive theory (Anderson et al., 1997), driving operations consist of three phases: the information perception, the decision, and the execution of controls. Thus, higher information accuracy makes simpler and correct decisions and operations.

According to Charlton (2007), drivers' errors on curve negotiation may result from three main behavioral issues: the incorrect perception of speed and curvature, the misjudgment of the transversal position in the lane, and the inability to moderate the attention level on more/less demanding elements. Accordingly, a correct perception of the roadway is possible if the visible space along the future path increases, i.e. when the available sight distance is adequate to receive visual information and to react properly. For this reason, standards require sufficient sight distances to perform safe maneuvers (i.e., stopping, overtaking, change lane).

Some researchers (Calvi, 2015b; Zakowska, 2010; Benedetto et al., 2009) investigated on drivers' perception errors with respect to the curve characteristics through driving simulation. Results specifically evidenced that the visible road path in front of the driver is fundamental to perceive and estimate horizontal curvature: a greater sight distance allows the driver to plan the operations in a longer time, and to adopt higher speeds (Moreno et al., 2013). This is an example of compensatory behavior: the free road path induces drivers to increase speed, while the perceived risk augments in segments with reduced visibility, leading to lower speeds (Brenac, 1990). This effect was observed and measured with sight distances lower than 500 m (Yagar and Van Aerde, 1983).

This knowledge is crucial to look for "self-explaining roads" (Theeuwes and Godthelp, 1995): the ambition of designers is that road geometrics and surrounding elements communicate appropriate information to the users, limiting conflicts and the possibility of errors. In this ideal framework, the warning traffic signs loses effectiveness. Hence, driver choices, in terms of speed and vehicle control, are the results of the subjective evaluation of the perceived risk while driving (Recarte and Nunes, 2002; De Waard et al., 1995).

FOCUS ON

The **Risk Compensation Theory** is a consolidated theoretical context for the analysis of driving behavior (Fuller and Santos, 2002). The driver is disposed to react to road environment changes and events occurrences according to her/his motivations and attitudes. The driver constantly and instantly controls the safety margin, and she/he changes her/his behavior if her/his perceived risk exceeds the subjective threshold. Behavior changes refer to driver operations on the driving controls, as speed reduction and/or adjustment of vehicle position in the lane, so as to lead the safety margin within the accepted limit (Bella, 2013; Summala, 1996). Hence, risk compensation is defined as a behavioral adaptation to a perceived risk situation (OECD, 1990). A wide literature has discussed such topic, leading to new theories of behavioral adaptation (Wilde, 1998). Recently, researchers are more focused on the effects of assisted/automated driving (e.g., Rudin-Brown and Parker, 2004; Brookhuis et al, 2001), that also influences and changes risk thresholds. Changing driver attitudes is considered a necessary condition for the improvement of road safety. However, there is not a direct relationship between road accidents and driver attitudes, but a complex of relationships between demographic (age and gender), behavioral, and other variables (emotional state, travel purpose, etc.) that affect the acceptable risk limits (Assum, 1997). According to Shinar (2017), engineering solutions to improve safety remain relatively ineffective unless they are "user-centered", in order to take into account all potential effects on behavior.

6.3 Literature Review on Vision Mechanisms

6.3.1 Eye movements

Eye movements are voluntary or involuntary generated by the neural system, that is the oculomotor system. The voluntary ones may be classified as gaze-shifting, gaze-stabilizing, or fixational (Gregory, 2015).

The former includes saccades and pursuit movements. A saccadic movement is a ballistic motion to propel the eye to a new object of interest; thus it is fundamental in searching activity. A period between 150 and 200 ms is required to plan and execute a saccade, while the actual movement only takes a maximum of 30 ms, reaching a speed of 900 deg/sec. The time between saccades is called fixation, and represents the time in which the visual information is processed. Conversely, pursuit movements are slower movements used to keep a moving object within the foveal view. Acquired information is elaborated by the system that is able to predict the speed of the moving object through ongoing feedbacks, and move the eyes coherently.

Gaze-stabilizing movements include vestibulo-ocular and optokinetic reflexes. The first are stabilizing eye movements that compensate for those of the head. In fact, the eyes may automatically stabilize the image on the retina by producing movements in the opposite direction with respect to the head, thus maintaining the image on the center of the visual field. Optokinetic response combines fast and slow phases, due to the optical transition of a moving object in the visual field. In this case, eyes follow the uniform movement of the target until it exits from the FOV, and move back to the initial position where the object was saw. As both are reflexes, they are involuntary eye movements.

As mentioned, fixations are those movements interposed between two consecutive saccades. In this case, the object of interest is placed in the center of

the fovea (point of clearest vision), in stationary conditions. The time length of these movements is strongly related to the activity to be performed: e.g., between 150 and 600 ms for reading, or between 100 and 300 ms for road driving (Sodhi et al., 2002; Land and Furneaux, 1997).

Eventually, a vergence is a slow motion of the eyes (10-30 deg/sec) useful to obtain and maintain a binocular vision. This type of movement helps in the perception of depth while looking the same point/object (Duchowski, 2007).

While driving, the eye movements that play a fundamental role in visual attention are the saccades, smooth pursuit, fixation, and vergence. Saccades express the voluntary manifestation of searching in the FOV, and moving the center of attention elsewhere; the smooth pursuit and fixation focus the user on the relation between her/his own motion and moving objects; and the vergence assists the driver in distance estimation.

6.3.2 Eye-tracking techniques

The monitoring of eye movements may be performed through basically two techniques: by measuring the position of the eye with respect to the movement of the head, or by surveying the orientation of the eye in space.

In literature, four different detection methodologies are reported:
- Electro-OculoGraphy (EOG);
- Galvanometric or scleral search coil;
- Photo-OculoGraphy (POG) or Video-OculoGraphy (VOG);
- Video-Based Combined Pupil/Corneal Reflection.

The former technique is an electrophysiological test used to evaluate the function of the retinal pigment epithelium and the outer retina. During successive periods of light and dark adaptation, the equipment records the change in the electrical potential between the ocular fundus and the cornea (Brown et al., 2006).

The second methodology consists in contact lenses embedded with a coil of wire. When they move in a magnetic field generated by field coils positioned on both side of the head, a voltage in the coil is induced. This is one of the most precise technique to record also microsaccades, but is the most intrusive, since lenses may cause discomfort.

The POG or VOG techniques consist in the monitoring of pupil, limbus (the iris-sclera boundary), and corneal reflection, but do not provide the gaze point measurement. Its evaluation may be made manually (frame-by-frame) but is tedious and prone to error of the operator.

The fourth methodology is based on the concept of corneal reflection. By means of a series of algorithms, the software is able to estimate the position of the pupil center. Nowadays, electronic and computation advancements have contributed to the wide diffusion of such technique, combined with the possibility of a real time capturing of the observer's point of view. The equipment adopted can be of two types: table-mounted or head-mounted (i.e., wearable like glasses).

The two devices are different is size and optic characteristics: wearable devices require light and small components, whereas fixed cameras must compensate the distance between the sensors and the eyes. Conversely, precision and performance depend on the sampling frequency and on the processing capacity of the calculator

where the system operates. In both cases, the calibration of the systems is required to estimate the position of the reference point on a perpendicular surface in the FOV, e.g., the screen of a driving simulator (Duchowski, 2007).

6.3.3 Eye movements while driving

More than 90% of the information useful for driving is from vision (Hartmann, 1970). In road engineering, the monitoring of eye activity has been developed since 1960s. It has been mainly focused in the evaluation of eye-guide interaction, as well as driver perception and behavior (Fuller and Santos, 2002). The optical guide supports many visual activities such as steering, adapting speed, detecting and avoiding obstacles, reading traffic signs (Land and Furneaux, 1997). Such activities are strongly affected by the user characteristics (age, experience, psycho-physical conditions), those of the infrastructure (road category, road geometry, pavement conditions, etc.), and those associated to the environment (presence of other users, vehicles, traffic signs, obstacles, weather conditions, etc.). There is still a large gap in knowledge in this field because of the considerable number of variables that influences driver vision, combined with the employed equipment and test environment (naturalistic or simulated).

Past research focused on driver gaze tracking when negotiating a tangent or curves (Shinar et al., 1977); others tried to correlate eyes activity with gender, aging, and experience (De Waard et al., 2004; Underwood et al., 2003; Maltz and Shinar, 1999; Crundall and Underwood, 1998; Serafin, 1993; Cohen and Studach, 1977). Relevant outcomes are synthetized here:

- negotiating curves is more complicated than traveling on tangents; the former implies a continuous search of reference and moving elements to maintain the best (and comfortable) trajectory; along tangents drivers look at the farthest point (stationary) and control lateral elements through the peripheral vision (Shinar et al., 1977);
- older drivers require longer visual search times with respect to younger one to elaborate the same information from the road scenario; in particular, main differences were found in the variability of data, and in occasional lapses that evidenced looking difficulties of older drivers (Maltz and Shinar, 1999);
- novice drivers tend to fixate more the part of road close to the vehicle in comparison to experienced drivers who spend more time on looking ahead (Mourant and Rockwell, 1972); in hazardous scenarios, experienced drivers scan the roadway more than novice ones, that tend to look principally to the road ahead (Underwood, 2007); conversely, Serafin (1993) argued that experience (and age) is not influential.

Focused on the relationship between road geometrics and driver behavior, some vision mechanisms were introduced in literature (Lappi, 2014; Lappi et al., 2013; Lehtonen et al, 2012; Robertshaw and Wilkie, 2008; Salvucci and Gray, 2004; Wann and Land, 2000; Boer, 1996; Land and Horwood, 1995; Land and Lee, 1994; Donges, 1978). In the following, main models for curve negotiation are presented and discussed.

Tangent point model

The seminal work related to the tangent point (TP) model was developed by Land and Lee (1994). They considered as TP the one on the lane (or pavement) edge on the inside of the curve, with the line of sight tangential to that edge. Accordingly, the driver's attention falls on that part of the roadway where the edge changes direction (Land and Furneaux, 1997).

The authors proposed a relationship between some factors describing the interaction between the driver gaze and the vehicle trajectory (Figure 6.2):

$$\cos \theta = 1 - \frac{t}{R} \qquad\qquad \text{(eq. 11)}$$

Considering the expansion of the cosine function with a shortened polynomial:

$$\cos \theta = 1 - \frac{\theta^2}{2} \qquad\qquad \text{(eq. 12)}$$

Substituting eq. 12 into eq. 11, the driving path curvature (c) become equal to:

$$c = \frac{\theta^2}{2t} \qquad\qquad \text{(eq. 13)}$$

where θ is the gaze angle (i.e., the deviation angle between the direction of the vehicle - direction of S, or heading - and the direction of driver's view - gaze direction), and t is the distance of the trajectory to the lane edge at the TP.
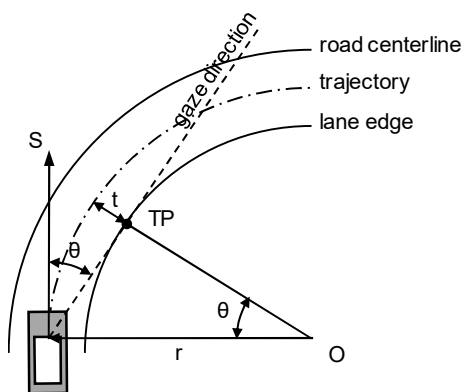
Figure 6.2. Scheme of tangent point model (r = radius of curvature of the trajectory)

Drivers use the TP before turning the steering wheel as a safe habit. Chattington et al. (2007) evaluated the coordination between eye and steering movements while driving. As well, Robertshaw and Wilkie (2008) found a direct link between the gaze direction and the steering direction. However, their results came from two distinguished experiments where only ten and nine participants were respectively observed.

Future path models

These models postulate the use of steering points on the planned trajectory, associating different control rules with respect to such points (Lappi et al., 2013).

The Boer model (1996) assumes that the driver controls the steering by judging the distance from her/his point of view to the target T along the future path (Figure 6.3). It could be obtained starting from the TP or any point of longitudinal elements inside the roadway (e.g., lane markings). When it is a point of the future path, the distance corresponds to the chord L_C, thus leading to:

$$c = \frac{1}{r} = \frac{2 \cdot \sin \theta}{L_C}$$ (eq. 14)

where r is the radius of curvature of the trajectory.
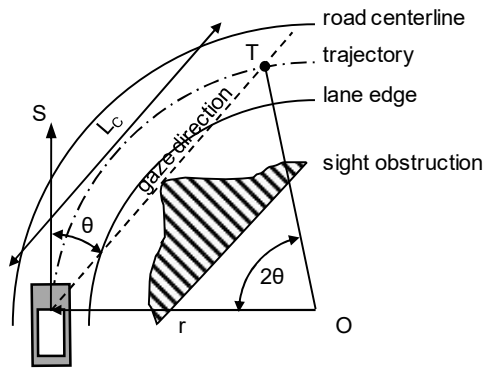
Figure 6.3. Scheme of the Boer model (1996) with a lateral sight obstruction

This mechanism is activated in situations where the driver anticipates or plans driving maneuvers, and does not look at a lateral element. It is also used when lateral sight obstruction limits the visibility (Figure 6.3): the driver regulates the speed and the driving path curvature on the basis of the available sight distance.

On the other hand, the Wann and Land (2000) model assumes that the driver refers to a fixed target (T) within the curve. Traveling at a constant speed along circular curves, the fixation of the steering point (T) generates a constant variation of the gaze angle (Figure 6.4).

This control mechanism is also at the basis of over- and understeering conditions recognition. Starting from eq. 14, the variation of the gaze angle during time is:

$$\frac{d\theta}{dt} = \frac{c}{2 \cdot \cos \theta} \cdot \frac{dL_C}{dt}$$ (eq. 15)

where dL_C/dt corresponds to the speed (S) component along the direction of observation.

Hence:

$$\frac{dL_C}{dt} = S \cdot \cos\theta \qquad \text{(eq. 16)}$$

Thus, substituting eq. 16 in eq. 15:

$$c = \frac{2}{S} \cdot \frac{d\theta}{dt} \qquad \text{(eq. 17)}$$
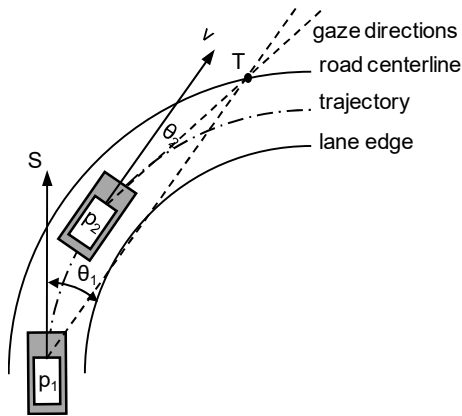
Figure 6.4. Scheme of the Wann and Land model (2000)

Other works that supported this model were developed by Wilkie and Wann (2003), who found that drivers focus more in the road (30%) and adjacent parts (50%), while only 1% relied on the TP. They stated that drivers who are free to scan the whole visual field allowed to steer more accurately with respect to imposed gaze condition. Lehtonen et al. (2012) observed the recourse of the occlusion point (OP), that is the most distant visible point along the roadway. Results evidenced that more drivers looking towards the OP along rightward curves than on leftward curves due to the reduced eccentricity of the target with respect the heading direction.

Two-level steering model

This model is based on the concept that the driver is not necessarily guided by the TP to negotiate the curve, but uses one or more reference points on the roadway (Salvucci and Gray, 2004; Land and Horwood, 1995; Donges, 1978). The visible road ahead may be divided in three different regions as a function of the relative distance from the driver viewpoint (nearest, middle-distance, farthest), as shown in Figure 6.5.

Results evidenced that the visibility of the middle zone allowed only to perform both a steering compliant with the curvature, and to maintain an adequate position inside the lane. At greater speed, drivers need more guiding elements to identify the curvature and anticipate maneuvers (through the far zone), and to control the vehicle position (through the near region).
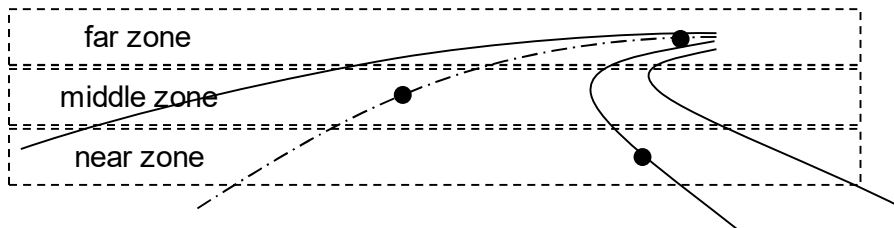
Figure 6.5. Scheme of future path model, where gaze point may fall in near, middle, and far zone

Although the effects of geometric parameters were widely investigated in the past, literature provides only qualitative information about the sight conditions in which drivers operated. Furthermore, studies that correlated the operational and behavioral performance of drivers with their visual activity are still valid but performed with outdated equipment (Wilkie and Wann, 2003; Boer, 1996; Land and Horwood, 1995; Land and Lee, 1994). Experiments were carried out considering a limited number of drivers (less than ten) while traveling in a limited number of curve types. In this framework, the direct relationship between the ASD and speed, trajectory, and visual attention was never investigated. Thus, there is more room to analyze the driver behavior in a wider range of sight conditions that usually occurs in rural road driving. The recourse to driving simulators allows the monitoring of human behavior in controlled, stationary, repeatable, and safe conditions.

7. Experiments

The objective of this research consists in evaluating the operational and behavioral effects of ASD. As mentioned, the ASD is influenced by geometric parameters that are controlled in road design activities and decisions: the radius of curvature (R) as well as the distance of the lateral sight obstruction from the lane centerline (D). In this study, these variables were employed to obtain a set of ASD values along a series of horizontal curves included in some test tracks. Voluntary TDs were involved, while driving speed, trajectory, and eye fixations were continuously collected and then manipulated for the analysis.

7.1 Equipment

This research activity was performed by means of the same fixed-base driving simulator already introduced in §3.1.

During the simulations, eye movements were monitored through the use of a wearable eye-tracking system ("eye-tracking glasses" in Figure 7.1) developed by Pupil Labs, whose settings are listed in Table 7.1.

The manufacturer released also the open source *Pupil* software to record (*Pupil Capture*) and analyze (*Pupil Player*) collected data. The former application presents the view-points of the three cameras, with the possibility of managing their settings and calibration factors before the acquisition. The second application uses the collected data to display and analyze gaze positions in the scene (e.g., fixations, scan-path, heatmap). Analyzed data can be exported in *.csv* (text) or *.png* (image) file.

Figure 7.1. Eye-tracking glasses manufactured by Pupil Labs [4]

Table 7.1. Eye-tracking glasses: components and characteristics

Function	Devices	Features
World monitoring	HD camera	Resolution: 1080p @ 30fps, 720p @ 60fps, 480p @ 120fps Field of view: 100° (maximum)
Pupil detection	No. 2 InfraRed (IR) cameras	Resolution: 480p @ 120fps
Support	3d printed headset	Laser sintered PA12
Connectivity	USB-Type C connector	-

7.2 Experiment Design and Research Variables

Two different experiments were consecutively performed: the former (#1) involved the design of the test tracks, and the evaluation of driving speeds and trajectories of drivers along horizontal curves with sight limitations; the second (#2) used similar road scenarios to analyze where drivers look during curve negotiation, in order to capture roadway information, and adopt appropriate speed and trajectory.

7.2.1 Experiment #1

<u>Test tracks and virtual scenarios</u>

Two alignments of a standard two-lane rural highway with a lane width (l_w) of 3.75 m, and a shoulder width (s_w) of 1.5 m were designed. To reduce the size of the virtual model, the test tracks included all combinations of the two main variables affecting ASD (Figure 7.2): the trajectory radius (r_i), and the distance of the ideal trajectory from the lateral sight obstruction (D_i).
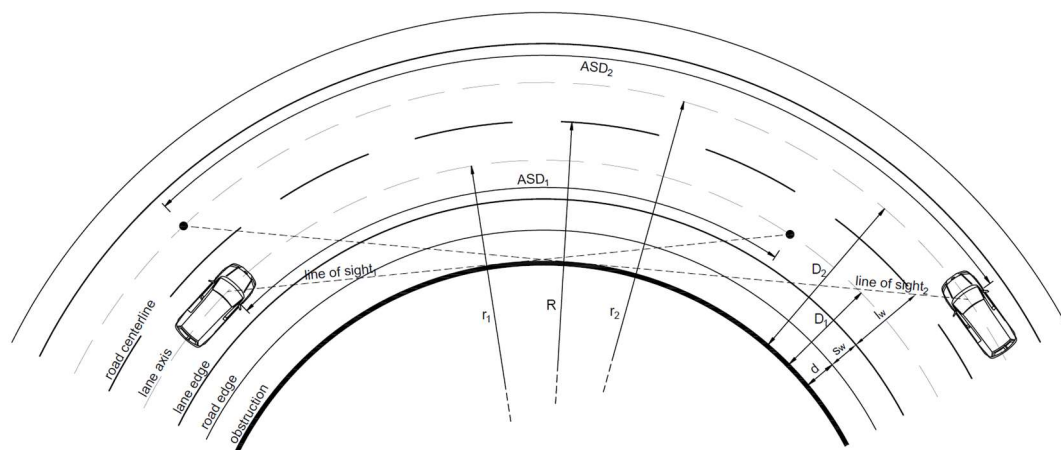
Figure 7.2. Nominal available sight distance (ASD) along a horizontal curve elaborated from road geometric policies (AASHTO, 2011; MIT, 2001). Subscript 1 refers to right-hand curve condition, subscript 2 to the left-hand curve one; R is the design radius; d is the distance of the lateral obstruction from the shoulder or pavement edge; s_w is the shoulder width; l_w is the lane width

It is worth noting that eq. 9 provides a nominal estimation of ASD under the simplified hypothesis, supported by current road geometric policies, in which the driver moves along the lane centerline. Eq. 9 is valid on flat grades only, and if the driver and the target are both on the circular arc, which is possible only in case of sufficiently long curves.

In real driving conditions, the actual driver position could be laterally shifted away from the lane axis, so the effective ASD slightly changes during the experiments. Hence, the reference (nominal) ASD was kept constant along the entire curve length in order to reflect stationary conditions.

Four curve radii (i.e., $R_1 = 120$ m, $R_2 = 225$ m, $R_3 = 300$ m, and $R_4 = 430$ m) were selected in the design speed variation range of 60-100 km/h according to Italian policy (MIT, 2001). For stability reasons, the cross slope along curves was set equal to 7% in accordance to the same policy; spirals were adopted also to accomplish the transition of cross slope from tangent to curve, and vice versa.

A continuous stone wall with a height of 1.5 m was employed to generate different ASD values. Walls were placed on the inner side of randomly selected curves at a predefined distance (D) from the driven lane centerline (Figure 7.3). ASD variations were obtained combining three specific distances d of the sight obstruction from the pavement edge (0, 1.5, and 3 m). Table 7.2 lists the ASD values computed from the combination of D and R and, also, of the driving direction.
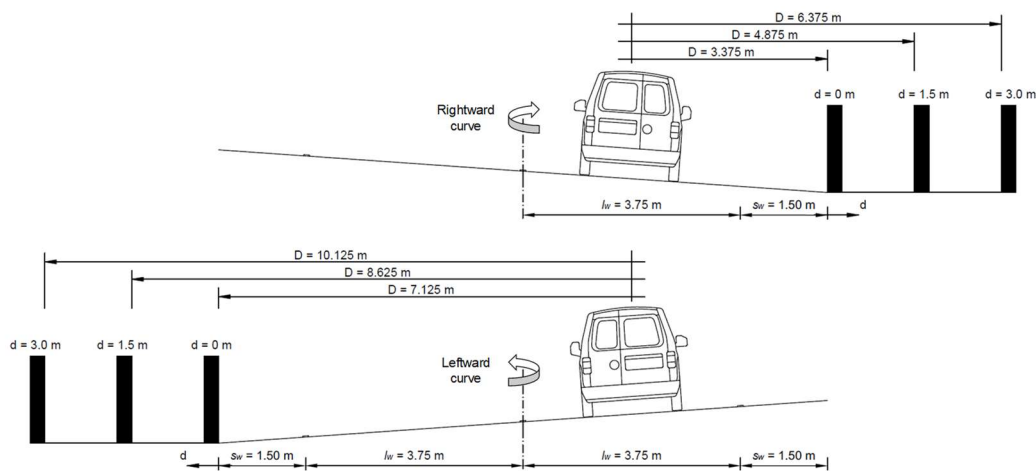
Figure 7.3. Cross section of the road configuration in right-hand and left-hand curves, with the sight obstruction at different distances (D) from the lane centerline

Table 7.2. Computed available sight distance (ASD) values according to eq. 9 for the combination of curve radius (R), direction (right- and leftward), and distance (D) from the lateral obstruction

Radius	Design speed	Rightward curves			Leftward curves		
		D_1	D_2	D_3	D_4	D_5	D_6
		3.375 m	4.875 m	6.375 m	7.125 m	8.625 m	10.125 m
(m)	(km/h)	(m)	(m)	(m)	(m)	(m)	(m)
$R_1 = 120$	61	56.61	68.11	77.97	83.76	92.25	100.06
$R_2 = 225$	77	77.72	93.46	106.93	114.02	125.52	136.07
$R_3 = 300$	86	89.80	107.98	123.53	131.43	144.67	156.81
$R_4 = 430$	100	107.59	129.34	147.95	157.11	172.91	187.40

Deflection angles were always larger than 60° to obtain a constant ASD value along curves, thus providing stationary sight conditions for a sufficient time (and space). The minimum travel time of 2.5 s required by Italian standards (MIT, 2001) was always guaranteed.

The combination of design variables R and d produced 12 (4 × 3) curve configurations, both for right- and leftward driving direction. Those were randomly distributed in the two road alignments, by adopting different deflection angles (equal to 60°, 75°, and 90°) that control the length of circular arcs. The first alignment had a length equal to 12,888 m; it was used to design track A (Figure 7.4) and track A-mod (Figure 7.5). Track A-mod was a variant of track A, which included also unlimited sight conditions along curves (D = infinite) without sight obstructions. The second alignment was 14,444 m long, and was used to implement track B (Figure 7.6). The choice of more tracks was consistent with the techniques to correct for confounding (McGwin, 2011). The total length of tracks was designed to limit the duration of the experiment to 20 minutes, thus minimizing fatigue, sickness, and boredom of drivers (Philip et al., 2003).
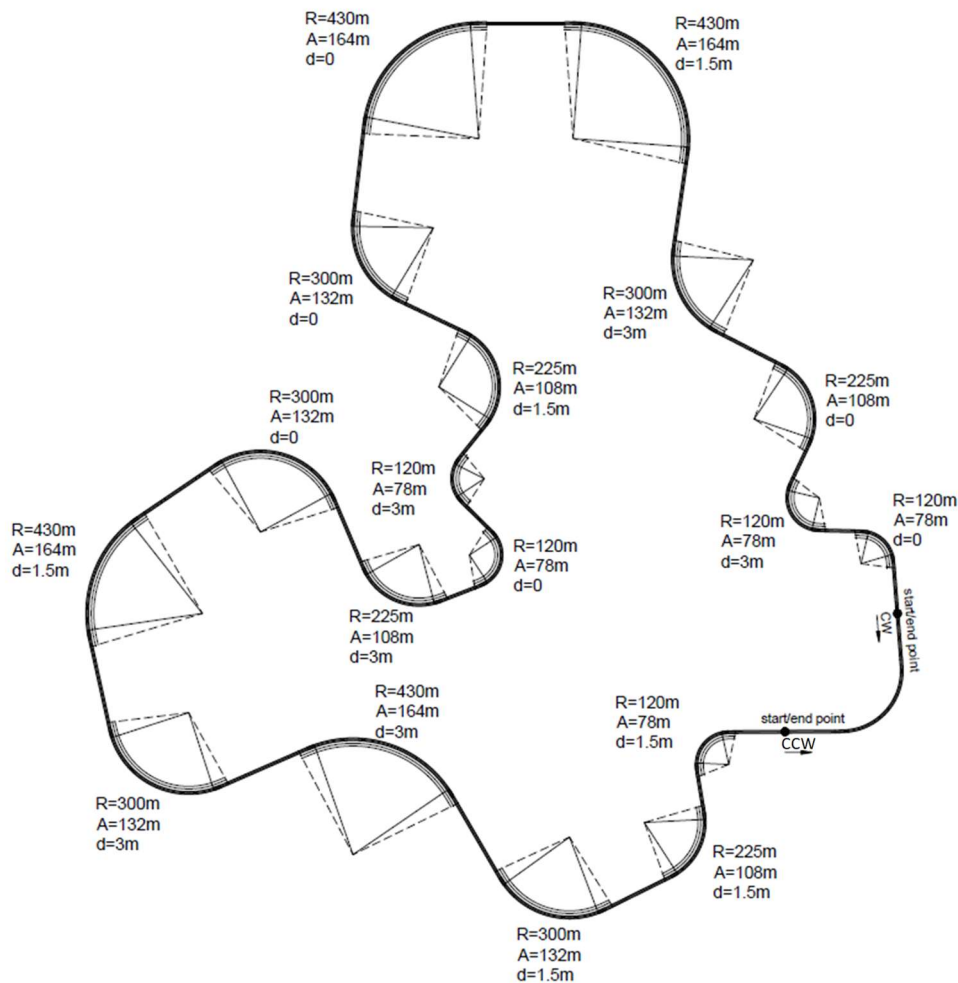
Figure 7.4. Horizontal alignment of track A with indication of the design radius (R), the scale parameter of the spiral (A), and the distance d of the sight obstruction from the shoulder
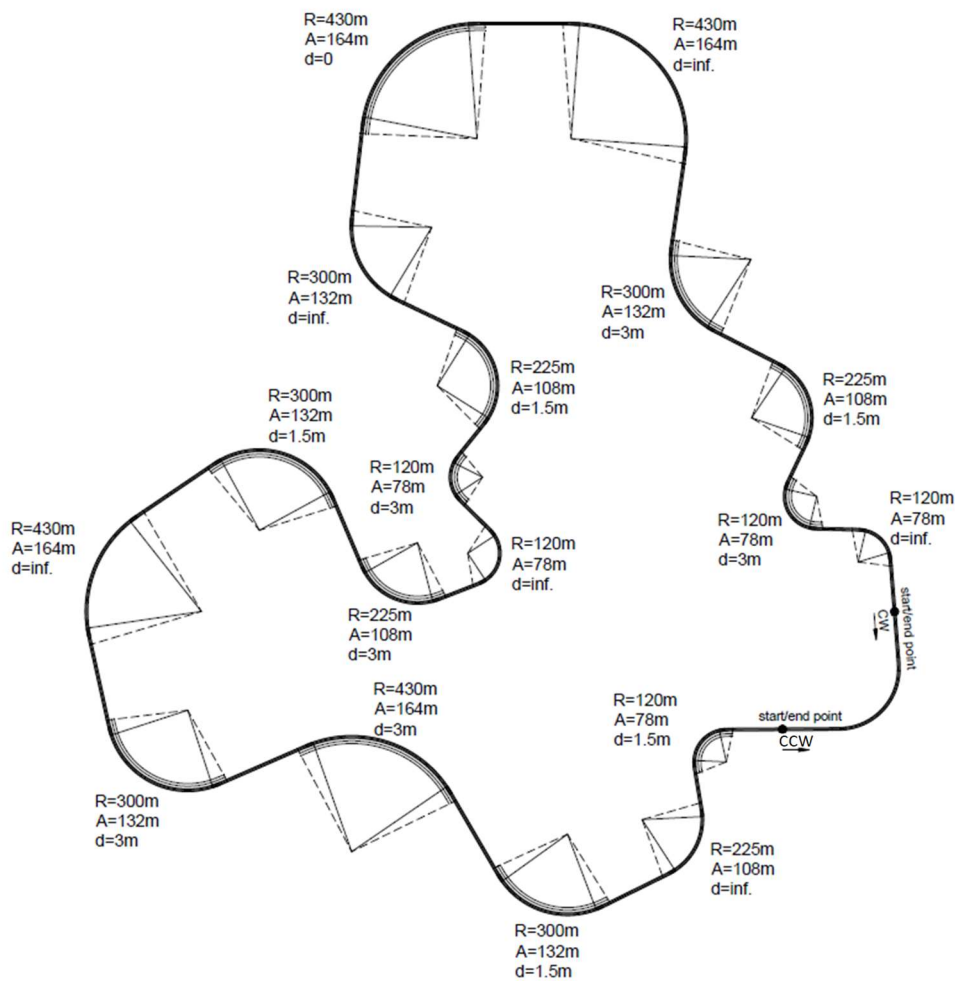
Figure 7.5. Horizontal alignment of track A-mod with indication of the design radius (R), the scale parameter of the spiral (A), and the distance d of the sight obstruction from the shoulder

The order of succession of left- and rightward curves along the tracks was set randomly. Only the curves with variable notation (eighteen per track) were further analyzed, while the other ones (one in the alignment A, and two in the alignment B) were introduced with the sole scope of completing the circuits. To be consistent with Italian and many other international standards (Brenac, 1996), particular care was taken to avoid the use of the smallest radius before or after the largest one, thus preventing unexpected situations. This was also necessary to avoid an excessive design and/or operating speed variation in two adjacent curves, thus meeting driver expectations when traversing curves of different radii (Castro et al., 2011; Leisch and Leisch, 1977). Figure 7.7 provides the curvature diagram of the three tracks, with the variables R and d, and the scale parameter A of the clothoids duly indicated.
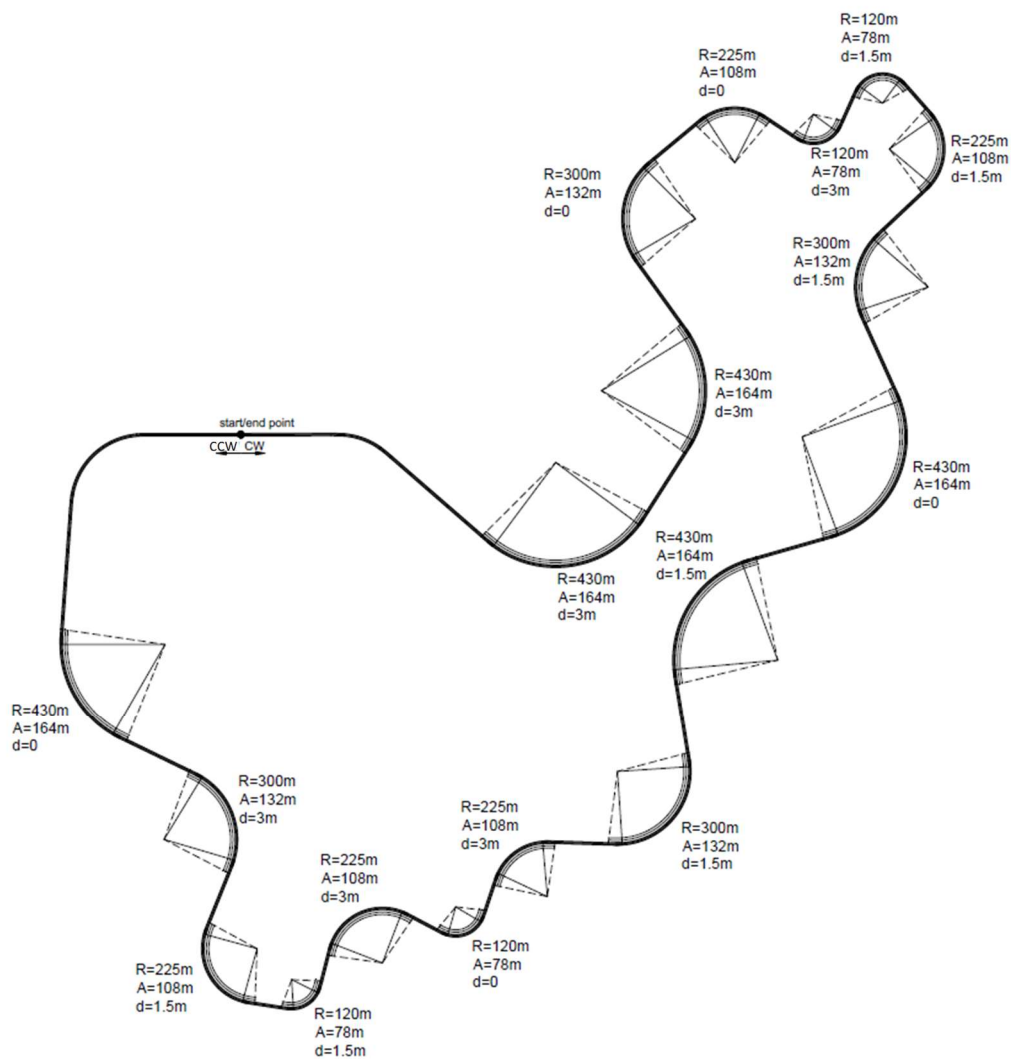
Figure 7.6. Horizontal alignment of track B with indication of the design radius (R), the scale parameter of the spiral (A), and the distance d of the sight obstruction from the shoulder

Circular curves were all placed between transition elements (clothoids), having a scale parameter set in the range between *R/3* and *R*. It is worth highlighting that spirals improve the optical perception of the road alignment (Zakowska, 2010). Tangents between curvilinear elements were designed to guarantee that $R > L_t$ for $L_t < 300$ m, and $R \geq 400$ m for $L_t \geq 300$ m (MIT, 2001). Therefore, their length was set in the range from 110 to 300 m.
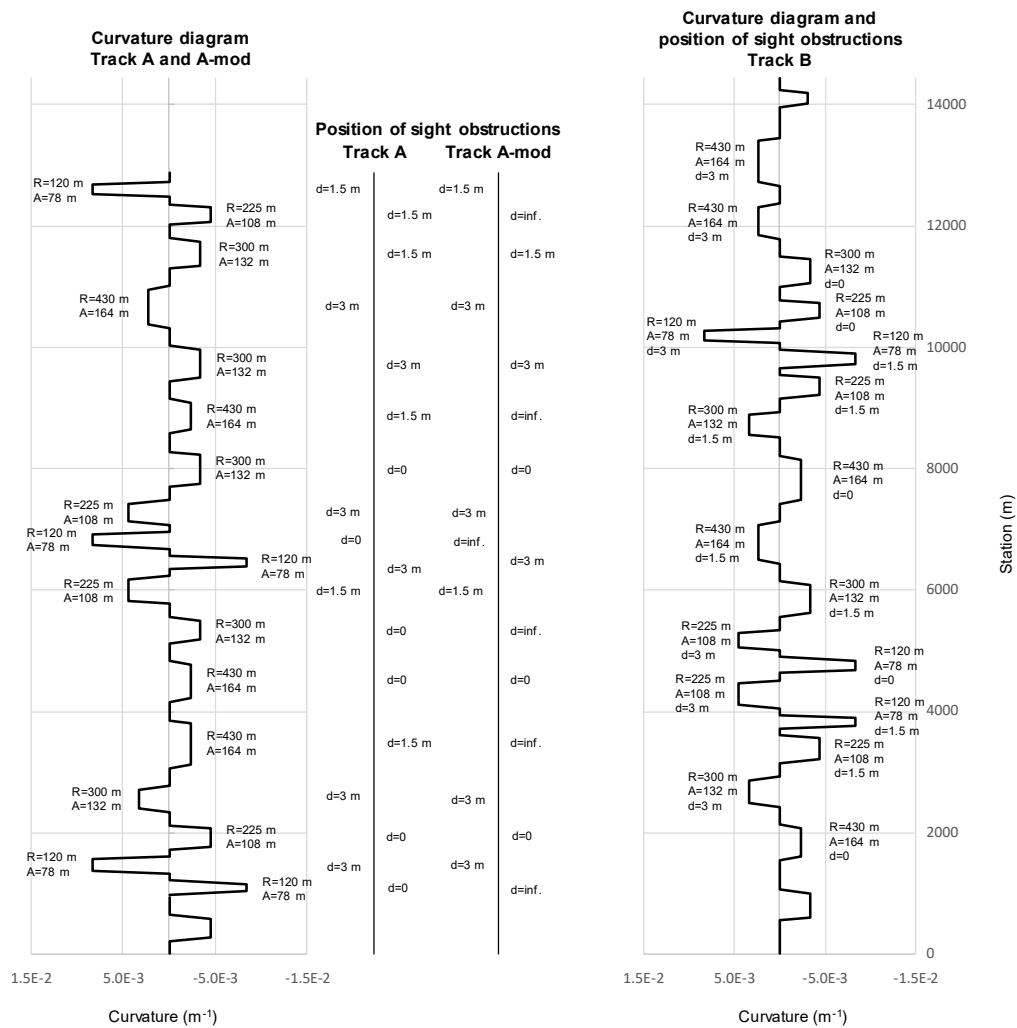
Figure 7.7. Curvature diagram for track A, A-mod, and B, with specification of curve radius R, scale parameter A of the clothoids, and distance d of the lateral obstruction from the road edge

To limit the number of design variables and including secondary effects, the terrain was kept flat. Figure 7.8 provides some frames taken from the simulations that depict the effects of the sight obstruction offset at different distances (*d*) from the shoulder for right- and leftward curves.

No vegetation, trees, and traffic barriers were placed along the roadside to exclude distractions and undesirable effects on subjects involved in the experiment. However, few objects (e.g., container, parked vehicle, cones) were positioned on the shoulder, close to the end of few curves to stimulate driver attention. No one vertical sign was used to indicate the posted speed limit (PSL); some signs provided warnings before dangerous curve ($R = 120$ m) only, and the right of way at few intersections placed along straights, again to promote attention. Margin delineators were positioned with a spacing of 50 m along curves and tangents (Italian Parliament, 1992a; Italian Parliament, 1992b).

	Leftward curves	Rightward curves
$d_1 = 0$ m		
$d_2 = 1.5$ m		
$d_3 = 3$ m		
No sight obstruction		
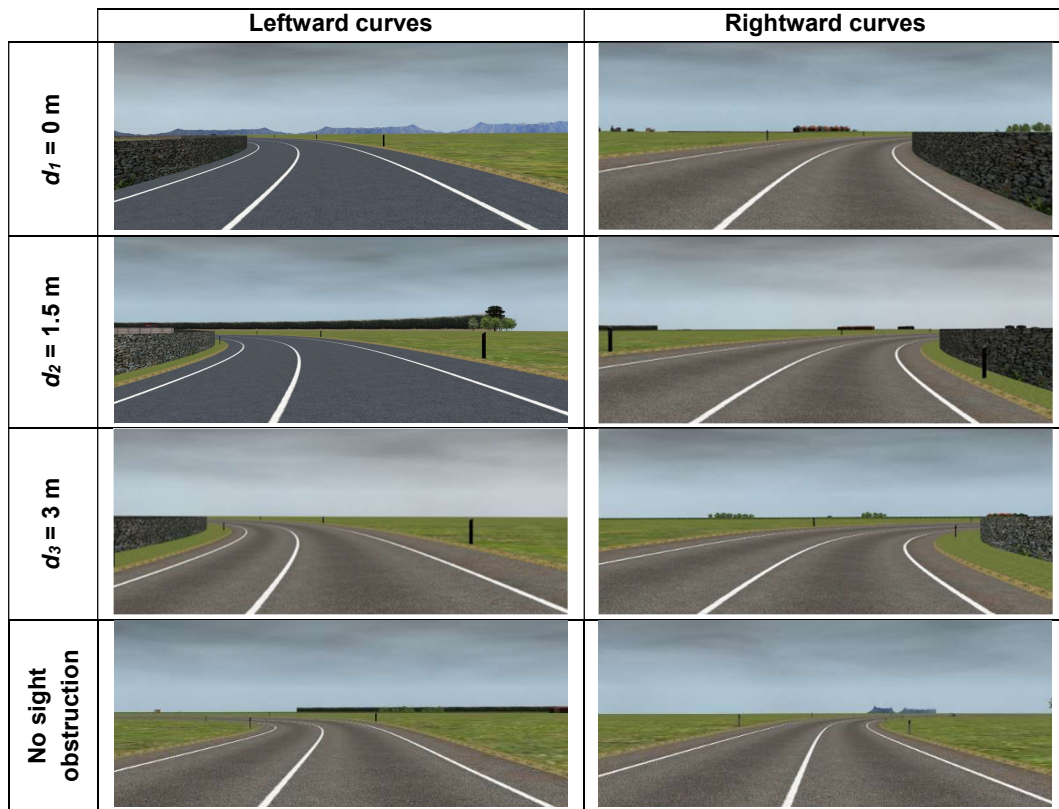
Figure 7.8. Frames of right-hand and left-hand curves with sight obstructions at distance d equal to 0, 1.5, 3 m, and without the lateral wall

The vehicle was the same for all participants. Its settings were similar to those of the average vehicle commonly found in Italy (UNRAE, 2016). The dynamic model corresponds to a passenger car powered by a 130 hp gas engine, with six manual gears. The brake pedal was set with the default regulation. The car model uses a numerical method with a constant time step.

Network traffic was reproduced through some isolated vehicles moving in the opposing lane, and just few in the same direction of the test vehicle. Simulated vehicles circulated inside the circuits through a secondary network and on predefined paths. Their trajectories were carefully programmed to be sufficiently far from the monitored driver, so as to avoid any impact on speed and sight distances (so free-flow traffic conditions were always obtained). The three tracks in Figure 7.7 were driven in both clockwise and counterclockwise directions.

Observed variables

Simulations were set to collect the following measurements of interest:
- speed;
- trajectory curvature;
- road and lane gaps;
- road logics, as road ID, road abscissa, road length, and lane ID.

All variables were gathered with the sampling rate of 10 Hz.

The lane gap (*LG*) is the transversal distance of the vehicle center of gravity (CoG) from the lane centerline. The software attributes positive values for

displacement on the left half of the lane, and negative values for the right one (Figure 7.9).

This sign convention is valid for all the lanes in the cross-section, shoulders included. For this reason, if the CoG enters in a different lane, the reference system changes according to the lane ID, and moves to the centerline of the new traveled lane. Thus, the road gap (RG, transversal distance of the CoG from the road axis) was used to correct such conditions and to calculate the correct lane gap (LG^*) according to:

$$LG^* = -RG + \frac{l_w}{2} \qquad\qquad \text{if } RG > l_w \qquad\qquad \text{(eq. 18)}$$

where l_w is the lane width. The RG has positive values when the vehicle is moving on the correct lane, negative if the CoG traversed the road centerline and the vehicle occupies the opposing lane (Figure 7.9).

The LG^* was employed to compute the dispersion of trajectory (DT). According to Calvi (2015b), DT is a synthetic indicator of the vehicle position into the lane, and along a road segment. DT considers the discrepancies between the adopted trajectory (red line of Figure 7.10) and the lane centerline (ideal trajectory), as per the:

$$DT = \int_{x=0}^{x=L} \left| LG^*(s) \right| ds \qquad\qquad \text{(eq. 19)}$$

where s is the curvilinear abscissa, and L is the total length of the element. The observed element includes 50 m of approaching and departure tangents, transitions (distance from TS to SC, and from CS to ST in Figure 7.10) and circular curves (distance from SC to CS). Differently from previous contributions (Montella et al., 2014; McFadden and Elefteriadou, 2000), the considered tangent length was limited to 50 m instead of 200 m in order to restrict the investigated segment and focus only on the trajectory variability related to the curve.
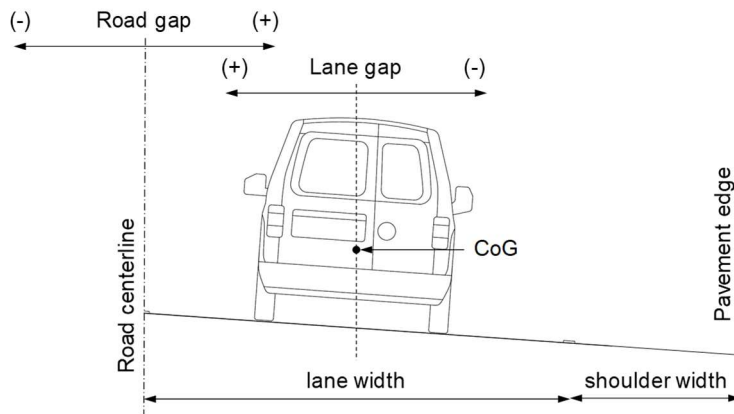
Figure 7.9 Sign convention for lane gap data treatment (CoG: center of gravity) of SCANeR^{TM}studio (driving simulator software)
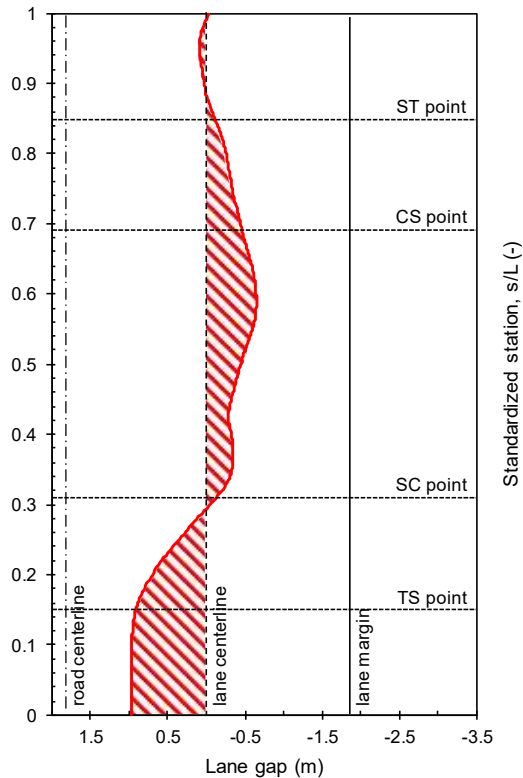
Figure 7.10. Scheme of DT measurement (red area) along the curved elements and adjacent tangents

Specifically, the *DT* evaluates the ability of the driver to select the appropriate steering angle, or to follow the correct geometry of the path. Low values of *DT* suggest that the geometry of the curve is well perceived (or also "read") by the TD. Thus, such data are safety related, since they describe the tendency of certain road alignments to induce frequent corrections (i.e., wrong steering wheel control) of drivers trajectory (McGehee et al., 2004).

Lastly, road logics refer to the intrinsic information of each element of the *SCANeR^TMstudio* database. The road ID is a number associated with a segment having the same cross section; the road abscissa is the relative station of the element identified with certain road ID; and lane ID is the number associated with a lane of the cross section. These are used for the definition of a methodology to transpose data collected in the time domain (10 Hz = ten data per second) to values attributed to a road station (§7.5).

7.2.2 Experiment #2

Vision mechanisms

When negotiating curves, drivers collect and elaborate visual information of the road space to control vehicle speed and trajectory. Thus, a vision mechanism identifies the model (or strategy) that the user adopts to estimate the curvature of a roadway element. On the basis of the literature review (§6.3.3), and the

geometrical relationships between road elements and gaze direction, four main vision mechanisms were considered in this research:

1.   tangent point (Land and Lee, 1994);
2.   distance to target estimation;
3.   motion of the fixation point (or gaze angle variation); and
4.   car following (Salvucci and Gray, 2004).

The first three mechanisms are used by drivers to have an estimation of the road curvature (through gaze angle, θ, or chord length, L_C) and to plan the future path; although the gaze targets are approximately in the same direction (in front of the driver), the steering strategies are guided by very different mechanisms (Lappi et al., 2013). The fourth mechanism is adopted to guarantee the preferred safety distance from the vehicle ahead. Few observations falling in this steering strategy were removed from the analyses since it is not related to the interpretation of curve geometrics.

The mechanisms were split into sub-classes to consider also the effects of the visible elements on the roadway.

With the vision mechanism (VM) #1, the tangent point (TP) is used to act on the steering wheel. Specifically, the driver focuses on right/left lane marking or pavement edges (i.e., the separation between the pavement and the roadside), or else the road centerline on leftward curves (VM 1a in Figure 7.11). With this steering strategy, the driver focuses on the TP with a fixed gaze angle (θ), and control the distance t from the tangency alignment.
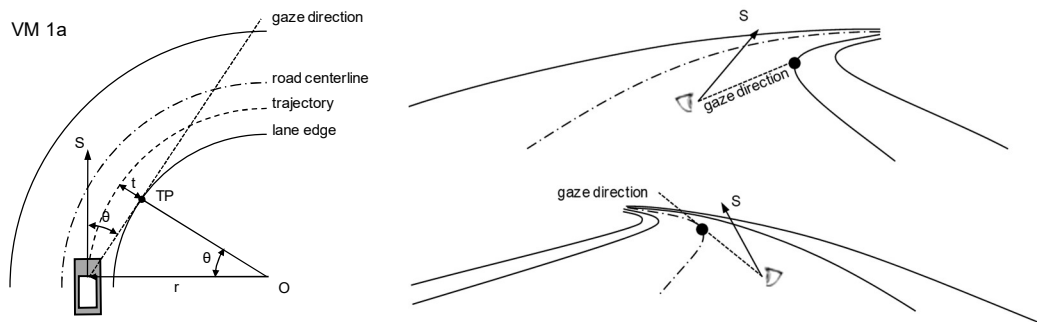
Figure 7.11. Horizontal and 3d schemes for vision mechanisms #1a

Conversely, the VM 1b occurs when the driver looks at the TP of the continuous lateral sight obstruction (Figure 7.12). It is valid both for rightward and leftward bends. In this case, the distance t corresponds to the distance (D) between the vehicle trajectory and the wall in the roadside (eq. 10).
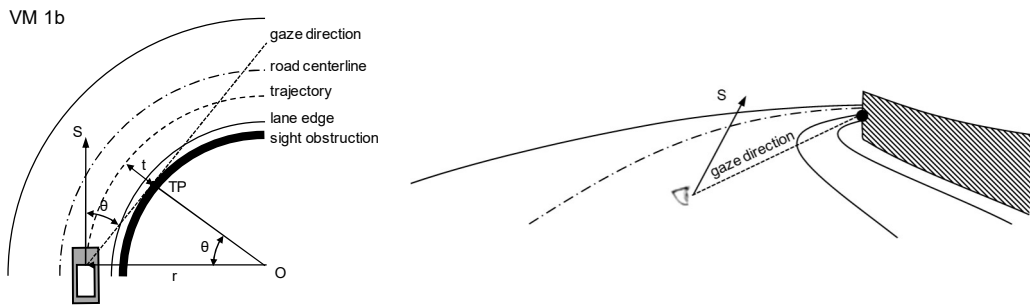
Figure 7.12. Horizontal and 3d scheme for vision mechanisms #1b on a right-hand curve

The vision mechanism #2 is related to the estimation and control of a fixed distance (L) from the point of view to the target (T) placed along a continuous alignment of the roadway (e.g., road axis, lateral markings, curbs, future path).

The VM 2a is defined as the strategy associated with focusing a target point on the road edge (Figure 7.13) or on the pavement edge. This is the alignment that separates the paved road from the natural terrain. In other words, the driver estimates the distance from her/his position to a possible out of the way point.
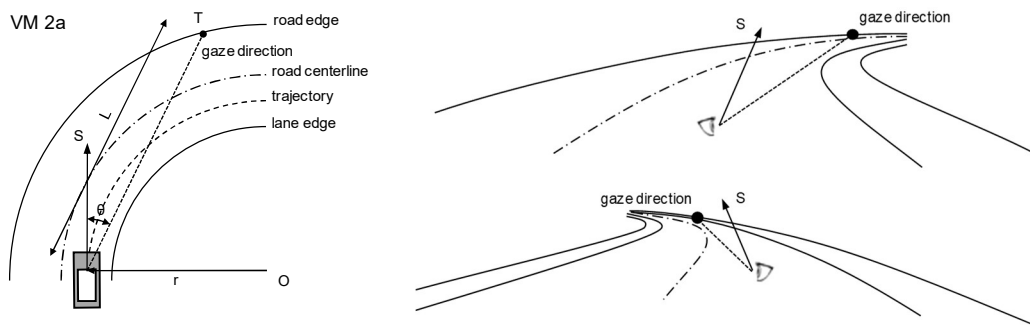
Figure 7.13. Horizontal and 3d schemes for vision mechanisms #2a

The VM 2b considers that the target (T) point is located along the future path. Specifically, the driver estimates the length of the chord (L_C) by maintaining a fixed gaze angle (Figure 7.14). This strategy is valid both for rightward and leftward bends.
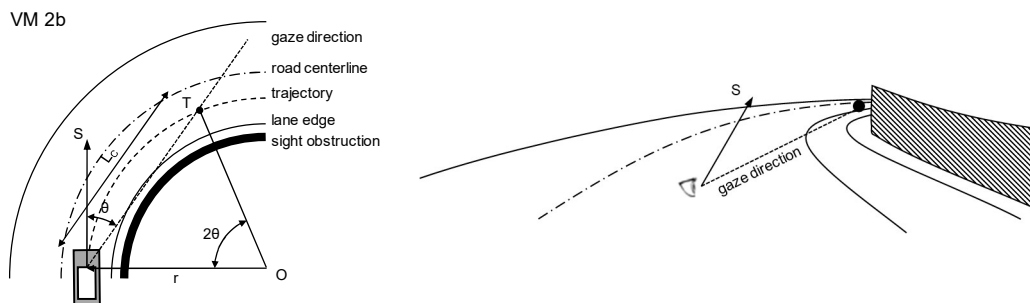
Figure 7.14. Horizontal and 3d scheme for vision mechanisms #2b on a right-hand curve

The VM 2c is adopted by drivers that look at the road centerline with a fixed gaze angle along the curve (Figure 7.15).
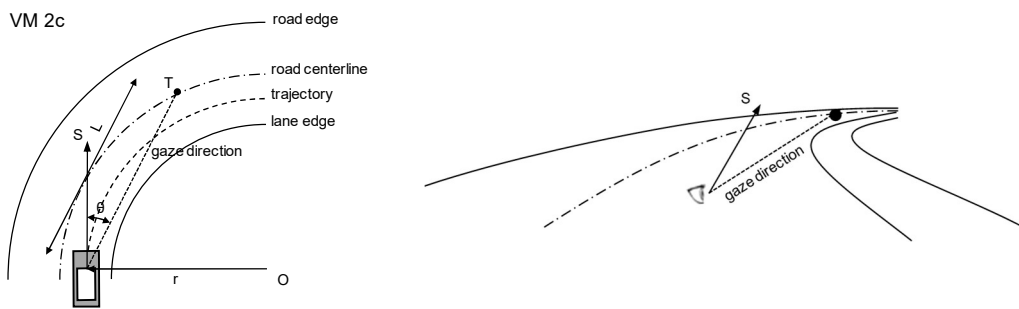
Figure 7.15. Horizontal and 3d scheme for vision mechanisms #2c on a right-hand curve

The VM 2d is identified when the driver fixates at the occlusion point (OP), that is the furthest visible point of the road track (Figure 7.16). This mechanism can be applied in both rightward and leftward bends.
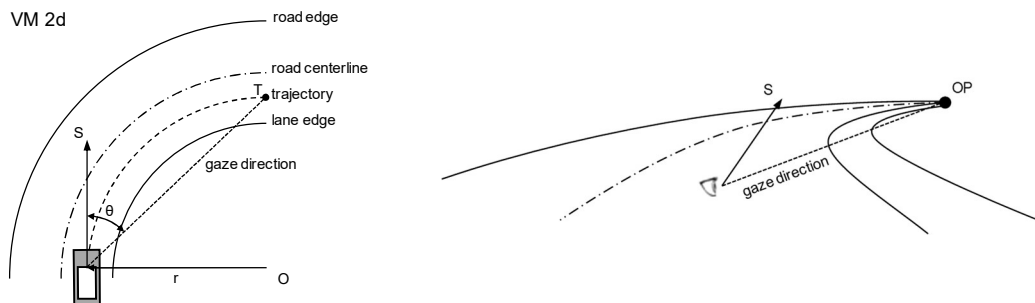
Figure 7.16. Horizontal and 3d scheme for vision mechanisms #2d on a right-hand curve

The third mechanism (VM #3) is related to the variation of the gaze angle over time ($d\theta/dt$). In this case, the observer fixates different and recurring elements of the roadway that are moving with specific path during curve negotiation. When the gaze angle reaches a minimum value (low eccentricity, $\theta \to 0$), the TD switch to the next element. For this experiment, margin delineators were adopted to stimulate such mechanisms (Figure 7.17).
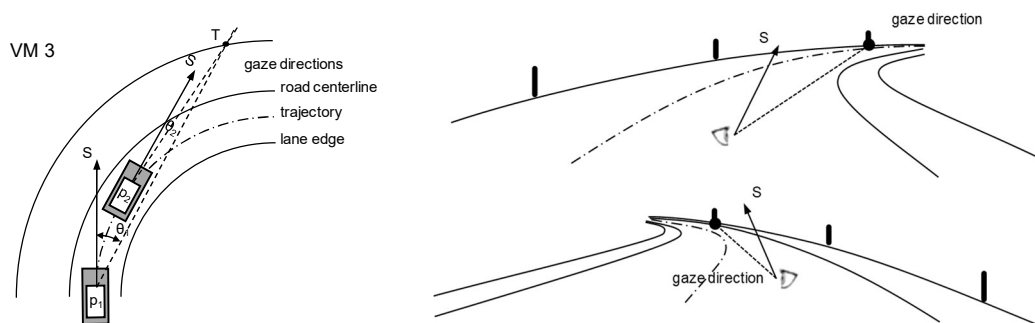
Figure 7.17. Horizontal and 3d schemes for vision mechanisms #3

Test tracks

The two road alignments presented in §7.2.1 were considered for the second experiment. However, some elements of the roadway (horizontal marking, lateral

obstruction, and margin delineators) were recombined in order to stimulate drivers in adopting different vision mechanisms.

Table 7.3 shows the seven combinations of the elements that were reproduced in the simulated scenarios, with the corresponding virtual views. Such combinations were attributed to the four curve radii (120, 225, 300, 430 m) selected in Experiment #1. This resulted in 28 (7 × 4) different curve configurations.

For the reasons above reported, the alignment of tracks A and B of Experiment #1 was maintained. Four experimental scenarios (A-mod, A2, B-mod, and B2) were designed by adjusting the presence/absence of the elements (road markings, lateral wall, margin delineators) along the curves. These combinations were randomly attributed to the whole sample of analyzed curves.

Table 7.3. Combinations of the three elements of the roadway in the virtual scenarios

Combination ID	Elements of the roadway			Representation in the virtual scenario
	Horizontal Marking (M)	Sight Obstruction (O)	Margin Delineator (D)	
1	X	X		
2	X		X	
3		X	X	
4			X	
5		X		
6	X			
7	X	X	X	

Table 7.4 and Table 7.5 report the configuration of the 18 curves respectively of track A-mod and A2, and B-mod and B2. In particular, d indicates the distance from the lateral sight obstruction to the pavement edge. The term "inf." indicates that the obstruction was not present. The presence of horizontal markings (M) and margin delineators (D) is indicated with "Y" (yes), their absence with "N" (no). Each scenario was driven both in clockwise and counterclockwise direction. This experimental approach prevented issues related to confounding effects (McGwin, 2011).

7.3 Driving Simulations

For the samples composition, the choice of drivers and their different ages was based on the attempt of reflecting Italian driver population characteristics (MIT, 2016).

In the Experiment #1 a total of 41 drivers, 26 males (63%) and 15 females (37%), aged between 20 and 60 years (Table 7.6) were involved. Participants were volunteers who did not received any benefit. All drivers passed the training phase to gain confidence with the use of the driving simulator (they all drive in a simple scenario for at least 10 minutes). None of them manifested simulation sickness during this phase. For the experimental task, participants were instructed to drive as they normally do, and to continue along the same lane for the whole duration of the experiment.

Table 7.4. Configuration of the curves in the tracks A-mod and A2 (d = inf. means no obstruction, M = markings, D = delineators)

Track A-mod						Track A2					
Curve #	R (m)	d (m)	M	D	Comb. ID	Curve #	R (m)	d (m)	M	D	Comb. ID
1	120	inf.	Y	Y	2	1	120	inf.	Y	Y	2
2	120	3	Y	Y	7	2	120	3	Y	Y	7
3	225	0	Y	N	1	3	225	inf.	Y	N	6
4	300	3	N	Y	3	4	300	3	Y	N	1
5	430	inf.	Y	Y	2	5	430	inf.	Y	Y	2
6	430	0	Y	Y	7	6	430	0	Y	Y	7
7	300	inf.	Y	N	6	7	300	inf.	Y	Y	2
8	225	inf.	N	Y	4	8	225	1.5	N	Y	3
9	120	3	Y	Y	7	9	120	3	Y	Y	7
10	120	inf.	Y	Y	2	10	120	inf.	Y	Y	2
11	225	3	N	N	5	11	225	3	Y	N	1
12	300	inf.	Y	Y	2	12	300	inf.	N	Y	4
13	430	inf.	Y	Y	2	13	430	inf.	Y	Y	2
14	300	3	Y	N	1	14	300	inf.	Y	N	6
15	430	3	Y	Y	7	15	430	inf.	Y	Y	2
16	300	1.5	N	N	5	16	300	1.5	N	N	5
17	225	inf.	Y	N	6	17	225	inf.	N	Y	4
18	120	1.5	Y	Y	7	18	120	1.5	Y	Y	7

Table 7.5. Configuration of the curves in the tracks B-mod and B2 (d = inf. means no obstruction, M = markings, D = delineators)

Track B-mod						Track B2					
Curve #	R (m)	d (m)	M	D	Comb. ID	Curve #	R (m)	d (m)	M	D	Comb. ID
1	430	0	N	Y	3	1	430	0	N	Y	3
2	300	3	Y	Y	7	2	300	3	Y	Y	7
3	225	inf.	Y	Y	2	3	225	inf.	Y	Y	2
4	120	1.5	Y	N	1	4	120	1.5	Y	N	1
5	225	3	Y	Y	7	5	225	3	Y	Y	7
6	120	inf.	N	Y	4	6	120	inf.	N	Y	4
7	225	3	Y	Y	7	7	225	3	Y	Y	7
8	300	1.5	Y	Y	7	8	300	inf.	Y	Y	2
9	430	inf.	N	Y	4	9	430	inf.	N	Y	4
10	430	0	Y	N	1	10	430	0	Y	N	1
11	300	inf.	Y	Y	2	11	300	inf.	Y	Y	2
12	225	1.5	Y	Y	7	12	225	1.5	Y	Y	7
13	120	1.5	N	Y	3	13	120	inf.	Y	N	6
14	120	3	N	N	5	14	120	3	N	Y	3
15	225	inf.	Y	Y	2	15	225	inf.	Y	Y	2
16	300	0	Y	Y	7	16	300	0	Y	Y	7
17	430	3	N	N	5	17	430	3	N	N	5
18	430	inf.	Y	N	6	18	430	inf.	Y	N	6

Table 7.6. Characteristics of the drivers' sample for Experiment #1

	No.	Age			Driving experience		No. accidents involved in	
		min	mean	max	mean	st.dev.	mean	st.dev.
	(-)	(yrs)	(yrs)	(yrs)	(yrs)	(yrs)	(-)	(-)
Males	26	20	36.3	60	17.3	11.5	1.1	1.5
Females	15	21	30.6	54	11.7	10.0	0.5	0.5
Total	41	20	34.2	60	15.2	11.2	0.9	1.2

Notes: M = mean, SD = standard deviation

The experimental protocol entailed the following steps:
- complete a pre-drive questionnaire;
- perform pre-drive (visual and auditory) cognitive tests;
- drive on the first pre-selected track;
- rest for at least 10 minutes;
- drive on a second pre-selected track;
- perform the same cognitive tests in post-driving; and
- complete a post-drive questionnaire.

The pre-drive questionnaire was used to ascertain the good health state of drivers and the absence of medical care. Pre- and post-drive cognitive tests [5] consisted in measuring the reaction time to visual and auditory stimuli. Mean values of 15 repetitions were computed. These were used to determine which driver suffered from an attention lapse due to simulator induced fatigue (Langner et al., 2010; Zhao et al., 2012).

Driving sessions lasted 10 to 15 minutes on the basis of the adopted speed. Two driving scenarios were randomly attributed to each TD from the six possible combinations derived from the three tracks (A, A-mod, and B) driven in the two

directions (clockwise and counterclockwise). This design allowed the removal of potentially confounding factors from the analyses (McGwin, 2011). From the summary of the experiments presented in Table 7.7, it is evident that the drivers were equally distributed across the six scenarios.

With the final questionnaire, based on the one proposed by Kennedy et al. (1993), drivers were asked to declare if they experienced any kind of simulation sickness.

The characteristics of drivers' sample that was involved in the Experiment #2 are shown in Table 7.8, with the indication of the mean and standard deviation of driving experience and number of accidents involved/caused in past. Drivers age ranged between 21 and 59 years, and there were 23 (64%) males and 13 (36%) females. Also in this case, participants were voluntary people appropriately trained before the tests. The experimental task remained the same of Experiment #1.

The experimental protocol slightly changed to include also the installation and use of eye-tracking equipment. It followed these steps:
- complete a pre-drive questionnaire;
- calibration of eye-tracking glasses;
- drive on the first pre-selected track A-type;
- rest for at least 10 minutes;
- control of eye-tracking glasses calibration;
- drive on a second pre-selected track B-type; and
- complete a post-drive questionnaire.

Drives were performed in both track types (A and B) in order to exclude any memory effect on participants. Details of attributed scenarios are listed in Table 7.9, where each scenario corresponds to a certain track, traveled in clockwise or counterclockwise direction. The timing of the activities was evaluated to engage voluntary participants for less than 1 hour.

Table 7.7. Summary of assigned scenarios in Experiment #1

Scenario #	Track name	Direction	# Drivers
1	A	Counterclockwise	14
2	A	Clockwise	13
3	A-mod	Counterclockwise	13
4	A-mod	Clockwise	14
5	B	Counterclockwise	14
6	B	Clockwise	14

Table 7.8. Characteristics of the drivers' sample for Experiment #2

	No.	Age			Driving experience		No. accidents involved in	
		min	mean	max	mean	st.dev.	mean	st.dev.
	(-)	(yrs)	(yrs)	(yrs)	(yrs)	(yrs)	(-)	(-)
Males	23	21	41.7	59	21.9	10.9	1.0	1.4
Females	13	27	35.6	49	16.6	7.3	0.7	0.8
Total	36	21	39.5	59	20.0	10.0	0.9	1.2

Notes: M = mean, SD = standard deviation

Table 7.9. Summary of assigned scenarios in Experiment #2

Scenario #	Track name	Direction	# Drivers
1	A-mod	Counterclockwise	10
2	A-mod	Clockwise	9
3	A2	Counterclockwise	8
4	A2	Clockwise	9
5	B-mod	Counterclockwise	9
6	B-mod	Clockwise	9
7	B2	Counterclockwise	5
8	B2	Clockwise	13

The eye-tracking system calibration consists in the adjustment of the algorithm parameters that transform acquired images (one from the world camera, two from the eye cameras) in image coordinates (or gaze points). In *Pupil Capture*, the *Screen Marker Calibration* displays on the simulator screen several reference points which the user must focus on for a short time. The operator manages the size of the reference point and the fixation time in function of the distance between the driver and the monitor. In this study, a sampling time of 100 ms and a marker size of 1.40 units were adopted. The calibration procedure resulted in a confidence level (from 0 to 1) that the software attributes to each monitored eye. When it was lower than 90%, the calibration was repeated after a correction of cameras orientation.

The area of interest (AoI), that corresponded to the three monitors, was identified through specific markers that the software (*Pupil Player*) used for the *Offline Surface Tracker* (Figure 7.18). In particular, only half of the lateral monitors was included in the AoI for two reasons: (i) the eight markers must be always visible from the world camera; (ii) the main research interest was related to roadway elements, that mostly appeared in the central monitor. The image coordinates were recalculated by the software with respect to the dimension of the AoI, and multiple analysis techniques were offered (i.e., *Fixation Detector*). For video recordings, the world camera was set with a sampling rate of 60 Hz, while the eye cameras collected images at 90 Hz.

7.4 Pilot Studies

A pilot study was performed before each experimental campaign to test the experimental protocol, define the timing of activities, evaluate issues, and establish the data analysis mode. In both cases, reduced samples of six test drivers out of the list of participants were involved. Their data were used for the pilot study only, and were discarded from the analysis.

The test of the Experiment #1 elicited the following observations:
- the designed scenarios were reproduced in fluid simulations, without any lag or flickers of images;
- each participant was engaged for 45 minutes;
- a methodology to transpose collected data from time to space (station) reference system was required (later described in §7.5).
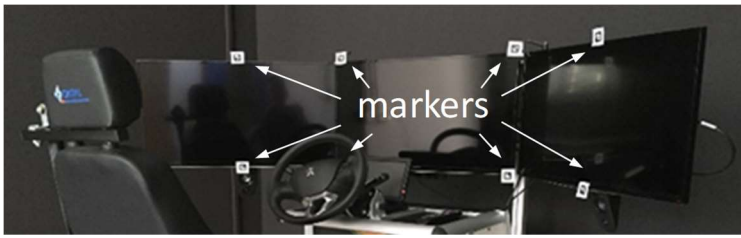
Figure 7.18. Position of the markers on the screens to define the area of interest

For the Experiment #2, from main outcomes it was deduced that:

- high confidence level of pupil detection required an adequate position of the cameras and calibration of the system;
- the use of eye shadow, eyeliner, and mascara must be avoided by women;
- the use of glasses was not compatible with the device; no problems were encountered in case of contact lenses;
- some checks for correct calibration must be carried out during the experiments;
- voluntary participants need to be involved for less than 1 hour each;
- a strategy to spatially synchronize simulator and eye-tracking data was needed.

Specifically, the 2d pupil detection was preferred to the 3d one: even if the 3d pupil detection is more accurate, it requires more time for setting and information provided was not relevant for research purposes. Moreover, the use of make-ups introduced noise during the calibration process, reducing the confidence level of collected data from the device. Conversely, contact lenses did not create disturbance to IR cameras.

The correct calibration of the eye-tracker must be tested before starting and at the end of each drive. This consisted of fixating three elements in the simulator screen, placed at a different distance from the observer. If discrepancies between the elements and gaze points were evident, their position could be corrected in post-processing by means of *Pupil Player*.

Road markings along curvilinear elements were modified in the virtual model to synchronize simulator and eye-tracking spatial data. If present, the road centerline was set as continuous, while dashed along tangents. In such way, during the frame-by-frame analysis the operator had spatial references of the initial and final points of the elements of interest.

7.5 Data Collection and Treatment

The driving simulator acquires data in the time domain. As the events (curves with specific ASD) were spatially distributed along the track, a conversion of the reference system was required. As mentioned, road logics information was used to define an algorithm that associated the measures to a specific road station. The problem was divided in two parts: (i) by computing the abscissa increments ($\Delta_{abscissa}$) between two samplings i and $i+1$; (ii) by referring data to the same road station (s) with a predefined discretization.

The (i) step was faced considering these three conditions:

1. i and $i+1$ recordings belong to the same road ID.

$$\Delta_{abscissa}(i+1) = Roadabscissa(i+1) - Roadabscissa(i) \qquad \text{(eq. 20)}$$

2. i and $i+1$ recordings belong to different road IDs.

$$\Delta_{abscissa}(i+1) = Roadlength_{(Road\,ID_i)} - Roadabscissa(i) + $$
$$+ \, Roadabscissa(i+1) \qquad \text{(eq. 21)}$$

3. i or $i+1$ recordings belong to the intersection area. The software did not attribute an abscissa to the vehicle positions inside intersections; thus, the traveled distance between two successive points was computed by multiplying the mean speed (in km/h) for the fixed sampling time (0.1 s).

$$\Delta_{abscissa}(i+1) = 0.1 \cdot \frac{Speed(i+1) + Speed(i)}{2 \cdot 3.6} \qquad \text{(eq. 22)}$$

The simplification introduced in (i.3) allowed the production of continuous speed profiles, and did not affect the data analyzed in further Sections. The road station s was computed as follows:

$$s(i+1) = s(i) + \Delta_{abscissa}(i+1) = $$
$$= \left(\sum_{i=1}^{i} \Delta_{abscissa} \right) + \Delta_{abscissa}(i+1) \qquad \text{(eq. 23)}$$

In the (ii) step, data were extrapolated from the recorded data in order to obtain a values every 1 m.

In Experiment #1, cognitive tests that measured reaction times to visual and auditory stimuli were conducted before and after the simulation sessions. According to Ting et al. (2008), excessive simulated driving times may contribute to fatigue in drivers leading to increased reaction times to stimuli. The average and standard deviation (SD) results for the drivers' sample are synthetized in Figure 7.19.

Results did not indicate any differences between the mean reaction times before and after the auditory and visual stimulus (i.e., difference Δ is lower than 5.3 ms). Similar conclusions were drawn from a comparison of the differences between before and after reaction times for each individual, thus confirming that no fatigue effects were observed in drivers involved in the experiments.
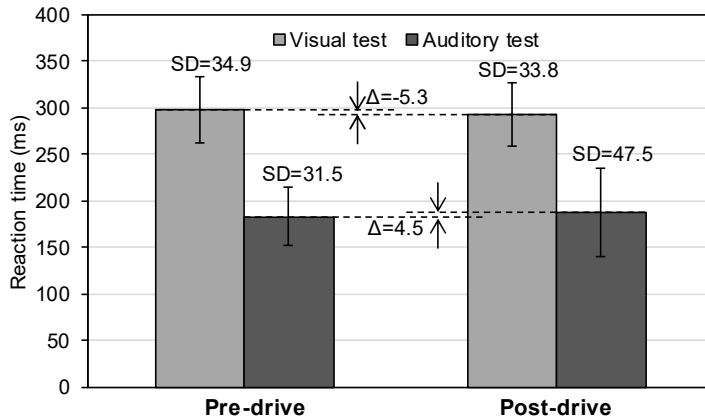
Figure 7.19. Pre- and post-drive visual and auditory reaction times (mean and standard deviation, SD) from the cognitive test of drivers involved in Experiment #1

Table 7.10 reports a summary of drivers' answers to the simulator sickness questionnaire: in few cases only, drivers declared symptoms that revealed a moderate degree of sickness. However, their performance on cognitive tests denoted a reduced Δ_i (difference between reaction times after and before the drives) for both visual and auditory tests, and they preserved their ability to drive for the whole experiment. For these reasons, their data were employed in further analyses.

The amount of driven curves was equal to 1,476; however, data referred to 67 curves were removed from the database due to the presence of a vehicle ahead, that influenced free-flow conditions. Analyzed speed data were restricted to the circular arc of curved sections only, excluding the entering and exiting spirals. Since curve length was variable, a normalized length (ratio between the distance from the initial point of the circular arc and the total arc length) was estimated to merge data collected from different curve lengths. Each curved section was discretized into 100 sub-sections and the average speed on each of them was then considered for the formation of speed profiles.

On the other hand, some curved sections were characterized by the presence of elements on the roadside (container, parked vehicles, cones; §7.2.1), that affected trajectory and speed data. Data from those 313 curves were completely neglected, as well as 9 curves where drivers accidentally exited from the carriageway. Hence, the number of analyzed curves was 1,103. Trajectory data were used to show the adopted paths of TDs in different curves, and to compute the standardized dispersion of trajectory (DT^S) as per the formula:

$$DT^S = \frac{DT}{L} \tag{eq. 24}$$

where L is the length of the observed segment (50 m of approaching and departure tangents, spirals, and circular arc).

Table 7.10. Summary of test drivers' symptoms after driving simulations of Experiment #1

Symptoms	None	Low	Moderate	High
General discomfort	68%	28%	2%	0%
Fatigue	83%	15%	2%	0%
Headache	68%	28%	2%	0%
Eyestrain	49%	46%	5%	0%
Difficulty focusing	81%	17%	2%	0%
Increased salivation	93%	7%	0%	0%
Sweating	88%	12%	0%	0%
Nausea	76%	17%	7%	0%
Difficulty concentrating	80%	20%	0%	0%
Fullness of head	56%	37%	7%	0%
Blurred vision	86%	12%	2%	0%
Dizziness	68%	32%	0%	0%
Vertigo	90%	10%	0%	0%
Stomach awareness	88%	10%	2%	0%
Burping	95%	5%	0%	0%

Table 7.11 shows the responses to post-drive questionnaires for Experiment #2. It is worth noting that one participant (TD#16) showed high level of both fatigue and eyestrain, and her/his data were excluded from the analysis. Furthermore, moderate level of eyestrain was reported by other five TDs: from the experience of previous works, it was presumably induced by the heating of the eye-tracking glasses but not by the simulator.

In addition to longitudinal and transversal measurements, information on drivers' fixations was collected by means of eye-tracking glasses. The total number of traveled curves was equal to 1,296. However, 36 observations were removed for simulator sickness, data of 52 bends were discarded for eye-tracker inaccuracies (too low confidence level), and three drives (54 observations along curves) were excluded due to the excessive aggressiveness of TDs (see §4.1.1 for discrimination criteria).

Table 7.11. Summary of test driver symptoms after driving simulations of Experiment #2

Symptoms	None	Low	Moderate	High
General discomfort	69%	28%	3%	0%
Fatigue	80%	14%	3%	3%
Headache	83%	17%	0%	0%
Eyestrain	33%	50%	14%	3%
Difficulty focusing	75%	19%	6%	0%
Increased salivation	94%	6%	0%	0%
Sweating	78%	19%	3%	0%
Nausea	83%	17%	0%	0%
Difficulty concentrating	86%	11%	3%	0%
Fullness of head	78%	22%	0%	0%
Blurred vision	83%	14%	3%	0%
Dizziness	89%	11%	0%	0%
Vertigo	97%	3%	0%	0%
Stomach awareness	94%	6%	0%	0%
Burping	100%	0%	0%	0%

Eye-tracking recordings consist of several files, among which the most relevant are the *pupil data*, and the video (*.mp4*) of the world camera. The former contains information both on the driver's pupil (detection method, confidence level, *x* and *y* position with respect to the reference system of the headset, etc.) and on eye activity (e.g., gaze position with respect to the reference surface). These data were associated with a single frame and with a unique recording time (timestamp, in ms).

Gaze positions were collected on *Pupil Player* by means of a frame-by-frame analysis to obtain fixation location and duration. For this purpose, the software has a dedicated plugin (*Offline Fixation Detector*) that identifies fixations as groups of consecutive points within a specified dispersion, or maximum separation.

Fixations typically have a duration equal to or greater than 100 ms (Salvucci and Goldberg, 2000). Thus, the plugin quantified the time in which the gaze was intent in a specific area of the image, on the basis of three inputs:

- Maximum Dispersion (in degrees), that measures the maximum distance between gaze points within the same fixation. It was set to 2°, according to Crundall and Underwood (1998);
- Minimum Duration (in ms), which is the lower threshold for fixation detection. It was set at 100 ms, according to the definition above;
- Maximum Duration (in ms), that is the maximum time length of a fixation. It was set at 1000 ms.

Fixations information was exported in a *.csv* file. For instance, data collected along curve #11 of track A2 for TD#18 were displayed in Figure 7.20. Fixation durations were variable and dispersed along the curve; the figure evidences the elements that the driver fixated while traveling, i.e. the road centerline and the left margin. In the whole cases, the employed vision mechanism was the "1a", for a total duration of 7.231 s (35% of the curve travel time). In the rest of the time, the driver used saccades to acquire information from the surrounding environment.
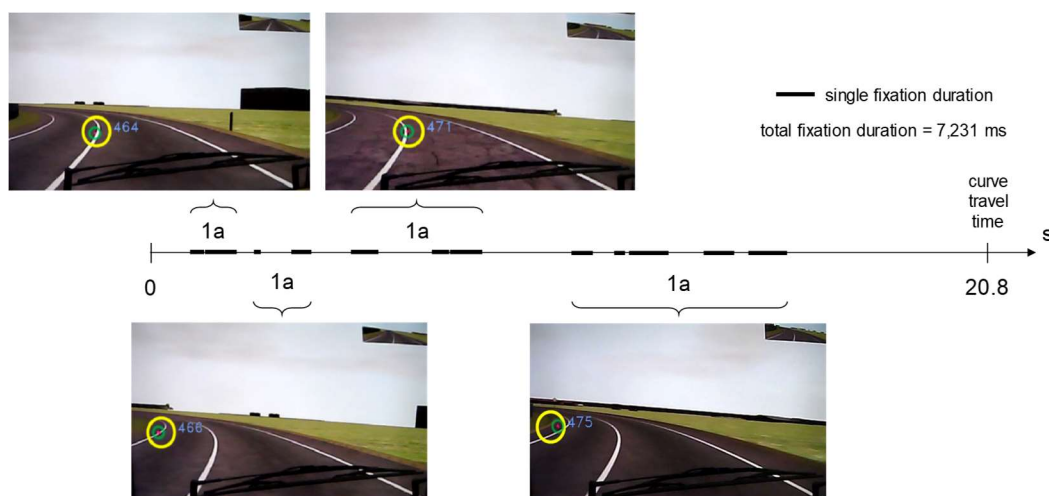
Figure 7.20. Chronological sequence of fixations adopted by TD#18 along curve #11 of track A2

Finally, the use of brake pedal was monitored in both experiments. In Part A of this document, the criticalities of this simulator component were highlighted for the different feeling with respect to actual vehicles. Curve negotiation implies the adjustment of vehicle trajectory and speed, that can be performed through the release of the throttle pedal or the use of brake.

However, collected data revealed that participants used the brake along seven curves of 1,103 in the Experiment #1, and approaching to five curves of 1,154 in the Experiment #2. Details on brake use are reported in Figure 7.21 and Figure 7.22, with the indication of test driver ID, and location along the different tracks. This observation evidenced the importance of the drivers training before the experiment, that allowed them to keep confidence with the equipment. They also developed different compensation strategies for speed regulation. As in real driving, participants reduced vehicle speed by reducing the pressure on gas pedal or by using the engine brake.
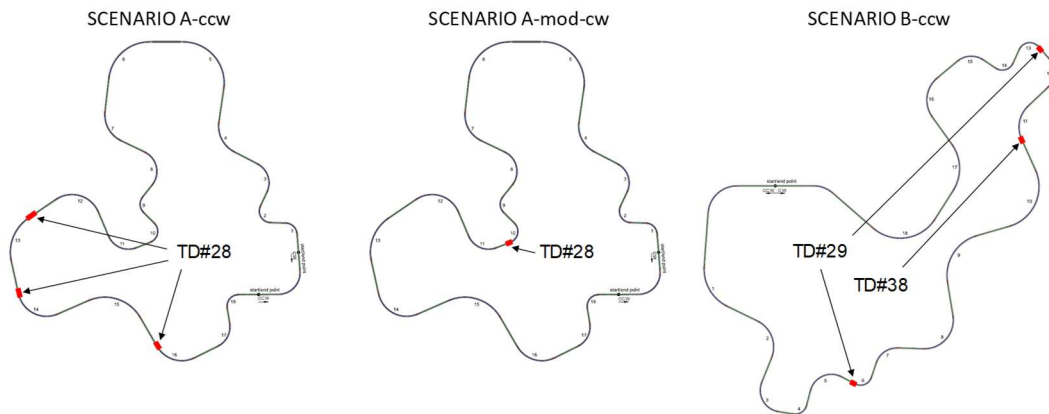
Figure 7.21. Locations of brake pedal use for the scenarios of Experiment #1 (cw = clockwise; ccw = counterclockwise)
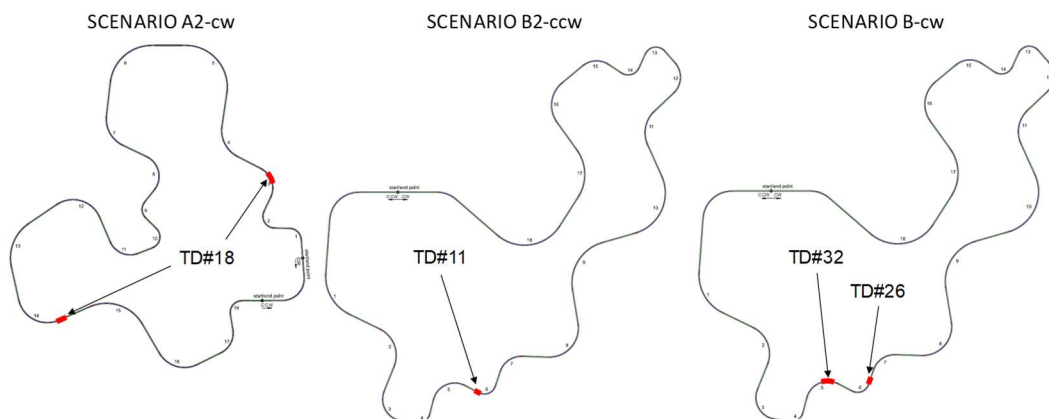
Figure 7.22. Locations of brake pedal use for the scenarios of Experiment #2 (cw = clockwise; ccw = counterclockwise)

8. Results and Discussion

This Section presents and discusses the data analysis of both experiments. For Experiment #1, driving speed profiles were firstly evaluated along different curve configurations, and then mean speeds were correlated to ASD values. A similar analysis was performed on vehicle trajectories: profiles of the lane gap on each curve at first, and the mean values of the dispersion of trajectory versus the ASD after were elaborated. In both cases, the Analysis of Variance (ANOVA) was used to identify the significance of research variables. Data from Experiment #2 were employed to evaluate the different vision mechanisms adopted and the effects on driving operations (speed and trajectory). Dedicated analyses were developed to find out how experienced/novice and aggressive/prudent drivers behaved in the same driving scenarios.

8.1 Speed Profiles along Curves

Figure 8.1 shows the average speed profiles along the circular arcs, as a function of the normalized curve length. Results were subdivided on the basis of radius, hand of curve, and distance of the sight obstruction from the shoulder (d). The case of no sight obstruction in the inner side of curves ("d∞" in Figure 8.1) was also included in the plots.

Speed data along the curves exhibit different trends depending on the hand and radius magnitude. Data in Figure 8.1 show that speed increases when the curve radius increases, a finding which is consistent with previous studies (Calvi, 2015b; Bella, 2013; Ben-Bassat and Shinar, 2011; Van Winsum and Godthelp, 1996). This indicates that drivers were able to distinguish differences in curvature between the road sections selected for investigation. Figure 8.1 also shows that sharp curves with radii of 120 m imposed a reduction in speed along their length, as a result of an excessive speed when the driver was travelling along the straight section and transition preceding the curve.

Conversely, drivers tended to accelerate along curves of higher radii, thus suggesting a more prudent speed choice before entering the curve (in line with findings of Montella et al., 2014). These behaviors reflect that drivers adjusted their speeds in accordance to curves of different radius magnitude, a phenomenon previously observed both in simulated (Coutton-Jean et al., 2009) and in real driving (Imberg and Palmberg, 2015).
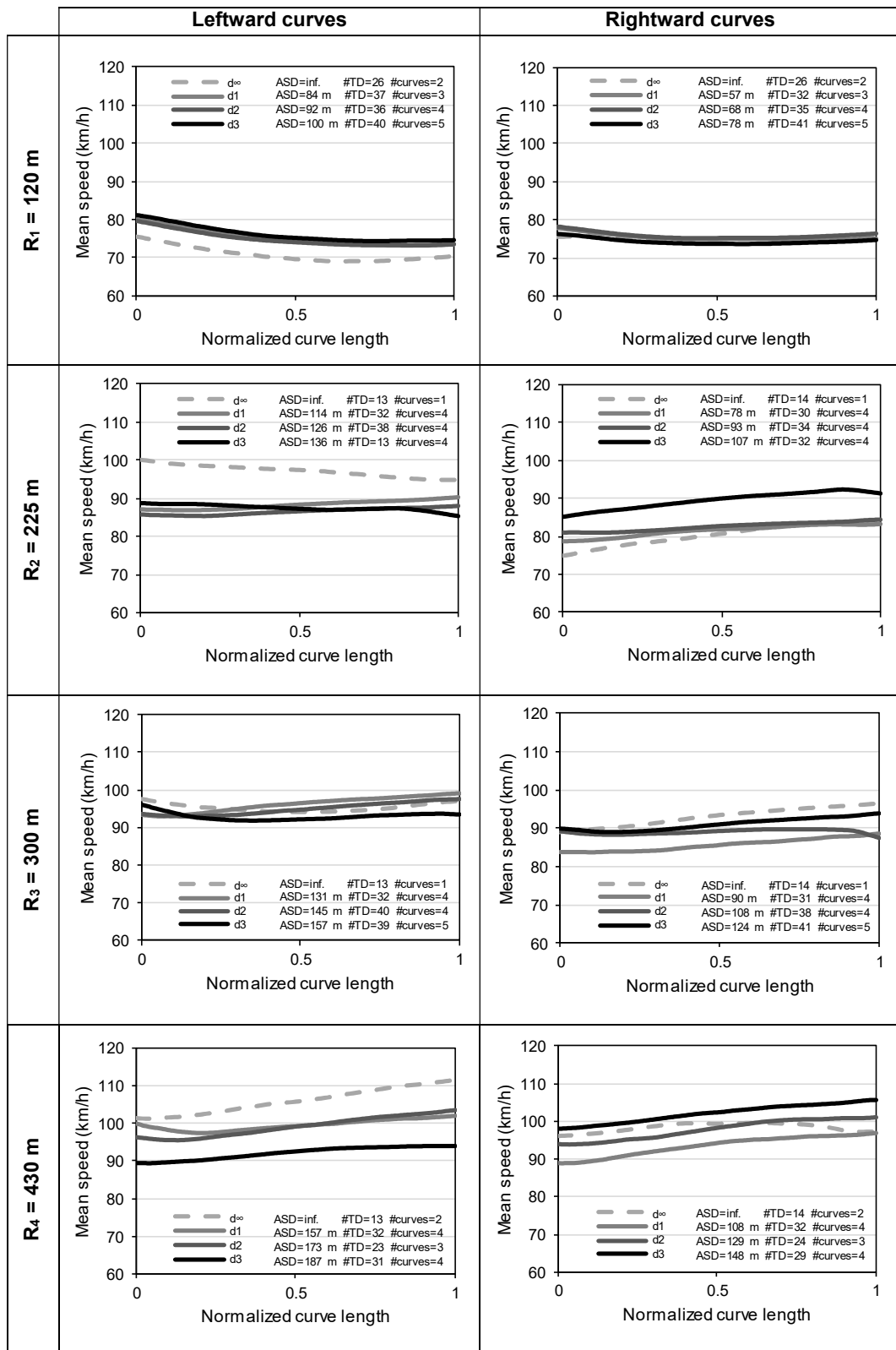
Figure 8.1. Average speed along arcs of different radius and hand, with and without sight obstructions (d1 = 0 m, d2 = 1.5 m, d3 = 3 m). Data in labels include the computed ASD, the total number of test drivers that travelled on that curve (#TD), and the number of curves considered (#curves)

In the curve of minimum radius (120 m), a lateral acceleration value of 0.42·g was recorded at 80 km/h. This value is slightly higher than the limit of 0.4·g which implies a linear interaction between tire and road at the contact (Doumiati et al. 2010). For curve radii equal to or greater than 225 m, the lateral acceleration was always lower than this limit (0.4·g) in the case of higher speeds as reported in Figure 8.1. Doumiati et al. (2010) asserted that when the tire operates in the non-linear region, a vehicle (real or simulated) tends to respond in a less predictable fashion. In fact, in this experiment the general behavior of drivers resulted in lateral accelerations which fell mostly within the expected handling region assumed by drivers in real driving conditions. This was also the case with the results for the minimum radius curve considered here.

Along leftward curves of 120 m in radius, drivers who had not been affected by sight obstructions ("d∞" line in Figure 8.1) tended to drive slower than those who, conversely, had a reduced ASD since they were conditioned by small d values. When the radius increased, the absence of sight obstructions led to an increase in driving speeds, with values higher than those recorded when d was limited to the range 0-3 m. Along curves of 430 m in radius, a correlation between speed and the position of the lateral obstruction was observed. Surprisingly, drivers tended to assume a more prudent speed behavior when d increased. When the obstruction was not present, drivers were observed operating at the maximum speeds.

Along rightward curves without sight obstruction, drivers always maintained a speed similar to that assumed when $0 \leq d \leq 3$ m. However, it was observed that when d increased, speed increased as well. Drivers benefitted from a higher d value, so they adjusted their speed in light of the more favorable sight conditions.

The variability of individual attitudes may also contribute to these substantial differences in longitudinal behaviors between left- and rightward curves. Drivers used different vision mechanisms for curve negotiation, which were mainly influenced by road characteristics and driver experience. Further discussion is postponed in §8.7 and §8.8.

8.2 Speed vs. Available Sight Distance

In a second analysis, considering the fact that speed data are affected by limited adaptation to curve conditions, the mean (M) and the standard deviation (SD) of all the speed values (*n*) collected along the circular arcs were estimated (Table 8.1), and shown in Figure 8.2. The dispersion of speed data around the mean (M) value reflects the variation in the speed values chosen by participants, results which are also evident in the field as a consequence of the range of behaviors and attitudes exhibited by the general driver population (Bassani et al., 2014). Data dispersion was also due to the fact that drivers adjusted their speeds along curves as discussed previously.

It is worth noting that in the case of curve of 120 m, SD values are, on average, lower than those for higher radii. Lower SD values occur for leftward curves without sight obstructions (11.6 km/h), and the corresponding rightward condition induces a SD of 12.4 km/h, which is close to the lower limit of those recorded on curves with obstructions (ranging from 12.2 to 14.9 km/h).

In the case of curves with a radius equal to or greater than 225 m, the SD values for unrestricted visibility conditions, on rightward curves, are lower than those measured in cases where $0 \leq d \leq 3$ m. The opposite is observed on leftward curves. Eventually, as is true for mean speed (M), the average SD increases with an increase in the radius, both for right- and leftward curves.

Table 8.1. Mean (M) and standard deviation (SD) of speed data collected along the circular arcs (n is the number of drivers travelling on this kind of curve) for different combination of radius (R) and distance of the obstruction from the roadway (d) and the trajectory (D). Symbol ∞ indicates that no sight obstruction was used, so ASD values are assumed to be higher

| R | Leftward curves | | | Speed | | | Rightward curves | | | Speed | | |
	d	D	ASD	M	SD	n	d	D	ASD	M	SD	n
(m)	(m)	(m)	(m)	(km/h)	(km/h)	#	(m)	(m)	(m)	(km/h)	(km/h)	#
120	0	7.125	83.76	75.2	14.7	41	0	3.375	56.61	75.2	13.9	41
	1.5	8.625	92.25	74.9	12.2	54	1.5	4.875	68.11	76.0	14.9	52
	3	10.125	100.06	76.3	13.6	65	3	6.375	77.97	74.2	13.1	67
	∞	∞	∞	70.9	11.6	26	∞	∞	∞	75.3	12.4	26
225	0	7.125	114.02	88.4	14.1	55	0	3.375	77.72	81.5	16.4	50
	1.5	8.625	125.52	86.6	13.3	49	1.5	4.875	93.46	82.6	14.7	49
	3	10.125	136.07	87.6	13.7	52	3	6.375	106.93	89.6	12.9	53
	∞	∞	∞	97.2	16.4	13	∞	∞	∞	80.3	11.0	14
300	0	7.125	131.43	96.1	14.7	52	0	3.375	89.80	85.7	17.3	53
	1.5	8.625	144.67	94.8	14.1	51	1.5	4.875	107.98	89.1	14.9	52
	3	10.125	156.81	92.8	16.1	61	3	6.375	123.53	91.0	15.7	68
	∞	∞	∞	95.3	17.6	13	∞	∞	∞	93.0	13.3	14
430	0	7.125	157.11	99.5	15.5	52	0	3.375	107.59	93.5	18.2	55
	1.5	8.625	172.91	99.1	14.4	42	1.5	4.875	129.34	98.0	19.4	37
	3	10.125	187.40	92.2	12.4	52	3	6.375	147.95	102.1	15.4	46
	∞	∞	∞	105.9	19.4	26	∞	∞	∞	98.4	13.9	28

(A)   (B)
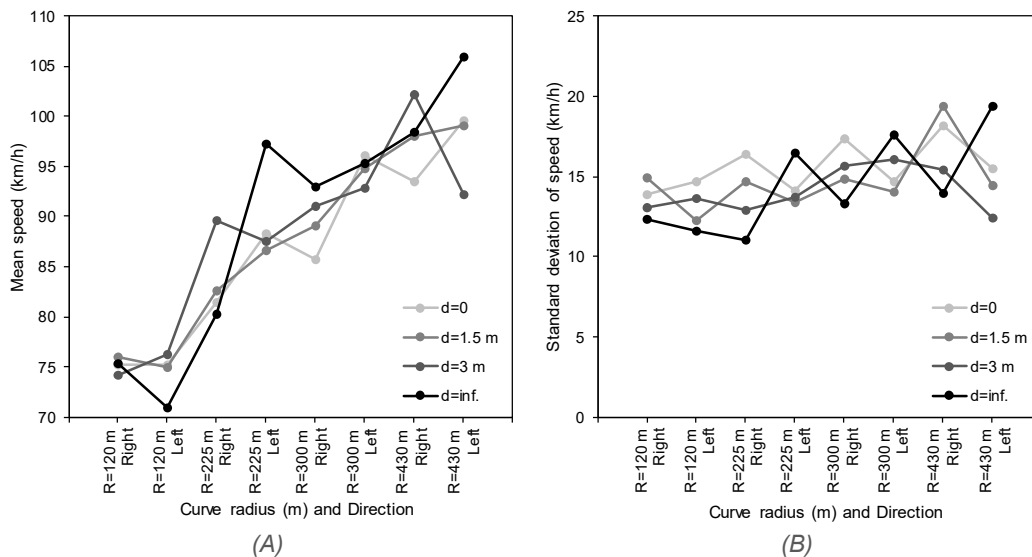
Figure 8.2. Mean and standard deviation of speed computed for the different combinations of curve radius and direction of travel

The results presented in this Section reflect the different responses of drivers to these specific conditions, in which the presence or absence of certain elements may trigger different visual mechanisms and individual driving abilities along curves.

Figure 8.3 exhibits the relationship between the mean speeds (Table 8.1) with the ASD in curves affected by sight obstruction only (please, note that data referred to $d = \infty$ were not represented, but simply indicated with an arrow oriented up or down if higher or lower than the data referred to $d = 3$ m). The different connections between points in the two graphs (Figure 8.3A and Figure 8.3B) reflect the two possible ways in which data can be interpreted: linking data obtained from experiments carried out with the same distance d (Figure 8.3A), and linking those obtained from experiments characterized by the same curve radius (Figure 8.3B).

Figure 8.3A emphasizes the direct proportionality between speed and ASD: when ASD increases speed increases too. As a result, the ASD affected the speed decision of drivers, the evidence for which was observed on both left (dashed lines) and right (continuous lines) curves. For the same ASD value, drivers adopted greater speeds as the distance d of the sight obstruction from the shoulder decreased; this means that the presence of a continuous element on the roadside provides a guidance effect to drivers, and reduces her/his perceived risk. Nonetheless, drivers were not able to discriminate between driving scenarios with the same ASD and to adjust their speed accordingly, demonstrating that the visual perception of curvature has a significant impact on driver speed choice. These observations were not evidenced by Moreno et al. (2013), since they used a single curve radius (265 m), and an ASD ranging from 109 to 198 m.

Along curves with $R = 120$ m, the mean speed remains almost constant even if the sight distance increases, both on right- and leftward curves (Figure 8.3B). This confirms that for small radii, speed choice has a strong correlation to the curvature captured from the inflection of road markings and roadsides. However, in the case of right curves with radii greater than 120 m, when ASD increases, so does speed while the opposite trend can be observed for left curves. Thus, on curves of the same radius, the proximity to the lateral obstruction induced drivers to travel prudently along rightward bends, and more fast along leftward ones (only for curves greater than 225 m in radius).

Figure 8.3B also includes the trend for unrestricted sight conditions (arrows on the right of "$d = 3$ m" series). Without sight obstructions along curves of $R \geq 225$ m, an increase in the average driving speed is evident in case of left curves. Like previous observations, it is the critical geometry of sharp curves ($R = 120$ m) independently of their ASD values which mostly influences driver speed decisions, a finding which emphasizes the relevant effect of road space guidance elements.

For validation purposes, the speed data collected in the Experiment #2 was treated accordingly to those presented up to here. Particular attention was given to free-flow speeds, and unconditioned data only. Furthermore, curves without horizontal markings (Combination ID #3, #4, and #5), were neglected in this analysis.
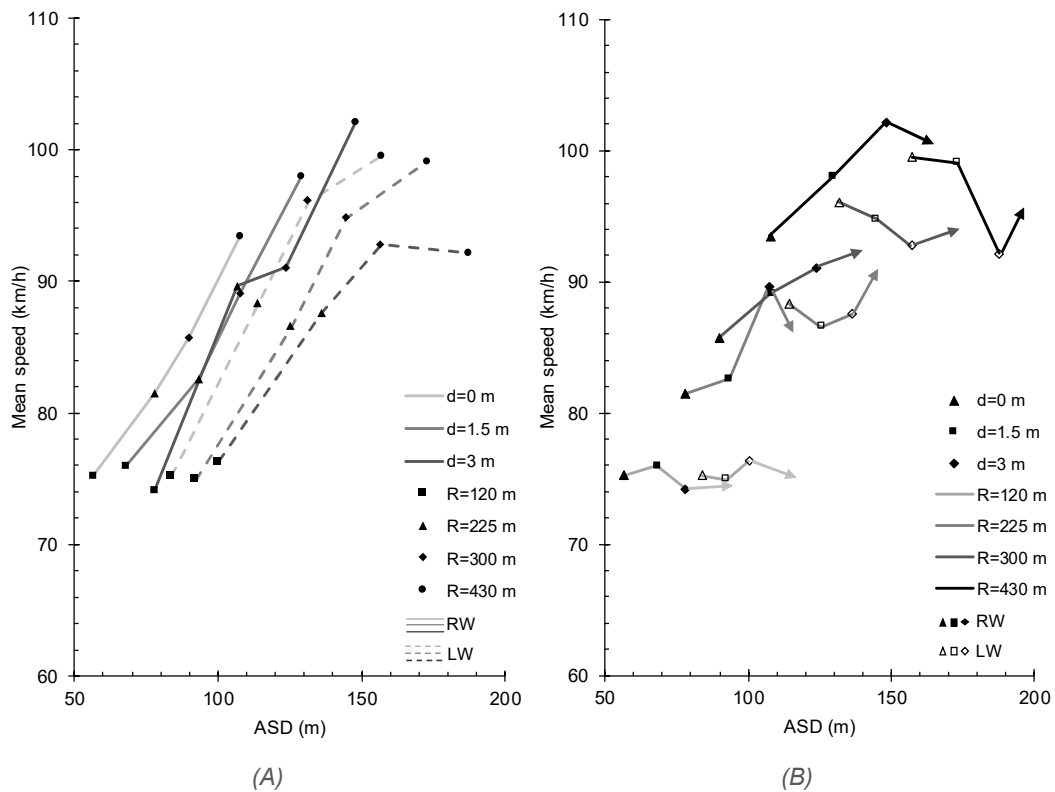
Figure 8.3. Relationship between ASD and average speed: data connected on the basis of distance of sight obstruction from the shoulder (A), and data connected on the basis of curve radius (B)

Figure 8.4A shows the match between the mean speed computed in Experiment #1 and #2, respectively. It is worth noting that the majority of values is closer to the equality line (dashed line). Only few points show a difference of mean speeds greater than 10 km/h (e.g., RW-300 m, LW-430 m). Similarly, the comparison of standard deviation of speed evidences that values are grouped nearby the equality line, with a higher discrepancy of 5 km/h (Figure 8.4B).
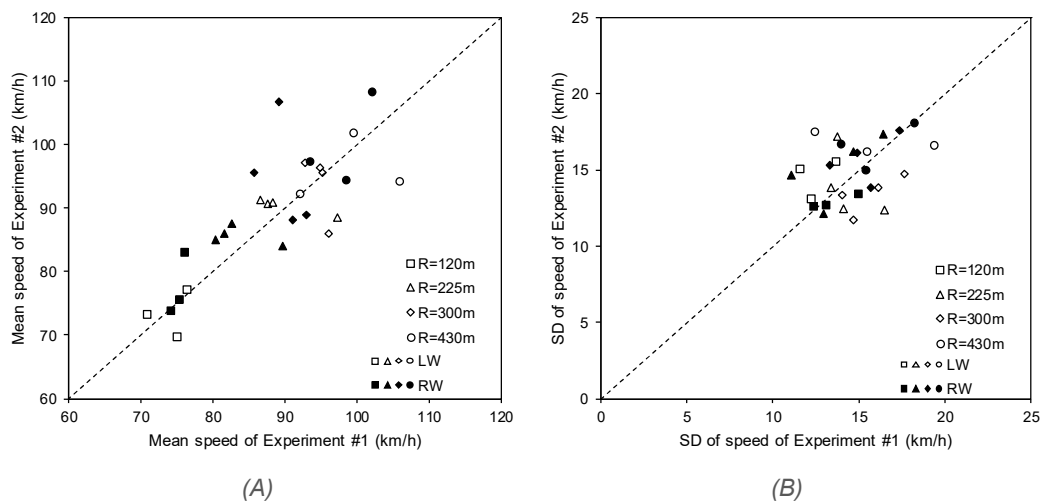
Figure 8.4. Comparison of mean and standard deviation (SD) of speed calculated for the two experiments for validation purposes

This comparison validates the Experiment #1, since it demonstrates that both drivers' sample produced comparable results, revealing the robustness of data and outcomes.

8.3 Significant Variables and Interactions

To support the inferences drawn from Figure 8.3, an ANOVA was performed by using R software (v3.1.1) to evaluate the significance of the investigated variables on the average speed (R Core Team, 2016). In this analysis, the mean speed along each investigated circular curve was repeatedly used as a measurement variable for drivers. The ANOVA was performed in two different ways: a 3-way ANOVA where the main effects were curve direction (*dir*), radius (*R*) and offset of the lateral obstruction from the road edge (*d*); and a 2-way ANOVA with radius (*R*) and aggregated distance (*D*) regarded as principal effects. The two ANOVAs were carried out to determine if *d* (the distance of sight obstruction from the carriageway) or *D* (the offset of the sight obstruction from the trajectory) had more influence on the driver speed decision in this experiment. In addition, Eta-squared (η^2) and partial Eta-squared (η^2_p) were computed to determine the variables effect size in ANOVA. In particular, the first measures the proportion of variance in dependent variable (e.g., speed) explained by the different groups defined for independent variables; partial Eta-squared is the variation of dependent variable associated with a given predictor, after excluding variance explained by the other ones (Richardson, 2001). In general, the Eta-squared is more conservative than the partial coefficient since it returns smaller or equal values.

In both cases, the statistical analysis required the speed datasets to be normally distributed. In the first step, the original speed samples which produced the data shown in Table 8.1 were subjected to the Chi-square test assuming a confidence level of 95% (χ^2_{crit} = 5.99). Results revealed that 29 out of 32 datasets were normally distributed, while the three that did not pass the test were not far from compliance (χ^2 / χ^2_{crit} equal to 1.02, 1.11, and 1.30, respectively).

Table 8.2 lists the results of the 3-way ANOVA clearly indicating that the radius (*F(3,1377)* = 154.57, *p* < .001, η^2 = .243) is the variable which has the most significant influence on operating speed, as well as on the direction of travel (*F(1,1377)* = 9.33, *p* = .002, η^2 = .005), while the offset of the lateral sight obstruction (*d*) was found to be insignificant (*F(3,1377)* = 1.24, *p* > .05, η^2 = .002). Therefore, the radius explains the 24.3% of the variation among speed values, whereas the direction of travel and distance *d* of lateral sight obstruction contribute less than 1% to the outcome variance. The offset *d* becomes significant in the interaction with the direction of travel (*F(3,1377)* = 5.14, *p* = .002, η^2 = .008), which means that the position of the sight obstruction plays a different role when evaluated on left- or right-hand curves. Other interactions between influencing factors are less significant and can be disregarded when explaining the variation in average speeds. Lastly, the proportion of speed variance that cannot be explained by designed variables is 72%.

Table 8.2. Results of 3-way ANOVA on driving speed

Principal Effects	Degree of Freedom	Sum of Squares	Mean of Squares	*F* value	Pr(>*F*)	η^2	Partial η^2	code
Direction (left/right hand), *dir*	1	2052	2052	9.334	0.00229	0.005	0.007	**
Radius, *R*	3	101946	33982	154.567	< 2.2e-16	0.243	0.252	***
Distance, *d*	3	820	273	1.243	0.29267	0.002	0.003	
Interaction Effects								
dir*R	3	1952	651	2.960	0.03129	0.005	0.006	*
dir*d	3	3387	1129	5.136	0.00156	0.008	0.011	**
R*d	9	2089	232	1.056	0.39308	0.005	0.007	
dir*R*d	9	4643	516	2.347	0.01259	0.011	0.015	*
Residuals	1377	302738	220			0.721		

Notes: significance of codes is 0 '***', 0.001 '**', 0.01 '*', 0.05 '.', 0.1 ' ', 1

The 3-way ANOVA confirmed the influence of the radius on driving speed. As already documented in previous studies (Said et al., 2009; Van Winsum and Godthelp, 1996), low curvatures facilitate the adoption of higher speeds since they generate reduced lateral accelerations. Although lateral acceleration cannot be detected on a fixed-base driving-simulator, drivers limited their speed on sharp curves for driving comfort based on their experience from real-life driving conditions. Furthermore, the second factor affecting speeds is curve direction (Table 8.2); the influence of direction is reduced in the case of sharp curves while it becomes dominant for wider radii, revealing also the significance of the interaction between *dir* and *R* ($F_{(3,1377)} = 2.96$, $p = .031$, $\eta^2 = .005$).

Bella (2013) found significant differences in speed between right- and left-hand curves in the 200 to 400 m range, consistent with the conclusions of this study. Conversely, Calvi (2015b) stated that only radius magnitude affected driver speed choice. In this case, any difference with respect to this investigation are attributed to roadside elements used in the various driving scenarios, which influence driver perceived safety levels and trigger specific visual mechanism strategies.

Results from this work confirmed the hypothesis of the influence of ASD on driver preferred speed along medium and shallow curves, although it is not the only factor affecting driver speed choice. The 3-way ANOVA carried out in this research revealed that the distance of the lateral wall from the road edge did not affect driver preferred speed. A sight obstruction was placed at three different offsets from the same shoulder, while in a previous investigation the traffic barrier used as a sight obstruction was offset by increasing the shoulder width. According to Ben-Bassat and Shinar (2011), when the lateral barrier is present, the operating speed on rightward curves increases in line with an increase in the distance of the obstruction from the road edge. The same wall provided a consistently higher sense of guidance on the right side than on the left one.

On the basis of previous outcomes, the aggregated distance *D* was used instead of the distinguished effects *direction* and *d* to perform a 2-way ANOVA, which returns the results listed in Table 8.3. In this case, speed samples were grouped as a function of the four radii and the seven road configurations (six with sight obstructions and one without). The outcomes confirmed the high significance of both *R* ($F_{(3,1381)} = 153.57$, $p < .001$, $\eta^2 = .243$) and *D* ($F_{(6,1381)} = 4.07$, $p < .001$, $\eta^2 = .013$), while their interaction proved to be fairly significant ($F_{(18,1381)} = 1.64$, $p < .05$, $\eta^2 = .016$).

Table 8.3. Results of 2-way ANOVA on driving speed

Principal Effects	Degree of Freedom	Sum of Squares	Mean of Squares	*F* value	Pr(>*F*)	η^2	Partial η^2	code
Radius, *R*	3	101985	33995	153.5676	< 2.2e-16	0.243	0.250	***
Distance, *D*	6	5408	901	4.0715	0.00047	0.013	0.017	***
Interaction Effects								
*R*D*	18	6525	362	1.6375	0.04445	0.016	0.021	*
Residuals	1381	305710	221			0.729		

Notes: significance of codes is 0 '***', 0.001 '**', 0.01 '*', 0.05 '.', 0.1 ' ', 1

This confirms the relevance of the radius (24.3%) and the effective distance *D* from the sight obstruction (1.3%) in affecting speed variance. The results from the 2-way ANOVA suggested that the distance between the sight obstruction and driving trajectory was the significant factor rather than the offset of the same obstruction from the roadway. This outcome reaffirmed the relevance of ASD when assessing driver behavior.

8.4 Trajectory Curvature Analysis

The adopted trajectory can be geometrically described in terms of curvature. The software *SCANeR™studio* collects the curvature value (in 1/mm) for each point of the traveled path, with a frequency of 10 Hz. Curvatures gathered along circular arcs were used to estimate the mean radius of curvature of the trajectory ($R_{trajectory,i}$) through the formula:

$$R_{trajectory,i} = \frac{1}{c_{t,i}}$$

(eq. 25)

where $c_{t,i}$ is the average value of curvature corresponding to the *i*-th curve with a specific configuration (in terms of *R* and *d* parameters).

Figure 8.5 shows the plots of the differences (ΔR) between the radius of the trajectory ($R_{trajectory,i}$) and the radius of the alignment (R_{design}) as a function of the design radius equal to 120, 225, 300, and 430 m. Specifically, Figure 8.5A reports the box-plots of all collected data (1,103 curves), distinguished in rightward (RW) and leftward (LW) bends; while Figure 8.5B displays the mean values only, computed for the different distances *d* of the sight obstruction from the road shoulder. The values referred to different R_d are connected through solid lines for rightward curves, and dashed lines for leftward ones.

The higher the R_{design}, the greater the dispersion of ΔR. Such differences are almost distributed across zero for RW bends, whereas the majority of data are concentrated in the positive part of the graph for LW curves, meaning that the adopted radius of curvature is larger than that of the alignment.
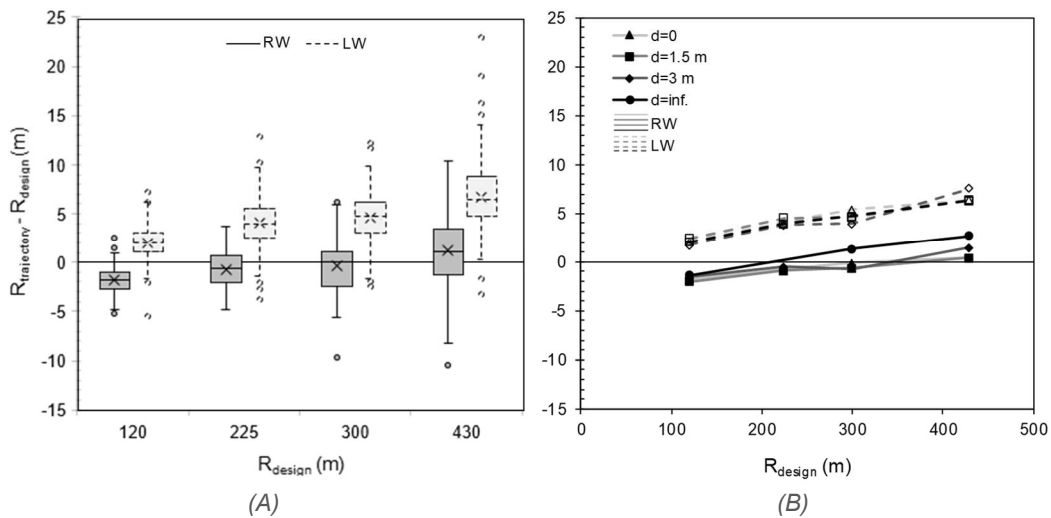
Figure 8.5. (A) Box-plot of ΔR = R_t – R_d data computed on the observed curves, distinguished in rightward (RW) and leftward (LW); (B) Mean ΔR values referred to different d distances are connected through solid (rightward curves) and dashed (leftward curves) lines

Trends in Figure 8.5B shows that ΔR values increase as the R_d increases. Along rightward curves, ΔR is negative when $R_d \leq 300$ m and the sight obstruction was present, indicating that the turning maneuvers was sharper than the ideal one. It seems that individuals initially moved to the center of the carriageway to increase the perceived ASD, and then steered to abrupt correct the trajectory. Further analyses of lane gaps may confirm this behavior (§8.5). Only when $R = 430$ m the ΔR is positive for all cases, suggesting that drivers "cut" the curves, moving to the right side of the lane.

It is evident in Figure 8.5 that trends of ΔR for right-hand and left-hand curves have approximately the same slope, with the second one shifted upward. For leftward bends, the greater the R_d, the larger the discrepancy ΔR. Lower curvature produces positive effects on driving comfort, limiting lateral accelerations. Thus, participants tended to move toward the road centerline, or to maintain the vehicle on the right mid of the lane. This behavior was preserved during the simulations even if the simulator does not return any physical feedback, indicating that visual information is sufficient for driving.

These results support the findings of Boer (1996), who stated that drivers were inclined to adopt a lateral acceleration control strategy. Thus, the path with the lowest maximum curvature is the one that minimize the centrifugal forces on the vehicle during the curve negotiation (Coutton-Jean et al., 2009). On the other hand, the mean values of R_t along sharp rightward curves are not consistent with the habit of cutting the curve. It could be an issue of synthetic estimate (mean) that conceals variations of the values within the observed interval. Therefore, a deep analysis is required to understand the specific transversal behavior along curves.

8.5 Transversal Behavior along Curves

Corrected lane gaps (LG^*) were used to plot the adopted trajectory along the observed segments in a stretched form (as exhibited by Spacek, 2005). As mentioned in §4.2, the observed segments include 50 m of approaching and departure tangents, the spirals, and the circular arcs. These elements were divided by reference points named TS (tangent-to-spiral), SC (spiral-to-curve), CS (curve-to-spiral), ST (spiral-to-tangent).

The following graphs (Figure 8.6, Figure 8.7, Figure 8.8, and Figure 8.9) show the measures of the corrected lane gap (LG^*) along a standardized station (s/L), for bends with a different radius R (120, 225, 300, and 430 m, respectively). Each line represents the profile of a single trajectory, while the mean profile is evidenced with a red thick line. Each graph is titled with the number of the curve ("Cx"), the track (A, B, or A-mod), and the direction of travel within the circuit (counterclockwise - ccw - or clockwise - cw). Details like direction of the curve, the length (L) and the distance D are reported on top of each graph. Finally, mean (M) and standard deviation (SD) of lane gap were computed and indicated for each reference point. The profiles of LG^* for the all investigated curves are reported in the Attachments (§A.3).
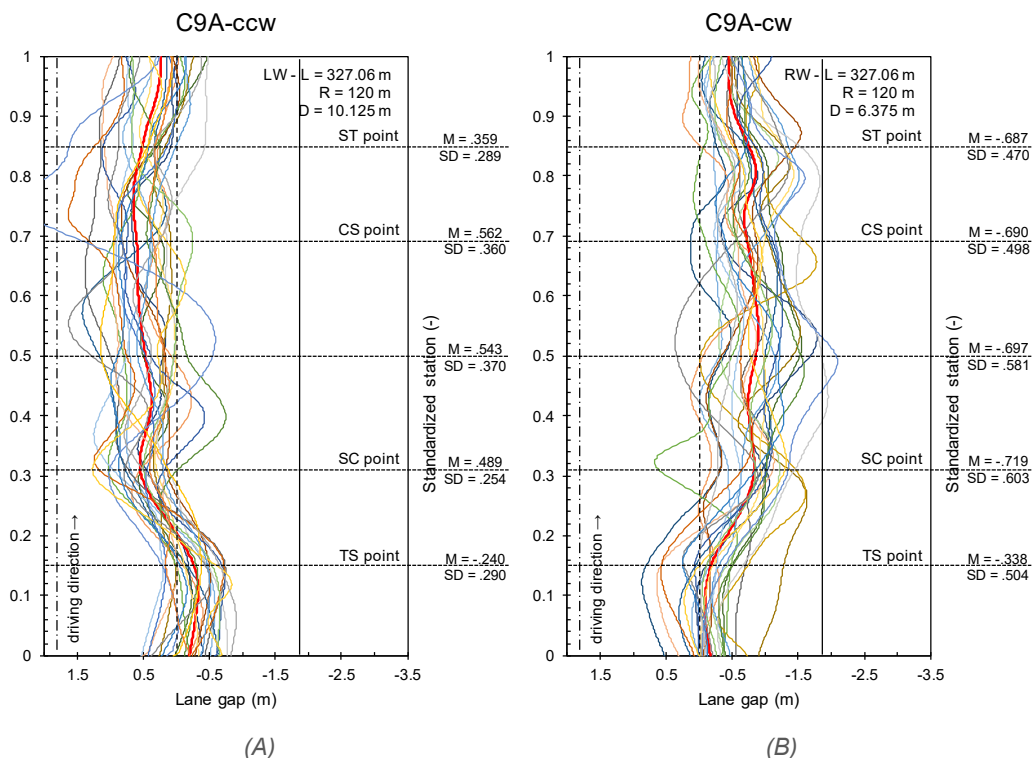
Figure 8.6. Lane gap profiles for the TDs who drove in the curve #9 of track A and A-mod in (A) counterclockwise and (B) clockwise direction. On top are reported the direction (RW or LW), the length L of the segment, the radius R, and the distance D
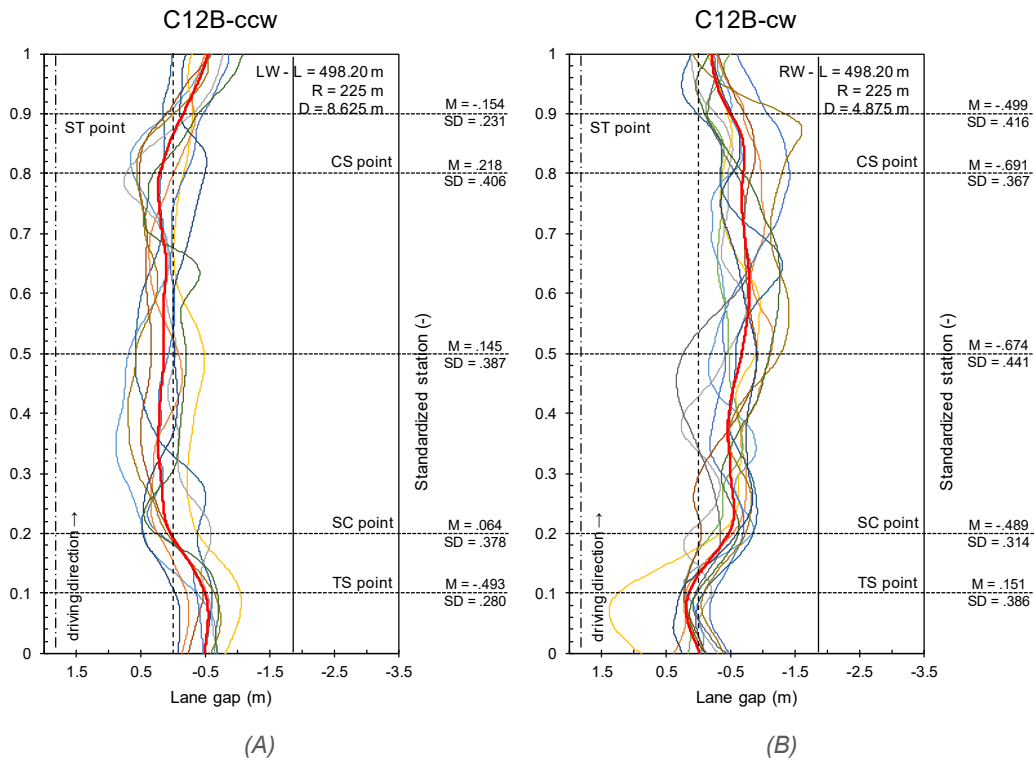
Figure 8.7. Lane gap profiles for the TDs who drove in the curve #12 of track B in (A) counterclockwise and (B) clockwise direction. On top are reported the direction (RW or LW), the length L of the segment, the radius R, and the distance D
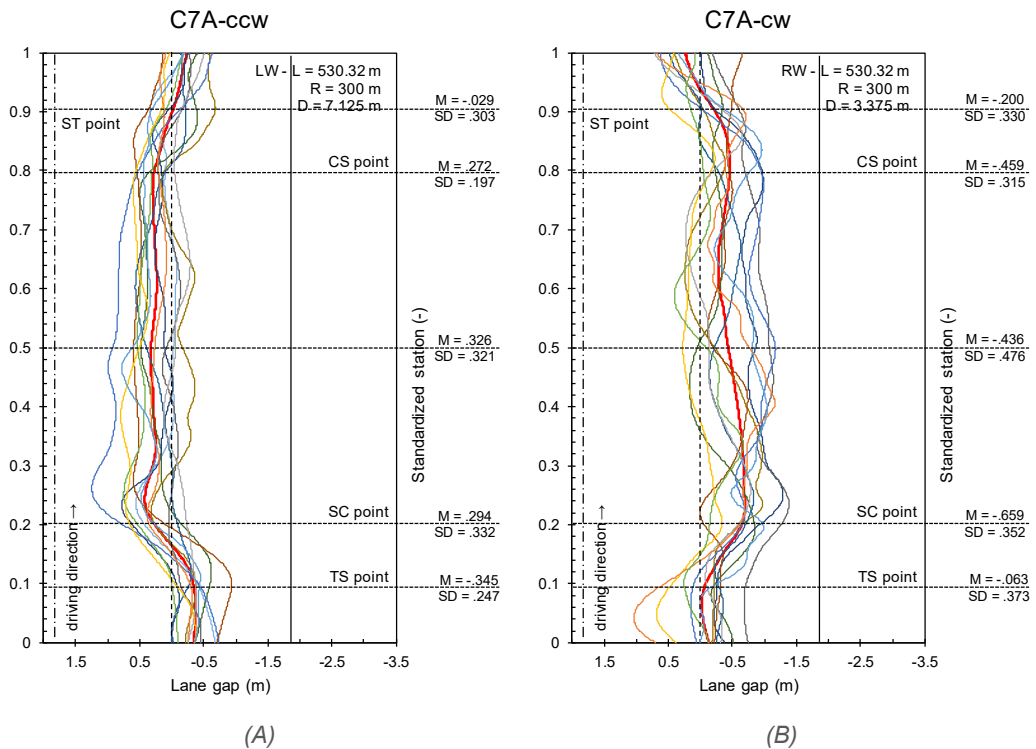
Figure 8.8. Lane gap profiles for the TDs who drove in the curve #7 of track A in (A) counterclockwise and (B) clockwise direction. On top are reported the direction (RW or LW), the length L of the segment, the radius R, and the distance D
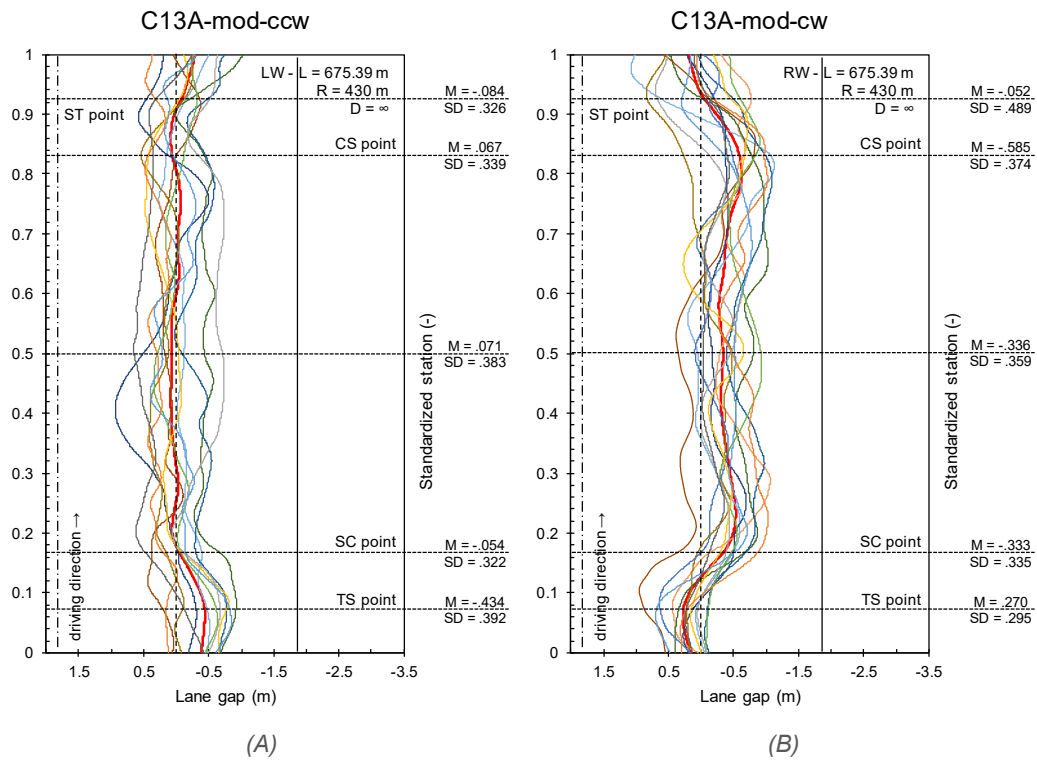
Figure 8.9. Lane gap profiles for the TDs who drove in the curve #13 of track A-mod in (A) counterclockwise and (B) clockwise direction. On top are reported the direction (RW or LW), the length L of the segment, the radius R, and the distance D

Values of the mean and standard deviation of the lane gap indicate that, for these four cases, drivers adopted trajectories close to the lane centerline more on the leftward bends than on the rightward ones. Their variability (SD) in correspondence of the reference points was greater in the B cases (rightward curves) due to the different behavior of TDs in curve negotiation, influenced by the distance D and the radius R. The profiles of sharp curves are characterized by continuous corrections to the steering angle, whereas those along shallow bends are smoother. In few cases, drivers traversed the right lane markings (on RW curves) or the road centerline (on LW bends) during the negotiation of sharp curves. This supports previous results (Bella, 2013; Ben-Bassat and Shinar, 2011; Bella, 2005b) that evidenced the steering effects of more demanding road elements (tight turns).

In Figure 8.10, plots of curves with different radius and same value of d (0) are compared. Along sharp curves, drivers tended to move laterally more than on shallow curves. This attitude of "cut" the curves, minimizing the traveled distance and centrifugal forces, is widely acknowledged in real driving (Felipe and Navin, 1998). These results, even if qualitative, evidence that the greater the ASD in front of the driver, the more the trajectory is centered along the lane centerline. Observations in Figure 8.10 stand out also in the trends for $d = 1.5$ m, 3 m, and infinite (∞), as visible in Figure 8.11, Figure 8.12, and Figure 8.13, respectively.

(A)   (B)
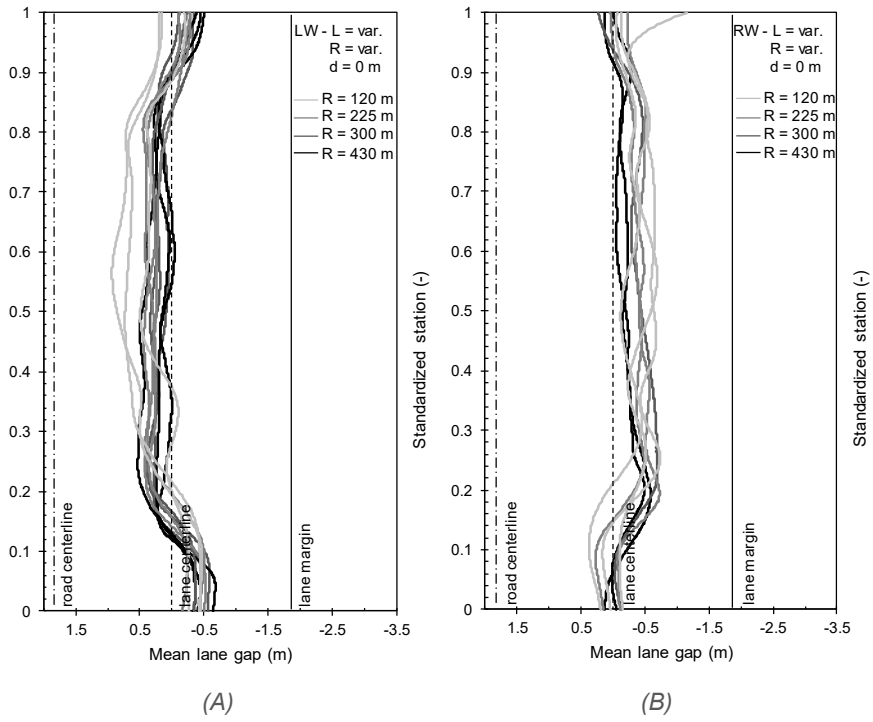
Figure 8.10. Mean lane gap profiles of TDs along (A) leftward and (B) rightward curves with d = 0

(A)   (B)
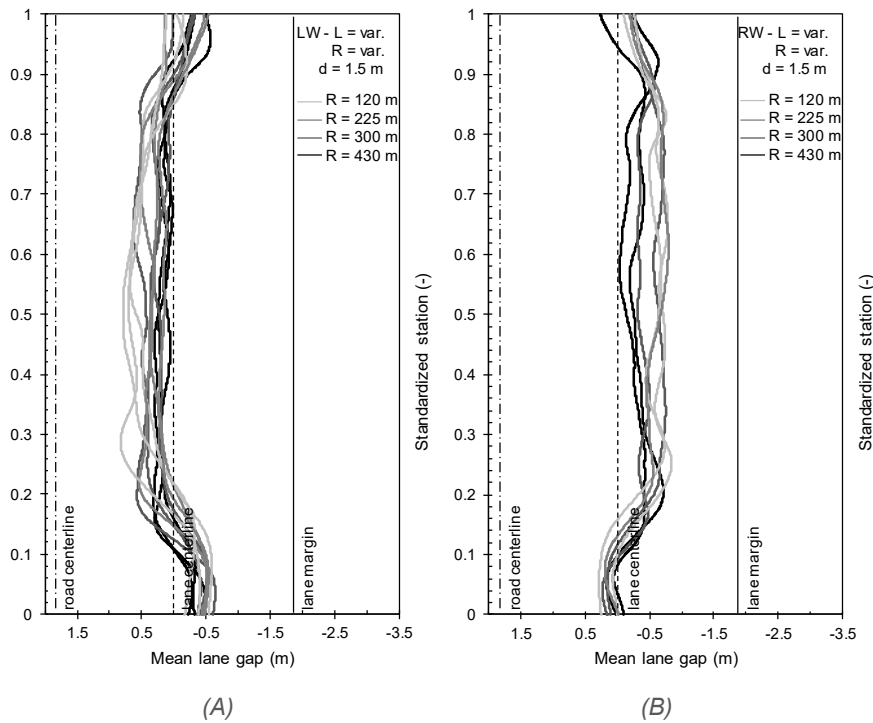
Figure 8.11. Mean lane gap profiles of TDs along (A) leftward and (B) rightward curves with d = 1.5 m
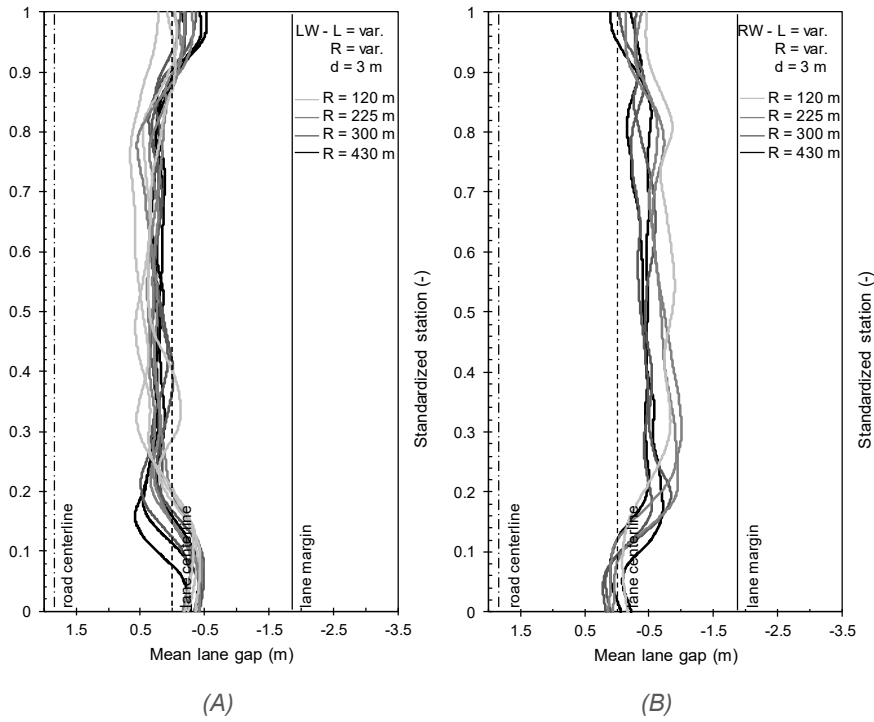
Figure 8.12. Mean lane gap profiles of TDs along (A) leftward and (B) rightward curves with d = 3 m
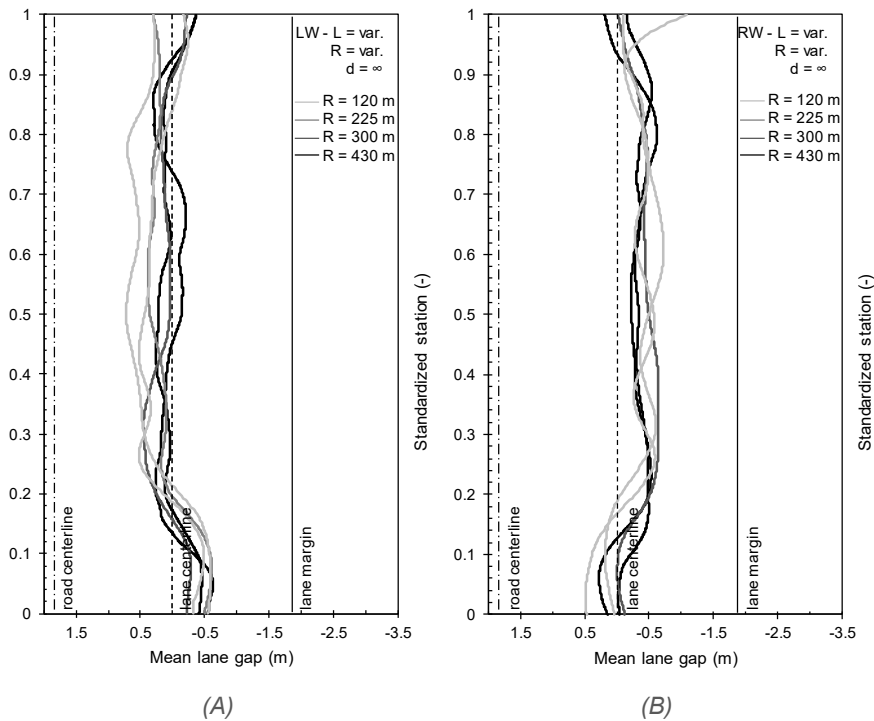
Figure 8.13. Mean lane gap profiles of TDs along (A) leftward and (B) rightward curves with d = ∞

According to Coutton-Jean et al. (2009), drivers did not maintain a stable position in the center of the lane. They took advantage of the approaching tangent and spiral to move the vehicle in the opposite lane side with respect the direction of the curve; in this condition, drivers gained the maximum ASD along the road segment ahead. Then, they crossed the lane centerline to enter in the circular arc, and to limit the perceived lateral accelerations. At the end of the circular arc, drivers reversed this behavior, passing from the inner to the outer lane side. This attitude was more evident along shallow than on sharp bends. In contrast, Van der Horst and De Ridder (2007) observed that drivers moved away from the roadside during curve negotiation.

It may be deduced that the computation of $R_{t,i}$ (eq. 25) was affected by the variability of the lane position along the circular arcs, that also influenced the curvature ($c_{t,i}$) values. The estimation of the average for a series of data hides its spatial variability within the observed stretch: this is appreciable on sharp rightward curves, where the mean R_t is lower than the R_d, even if the lateral displacements on the right side of the lane are considerable (e.g., Figure 8.6B). In fact, a curve cutting path should result in lowering the trajectory curvature, thus increasing its radius. On the other hand, curves of greater radii were characterized by reduced steering wheel corrections (smoother profiles of lane gap), leading to mean curvatures more similar to the actual data. Although adopted radii were greater than the design radius, they allowed drivers to maintain the vehicle within the traveled lane.

8.6 Transversal Behavior vs. Available Sight Distance

The dispersion of trajectory (DT) is a measure of accuracy of the trajectory with respect to the lane centerline. For comparison purposes, such values were standardized (DT^S) as a function of the different segments length. Among the sample of drivers who traveled on the curves, mean (M) values of DT^S were computed and shown in Table 8.4. It also reports the standard deviation (SD) of the values and the number of observations (n) for each curve configuration.

Mean values of DT^S are plotted in Figure 8.14A in function of the designed radius (R). Data was connected on the basis of the d distance, and distinguished for the direction of travel (solid line for right-hand, and dashed line for left-hand bends). In general, the higher the radius, the lower the DT^S. These results support the observations of Zakowska (2010). In few cases, this tendency is opposed: e.g., when $d \geq 3$ m on RW bends, the observed DT^S corresponding to $R = 300$ m is lower than the one on curves with $R = 430$ m. In these conditions, the perceived distance to the lateral wall increased, and diminished the guidance effect provided by the sight obstruction.

On the other hand, LW bends are characterized by smaller DT^S with respect to the corresponding RW curves. This statement is refused only for curves of $R = 120$ m, with $d = 0$ m and infinite (∞). Therefore, the greater the ASD, the smaller the deviation from the ideal trajectory, but only when the sight obstruction was present.

Table 8.4. Mean (M) and standard deviation (SD) of dispersion of trajectory collected along the entire curve length (n is the number of drivers travelling on this kind of curve) for different combination of radius (R) and distance of the obstruction from the roadway (d) and the trajectory (D). Symbol ∞ indicates that no sight obstruction was used, so ASD values are assumed to be higher

R				Leftward curves						Rightward curves		
	d	D	ASD	DT^S			d	D	ASD	DT^S		
				M	SD	n				M	SD	n
(m)	(m)	(m)	(m)	(m)	(m)	#	(m)	(m)	(m)	(m)	(m)	#
120	0	7.125	83.76	0.51	0.19	41	0	3.375	56.61	0.45	0.18	41
	1.5	8.625	92.25	0.50	0.20	52	1.5	4.875	68.11	0.58	0.22	40
	3	10.125	100.06	0.43	0.19	65	3	6.375	77.97	0.66	0.27	26
	∞	∞	∞	0.48	0.20	25	∞	∞	∞	0.46	0.20	26
225	0	7.125	114.02	0.38	0.16	55	0	3.375	77.72	0.43	0.18	23
	1.5	8.625	125.52	0.40	0.19	49	1.5	4.875	93.46	0.54	0.17	12
	3	10.125	136.07	0.36	0.13	52	3	6.375	106.93	0.63	0.21	26
	∞	∞	∞	0.40	0.16	12	∞	∞	∞	-	-	-
300	0	7.125	131.43	0.34	0.13	52	0	3.375	89.80	0.47	0.21	12
	1.5	8.625	144.67	0.38	0.16	51	1.5	4.875	107.98	0.48	0.18	25
	3	10.125	156.81	0.34	0.12	61	3	6.375	123.53	0.46	0.22	41
	∞	∞	∞	0.37	0.16	13	∞	∞	∞	0.45	0.23	14
430	0	7.125	157.11	0.34	0.15	52	0	3.375	107.59	0.36	0.15	41
	1.5	8.625	172.91	0.30	0.14	42	1.5	4.875	129.34	0.42	0.17	26
	3	10.125	187.40	0.34	0.15	52	3	6.375	147.95	0.46	0.21	22
	∞	∞	∞	0.37	0.20	26	∞	∞	∞	0.41	0.20	28

(A)

(B)
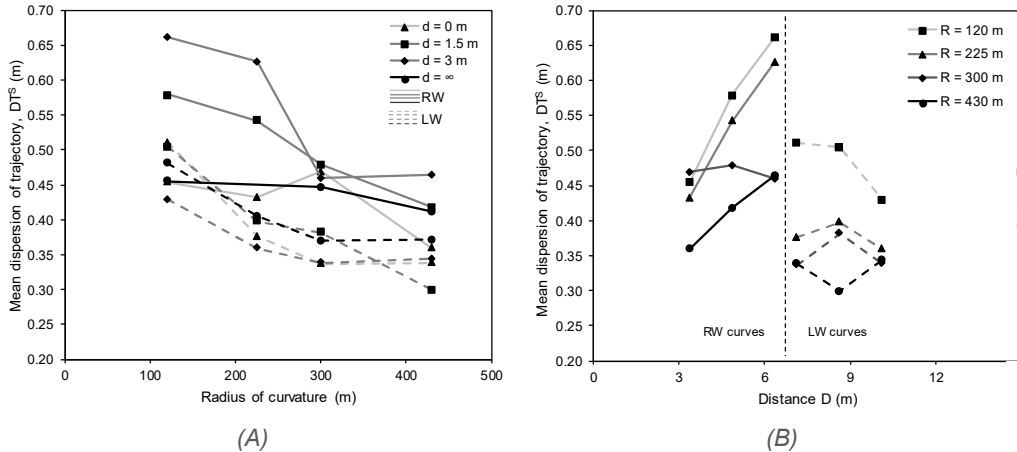
Figure 8.14. Trends of mean values of the standardized dispersion of trajectory as a function (A) of the radius of curvature, and (B) of the distance D of the trajectory from the lateral sight obstruction

DT^S values were then displayed in function of the distance D (Figure 8.14B). It is worth remarking that when R increases, DT^S decreases both for RW and LW bends. Along RW curves, when D grows, the DT^S raises too. This trend is not valid for the curves with $R = 300$ m only. Hence, when the sight limitation was present, its effect as optical guidance is appreciated by drivers along RW bends; however, there is not a clear behavior for LW curves, where the effect of the radius on lane position was more significant.

These outcomes are consistent with findings of Calvi (2015b). By comparing the case of $d = ∞$, and the cases of $d ≤ 1.5$ m respectively with "Road A" and "Road B/C" of his work, the results are equivalent: unrestricted sight conditions lead to

lower *DT* with respect to curves with sight limitations. Conversely, absolute values in this experiment are larger than those obtained by Calvi (2015b): this is attributable to the computation of *DT*, that here included also 50 m of adjacent tangents, or to the different effects provided by the equipment. However, Calvi considered only two discrete visibility conditions ("restricted" and "unrestricted") that did not allow to explore driver behavior in a wider range of sight conditions.

In Figure 8.15, the mean values of the *DT* were related to the corresponding mean driving speeds. For comparable speeds, the *DT* of rightward curves (black filled symbols) is greater than leftward ones (empty symbols). As already mentioned, the values collected on sharp curves ($R = 120$ m - squares) present similar speeds and $DT^S > 0.4$ m. Greater radii are characterized by higher driving speeds, and a gradual reduction of *DT*.

According to Van Winsum and Godthelp (1996), Figure 8.15 highlights that sharp curves allowed the adoption of larger *DT* values (> 0.5 m) since they were traveled at lower speeds. In these conditions, the driver was able to adequate and correct her/his trajectory without compromising her/his perceived risk. Along shallow bends, the driver opts for higher speed when her/his risk perception is reduced. Nonetheless, the cognitive skills employed in such operations increases, leading to more precise and stable trajectories. In a two-lane road, the ideal trajectory is, per definition, the farthest from plausible collision points (i.e., road centerline for head-on crashes; carriageway edge for collisions with fixed elements close to the shoulder). Thus, the driver that accepts a higher risk threshold (i.e., driving faster), at the same time she/he tries to adopt the best trajectory. This analysis suggests that steering strategy and speed choice are closely related in curve negotiation.

Moreover, the analysis of transversal variability of the vehicle position within the lane was performed with respect to the ASD, that combines the effects of *R* (radius) and *d* (cross section) together.
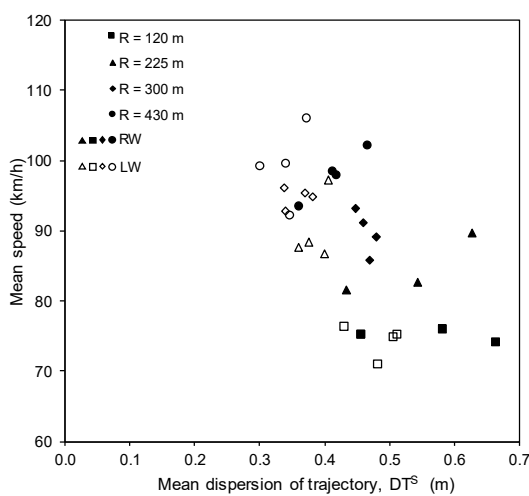
Figure 8.15. Relationship between mean values of dispersion of trajectory and speed, distinguished for radius of curvature and direction

Figure 8.16 exhibits the data of Table 8.4, showing the relationship between the mean dispersion of trajectory and ASD along curves affected by sight obstruction only. The different connections between points in the two graphs (Figure 8.16A and Figure 8.16B) reflect the two possible ways in which data can be interpreted: linking data with the same distance d (Figure 8.16A), and connecting those characterized by the same curve radius (Figure 8.16B).

Figure 8.16A emphasizes the direct proportionality between DT^S and ASD: when ASD increases the mean dispersion of trajectory decreases. It means that the greater the ASD, the greater is the tendency to adopt more precise vehicle trajectories, both along leftward (dashed lines) and rightward (continuous lines) curves. It is worth noting that for the same ASD, drivers' trajectories were characterized by different DT: their transversal behavior was affected by the radius R more on right- than on left-hand bends, which show closer trends. Lower values of DT^S were observed only when the sight limitation was placed near the shoulder ($d = 0$ m) or when the ASD was higher than 150 m. Accordingly, it may highlight the guidance effect of the lateral wall on steering behavior.

Referring to Figure 8.16B, along rightward curves with $R \leq 225$ m the mean DT^S increases with a higher slope than on curves of 430 m of radius. Along left-hand curves where ASD was greater than 120 m, the mean values of DT^S range between 0.3 and 0.4 m.
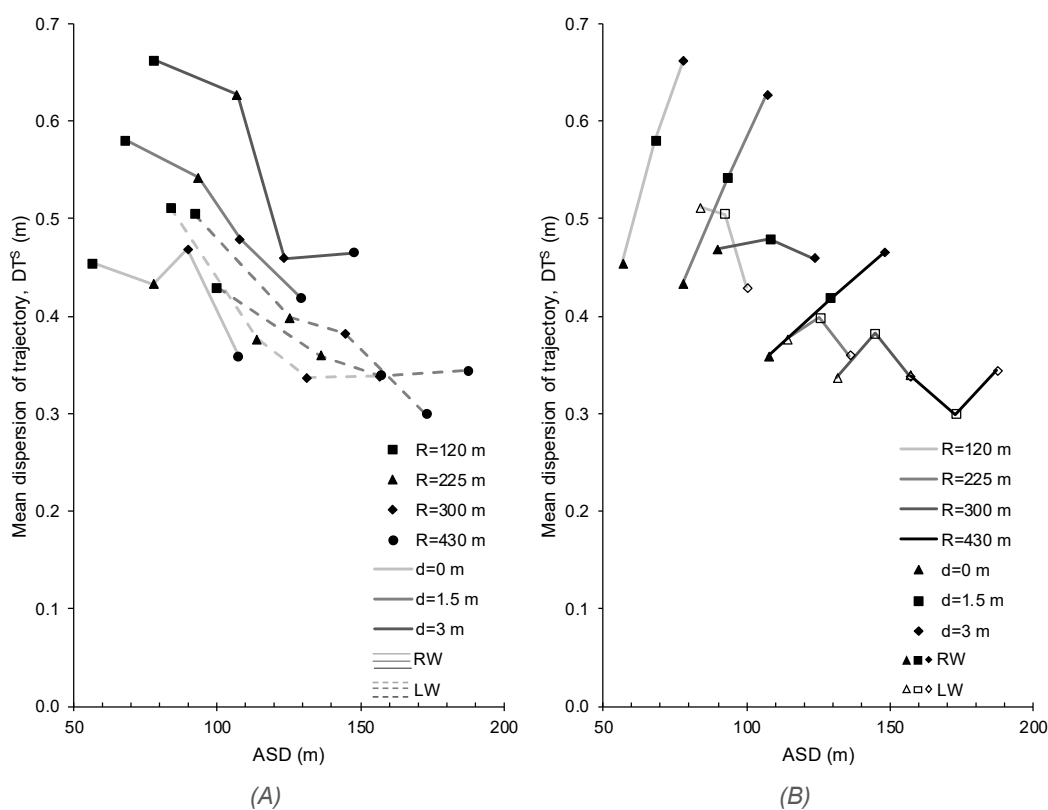
Figure 8.16. Relationship between ASD and the dispersion of trajectory: data connected on the basis of distance d of sight obstruction from the shoulder (A), and data connected on the basis of curve radius R (B)

To support the inferences derived from Figure 8.16, the ANOVA was carried out also to evaluate the significance of the investigated variables on the dispersion of trajectory. In this analysis, the *DT* of drivers that traveled along each investigated curve was used as repeated measures. Also in this case, the 3-way ANOVA considers the main effects are curve direction (*dir*), radius (*R*) and offset of the lateral obstruction from the road edge (*d*); and the 2-way ANOVA with radius (*R*) and aggregated distance (*D*) regarded as principal effects. In both cases, the Normal distribution of data was checked by means of the Chi-square test assuming a significance level of 5% ($\chi^2_{crit} = 5.99$).

Table 8.5 lists the results of the 3-way ANOVA, clearly indicating that the direction ($F(1,1072) = 69.31$, $p < 2.6 \cdot 10^{-16}$, $\eta^2 = .053$) and radius ($F(3,1072) = 31.47$, $p < 2.2 \cdot 10^{-16}$, $\eta^2 = .072$) are the variable which have the most significant influence on dispersion of trajectory. Also the distance *d* is significant ($F(3,1072) = 2.92$, $p = .033$, $\eta^2 = .007$). Once again, the radius of curvature is the variable that explains the outcome more than others (7.2%), whereas the direction of travel influences only 5.3% of the dispersion of trajectory variance. The interaction between the direction of travel and the distance *d* has high significance ($F(3,1072) = 10.17$, $p = 1.3 \cdot 10^{-6}$, $\eta^2 = .023$), which means that the position of the sight obstruction plays a different role when evaluated on left- or rightward curves; furthermore, the interaction of the radius and the direction of the curve presents $F(3,1072) = 3.34$, $p < .02$, $\eta^2 = .008$. Other interactions between influencing factors are less significant. The proportion of variance that cannot be explained with the considered variables is about 82%.

Results are consistent with outcomes of Calvi (2015b), that found significant differences between bends of the same radius but traveled in opposite direction.

On the basis of previous outcomes, the 2-way ANOVA aggregated the main effects *d* and *dir* into the distance *D*, whose results are listed in Table 8.6. The results confirm the high significance of both *R* ($F(3,1075) = 32.90$, $p < 2 \cdot 10^{-16}$, $\eta^2 = .075$) and *D* ($F(6,1075) = 17.87$, $p < 2 \cdot 10^{-16}$, $\eta^2 = .082$), while their interaction proved to be fairly significant ($F(18,1075) = 1.65$, $p < .05$, $\eta^2 = .023$). In this case, the *DT* variance is more associated with the variation of *D* (8.2%) than the variation of *R* (7.5%). The results of this 2-way ANOVA are the same of those referred to the driving speed, evidencing that *R* and *D* significantly influence the driver longitudinal and transversal behavior. Such outcomes remark once again the relevance of ASD on driver performance.

Table 8.5. Results of 3-way ANOVA on dispersion of trajectory

Principal Effects	Degree of Freedom	Sum of Squares	Mean of Squares	F value	Pr(>F)	η^2	Partial η^2	code
Direction (left/right hand), *dir*	1	2.224	2.22388	69.309	2.542e-16	0.053	0.061	***
Radius, *R*	3	3.029	1.00962	31.466	< 2.2e-16	0.072	0.081	***
Distance, *d*	3	0.281	0.09357	2.916	0.03330	0.007	0.008	*
Interaction Effects								
dir*R	3	0.321	0.10704	3.336	0.01885	0.008	0.009	*
dir*d	3	0.979	0.32617	10.165	1.325e-06	0.023	0.028	***
R*d	9	0.308	0.03426	1.068	0.38403	0.007	0.009	
dir*R*d	8	0.483	0.06035	1.881	0.05945	0.011	0.014	.
Residuals	1072	34.397	0.03209			0.819		

Notes: significance of codes is 0 '***', 0.001 '**', 0.01 '*', 0.05 '.', 0.1 ' ', 1

Table 8.6. Results of 2-way ANOVA on dispersion of trajectory

Principal Effects	Degree of Freedom	Sum of Squares	Mean of Squares	F value	$Pr(>F)$	η^2	Partial η^2	code
Radius, R	3	3.164	1.05481	32.8994	< 2e-16	0.075	0.084	***
Distance, D	6	3.438	0.57294	17.8699	< 2e-16	0.082	0.091	***
Interaction Effects								
$R*D$	18	0.952	0.05291	1.6503	0.04238	0.023	0.027	*
Residuals	1075	34.466	0.03206			0.820		

Notes: significance of codes is 0 '***', 0.001 '**', 0.01 '*', 0.05 '.', 0.1 ' ', 1

Also in this case, the comparison of DT values computed in the Experiment #1 and Experiment #2 is shown in Figure 8.17. Only values belonging to the Combination ID #1, #2, #6, and #7 of the Experiment #2 were considered in this analysis, since the other data are affected by the absence of horizontal markings.

The great part of mean values of DT^S is close to the equality line (dashed line), meaning that the two TD samples behave similarly in both experiments. Only one point referred to a curve of 225 m of radius shows the largest DT difference equal to 0.2 m. Once again, this result strengthens the robustness of collected data and the significance of the outcomes.

8.7 Vision Mechanisms

The analysis of vision mechanisms required the acquisition of the following information for all traveled curves:

- the road elements used by participants for driving, that allowed the identification of the vision mechanisms;
- the duration of each fixation; and
- the curve travel times, that is the time employed to drive along the curved segments (spirals and circular arc).
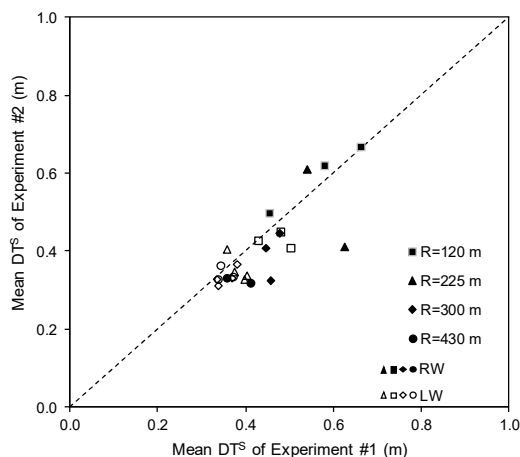
Figure 8.17. Comparison of mean dispersion of trajectory (DT^S) calculated for the two experiments for validation purposes

In the following discussion, the analysis focused on the use of vision mechanisms along curves with different combinations of roadway elements (Comb. ID in Table 7.3). The time spent by drivers for fixating reference elements was related to the time devoted for curve negotiation, to carry out a quantitative evaluation.

For each curve, two quantities were computed: (i) the total time employed for fixations, as the sum of the single durations, for each vision mechanism; and (ii) the total travel time on curve, by adding the time employed by TDs to traverse the curve. The ratio between these two quantities returns the percentage of use of each visual strategy. In such way, the percentages can be compared among curves of different radii, where the fixation and travel times significantly change.

Following graphs show these values computed along curves where each vision mechanism (VM) may be effectively employed (e.g., the VM 2c). Figure 8.18 reports an excerpt of a graph. Participants who drove in the leftward curve with R = 120 m, $d2$ = 1.5 m, with the Comb. ID #1, fixated for 17% of the time the tangent points (VM 1) on the road pavement (horizontal markings, road edges), for 5% of the time the points on the road edges, and for 6% of the time the points on the future path, by using the VM 2. Anyone employed the sight obstruction (VM 1b) as a steering guidance; the percentage of use of the VM 3 is equal to zero since the margin delineators were not present. For the rest of the time, drivers spread the gaze in other points of the road environment.

Afterwards, the analysis considers the use of combined vision mechanisms (more than one along the traveled curve) to evaluate their adoption on the basis of road configurations, and the different visual attitudes of experienced and unexperienced drivers when negotiating curves.
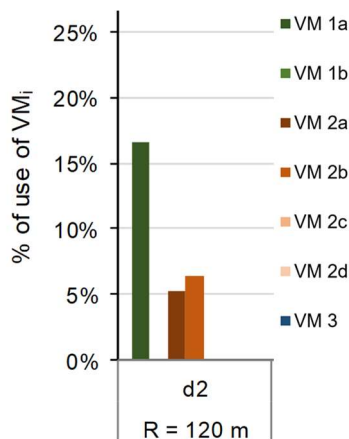
Figure 8.18. Example of fixations data analysis and representation

8.7.1 Fixations analysis

<u>Combination #1</u>

The first combination of elements considers the presence of the road markings and the sight obstruction (Figure 8.19A).

The graphs in Figure 8.19 evidence that VM 1a was the most used. Drivers used the lateral wall (VM 1b) as a guiding element instead of the lane markings on two leftward bends with sight obstruction close to the shoulder ($d1$ = 0 m). Only in few cases, participants used the gaze direction tangent to the lateral wall on rightward curves with d = 3 m. The use of VM 2a increased from sharp to shallow curves, but greater values were observed on leftward bends than on right ones. Thus, some drivers tended to substitute the TP mechanism with the estimation of the distance-to-target (VM 2) when the sight distance increased.

(A)

(B)   *(C)*
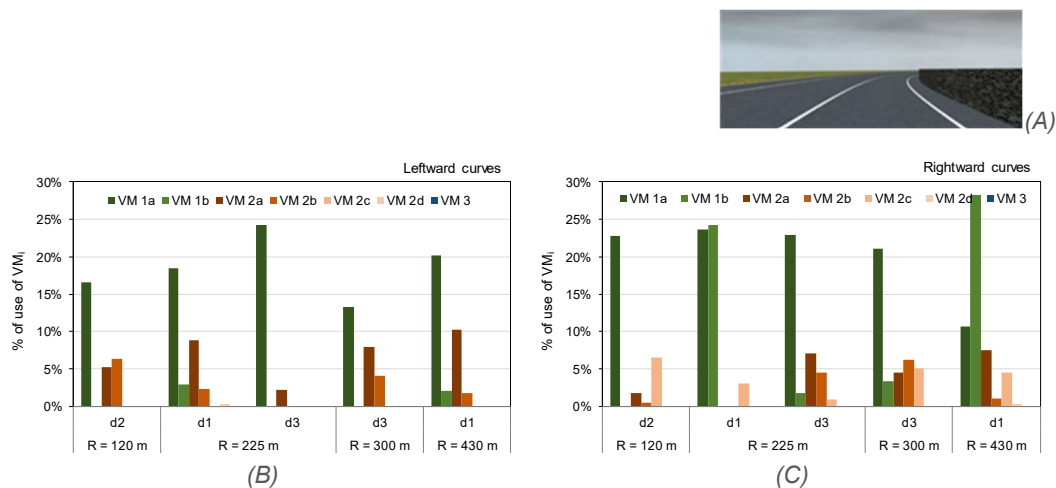
Figure 8.19. (A) Picture of the virtual scenario; in the graphs, the percentage of use of VMs for the Combination #1 along (B) leftward and (C) rightward curves (d1 = 0 m; d2 = 1.5 m; d3 = 3 m)

<u>Combination #2</u>

The second combination of elements considers the presence of the horizontal markings and margin delineators along curves (Figure 8.20A).

The graphs in Figure 8.20 show once again that VM 1a was the most employed by participants (mean of 18% of the total travel time on RW curves, and equal to 15% on LW bends). The use of VM 2a decreased along rightward curves when the radius increased; conversely, it grew on leftward bends, except for the case with R = 400 m. It is appreciated that the reduction of VM 1a on leftward bends is associated with the increasing adoption of VM 3 thanks to the presence of margin delineators. Longer fixations to the future path (VM 2b) were observed when R = 120 m; the road axis (VM 2c) was fixated only on rightward curves, more on sharper than on shallower ones.
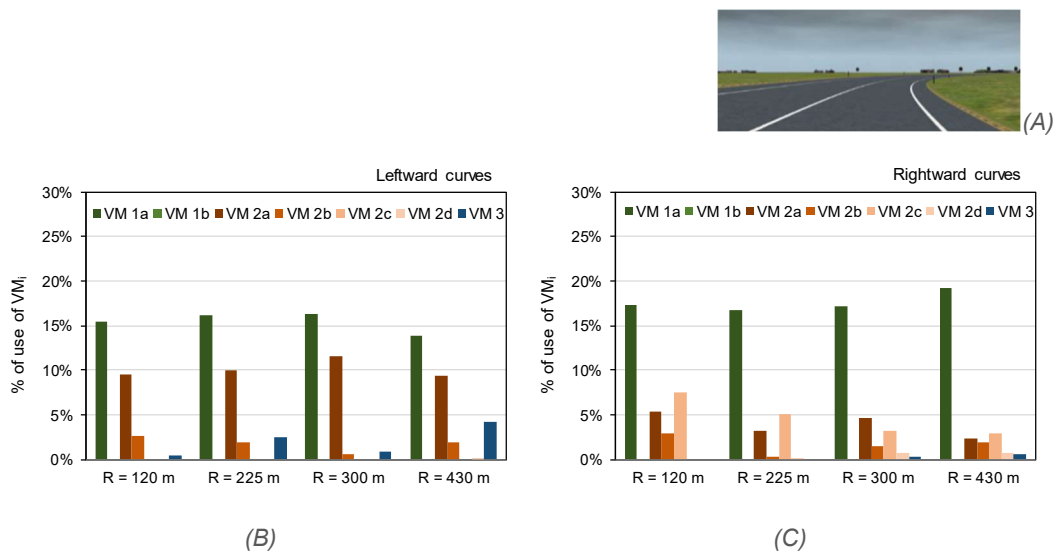
Figure 8.20. (A) Picture of the virtual scenario; in the graphs, the percentage of use of VMs for the Combination #2 along (B) leftward and (C) rightward curves

Combination #3

The third combination of elements considers the presence of the sight obstruction and margin delineators along the curve.

The VM 1a was the most used (mean of 21% of the total travel time on RW curves, and equal to 14% on LW bends) even if the road markings are absent (Figure 8.21A). It is worth noting in the graphs of Figure 8.21 that VM 1a was the only visual strategy employed in the rightward curve with $R = 120$ m, and sight obstruction at 3 m to the shoulder. Once again, the use of a gaze direction tangent to the lateral wall (VM 1b) is preferred to the VM 1a when the sight obstruction is close to the driver ($d1 = 0$ m).

The participants recurred to VM 2 when the radius of curvature increased (except for $R = 120$ m and $d = 1.5$ m). Fixations to the future path (VM 2b) also increased according to the increase of the radius, that is as the ASD grows. Conversely, VM 3 has not a defined trend, but it was observed mostly on leftward curves.

(A)

(B)

(C)
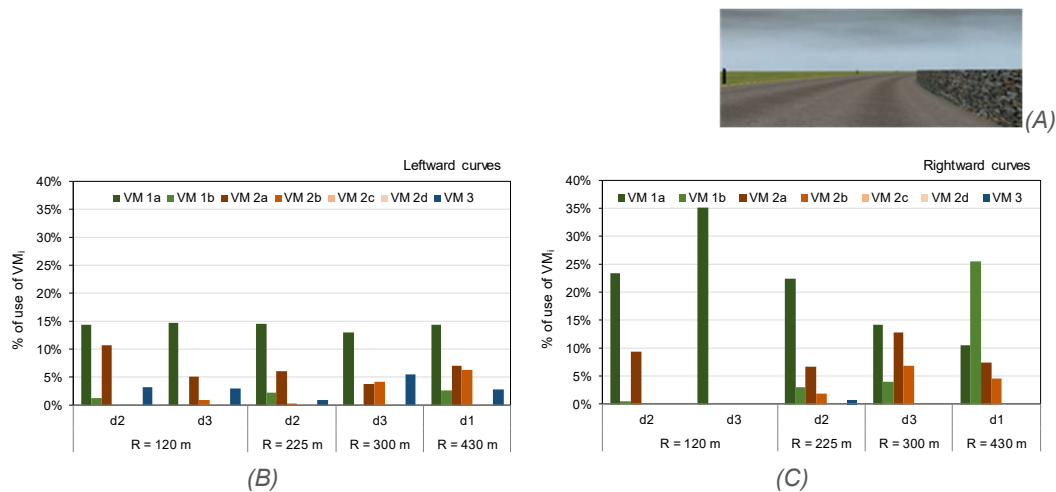
Figure 8.21. (A) Picture of the virtual scenario; in the graphs, the percentage of use of VMs for the Combination #3 along (B) leftward and (C) rightward curves (d1 = 0 m; d2 = 1.5 m; d3 = 3 m)

Combination #4

The fourth combination of elements considers the presence of margin delineators only (Figure 8.22A).

Although the horizontal markings were not present, the VM 1a was still the most used on rightward curves (Figure 8.22C). Also in this case, the participants fixated to targets on the road margins (VM 2a) to set the preferred trajectory, more on left- than on right-hand bends. For leftward curves with $R \geq 225$ m, the percentage of VM 2a use was greater than that of VM 1a. Points of the future path (VM 2b) and margin delineators (VM 3) were fixated more on shallow leftward bends than on sharper ones.

(A)

(B)

(C)
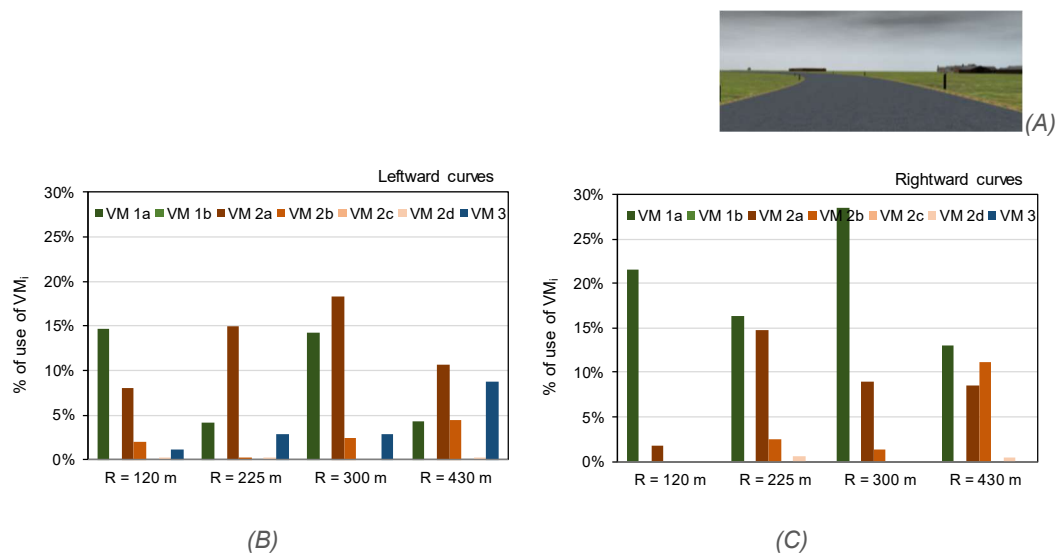
Figure 8.22. (A) Picture of the virtual scenario; in the graphs, the percentage of use of VMs for the Combination #4 along (B) leftward and (C) rightward curves

Combination #5

The fifth combination of elements considers the presence of the sight obstruction only (Figure 8.23A).

It is worth noting that the absence of horizontal markings led to a gradual adaptation of drivers, who substituted the VM 1a with the VM 2a moving from tight to shallow curves (Figure 8.23). This is evident also from the comparison between right- and leftward bends: the lack of the tangent point in the nearest zone induced participants to look towards targets on the road ahead. The percentage of VM 1b usage was considerable on rightward shallow bends only ($R \geq 300$ m). The use of references on the future path (VM 2b) was greater on rightward than of leftward curves, except for the case of $R = 300$ m.
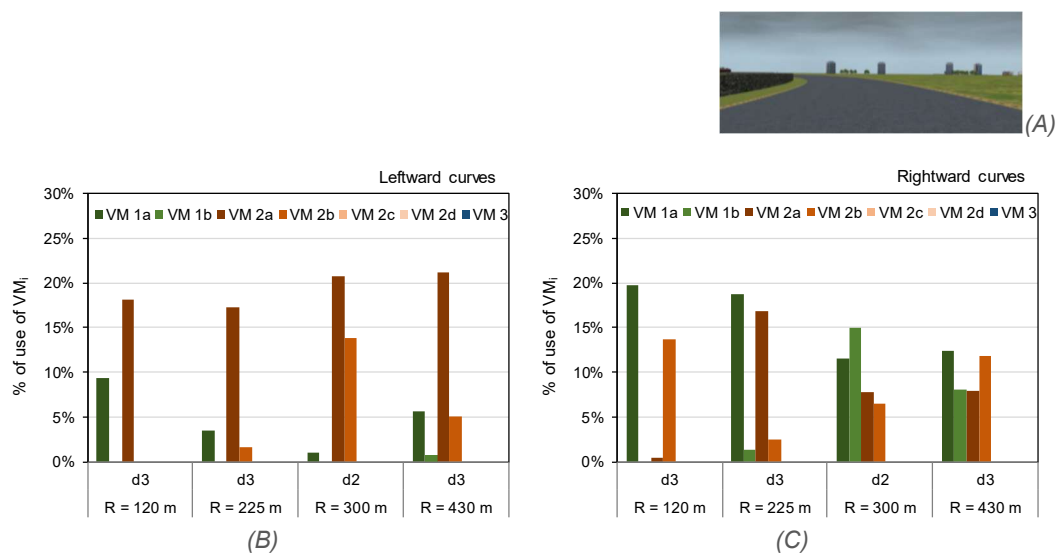
Figure 8.23. (A) Picture of the virtual scenario; in the graphs, the percentage of use of VMs for the Combination #5 along (B) leftward and (C) rightward curves (d1 = 0 m; d2 = 1.5 m; d3 = 3 m)

Combination #6

The sixth combination of elements considers the presence of horizontal markings only (Figure 8.24A).

It is worth noting that horizontal markings and road margins (VM 1a) were highly employed when negotiating both rightward and leftward curves (Figure 8.24). However, along left-hand bends of 120 and 300 m of radius, VM 2a was preferred to VM 1a. On the other hand, few drivers adopted VM 2 on rightward curves: fixations on the future path and on the road axis increased as the radius increased as well.

(A)

(B)

(C)
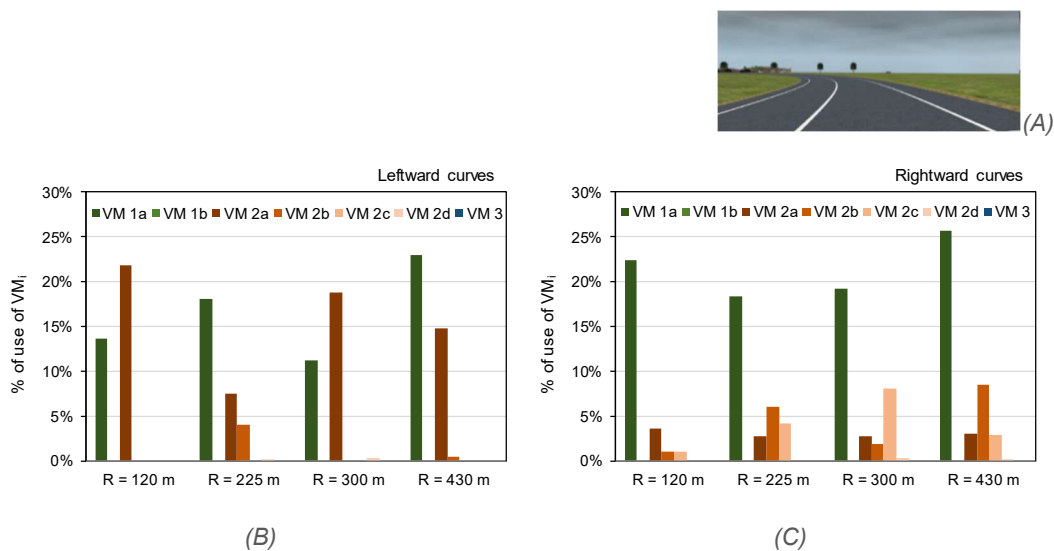
Figure 8.24. (A) Picture of the virtual scenario; in the graphs, the percentage of use of VMs for the Combination #6 along (B) leftward and (C) rightward curves

Combination #7

With this combination, the roadway included three reference elements (Figure 8.25A). Their contextual presence divided the drivers' attention on more elements of the roadway.

Graphs of Figure 8.25 reveal that VM 1a was the most used (mean of 15% of the total travel time on RW curves, and equal to 16% on LW bends). Nevertheless, the lateral wall seemed to guide participants (VM 1b) along rightward curves with $R \geq 300$ m, especially where the sight obstruction was close to the shoulder (*d1*).

The percentage of use of VM 2a and 2b was greater on leftward curves than on rightward ones, without a defined trend among different variables combinations. The distance to points of the road centerline (VM 2c) was useful on the right bends only.

Only few drivers adopted the VM 3 on left-hand bends with R equal and greater than 225 m.

(A)

(B)

(C)
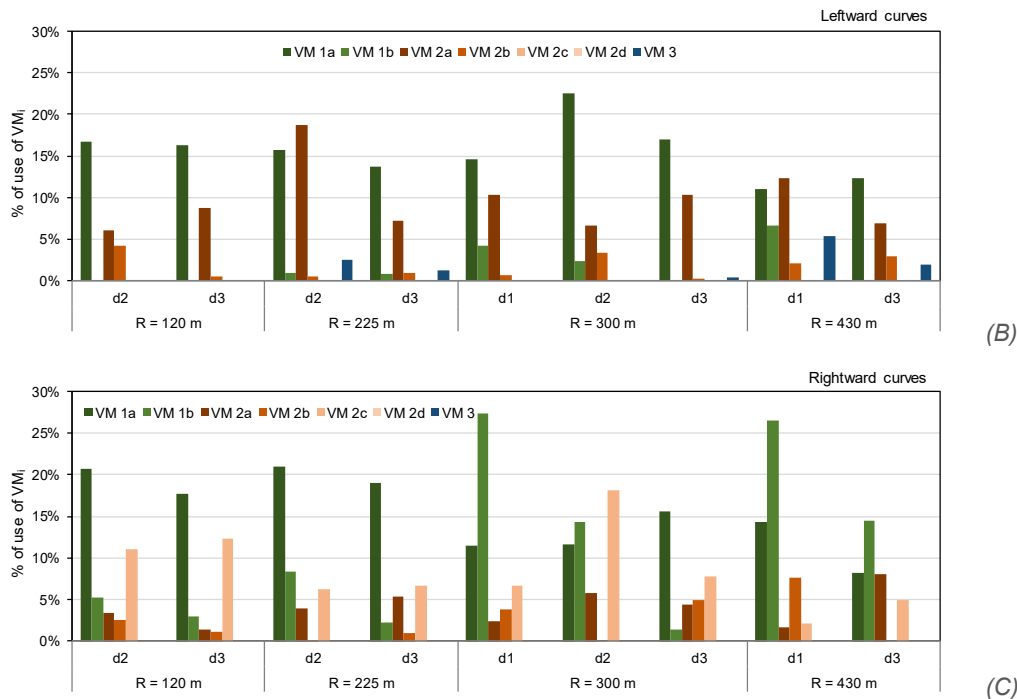
Figure 8.25. (A) Picture of the virtual scenario; in the graphs, the percentage of use of VMs for the Combination #7 along (B) leftward and (C) rightward curves (d1 = 0 m; d2 = 1.5 m; d3 = 3 m)

Summary

The mean time used for fixations of reference elements that help for steering was always higher than 30% for all combinations. Along rightward curves drivers spent more time in fixating guidance elements (average of 38%) than on leftward curves (average of 30%). For about 70% of the travel time, drivers were occupied in doing by saccades movements or fixations on other parts of the field of vision. The former represent the time employed for move the gaze from one fixation to the next one; in addition, drivers tended to monitor and explore the road space ahead in order to comprehend events occurring in the scenario (Lehtonen et al., 2013).

Presented figures elicit the following observations:
- the tangent point model is the simplest and most feasible mechanism that participants employed while driving;
- the lateral wall on the roadside is used as a reference element, especially when it is close to the shoulder;
- the presence of lateral continuous obstruction guides the curve negotiation on rightward curves, more on shallow than on sharp ones;
- when the horizontal markings are absent, drivers made use of the road margins as longitudinal alignments where to find the tangent point;
- the lack of tangent points in the nearest zone induces drivers to look towards targets along the road ahead. Specifically, they recurred to

VM 2a, that refers to the extreme point of the roadway that drivers look along the gaze direction;

- VM 2c was used on rightward curves only, since on the left curves drivers turned to VM 1a;
- margin delineators helped steering strategies only on leftward shallow curves; their use increased when the radius of curvature increased as well.

Table 8.7 summarizes the number of events where each VM was adopted in comparison to the number of bends where they can be applied, on the basis of the configuration of the road elements. It is evident from the above discussion that VM 1a was most frequently used (63%), followed by the VM 2a (36%), and the VM 1b (23%). It is worth noting that the sum of frequencies is not equal to 1 because they refer to different subsets of curves (each percentage refers to the total number of occasions in which that VM could be effectively used).

Results are in line with those observed in real driving by Kandil et al. (2010) and Kandil et al. (2009). They reported that drivers used the tangent point model for 59 to 75% of the fixation time. In general, the TP is more used along right bends than on left ones. This indicates that the available sight distance also influences the visual strategies, since for the same radius (and obstruction conditions) leftward bends benefit of a greater ASD than right-hand ones (Kandil et al., 2010). Although these experiences (those of Kandil and the one here presented) were performed in different environments (real and simulated respectively), manifested driver behavior seems to be comparable.

Table 8.8 reports the time of use of single mechanisms in the whole experiment, compared to the travel time employed by drivers to negotiate the observed curves. For 15.1% of the time, participants fixated the tangent points on the road surface, and for 7% the gaze direction was tangent to the lateral sight obstruction. The road edges (VM 2a) were fixated for 8% of the time, while the occlusion point (VM 2d) was used for 0.2% of the time only.

Table 8.7. Counts and frequency of events where each vision mechanism was adopted in comparison to the possible number of events

VM	# identified events	# possible events	Frequency
1a	726	1,154	62.9%
1b	147	641	22.9%
2a	417	1,154	36.1%
2b	149	1,154	12.9%
2c	121	847	14.3%
2d	27	513	5.3%
3	71	814	8.7%

Table 8.8. Time of use and frequency of application of each vision mechanism with respect to the time employed to negotiate curves

VM	Fixation time (ms)	Travel time along curves (ms)	Frequency
1a	3,501,270	23,123,513	15.1%
1b	850,414	12,106,512	7.0%
2a	1,788,035	23,123,513	7.7%
2b	622,150	23,123,513	2.7%
2c	457,184	17,145,767	2.7%
2d	22,650	11,017,001	0.2%
3	199,749	16,212,658	1.2%

8.7.2 Combined vision mechanisms

The previous analysis considered the single fixations adopted by participants when negotiating curves. However, in some cases they fixated different elements during the driving task, to balance "guidance information" with "stabilization information" (Donges, 1978). The former is used by the driver to observe the desired path, whereas the second allows to maintain the vehicle and the actual path along the desired one.

Table 8.9 shows the number of curves where combined vision mechanisms (more than one) were employed by participants. In almost all the cases the number of occurrences increases as the radius increases too. This is mainly due to the length of the segment (that also increases with the radius of curvature), thus giving more time to the driver to fixate different reference elements.

The highest total number of combined vision mechanisms occurred in the Combination ID #7, that is also the richest of road reference elements (i.e., horizontal markings, lateral wall, margin delineators). In such framework, the driver had the chance to select the preferred elements to fix. Conversely, the number of combined vision mechanisms is reduced in the Combinations #5 and #6, where only the lateral wall and the horizontal markings were respectively provided. In these curves, the drivers maintained the attention on a single element or a single vision strategy along the entire curve.

Figure 8.26 exhibits the number of occurrences of combined vision mechanisms for each combination of elements. Combined strategies were defined according to the two most employed VMs. It is worth noting that in 100 observations the adopted visual strategy included the VM 1a and the VM 2a, and that drivers used VM 1a combined with the VM 2b in 79 occasions. In both cases, the adopted strategy for curve negotiation was based on the two-points steering model, since the "near zone" was fixated by means of the tangent point model, while the "far zone" was observed for the estimation of the target distance (Robertshaw and Wilkie, 2008; Salvucci and Gray, 2004).

According to Lehtonen et al. (2012), the use of the occlusion point (VM 2d) was always combined with other mechanisms, which contributed in lane keeping. The VM 3 was employed preferably with the VM 2a, since they both refer to the boundary of the roadway.

Table 8.9. Number of combined vision mechanisms distinguished for radius of curvature and combination ID

Combination ID	$R_1 = 120$ m	$R_2 = 225$ m	$R_3 = 300$ m	$R_4 = 430$ m	Total
1	7	11	14	21	53
2	16	21	33	41	111
3	6	6	9	19	40
4	5	12	7	17	41
5	1	5	11	14	31
6	3	9	6	15	33
7	24	38	38	32	132
					441
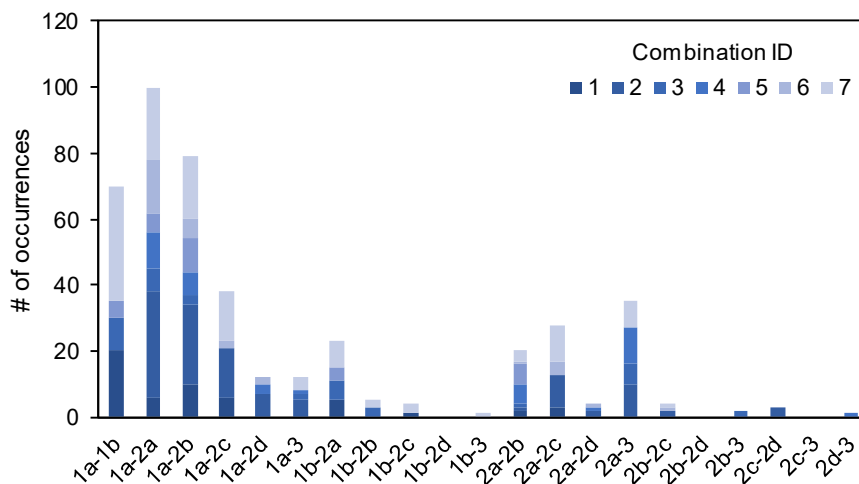
Figure 8.26. Distribution of the combined vision mechanisms among the different combinations of roadway elements along curves

Results evidenced the fundamental role of tangent points while negotiating curves. The curvature of longitudinal elements provides a beneficial information to drivers, who can simply estimate the road curvature ant properly act on the steering wheel. In addition, other elements on the carriageway/platform (i.e., road markings, road edges) give evidence of the lane/road width, where the vehicle can safely operate, preventing off track maneuvers.

On the other side, drivers need to control the road conditions ahead in order to anticipate possible events that may occur in the future path. For this reason, look-ahead fixations are used to plan in advance driving speed and trajectory as a function of the road alignment (Lehtonen et al, 2013; Wilkie et al., 2008), and to detect the presence of obstacles along the desired path.

Hence, the combination of these strategies is essential while driving along bends, where both the road geometry and the sight conditions are critical if compared to straight segments.

8.7.3 Effect of experience on fixations

Data referred to nine experienced and nine novice drivers were isolated from the database to analyze their behavior during the experiments. The group of experts (E) is composed by participants who obtained the driving license from at least 28

years; this subset declared an average traveled distance greater than 21,000 km/year. The group of novice (N) drivers is composed by those who took the license less than 13 years ago; such volunteers reported a traveled distance lower than 9,000 km/year.

Figure 8.27 displays the mean of fixation duration along left- and rightward bends of different radii. The numbers on the bottom of each column indicate the number of fixations from which the mean values were computed. It is worth noting that the greater the radius, the higher the mean fixation duration. In every cases, experienced drivers used averagely longer fixations than novice ones, in accordance with previous investigations (Lehtonen et al., 2014; Chapman and Underwood, 1998; Crundall and Underwood, 1998). Thus, expert participants tended to spend more time in fixating roadway elements, by using a reduced number of glances with respect to novice drivers. Cohen and Studach (1977) found opposite outcomes by monitoring only five experienced and four inexperienced drivers with a completely different background (only students with mean age of 23.5 years) with respect to the present work.

In the majority of cases, a greater number of fixations were observed for experienced drivers than novice ones, along the same number of curves (324). Average fixations duration were higher for rightward than for leftward curves. Hence, selected drivers tended to fixate for longer times those curves with a reduced ASD than on curves to the left. This observation suggests also a difference in quantity than in quality of drivers' fixation behavior (Lehtonen et al., 2014).

The ANOVA was employed to determine the relevance of the driving experience on fixations duration. Once again, the K-S test was used to verify that data shown in Figure 8.27 were normally distributed, with a level of significance equal to 5%. The analysis considers the sole experience of drivers (E or N) as principal effect, evidencing its high significance on results ($F(1,852) = 36.16$, $p = 6 \cdot 10^{-10}$, $\eta^2 = .046$; Table 8.10).
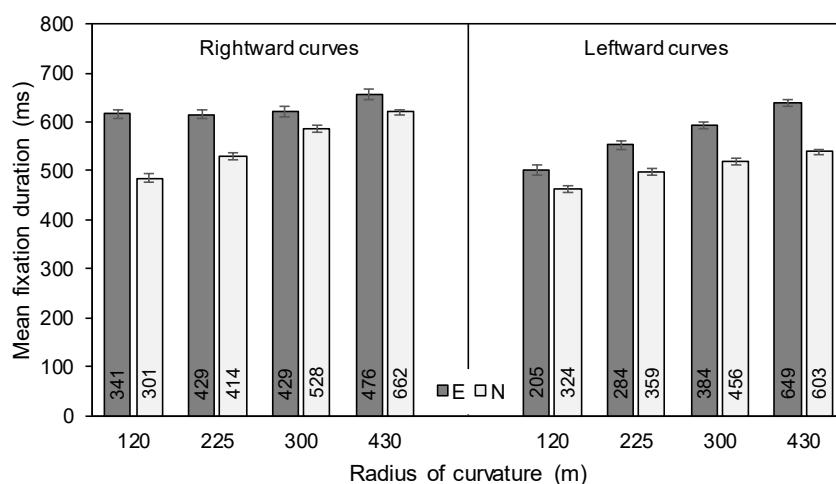
Figure 8.27. Mean fixation duration of expert (E) and novice (N) drivers distinguished for direction of the curve, and radius of curvature. On the bottom of columns, the number of fixations from which the mean and standard error (vertical bars) values were computed. Observations are referred to 324 curves of 1,154

Table 8.10. Results of one-way ANOVA on fixations duration of experienced and novice drivers

Principal Effects	Degree of Freedom	Sum of Squares	Mean of Squares	*F* value	Pr(>*F*)	η^2	code
Experience, *exp*	1	1104519	1104519	36.161	6.175e-10	0.046	***
Residuals	852	24030351	28205				

Notes: significance of codes is 0 '***', 0.001 '**', 0.01 '*', 0.05 '.', 0.1 ' ', 1

Nonetheless, the experience explains only 4.6% of the outcomes variance, meaning that there are also other factors that influence visual behavior along curves.

However, the fixation time could be also influenced by the driving speed adopted by the two subsets of participants. For this reason, a deeper analysis was focused on the evaluation of fixations belonging to different strategies, adopted by drivers who travelled on the same track. The total fixation time of use of each VM was computed according to the hypothesis that drivers traveled with similar speeds (they were not classified as aggressive or prudent, see §8.8.2 for discrimination criteria).

Figure 8.28 shows the comparison between visual strategies of experienced (E) and novice (N) drivers along the same test tracks: the case (A) considers three expert and three inexperienced participants who drove on the track A-mod, in counterclockwise direction; the case (B) includes four drivers (two E and two N) who performed the test on track B2, in clockwise direction.

Novice drivers preferably used simple visual strategies (i.e., tangent point model, VM 1a and VM 1b), compared to experienced ones that rather employed for more time those associated with the distance to target estimation (VM 2a and VM 2c). Thus, novice drivers fixated often the parts of the road close to the vehicle (i.e., road markings) in order to control their position within the lane, compared to more experienced ones who were more prone to plan their future trajectory (Lehtonen et al., 2014; Mourant and Rockwell, 1972; McLean and Hoffmann, 1971).

The numbers on top of the columns in Figure 8.28 indicate the number of fixations that contributed to reach the total fixation time. Expert participants used less glances for longer times (e.g., in the case of VM 1b in Figure 8.28B) with respect to unexperienced ones, confirming previous outcomes of Maltz and Shinar (1999) and Crundall and Underwood (1998).

Eventually, expert drivers were more prone to estimate the road curvature by means of the variation of the gaze angle (VM 3).

This analysis evidenced the different behavior of novice and experienced drivers. Visual skills demonstrated the inclination of expert drivers to scan widely, with shorter fixations. Results are in line with those of Underwood (2007), revealing also a more efficient ability to focus the visual attention on possible hazards on the roadway. In contrast, novice drivers showed less ocular activity and fixations felt on the near zone (close to the vehicle) for shorter durations.
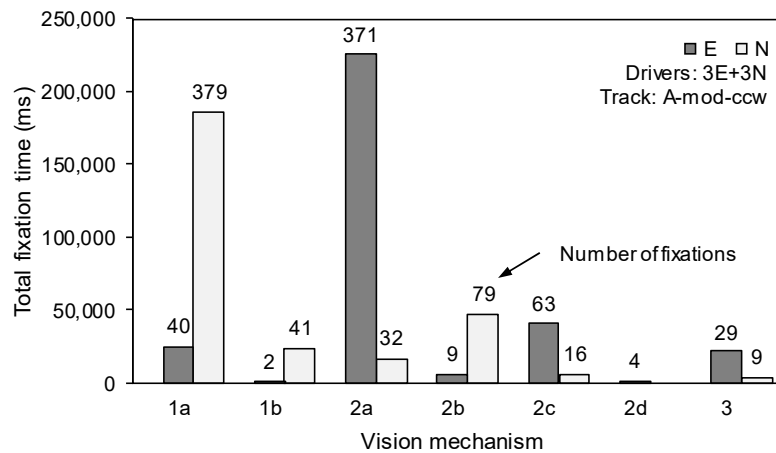
(A)
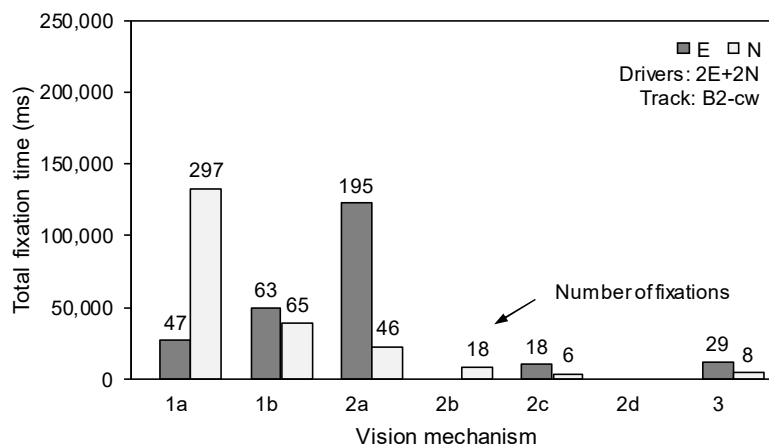
(B)

Figure 8.28. Distribution of total fixation time among the different vision mechanisms for (A) three expert (E) and three novice (N) drivers who traveled on the track A-mod in counterclockwise direction, and (B) two expert (E) and two novice (N) drivers who traveled on the track B2 in clockwise direction. The numbers on top of each column indicate the employed number of fixations

8.8 Vision Mechanisms vs. Operational Effects

In the following Section, the analysis focused on drivers' performance (driving speed and dispersion of trajectory collected in the Experiment #2) associated with the use of different visual strategies.

8.8.1 Effects of vision mechanism on driver behavior

Mean driving speed and the dispersion of trajectory adopted by participants were computed for each investigated curve. Also in this case, the data analysis was performed for the different combinations of roadway elements, in order to compare scenarios with similar visual inputs. The following figures show: (A) the box-plots that display the distributions of mean speeds along the curves characterized by the same ASD value (curves are distinguished in rightward and leftward directions);

and (B) the plots with mean speed and DT^S, to evaluate the different performance produced by vision mechanisms. Specifically, the most employed vision mechanism was considered as the most influential for driving behavior.

In this analysis, only in free-flow speeds were considered. In addition, DT^S was not computed along those bends where obstacles were placed on the roadside (§7.2.1, §7.5), since trajectories would be not influenced by the road geometry only. For these reasons, in the following figures the number of speed values on (A) graphs could be higher than those shown on (B) plots.

Combination #1

The first combination of elements considered the contextual presence of the horizontal markings and the lateral wall.

Figure 8.29A does not evidence a trend of speeds distribution along rightward curves, while on left-hand bends drivers who adopted the VM 1 increased their speed as the ASD increased too. The dispersion of speed data across the mean was wider along rightward than leftward curves; in fact, it decreased when the ASD increased. Corresponding dispersion of trajectory ranged between 0.12 and 0.68 m.

In the case of VM 2a, the greater the ASD, the larger the deviation from mean speeds, both on right-hand (for ASD from 68 to 108 m) and on left-hand curves (for ASD from 136 to 157 m). When the ASD < 107 m, participants who recurred to the VM 2c travelled faster than those who employed the VM 2a and VM 2b. The distribution of DT values (Figure 8.29B) ranged between 0.15 and 0.64 m for VM 2a data; reduced values were associated with VM 2b strategy (0.20-0.48 m).

(A)   *(B)*
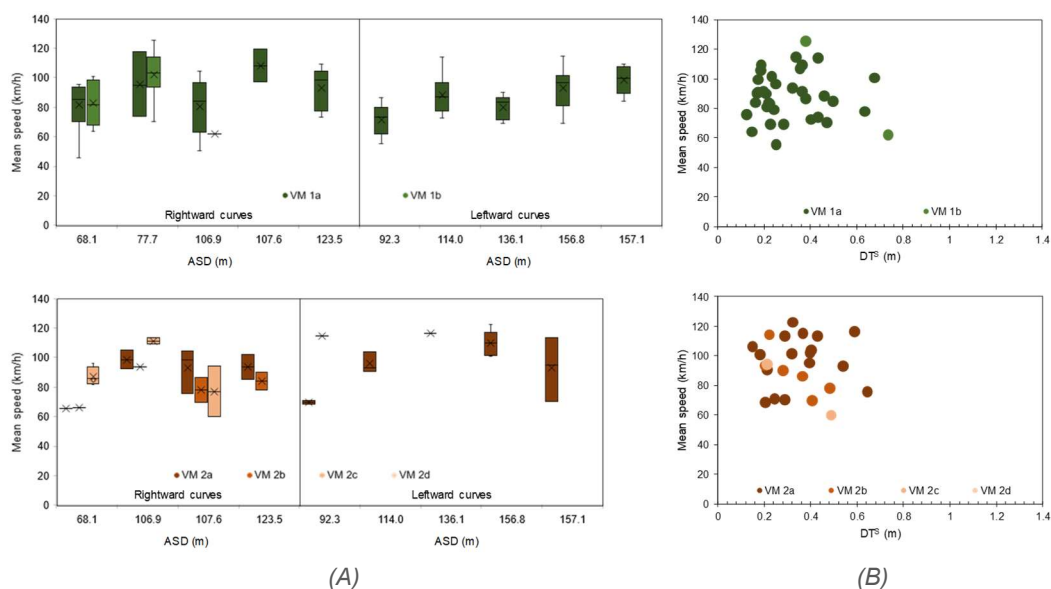
Figure 8.29. (A) Box-plots of mean speeds along curves with different ASD; and (B) plot of the correlation between dispersion of trajectory values and mean speeds, distinguished for classes of vision mechanisms. Observations are referred to curves with elements Combination #1

Combination #2

The second combination of elements included the road markings and margin delineators along the bend. The lack of lateral obstruction provided unrestricted sight conditions (ASD = ∞); in addition, VM 1b could not be employed by participants.

Figure 8.30A shows that mean values (× symbol inside the box) associated with the different VMs did not change between rightward and leftward curves, but the dispersion of speeds increased. In contrast, the dispersion of data decreased passing from VM 1 to VM 3.

In Figure 8.30B, DT^S ranged between 0.14 and 1.00 m for VM 1a, but it reduces for the other visual strategies: from 0.11 to 0.71 m for VM 2a, from 0.12 to 0.56 m for VM 2b, from 0.16 to 0.76 m for VM 2c, and from 0.10 to 0.47 m for VM 3. It is worth noting that VM 3 was preferably used on leftward curves. When employed by drivers, it contributed to adopt higher speeds and less errant trajectories across the theoretical one (lane centerline).
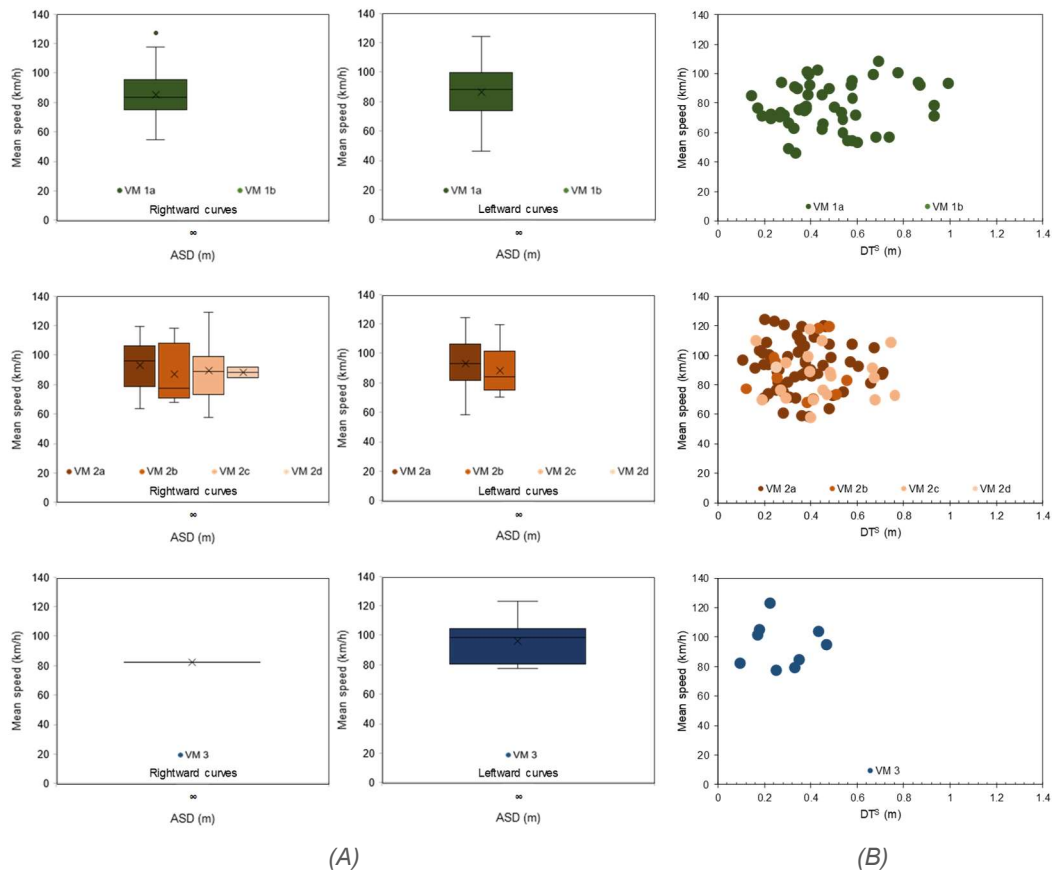
Figure 8.30. (A) Box-plots of mean speeds along curves with different ASD; and (B) plot of the correlation between dispersion of trajectory values and mean speeds, distinguished for classes of vision mechanisms. Observations are referred to curves with elements Combination #2

Combination #3

The third combination of elements considered the sight obstruction and margin delineators along the curve.

Figure 8.31A evidences that speed distributions increased their dispersion when the ASD became longer, for all VMs. Mean speeds grow as the ASD increases along right-hand curves; on the other hand, there is not a defined trend of data. VM 1b was employed along curves with reduced ASD (< 93 m): it produced a DT^S ranging between 0.28 to 0.77 m, and speeds higher than 78 km/h (Figure 8.31B). The adoption of VM 1a spread the dispersion of DT^S values until 1.09 m at 84 km/h.

In the case of VM 2, it is worth noting that the mean speeds referred to VM 2b were greater than those attributed to VM 2a both on rightward and leftward sharp curves. Along shallow rightward curves, the opposite trend occurred when ASD was longer than 107 m. DT^S values referred to VM 2a ranged between 0.10 m (at 54 km/h) to 0.84 m (at 69 km/h). Participants who adopted VM 2b demonstrated better performance in terms of DT (< 0.50 m).

The VM 3 was adopted only along leftward curves with an ASD longer than 100 m. Also in this case, the interval of DT^S is reduced in comparison to the other VMs (1a, 1b, and 2a).
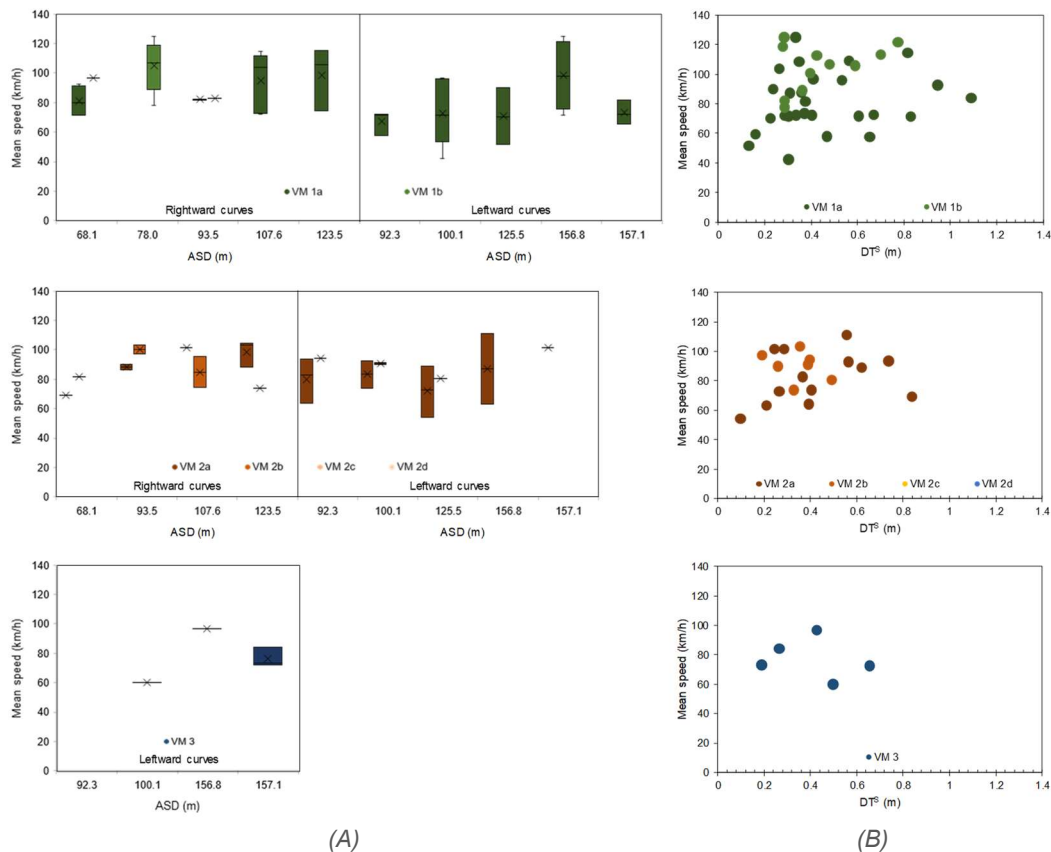
Figure 8.31. (A) Box-plots of mean speeds along curves with different ASD; and (B) plot of the correlation between dispersion of trajectory values and mean speeds, distinguished for classes of vision mechanisms. Observations are referred to curves with elements Combination #3

Combination #4

The fourth combination of elements considered the presence of margin delineators only. The absence of the lateral wall supplied to drivers unrestricted sight conditions (ASD = ∞).

Once again, Figure 8.32A shows that mean speed distributions of rightward curves were characterized by a lower mean values and dispersion with respect to leftward bend, both for data referred to VM 1 and VM 2. The use of occlusion point (VM 2d) was observed on one rightward curve only, providing a mean speed lower than those computed for VM 2a and VM 2b.

In Figure 8.32B, DT^S for the VM 1a ranged between 0.21 and 1.24 m; mean speeds associated with these limit cases were higher than 100 km/h. The interval of DT^S values reduced when other strategies were adopted: from 0.17 to 1.06 m for VM 2a, from 0.41 to 0.58 m for VM 2b, and from 0.21 to 0.77 m for VM 3.

(A)   *(B)*
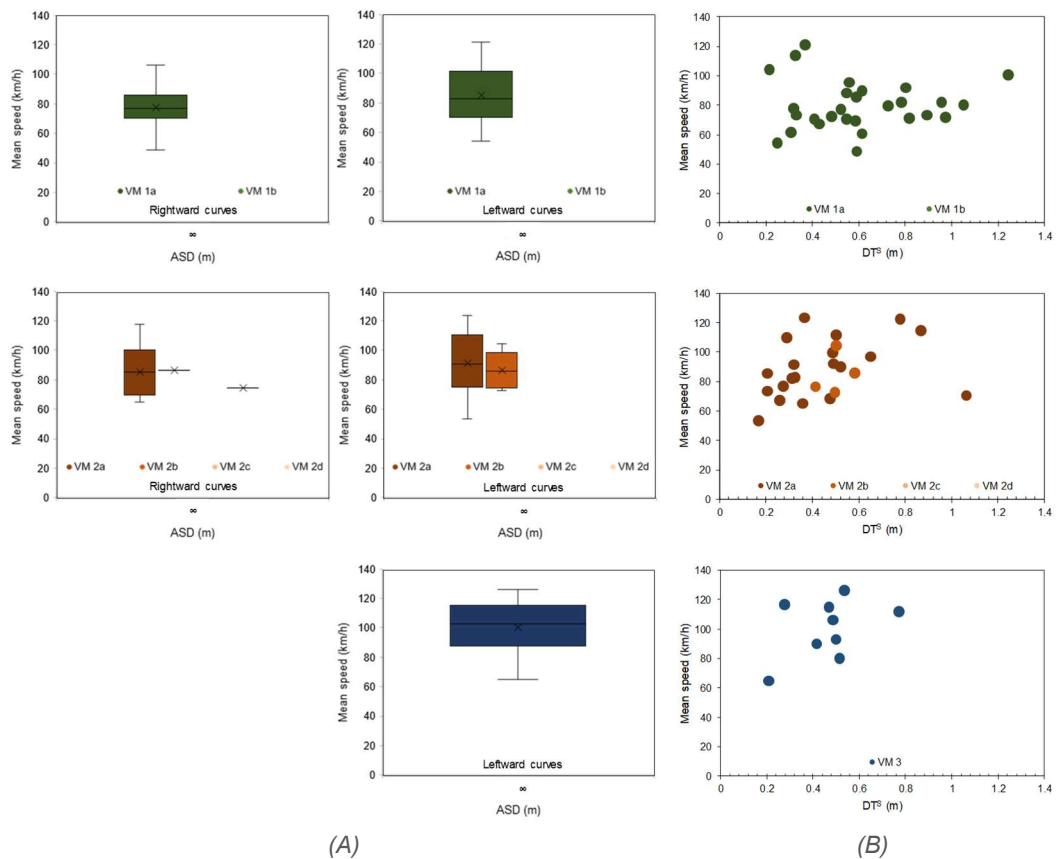
Figure 8.32. (A) Box-plots of mean speeds along curves with different ASD; and (B) plot of the correlation between dispersion of trajectory values and mean speeds, distinguished for classes of vision mechanisms. Observations are referred to curves with elements Combination #4

Combination #5

The fifth combination of elements presented the lateral sight obstruction only.

Figure 8.33A shows that the greater the ASD, the higher the mean speeds for drivers who adopted VM 1 and VM 2. In addition, the dispersion of speed data increased when ASD became longer. Participants principally referred to the lateral obstruction (VM 1b) only along rightward curves (ASD ≤ 108 m). Corresponding dispersion of trajectory ranged between 0.18 and 0.93 m for VM 1a, and between 0.37 and 0.63 m for VM 1b (Figure 8.33B).

In the case of VM 2, neither VM 2c nor VM 2d were used as main visual strategy for curve negotiation. The distribution of DT^S values for the VM 2a ranged between 0.20 and 1.25 m, but it reduced for those who adopted the VM 2b (from 0.18 to 0.95 m).

In this combination, the use of the VM 2 did not provide more efficient performance than the use of the VM 1.
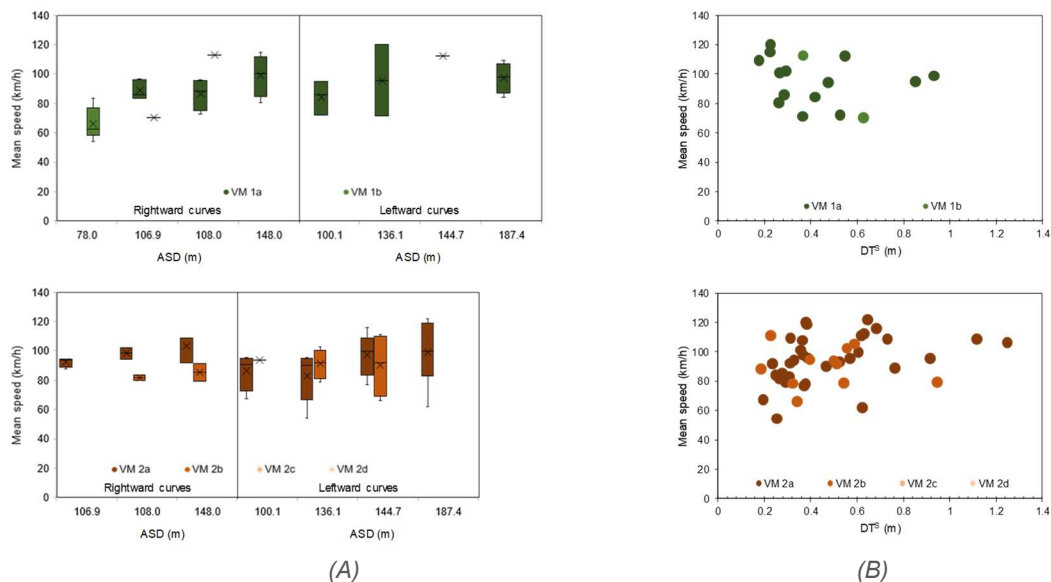
Figure 8.33. (A) Box-plots of mean speeds along curves with different ASD; and (B) plot of the correlation between dispersion of trajectory values and mean speeds, distinguished for classes of vision mechanisms. Observations are referred to curves with elements Combination #5

Combination #6

The sixth combination of elements considered the presence of horizontal markings only. The absence of any lateral obstruction provided unrestricted sight conditions (ASD = ∞).

Figure 8.34A shows that leftward curves induced higher mean speeds and dispersion of data with respect to rightward curves. This was observed both for VM 1a and VM 2a.

In Figure 8.34B, the more dispersed distribution of DT^S was that referred to VM 1a, which ranged between 0.10 (at 103 km/h) and 0.94 m (at 100 km/h). The DT^S dispersion reduced for the other visual strategies: from 0.18 to 0.75 m for VM 2a, from 0.08 to 0.43 m for VM 2b, and from 0.21 to 0.36 m for VM 2c.
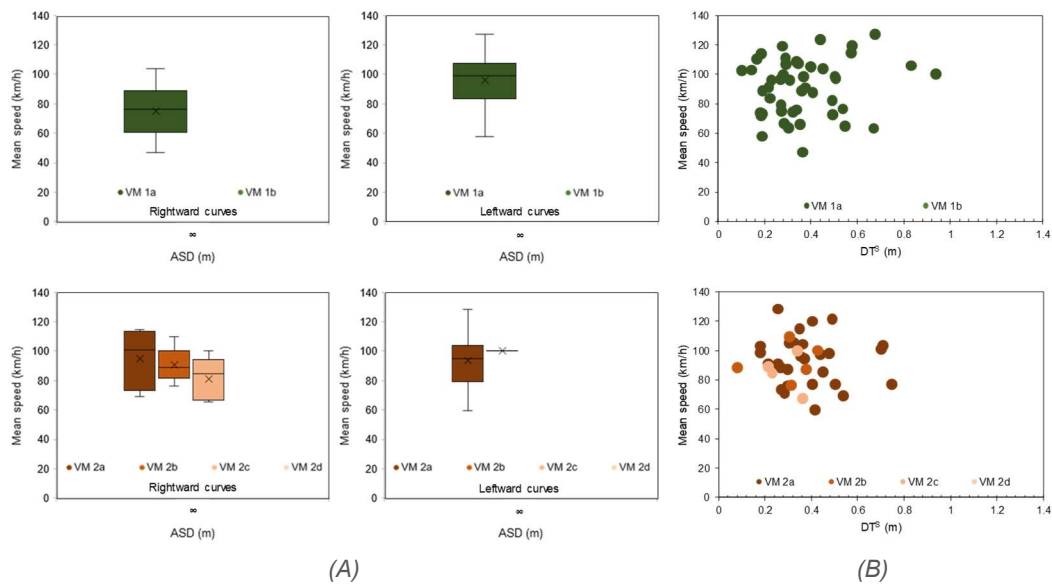
Figure 8.34. (A) Box-plots of mean speeds along curves with different ASD; and (B) plot of the correlation between dispersion of trajectory values and mean speeds, distinguished for classes of vision mechanisms. Observations are referred to curves with elements Combination #6

Combination #7

The last (seventh) combination of elements combined all the three guidance elements.

For VM 1a and VM 1b, Figure 8.35A evidences that there is not a defined trend for the distribution of mean speed along rightward curves, whereas those increased when ASD became longer along leftward curves. Also in this case, the distribution of DT^S (Figure 8.35B) was wider for VM 1a (0.12-1.01 m) with respect to VM 1b (0.22-0.88 m). The adoption of the VM 1b provided driving speeds higher than 68 km/h.

The dispersion of mean speeds along leftward curves increased with respect to rightward ones, when drivers adopted the VM 2a. The VM 2b was employed only when the ASD < 130 m, whereas the VM 2c was mainly employed on right-hand bends. Corresponding DT^S values ranged between 0.14 m (at 108 km/h) and 0.82 m (at 110 km/h) for VM 2a, from 0.21 to 0.46 m for VM 2b, and from 0.18 to 1.11 m for VM 2c. Conversely from previous results, participants who adopted the VM 2c showed worse performance than those who used the other steering strategies related to the estimation of the distance to target.

The VM 3 was adopted exclusively along leftward bends with ASD longer than 125 m. The related interval of DT^S (from 0.26 to 0.47 m) is reduced in comparison to those associated with the other VMs (Figure 8.35B).
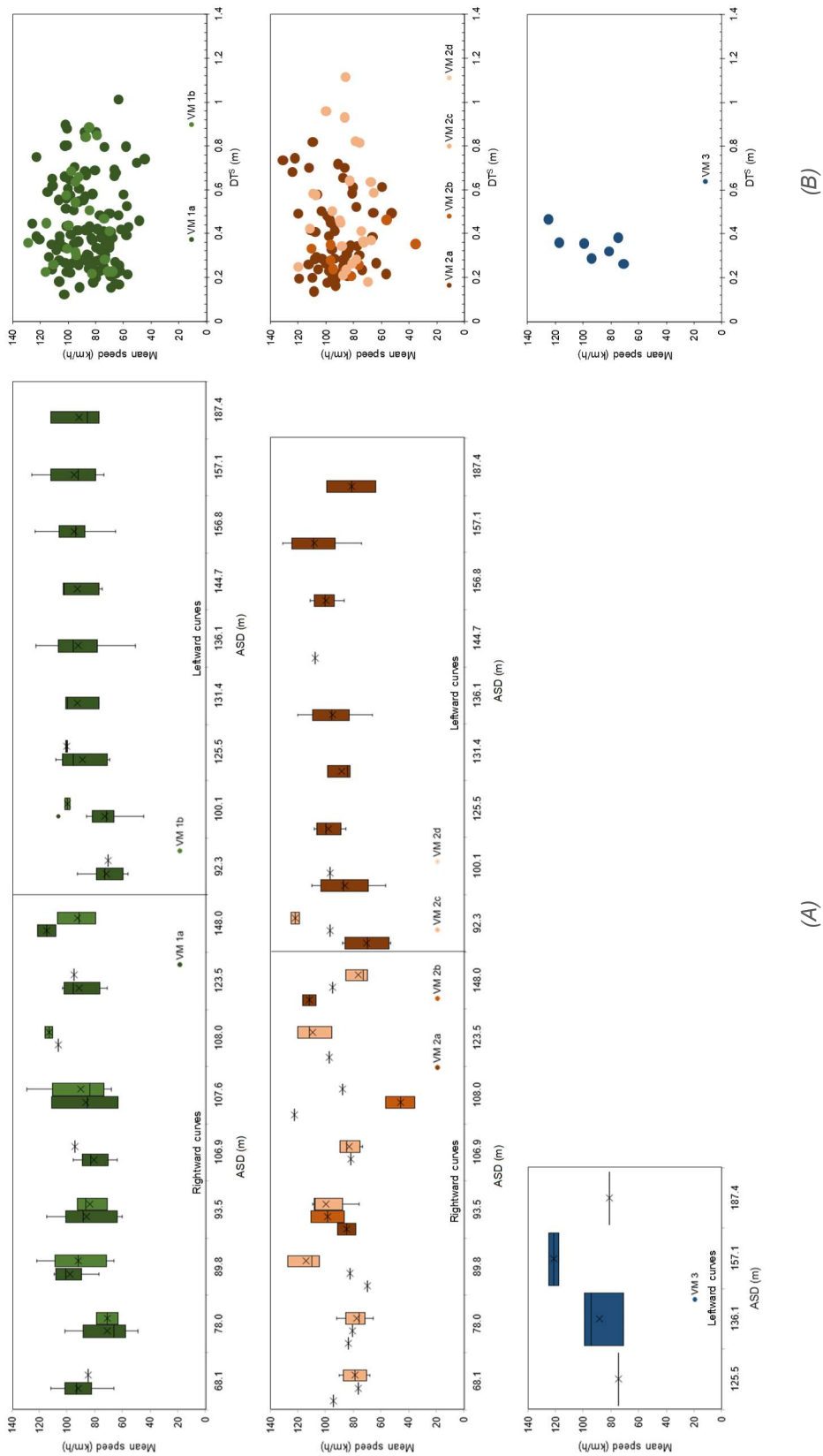
Figure 8.35. (A) Box-plots of mean speeds along curves with different ASD; and (B) plot of the correlation between dispersion of trajectory values and mean speeds, distinguished for classes of vision mechanisms. Observations are referred to curves with elements Combination #7

Table 8.11 listed the average values both for speeds (S) and standardized dispersion of trajectory (DT^S) showed in the preceding figures. It is evident that there is not a defined trend of data for the different combinations of elements. Moreover, it is worth noting that increasing the number of guidance elements on the road (i.e., Comb. ID #7) does not always produce greater speeds or more correct trajectories (De Waard et al., 2004). In fact, the highest values of DT^S were recorded when the road markings were added on the pavement.

<u>Summary</u>
Presented graphs lead to the following observations:

- drivers' behavior associated with the use of VM 1a (the most preferred strategy when negotiating curves) was characterized by a wider dispersion of mean speeds and trajectory;
- the line of sight tangent to the sight obstruction produced more stable trajectories and higher operating speeds;
- VM 2a led to safer mechanism since drivers better controlled the distance from the roadway out point. Its use entailed a more correct trajectory only when the road markings were present;
- wider dispersion of DT data were due to the absence of lane markings (Combinations #3, #4, #5). In such conditions, the VM 2b (control of the desired path) produced more accurate performance;
- VM 2d was used as a principal visual strategy in few occasions on rightward bends only. This confirms that drivers preferred to look at the road ahead (reduced eccentricity of the gaze direction), and sporadically plan the future path by looking towards the occlusion point (Lehtonen et al., 2012);
- in those few cases recorded, VM 3 was adopted in case of higher speeds and less dispersed trajectories in comparison to other vision strategies.

The great dispersion of DT^S produced by the tangent point model is consistent with previous investigations (Robertshaw and Wilkie, 2008), in which participants drove the vehicle towards the TP instead of following the road curvature. In such a way, the distance of the vehicle trajectory from the ideal one (lane gap) increased.

In general, a correlation between gaze direction and steering control may exist (Kandil et al., 2009). Here, the investigated vision mechanisms refer to different elements of the roadway and positions (near, middle, far) in the users' field of vision. The main interest is not related to the direction of the gaze (eccentricity from the straight direction), but on the variation of such gaze direction while driving along horizontal curves. In fact, the three strategies were defined by considering a constant angle θ (null variation, VM #1 and #2) or a change of θ in time (VM #3; see §7.2.2). The analysis of these strategies adopted by drivers revealed that there is a relationship between operating speed and trajectory accuracy: the higher the speeds, reduced is the dispersion of trajectory, when road markings are painted on the pavement. In addition, the more adequate steering control was observed for those who applied the VM #3, considered the most complex strategy since it was adopt principally by experienced participants.

Table 8.11. Summary of mean speed (S in km/h) and dispersion of trajectory (DT in m) values associated to each vision mechanism and combination of elements

Comb. ID	VM 1a		VM 1b		VM 2a		VM 2b		VM 2c		VM 2d		VM 3	
	S	DT	S	DT	S	DT	S	DT	S	DT	S	DT	S	DT
1	87.3	.30	94.7	.56	96.1	.35	85.3	.33	90.7	.35	-	-	-	-
2	86.0	.42	-	-	93.1	.37	87.8	.36	89.2	.45	88.2	.25	94.6	.28
3	82.4	.45	102.5	.45	85.6	.43	88.1	.35	-	-	-	-	77.2	.41
4	80.2	.60	-	-	89.3	.45	86.4	.50	-	-	74.4	-	100.3	.46
5	92.7	.42	72.5	.50	94.8	.49	88.7	.47	-	-	-	-	-	-
6	90.2	.37	-	-	94.0	.39	92.2	.30	81.3	.29	-	-	-	-
7	85.5	.44	91.0	.46	93.9	.39	81.6	.30	89.3	.51	-	-	94.6	.35

8.8.2 Effect of driving attitudes on fixations

The following analysis considers the driving performance (in terms of visual attention) of five aggressive (A) and five prudent (P) participants, selected among the whole sample for the speeds adopted along the experimental tracks. In particular, the profiles corresponding to the 15th and the 85th speed percentiles were computed for each track. Aggressive drivers were selected from those who overcome the profile corresponding to the 85th percentile, while prudent drivers between those who adopted speeds lower than the 15th percentile of recorded speeds.

Figure 8.36 reports the values of the ratio between the total fixation time (TFT) and the total travel time (TTT) along curves, computed for right- and left-hand curves of different radius (R). The TFT is the sum of fixation durations along the observed curves, whereas the TTT is the time spent to travel the correspondent bends. Therefore, the ratio TFT/TTT indicates the percentage of time in which drivers focused on roadway elements to read the road alignment; the ratio also excludes any effect of driving speed on compared values. Figure 8.36 includes data referred to 180 curves.

The distribution of data in Figure 8.36 evidences that:

- the percentage of fixations is higher along rightward curves than on leftward ones, in accordance with Lehtonen et al. (2014);
- the percentage of fixations along rightward curves with sight obstruction close to the shoulder ($d1 = 0$ m) was greater for prudent drivers than for aggressive ones;
- along right-hand bends, the farther the sight obstruction, the lower the percentage of fixations use; on shallow leftward bends, the trend was the opposite;
- with few exceptions, the percentage of fixation for aggressive drivers was higher than that for prudent ones.

Such observations highlight again the importance of the lateral element as a guidance reference when negotiating rightward curves. The attitude differences that emerged between aggressive and prudent participants are mainly related to their visual attention: drivers who adopted greater speeds were also more focused on the roadway characteristics; in contrast, cautious drivers spread their glances elsewhere in the surrounding environment.
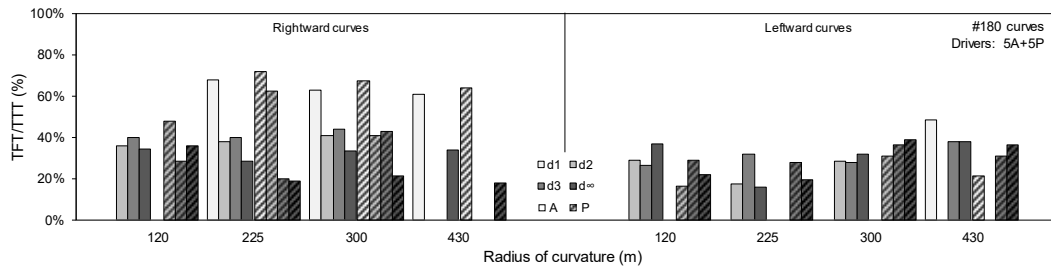
Figure 8.36. Distribution of the ratio between the total fixation time (TFT) and the total travel time (TTT) along rightward and leftward curves of different radius and distance of the obstruction from the shoulder (d1 = 0 m; d2 = 1.5 m; d3 = 3 m; d∞ = infinite). Ratios were compute for five aggressive (A) and five prudent (P) drivers, who drove on 180 curves

9. Conclusions

Previous studies investigated the effects of horizontal alignment and cross-sectional factors on the longitudinal behavior of drivers (Calvi, 2015b; Bella, 2013; Ben-Bassat and Shinar, 2011). These works did not measure the effects associated to variations in the available sight distance (ASD) along curves with limited visibility. According to Weller et al. (2008), the available sight distance is a key factors in the perception of road category, which in turn has a great influence on drivers' preferred speeds and trajectories.

The main aim of this experimental work was to evaluate if it (the sight distance available) actively affects a wide range of longitudinal and transversal behaviors of drivers. More specifically, this study examined the effects of ASD on driver preferred speed, trajectory, and visual strategy. The analyses were carried out by means of the fixed-base driving simulator at the *Politecnico di Torino*, and eye-tracking glasses for eye monitoring and fixations detection. ASD values were generated by the placement of a continuous sight obstruction at different offsets (D) from the traveled lane along curves of different radii (R) within a range from 120 to 430 m.

The study was organized into two consecutive experiments. Experiment #1 investigated the longitudinal (speed) and transversal (curvature, and lane gap) behaviors of participant drivers. Experiment #2 analyzed the vision mechanisms employed by TDs while negotiating curves, identifying the operational effects associated with the different visual strategies. Two different sets of volunteer drivers were involved in the experiments. A comparison of collected data was performed at the end of each analysis to assess the validity of results, and to support the robustness of the conclusions reached.

Pilot studies were performed in advance to evaluate the consistency of the experimental protocol, the time optimization during the driving sessions, and the methodologies for data manipulation and analysis. Driving speeds were examined by computing (i) the speed profiles of TDs along the circular arc portion of the investigated curves, and (ii) the mean speed of TDs by considering the factors controlling ASD (R and D).

The first set of output highlighted the effects of radius and the distance of sight obstructions from the vehicle trajectory on the operating speed profile. Along tight bends, the speed was not influenced by the position of the sight obstruction (i.e., by the ASD). The different attitudes became more appreciable with an increase in the radius of curvature, where the effect of the distance from the lateral obstruction was significant, more on right- than on leftward curves. Moreover, no substantial difference in speed was identified between sharp right and left curves, although a guidance effect from the continuous sight obstruction was evidenced in the outcomes.

The second set of output was directly associated with the actual ASD that drivers perceived along the traveled curves. Results confirmed that the road curvature had the greatest impact on driver preferred speed. On sharp curves, the speed choice was affected more by the curvature of the segment than by the ASD. For higher radii, the effect of the distance from the sight obstruction is also evident on driving speed, leading to increasing values when it moved far away from the vehicle trajectory (for rightward curves only). Conversely, on leftward bends the speed decreased even when the sight distance increased. Along the investigated interval of alignment radii, results indicated that the relationship between the mean driving speed and the ASD is linear: the greater the ASD, the higher the speed. The 2-way ANOVA highlighted the contextual statistical significance of both the radius and the offset of the obstruction from the vehicle trajectory on operating speed; the 3-way ANOVA confirmed that the offset of the sight obstruction from the pavement edge did not affect the speed choice of drivers.

Driver transversal behavior was analyzed in terms of (i) mean radius of curvature of the adopted trajectory along the circular arc only, (ii) the gap between the traveled path and the lane centerline, and (iii) the trajectory dispersion along the investigated curves. These quantities were computed and compared to the design variables and the actual ASD along each curve.

The mean trajectory curvature values along the circular arc were found to be similar to the design values on rightward curves, whereas those for left-hand bends were always greater. This means that the TDs were more inclined to "cut" the curves when traveling to the left than to the right. This is in line with previous observations by Coutton-Jean et al. (2009) and Boer (1996), who stated that drivers are prone to adopt the path with the lowest maximum curvature to minimize the centrifugal forces on the vehicle. However, this experiment evidenced that drivers tended to "cut" the leftward bends since this maneuver did not significantly limit their perceived ASD, while they adopted trajectory curvatures close to the design ones thereby not compromising their restricted sight distance. These outcomes derive from the analysis of several sight distances provided to TDs, which the previously mentioned works omitted. These results affirm the relevance of visual information that drivers process when negotiating curves, although the simulator is not able to return any acceleration to participants.

The lane gap profiles along the observed segments (50 m of approaching and departure tangents, spirals, and circular arc) showed that the greater the radius of curvature, the lower their variability (standard deviation). This indicates that the traveled paths along sharp curves are characterized by a less stable position, which becomes more accurate on shallow bends. Their tendency to "cut" curves was also revealed by participants, albeit this was more evident on tight rather than on shallow bends (Bella, 2013; Ben-Bassat and Shinar, 2011). Although the movement toward the roadside (on rightward curves) is risky for the driver, moving leftward is no less so since it may lead to a frontal collision with vehicles traveling in the opposite direction.

The computation of the standardized dispersion of trajectory (DT^S) confirmed that the accuracy of the trajectory increased for greater radii, and for leftward curves (Calvi, 2015b; Van Winsum and Godthelp, 1996). The trends of the DT^S also

evidenced the guidance role of the lateral sight obstruction on rightward bends. Specifically, for the same radius of curvature, reduced values were observed when the obstruction was close to the vehicle trajectory. The distance (D) from the lateral wall was less effective than the radius of curvature when negotiating leftward bends. A direct proportionality was also observed between the dispersion of trajectory and the ASD: the greater the ASD, the lower the DT^S. The ANOVA supports the high significance of the main geometric variables, like the radius (R) and the distance D from the vehicle path to the sight obstruction, on the dispersion of trajectory values.

Driving speed and trajectory data collected in Experiment #1 were compared to those gathered in Experiment #2. Despite the different goals of the second research activity, it was nevertheless useful for the validation of the results obtained in Experiment #1. The similarity in performance realized by different groups of participants bears out the robustness of collected data and the significance of the outcomes.

Experiment #2 considered the same road tracks in terms of geometrics, but some adjustments were made to the roadway elements (horizontal markings, lateral wall, margin delineator) in order to encourage drivers to activate different visual strategies while negotiating curves. Starting from the basic vision mechanisms already presented in literature (e.g., Salvucci and Gray, 2004; Wann and Land, 2000; Boer, 1996; Land and Lee, 1994), three classes of vision mechanisms were defined on the basis of the adopted gaze angle: (i) tangent point model, (ii) distance to target estimation, (iii) motion of the fixation point (or gaze angle variation). Fixations were analyzed in terms of the observed roadway element and length, to evaluate the adopted visual strategies, the different attitudes of expert/novice and aggressive/prudent drivers, and relationship to driving performance.

Firstly, the tangent point was the most used steering strategy adopted by drivers. Secondly, the lateral wall (sight obstruction) guides the steering strategy and enhanced the confidence of drivers along shallow curves. Thirdly, the margin delineators were used only on shallow leftward curves. In general, participants tended to fixate the near zone of the road when traveling on tight curves, and to look towards more distant zones as the radius (and the ASD) increased. According to Bella (2013), the right edge (or marking) had more of a guidance effect on right- than on leftward sharp curves.

Contrary to expectations, the lack of horizontal markings caused drivers to focus more on the same reference elements (or direction); when markings are painted on the pavement, the frequency of combined vision mechanisms grew. Hence, the dearth of information provided by the road environment resulted in a shift of focus to the elements that drivers judge most reliable; the greater the number of references, the more dispersed the scan-path.

The driving experience of the TDs played a fundamental role in visual strategy: expert drivers tended to fixate more on distant points ("guidance information") than novice ones did, who spent more fixation time on near zone ("stabilization information"). This was evidenced by selecting nine experienced and nine unexperienced drivers, and observing their behavior along two test tracks.

The different visual strategies affected the operational effects of TDs, both in terms of driving speed and lane position variability (DT^S). The high number of observations for the VM 1 (tangent point model) also increased the dispersion of this performance among the proposed ASD values. The use of different and more complex strategies (VM 2 and 3) encouraged participants to exert greater control over their lane position, even if the horizontal markings were not painted on the pavement. This means that some drivers were abler to adapt their steering strategies on the basis of the available information on the roadway; conversely, the absence of this fundamental street furniture may lead to unsafe travel conditions.

The driving attitudes of five participants manifesting a more aggressive behavior and five displaying a more prudent conduct were also compared. The analysis demonstrated that the percentage of fixation for aggressive drivers is higher than that for prudent drivers. Thus, speed management while driving requires attentiveness, which in turn is supported by visual information and adequate sight distance.

9.1 Implications of results

This investigation demonstrates that drivers adjusted their longitudinal behavior and vehicle trajectory in response to different ASD conditions. From the road designers' point of view, a knowledge of the range of possible driver behaviors would help the assumption of consistent design decision. In this way, the effects of road geometrics on driver behavior can be anticipated, and plausible driving errors and unexpected/undesired behaviors can be eliminated.

Hence, road geometric policy makers should integrate ASD as a fundamental parameter in operational analysis and road safety. Designers should avoid situations in which the ASD is much greater than the RSD. Based on the study results, limiting the ASD to the lowest possible value (but ensuring that ASD > RSD) is recommended in order to discourage drivers from adopting inappropriate speeds. This is also necessary to help drivers in "reading" the road characteristics, and assuming a more correct trajectory. Accordingly, limitations to the ASD could be used in conjunction with other environmental factors in the quest for a more prudent longitudinal behavior and a safer vehicle control.

Visual strategies confirmed that drivers were able to steer by adopting different mechanisms, but new insights revealed the influence of ASD when negotiating road scenarios with different combinations of lateral sight obstructions and reference lines. Fundamental visual information is provided by the road markings which drivers use as a reference more than other elements on the roadway. In this context, it is worth mentioning a recent research study that investigated how to use road markings for speed mitigation (Charlton et al., 2018). Therefore, road Agencies should take into account such observations and adopt maintenance plans to preserve the visibility of horizontal markings in any kind of environmental lighting conditions.

Reliability analysis is, nowadays, one of the solutions promoted to account for uncertainties in the geometric design and to evaluate the risk associated with particular design choices (Hussein et al., 2014). Thus, the results of this thesis

could be employed in the validation of risk-based reliability analysis to assess the effectiveness of design guides.

Furthermore, the results reported here are consistent with the "self-explaining road" concept and framework (Theeuwes and Godthelp, 1995). ASD is most definitely a factor that conveys a specific message to drivers, who use it to regulate their behavior.

9.2 Limitations of the study

The limitations in the results of this investigation follow:

- the selected road category corresponds to a two-lane highway set in a rural environment; other road categories should be considered in future studies;
- the range of curvature radii employed only considers bends with design speeds in the 60-100 km/h range, but with the maximum cross slope allowed by the Italian standards (i.e., 7%; MIT, 2001); other curve radii and pavement cross slopes could be taken into account in future investigations;
- the road tracks were developed on a flat terrain, thus the ASD was limited only in the horizontal plain and did not consider the effect(s) of the vertical alignment of the road which is something that could be included in further analyses;
- the reduced sample of TDs allows to categorize only small groups of participants as a function of their driving attitudes (aggressive/prudent and experienced/novice). A wider investigation is necessary to explore in deep their behavior on road.

General conclusions

This thesis presented the first research activities conducted using the fixed-base driving simulator at the *Politecnico di Torino*. Its use in research is primarily related to road design and road safety issues. In these fields, the understanding of human behavior is of primary interest, together with the operational effects produced by road geometrics, street furniture, and the general road environment. Therefore, the driving simulation plays an essential role in assuring the control of research variables, guaranteeing the repeatability of the experiments, and increasing operative safety conditions.

The key factors of this work consider that:
- the data analysis method proposed in the validation study has proved to be robust thereby highlighting the potential that the driving simulator has for the generation of field speeds and trajectories for different road elements and features;
- the assessment of the relative validity of the driving simulator (for the investigated road and environment characteristics) will be fundamental for the interpretation of simulated data from different road elements for real applications;
- the heterogeneity of selected participants results in a diversity of driver behavior due to differences in terms of experience and attitudes (or style). However, these analyses must be extended to a more sizeable sample of drivers to obtain more significant results;
- the drivers' performance, in terms of speed and trajectory, and ASD are linked by a direct proportionality. The greater the ASD, the higher the speed, while the dispersion of trajectory decreases;
- visual information is essential for drivers to "read" the road geometry and choose the adequate speed and trajectory. The lack of reference elements (i.e., horizontal markings) results in drivers adopting unsafe behaviors, increasing their perceived risk.

In future, there is a need to assess the potential for alternative visual equipment (i.e., Virtual Reality headset) to compensate for the limited field of view that drivers experienced with the simulator screens. A new validation work is required to assess its performance in the reproduction of real driving conditions.

Less invasive equipment (reduced heating of the cameras) is also preferred for future investigations into driver eye movement while driving. In fact, eye-tracking technology is continuously improving while costs are decreasing, making the inclusion of this precious surveying technique in future research activity a distinct possibility (Crundall and Underwood, 2011).

In conclusion, a complete exploration of the operational and behavioral effects of sight conditions requires that the ASD is also influenced by the vertical alignment of the road. This will be the objective of future work, to attain a comprehensive understanding of the role of ASD in driver performance.

But, will autonomous driving override the need for driver decisions in the near future?

References

AASHTO (2011). *A Policy on Geometric Design of Highways and Streets, 6th edition*. American Association of State Highway, and Transportation Officials, Washington, D.C. ISBN: 978-1-56051-508-1

Abele, L., and Møller, M. (2011). The relationship between road design and driving behavior: A simulator study. In *3rd International Conference on Road Safety and Simulation*.

Anderson, J. R., Matessa, M., and Lebiere, C. (1997). ACT-R: A theory of higher level cognition and its relation to visual attention. *Human-Computer Interaction*, *12*(4), 439-462.

Antonson, H., Mårdh, S., Wiklund, M., and Blomqvist, G. (2009). Effect of surrounding landscape on driving behaviour: A driving simulator study. *Journal of Environmental Psychology*, *29*(4), 493-502.

Assum, T. (1997). Attitudes and road accident risk. *Accident Analysis and Prevention*, *29*(2), 153-159.

Bassani, M., Dalmazzo, D., Marinelli, G., and Cirillo, C. (2014). The effects of road geometrics and traffic regulations on driver-preferred speeds in northern Italy. An exploratory analysis. *Transportation Research Part F: Traffic Psychology and Behaviour*, *25*, 10-26.

Bella, F. (2005b, October). Speeds and lateral placements on two-lane rural roads: analysis at driving simulator. In *Proceedings of the 13th International Conference "Road Safety on Four Continents"*. Warsaw, Poland.

Bella, F. (2013). Driver perception of roadside configurations on two-lane rural roads: Effects on speed and lateral placement. *Accident Analysis and Prevention*, *50*, 251-262.

Ben-Bassat, T., and Shinar, D. (2011). Effect of shoulder width, guardrail and roadway geometry on driver perception and behavior. *Accident Analysis and Prevention*, *43*, 2142-2152.

Benedetto, A., Calvi, A., D'Amico, F., and Zakowska, L. (2009, January). The effect of curve characteristics on driving behavior: A driving simulator study. In

Proceedings of 88ᵗʰ Annual Meeting of the Transportation Research Board. Washington, D.C.

Boer, E. R. (1996, September). Tangent point oriented curve negotiation. In *Proceedings of the Intelligent Vehicles Symposium* (pp. 7-12). IEEE.

Brenac, T. (1990) *Speed, Safety and Highway Design.* Recherche Transports Securite, Vol. 5, 69-74.

Brenac, T. (1996). Safety at curves and road geometry standards in some European countries. *Transportation Research Record, No. 1523*, 99-106.

Brookhuis, K. A., De Waard, D., and Janssen, W. H. (2001). Behavioural impacts of advanced driver assistance systems–an overview. *European Journal of Transport and Infrastructure Research, 1*(3), 245-253.

Brown, M., Marmor, M., Zrenner, E., Brigell, M., and Bach, M. (2006). ISCEV standard for clinical electro-oculography (EOG) 2006. *Documenta Ophthalmologica, 113*(3), 205-212.

Calvi, A. (2015a). Does roadside vegetation affect driving performance? Driving simulator study on the effects of trees on drivers' speed and lateral position. *Transportation Research Record: Journal of the Transportation Research Board, No. 2518*, 1-8.

Calvi, A. (2015b). A study on driving performance along horizontal curves of rural roads. *Journal of Transportation Safety and Security, 7*(3), 243-267.

Campbell, J. L., Lichty, M. G., Brown, J. L., Richard, C. M., Graving, J. S., Graham, J., O'Laughlin, M., Torbic, D., Harwood, D. (2012). *Human factors guidelines for road systems*. NCHRP Report 600 (2ⁿᵈ edition). Transportation Research Board, Washington, D.C.

Castro, M., Sánchez, J. F., Sánchez, J. A., and Iglesias, L. (2011). Operating speed and speed differential for highway design consistency. *Journal of Transportation Engineering, 137*(11), 837-840.

Chapman, P. R., and Underwood, G. (1998). Visual search of driving situations: Danger and experience. *Perception, 27*(8), 951-964.

Charlton, S. G. (2007). The role of attention in horizontal curves: A comparison of advance warning, delineation, and road marking treatments. *Accident Analysis and Prevention, 39*(5), 873-885.

Charlton, S. G., Starkey, N. J., and Malhotra, N. (2018). Using road markings as a continuous cue for speed choice. *Accident Analysis and Prevention, 117*, 288-297.

Chattington, M., Wilson, M., Ashford, D., and Marple-Horvat, D. E. (2007). Eye-steering coordination in natural driving. *Experimental Brain Research, 180*, 1-14.

Choueiri, E. M., Lamm, R., Kloeckner, J. H., and Mailaender, T. (1994). Safety aspects of individual design elements and their interactions on two-lane highways: international perspective. *Transportation Research Record, No. 1445*, 34-46.

Cohen, A. S., and Studach, H. (1977). Eye movements while driving cars around curves. *Perceptual and Motor Skills, 44*(3), 683-689.

Coutton-Jean, C., Mestre, D. R., Goulon, C., and Bootsma, R. J. (2009). The role of edge lines in curve driving. *Transportation Research Part F: Traffic Psychology and Behaviour, 12*(6), 483-493.

Crundall, D. E., and Underwood, G. (1998). Effects of experience and processing demands on visual information acquisition in drivers. *Ergonomics*, *41*(4), 448-458.

Crundall, D. E., and Underwood, G. (2011). Visual attention while driving. In: *Handbook of traffic psychology* (pp. 137-148). London, UK: Academic Press.

De Waard, D., Jessurun, M., Steyvers, F. J., Reggatt, P. T., and Brookhuis, K. A. (1995). Effect of road layout and road environment on driving performance, drivers' physiology and road appreciation. *Ergonomics*, *38*(7), 1395-1407.

De Waard, D., Steyvers, F. J., and Brookhuis, K. A. (2004). How much visual road information is needed to drive safely and comfortably?. *Safety Science*, *42*(7), 639-655.

Donges, E. (1978). A two-level model of driver steering behavior. *Human Factors*, *20*(6), 691-707.

Doumiati, M., Victorino, A., Charara, A., and Lechner, D. (2010). A method to estimate the lateral tire force and the sideslip angle of a vehicle: Experimental validation. In *Proceedings of the American Control Conference (ACC) 2010* (pp. 6936-6942). IEEE.

Duchowski, A. T. (2007). *Eye tracking methodology: Theory and Practice, 2nd edition*. London, UK: Springer

Fitzpatrick, C. D., Samuel, S., and Knodler Jr, M. A. (2016). Evaluating the effect of vegetation and clear zone width on driver behavior using a driving simulator. *Transportation Research Part F: Traffic Psychology and Behaviour*, *42*, 80-89.

Felipe, E., and Navin, F. (1998). Automobiles on horizontal curves: experiments and observations. *Transportation Research Record, No. 1628*, 50-56.

Fuller, R., and Santos, J. A. (2002). *Human factors for highway engineers*. Amsterdam, The Netherlands: Pergamon.

Gawron, V. J., and Ranney, T. A. (1990). Curve negotiation performance in a driving simulator as a function of curve geometry. *Applied Ergonomics*, *21*(1), 33-38.

Glennon, J. C., Neuman, T. R., and Leisch, J. E. (1983*). Safety and operational considerations for design of rural highway curves. Final report* (No. FHWA-RD-83-035). FHWA, U.S. Department of Transportation.

Godley, S. T., Triggs, T. J., and Fildes, B. N. (2004). Perceptual lane width, wide perceptual road centre markings and driving speeds. *Ergonomics*, *47*(3), 237-256.

Gregory, R. L. (2015). *Eye and Brain: The Psychology of Seeing, 5th edition*. Princeton, NJ: Princeton University Press.

Hartmann, E. (1970). Driver vision requirements. In *Proceedings of Society of Automotive Engineers*. New York, NY.

Hummer, J. E., Rasdorf, W., Findley, D. J., Zegeer, C. V., and Sundstrom, C. A. (2010). Curve collisions: road and collision characteristics and countermeasures. *Journal of Transportation Safety and Security*, *2*(3), 203-220.

Hussein, M., Sayed, T., Ismail, K., and Van Espen, A. (2014). Calibrating road design guides using risk-based reliability analysis. *Journal of Transportation Engineering*, *140*(9), 04014041.

Imberg, J., and Palmberg, A. (2015). *How curve geometry influences driver behavior in horizontal curves. A study of naturalistic driving*. Master's Thesis. Chalmers University of Technology, Gothenburg, Sweden.

Italian Parliament (1992a). *Nuovo Codice della Strada* (in Italian). D.Lgs. no. 285 of April, 30th.

Italian Parliament (1992b). *Regolamento di esecuzione e di attuazione del nuovo Codice della Strada* (in Italian). D.P.R. no. 495 of December, 16th.

Jamson, S., Lai, F., and Jamson, H. (2010). Driving simulators for robust comparisons: A case study evaluating road safety engineering treatments. *Accident Analysis and Prevention*, *42*(3), 961-971.

Kandil, F. I., Rotter, A., and Lappe, M. (2009). Driving is smoother and more stable when using the tangent point. *Journal of Vision*, *9*(1):11, 1-11.

Kandil, F. I., Rotter, A., and Lappe, M. (2010). Car drivers attend to different gaze targets when negotiating closed vs. open bends. *Journal of Vision*, *10*(4):24, 1-11.

Kanellaidis, G., Zervas, A., and Karagioules, V. (2000). Drivers' risk perception of road design elements. *Transportation Human Factors*, *2*(1), 39-48.

Kraus, J. F., Anderson, C. L., Arzemanian, S., Salatka, M., Hemyari, P., and Sun, G. (1993). Epidemiological aspects of fatal and severe injury urban freeway crashes. *Accident Analysis and Prevention*, *25*(3), 229-239.

Land, M. F., and Horwood, J. (1995). Which parts of the road guide steering?. *Nature*, *377*(6547), 339-340.

Land, M. F., and Lee, D. N. (1994). Where we look when steer, *Nature*, *369*(6483), 742-744.

Land, M. F., and Furneaux, S. (1997). The knowledge base of the oculomotor system. *Philosophical Transactions of the Royal Society of London B: Biological Sciences*, *352*(1358), 1231-1239.

Langner, R., Steinborn, M. B., Chatterjee, A., Sturm, W., and Willmes, K. (2010). Mental fatigue and temporal preparation in simple reaction-time performance. *Acta Psychologica*, *133*(1), 64-72.

Lappi, O., Lehtonen, E., Pekkanen, J., and Itkonen, T. (2013). Beyond the tangent point: gaze targets in naturalistic driving. *Journal of Vision*, *13*(13):11, 1-18.

Lappi, O. (2014). Future path and tangent point models in the visual control of locomotion in curve driving. *Journal of Vision*, *14*(12):21, 1-22.

Lehtonen, E., Lappi, O., and Summala, H. (2012). Anticipatory eye movements when approaching a curve on a rural road depend on working memory load. *Transportation Research Part F: Traffic Psychology and Behaviour*, *15*, 369-377.

Lehtonen, E., Lappi, O., Kotkanen, H., and Summala, H. (2013). Look-ahead fixations in curve driving. *Ergonomics*, *56*(1), 34-44.

Lehtonen, E., Lappi, O., Koirikivi, I., and Summala, H. (2014). Effect of driving experience on anticipatory look-ahead fixations in real curve driving. *Accident Analysis and Prevention*, *70*, 195-208.

Leisch, J. E., and Leisch, J. P. (1977). New concepts in design-speed application. *Transportation Research Record, No. 631*, 4-14.

Maltz, M., and Shinar, D. (1999). Eye movements of younger and older drivers. *Human Factors*, *41*(1), 15-25.

Martens, M. H., Compte, S., and Kaptein, N. A. (1997). The effects of road design on speed behaviour: a literature review. *Deliverable D1 (Report 2.3.1), MASTER Project*.

McFadden, J., and Elefteriadou, L. (2000). Evaluating horizontal alignment design consistency of two-lane rural highways: Development of new procedure. *Transportation Research Record: Journal of the Transportation Research Board, No. 1737*, 9-17.

McGehee, D. V., Lee, J. D., Rizzo, M., Dawson, J., and Bateman, K. (2004). Quantitative analysis of steering adaptation on a high performance fixed-base driving simulator. *Transportation Research Part F: Traffic Psychology and Behaviour, 7*(3), 181-196.

McGwin, G. Jr. (2011). Independent variables: The role of confounding and effect modification. In: *Handbook of driving simulation for engineering, medicine, and psychology* (pp. 15:1-8). Boca Raton, FL: CRC Press.

McLean, J. R., and Hoffmann, E. R. (1971). Analysis of drivers' control movements. *Human Factors, 13*(5), 407-418.

MIT (2001). *Norme funzionali e geometriche per la costruzione delle strade* (in Italian). Ministero delle Infrastrutture e dei Trasporti, D.M. no. 6792 of November 5th.

MIT (2016). *Conto Nazionale delle Infrastrutture e dei Trasporti: Anni 2014-2015* (in Italian). Ministero delle Infrastrutture e dei Trasporti, Istituto Poligrafico e Zecca dello Stato S.p.A. Roma, Italy.

Montella, A., Galante, F., Imbriani, L. L., Mauriello, F., and Pernetti, M. (2014). Simulator evaluation of drivers' behaviour on horizontal curves of two-lane rural highways. *Advances in Transportation Studies: An International Journal, 34*, 91-104.

Moreno, A. T., Garcia, A., Camacho-Torregrosa, F. J., and Llorca, C. (2013). Influence of highway three-dimensional coordination on drivers' perception of horizontal curvature and available sight distance. *IET Intelligent Transport Systems, 7*(2), 244-250.

Mourant, R. R., and Rockwell, T. H. (1972). Strategies of visual search by novice and experienced drivers. *Human Factors, 14*(4), 325-335.

Nelson, T. M. (1997). Fatigue, mindset and ecology in the hazard dominant environment. *Accident Analysis and Prevention, 29*(4), 409-415.

Organization for Economic Co-operation and Development (1990). *Behavioural adaptations to changes in the road transport system*. Organization for Economic Co-operation and Development, Paris, France.

Philip, P., Taillard, J., Klein, E., Sagaspe, P., Charles, A., Davies, W. L., Guilleminault, C., and Bioulac, B. (2003). Effect of fatigue on performance measured by a driving simulator in automobile drivers. *Journal of Psychosomatic Research, 55*(3), 197-200.

R Core Team (2016). *R: A language and environment for statistical computing*. R Foundation for Statistical Computing, Vienna, Austria. http://www.R-project.org/

Recarte, M. A. and Nunes, L. (2002). Mental load and loss of control over speed in real driving. Towards a theory of attentional speed control. *Transportation Research Part F: Traffic Psychology and Behaviour*, *5*(2), 133-144.

Richardson, J. T. (2011). Eta squared and partial eta squared as measures of effect size in educational research. *Educational Research Review*, *6*(2), 135-147.

Robertshaw, K. D., and Wilkie, R. M. (2008). Does gaze influence steering around a bend? *Journal of Vision*, *8*(4):18, 1-13.

Rosey, F., Auberlet, J. M., Moisan, O., and Dupré, G. (2009). Impact of narrower lane width: Comparison between fixed-base simulator and real data. *Transportation Research Record: Journal of the Transportation Research Board, No. 2138*, 112-119.

Rosey, F., and Auberlet, J. M. (2012). Trajectory variability: Road geometry difficulty indicator. *Safety Science*, *50*(9), 1818-1828.

Rudin-Brown, C. M., and Parker, H. A. (2004). Behavioural adaptation to adaptive cruise control (ACC): implications for preventive strategies. *Transportation Research Part F: Traffic Psychology and Behaviour*, *7*(2), 59-76.

Rushton, S. K., and Salvucci, D. D. (2001). An egocentric account of the visual guidance of locomotion. *Trends in Cognitive Sciences*, *5*(1), 6-7.

Said, D., Abd El Halim, A., and Hassan, Y. (2009). Desirable spiral length based on driver steering behavior. *Transportation Research Record: Journal of the Transportation Research Board, No. 2092*, 28-38.

Salvucci, D. D., and Goldberg, J. H. (2000, November). Identifying fixations and saccades in eye-tracking protocols. In *Proceedings of the 2000 Symposium on Eye Tracking Research & Applications* (pp. 71-78). ACM.

Salvucci, D. D. and Gray, R. (2004). A two-point visual control model of steering. *Perception*, *33*(10), 1233-1248.

Serafin, C. (1993). *Preliminary examination of driver eye fixations on rural roads: Insight into safety driving behavior*, Transportation Research Institute, University of Michigan, Ann Arbor, MI.

Shinar, D. (2017). *Traffic safety and human behavior, 2nd edition*. Bingley, UK: Emerald Publishing Limited.

Shinar, D., McDowell, E. D., and Rockwell, T. H. (1977). Eye movements in curve negotiation. *Human Factors*, *19*(1), 63-71.

Shinar, D., Rockwell, T. H., and Malecki, J. A. (1980). The effects of changes in driver perception on rural curve negotiation. *Ergonomics*, *23*(3), 263-275.

Singh, S. (2015). *Critical reasons for crashes investigated in the national motor vehicle crash causation survey* (No. DOT-HS-812-115). National Highway Traffic Safety Administration, U.S. Department of Transportation.

Sodhi, M., Reimer, B., Cohen, J. L., Vastenburg, E., Kaars, R., and Kirschenbaum, S. (2002, March). On-road driver eye movement tracking using head-mounted devices. In *Proceedings of the 2002 Symposium on Eye Tracking Research & Applications* (pp. 61-68). ACM.

Spacek, P. (2005). Track behavior in curve areas: attempt at typology. *Journal of Transportation Engineering*, *131*(9), 669-676.

Stamatiadis, N., Pigman, J., Sacksteder, J., Ruff, W., and Lord, D. (2009). *Impact of Shoulder Width and Median Width on Safety*. NCHRP Report 633. Transportation Research Board, Washington, D.C.

Stamatiadis, N., Bailey, K., Grossardt, T., and Ripy, J. (2010). Evaluation of highway design parameters on influencing operator speeds through casewise visual evaluation. *Transportation Research Record: Journal of the Transportation Research Board, No. 2195*, 143-149.

Summala, H. (1996). Accident risk and driver behaviour. *Safety Science*, *22*(1), 103-117.

Taylor, J. I., McGee, H. W., Seguin, E. L., and Hostetter, R. S. (1972). *Roadway delineation systems. National Cooperative Highway Research Program* (Report No. 130). Highway Research Board, Washington, D.C.

Theeuwes, J., and Godthelp, H. (1995). Self-explaining roads. *Safety Science*, *19*(2), 217-225.

Ting, P. H., Hwang, J. R., Doong, J. L., and Jeng, M. C. (2008). Driver fatigue and highway driving: A simulator study. *Physiology and Behavior*, *94*(3), 448-453.

Underwood, G., Chapman, P., Brocklehurst, N., Underwood, J., and Crundall, D. (2003). Visual attention while driving: sequences of eye fixations made by experienced and novice drivers. *Ergonomics*, *46*(6), 629-646.

Underwood, G. (2007). Visual attention and the transition from novice to advanced driver. *Ergonomics*, *50*(8), 1235-1249.

UNRAE (2016). *L'auto 2015: Sintesi Statistica. Il Mercato Italiano negli ultimi 10 anni* (in Italian). Unione Nazionale Rappresentanti Autoveicoli Esteri.

Van der Horst, R., and De Ridder, S. (2007). Influence of roadside infrastructure on driving behavior: Driving simulator study. *Transportation Research Record: Journal of the Transportation Research Board, No. 2018*, 36-44.

Van Winsum, W., and Godthelp, H. (1996). Speed choice and steering behavior in curve driving. *Human Factors*, *38*(3), 434-441.

Wann, J. P., and Land, M. F. (2000). Steering with or without the flow: Is the retrieval of heading necessary? *Trends in Cognitive Sciences*, *4*(8), 319-324.

Weller, G., Schlag, B., Friedel, T., and Rammin, C. (2008). Behaviourally Relevant Road Categorisation: A Step Towards Self-explaining Rural Roads. *Accident Analysis and Prevention*, *40*(4), 1581-1588.

Wilde, G. J. (1998). Risk homeostasis theory: An overview. *Injury Prevention*, *4*(2), 89-91.

Wilkie, R. M., and Wann, J. P. (2003). Eye-movements aid the control of locomotion. *Journal of Vision*, *3*(11), 677-684.

Wilkie, R. M., Wann, J. P., and Allison, R. S. (2008). Active gaze, visual look-ahead, and locomotor control. *Journal of experimental psychology: Human perception and performance*, *34*(5), 1150-1164.

Xiao, R. M., Yun, W. G., and Xu, T. B. (2007). Driving safety on long-even-straight-line road on highland. *Chang'an Daxue Xuebao (Ziran Kexue Ban)*, *27*(3), 76-79.

Yagar, S., and Van Aerde, M. (1983). Geometric and environmental effects on speeds of 2-lane highways. *Transportation Research Part A: General*, *17*(4), 315-325.

Zador, P., Stein, H. S., Wright, P., Hall, J. (1987). Effects of chevrons, post-mounted delineators, and raised pavement markers on driver behaviour at roadway curves. *Transportation Research Record*, *No. 1114*, 1-10.

Zakowska, L. (2010). Operational and safety effects of transition curves in highway design-A driving simulator study. In *4th International Symposium on Highway Geometric Design, Polytechnic University of Valencia, Transportation Research Board*.

Zhao, C., Zhao, M., Liu, J., and Zheng, C. (2012). Electroencephalogram and electrocardiograph assessment of mental fatigue in a driving simulator. *Accident Analysis and Prevention*, *45*, 83-90.

Zhao, X., Guan, W., and Liu, X. (2013). A pilot study verifying how the curve information impacts on the driver performance with cognition model. *Discrete Dynamics in Nature and Society*, *2013*. Hindawi Publishing Corporation.

Webography

[3] TRB Committee AHB65, Operational Effects of Geometrics: https://sites.google.com/site/trbcomahb65/home.

[4] Pupil labs: https://pupil-labs.com/

[5] Cognitivefun website for cognitive tests: cognitivefun.net

Attachments

A.1 MATLAB® scripts

<u>Field data</u>

```
clc;
clear all;
close all;

load TD19x_Trtt1.txt;
load POS_1.txt;

TRA=TD19x_Trtt1(:,:);
POS=POS_1(:,:);

[t1,t2]=size(TRA);
[p1,p2]=size(POS);

for a=1:p1 %start to read the vector POS
t=1;
pts_in_square=zeros(1,6); %variable that contains the points
inside the search window
for b=1:t1 %start to read the vector TRA
deltaE=(POS(a,1)-TRA(b,4)); %evaluate the difference between East
coordinate of two points
deltaN=(POS(a,2)-TRA(b,5)); % evaluate the difference between
North coordinate of two points
if abs(deltaE)<10 && abs(deltaN)<10
pts_in_square(t,1)=TRA(b,4); %save the coordinate X of the
trajectory point
pts_in_square(t,2)=TRA(b,5); %save the coordinate Y of the
trajectory point
pts_in_square(t,3)=sqrt((TRA(b,4)-POS(a,1))^2+(TRA(b,5)-
POS(a,2))^2); %compute the distance between the point on TRA and
the point on POS vectors
pts_in_square(t,4)=TRA(b,6); %save the speed of the trajectory
point
t=t+1;
end
end

[pts1,pts2]=size(pts_in_square); %determine the size of the
variable pts_in_square
if pts1==1 %if no point fall inside the search window...
PTS(a,1)=NaN; %save one row of NaN (coordinate x)
PTS(a,2)=NaN; %save one row of NaN (coordinate y)
PTS(a,3)=NaN; %save one row of NaN (distance)
PTS(a,4)=NaN; %save one roe of NaN (speed)
else
pts_ord=sortrows(pts_in_square,3); %sort in increasing order the
whole matrix pts_in_square on the basis of values in the column 3
(distance)
PTS(a,1)= pts_ord(1,1); %save the coordinate of the closest point
in the vector PTS
PTS(a,2)= pts_ord(1,2);
PTS(a,3)= pts_ord(1,4); %save the speed of the closest point in
the vector PTS
end
```

```
clear pts_in_square
end

save('TD19_xass_Tr1.txt','PTS','-ASCII','-double'); %export file
```

Driving simulator data

```
clc;
clear all;
close all;

load TD19s_Trtt1.txt;
load POS_1.txt;

TRA=TD19s_Trtt1(:,:);
POS=POS_1(:,:);

[t1,t2]=size(TRA);
[p1,p2]=size(POS);

for a=1:p1 %start to read the vector POS
t=1;
pts_in_square=zeros(1,6); %variable that contains the points
inside the search window
for b=1:t1 %start to read the vector TRA
deltaE=(POS(a,1)-TRA(b,5)); %evaluate the difference between East
coordinate of two points
deltaN=(POS(a,2)-TRA(b,6)); % evaluate the difference between
North coordinate of two points
if abs(deltaE)<5 && abs(deltaN)<5
pts_in_square(t,1)=TRA(b,5); %save the coordinate X of the
trajectory point
pts_in_square(t,2)=TRA(b,6); %save the coordinate Y of the
trajectory point
pts_in_square(t,3)=sqrt((TRA(b,5)-POS(a,1))^2+(TRA(b,6)-
POS(a,2))^2); %compute the distance between the point on TRA and
the point on POS vectors
pts_in_square(t,4)=TRA(b,2); %save the speed of the trajectory
point
t=t+1;
end
end

[pts1,pts2]=size(pts_in_square); %determine the size of the
variable pts_in_square
if pts1==1 %if no point fall inside the search window...
PTS(a,1)=NaN; %save one row of NaN (coordinate x)
PTS(a,2)=NaN; %save one row of NaN (coordinate y))
PTS(a,3)=NaN; %save one row of NaN (distance)
PTS(a,4)=NaN; %save one roe of NaN (speed)
else
pts_ord=sortrows(pts_in_square,3); %sort in increasing order the
whole matrix pts_in_square on the basis of values in the column 3
(distance)
PTS(a,1)= pts_ord(1,1); %save the coordinate of the closest point
in the vector PTS
PTS(a,2)= pts_ord(1,2);
PTS(a,3)= pts_ord(1,4); %save the speed of the closest point in
the vector PTS
end
clear pts_in_square
end

save('TD19_sass_Tr1.txt','PTS','-ASCII','-double'); %export file
```

A.2 Data and results of statistical tests (Validity study)

The following tables report the data used to carry out the statistical tests of Experiment #1, and the obtained results.

The procedure adopted for the computation was that proposed in Bella (2005a), which considers these steps:

$$\sigma_{(X_F - X_S)} = \sqrt{\frac{\sigma_F^2}{N_F} + \frac{\sigma_S^2}{N_S}}$$

$$Z = \frac{(X_F - X_S)}{\sigma_{(X_F - X_S)}}$$

$$CI = 0 \pm Z_{crit} \cdot \sigma_{(X_F - X_S)}$$

$$Z_\beta = \left(Z_{crit} \cdot \sigma_{(X_F - X_S)} - \Delta \right) \cdot \frac{1}{\sigma_{(X_F - X_S)}}$$

$$\beta = \frac{1}{\sqrt{2\pi}} \cdot e^{-\frac{Z_\beta^2}{2}}$$

where X_F and X_S are the mean values of the observations (speed, anticipatory distance, curvature, curvature change rate), σ_F and σ_S are the associated standard deviations, in the field and at the simulator, respectively; CI is the confidence interval.

Speed data

Segment #1

Station (m)	Field			Simulation			S_F-S_S (km/h)	σ^2_{comb} (km/h)^2	Δ (km/h)	$\sigma(S_F$-$S_S)$ (km/h)	$|Z|$	$|Z_{crit}|$	Result of test	Confidence interval		Z_β	β	Power (1-β)	Hedges's effect size, g
	Mean speed S_F (km/h)	#	Standard deviation (km/h)	Mean speed S_S (km/h)	#	Standard deviation (km/h)								Lower limit	Upper limit				
0	34.41	27	3.81	32.15	26	4.59	2.3	17.7	3.4	1.2	1.95	1.96	H₀ acc.	-2.3	2.3	-1.00	0.16	0.84	0.54
100	45.78	27	4.42	43.70	26	7.94	2.1	40.9	4.6	1.8	1.18	1.96	H₀ acc.	-3.5	3.5	-0.62	0.27	0.73	0.33
200	51.06	27	5.28	51.92	26	8.75	-0.9	51.7	5.1	2.0	0.43	1.96	H₀ acc.	-3.9	3.9	-0.60	0.27	0.73	0.12
300	57.82	27	5.34	57.58	26	9.86	0.2	62.2	5.8	2.2	0.11	1.96	H₀ acc.	-4.3	4.3	-0.68	0.25	0.75	0.03
400	58.14	27	6.76	55.39	26	8.81	2.8	61.4	5.8	2.2	1.27	1.96	H₀ acc.	-4.2	4.2	-0.73	0.23	0.77	0.35
500	50.10	27	4.17	48.03	26	7.09	2.1	33.5	5.0	1.6	1.29	1.96	H₀ acc.	-3.1	3.1	-1.16	0.12	0.88	0.36
600	58.37	27	4.80	55.65	26	7.20	2.7	37.2	5.8	1.7	1.61	1.96	H₀ acc.	-3.3	3.3	-1.50	0.07	0.93	0.45
700	56.87	26	5.38	58.47	26	7.53	-1.6	42.8	5.7	1.8	0.88	1.96	H₀ acc.	-3.6	3.6	-1.17	0.12	0.88	0.24
800	60.17	26	6.52	58.97	26	8.48	1.2	57.2	6.0	2.1	0.57	1.96	H₀ acc.	-4.1	4.1	-0.91	0.18	0.82	0.16
900	61.75	26	6.68	62.72	26	7.64	-1.0	51.5	6.2	2.0	0.49	1.96	H₀ acc.	-3.9	3.9	-1.14	0.13	0.87	0.13
1000	61.59	27	6.06	63.66	26	8.85	-2.1	57.1	6.2	2.1	0.99	1.96	H₀ acc.	-4.1	4.1	-0.98	0.16	0.84	0.27
1100	60.94	27	6.00	64.73	26	9.21	-3.8	59.9	6.1	2.1	1.77	1.96	H₀ acc.	-4.2	4.2	-0.88	0.19	0.81	0.49
1200	61.70	27	5.56	60.10	26	9.15	1.6	56.8	6.2	2.1	0.77	1.96	H₀ acc.	-4.1	4.1	-0.99	0.16	0.84	0.21
1300	57.11	27	6.03	52.87	26	8.87	4.2	57.1	5.7	2.1	2.03	1.96	H₀ ref.	-4.1	4.1	-0.77	0.22	0.78	0.56

Note: α = .05; Δ = 0.1 × S_F

Segment #2

Station (m)	Field Mean speed S_F (km/h)	#	Standard deviation (km/h)	Simulation Mean speed S_S (km/h)	#	Standard deviation (km/h)	S_F-S_S (km/h)	σ^2_{comb} (km/h)^2	Δ (km/h)	$\sigma(S_F$-$S_S)$ (km/h)	$|Z|$	$|Z_{crit}|$	Result of test	Confidence interval Lower limit	Upper limit	Z_β	β	Power (1-β)	Hedges's effect size, g
0	53.34	27	6.93	37.82	26	7.49	15.5	52.0	5.3	2.0	7.82	1.96	H₀ ref.	-3.9	3.9	-0.73	0.23	0.77	2.15
100	63.95	27	5.78	60.53	26	6.47	3.4	37.5	6.4	1.7	2.03	1.96	H₀ ref.	-3.3	3.3	-1.83	0.03	0.97	0.56
200	70.81	27	6.47	71.02	26	6.82	-0.2	44.1	7.1	1.8	0.12	1.96	H₀ acc.	-3.6	3.6	-1.91	0.03	0.97	0.03
300	74.47	27	7.77	76.15	26	9.30	-1.7	73.2	7.4	2.4	0.71	1.96	H₀ acc.	-4.6	4.6	-1.20	0.12	0.88	0.20
400	74.82	26	8.25	77.23	26	12.36	-2.4	110.5	7.5	2.9	0.83	1.96	H₀ acc.	-5.7	5.7	-0.61	0.27	0.73	0.23
500	73.85	26	8.67	80.28	26	12.67	-6.4	117.9	7.4	3.0	2.14	1.96	H₀ ref.	-5.9	5.9	-0.49	0.31	0.69	0.59
600	75.05	25	9.01	83.24	26	13.43	-8.2	131.8	7.5	3.2	2.57	1.96	H₀ ref.	-6.3	6.3	-0.39	0.35	0.65	0.71
700	76.24	25	8.36	84.00	26	13.42	-7.8	126.1	7.6	3.1	2.49	1.96	H₀ ref.	-6.1	6.1	-0.48	0.31	0.69	0.69
800	76.95	25	8.13	83.91	26	13.82	-7.0	129.8	7.7	3.2	2.20	1.96	H₀ ref.	-6.2	6.2	-0.47	0.32	0.68	0.61
900	76.27	25	9.05	82.26	26	13.42	-6.0	132.0	7.6	3.2	1.88	1.96	H₀ acc.	-6.3	6.3	-0.43	0.33	0.67	0.52
1000	71.92	24	10.36	77.16	26	12.70	-5.2	135.4	7.2	3.3	1.60	1.96	H₀ acc.	-6.4	6.4	-0.24	0.40	0.60	0.45
1100	61.53	25	9.24	64.07	26	14.53	-2.5	149.5	6.2	3.4	0.75	1.96	H₀ acc.	-6.7	6.7	0.15	0.56	0.44	0.21
1200	28.54	25	8.30	37.93	26	9.43	-9.4	79.1	2.9	2.5	3.78	1.96	H₀ ref.	-4.9	4.9	0.81	0.79	0.21	1.06

Note: α = .05; Δ = 0.1 × S_F

Segment #3

Station (m)	Field			Simulation			S_F-S_S (km/h)	σ^2_{comb} (km/h)^2	Δ (km/h)	$\sigma(S_F$-$S_S)$ (km/h)	$|Z|$	$|Z_{crit}|$	Result of test	Confidenceinterval		Z_β	β	Power (1-β)	Hedges's effect size, g
	Mean speed S_F (km/h)	#	Standard deviation (km/h)	Mean speed S_S (km/h)	#	Standard deviation (km/h)								Lower limit	Upper limit				
0	32.73	23	2.92	32.60	26	3.89	0.1	12.0	3.3	1.0	0.14	1.96	H_0 acc.	-1.9	1.9	-1.39	0.08	0.92	0.04
100	49.67	23	4.75	50.52	26	7.39	-0.8	39.6	5.0	1.8	0.48	1.96	H_0 acc.	-3.4	3.4	-0.87	0.19	0.81	0.13
200	61.53	23	4.82	63.65	26	8.00	-2.1	44.9	6.2	1.9	1.14	1.96	H_0 acc.	-3.6	3.6	-1.34	0.09	0.91	0.32
300	69.00	23	5.07	73.33	26	8.02	-4.3	46.2	6.9	1.9	2.28	1.96	H_0 ref.	-3.7	3.7	-1.68	0.05	0.95	0.64
400	74.57	23	5.41	78.80	26	9.93	-4.2	66.1	7.5	2.2	1.88	1.96	H_0 acc.	-4.4	4.4	-1.35	0.09	0.91	0.52
500	78.11	23	5.99	81.74	26	11.35	-3.6	85.3	7.8	2.6	1.42	1.96	H_0 acc.	-5.0	5.0	-1.10	0.14	0.86	0.39
600	80.13	23	7.03	83.73	26	12.31	-3.6	103.8	8.0	2.8	1.27	1.96	H_0 acc.	-5.5	5.5	-0.88	0.19	0.81	0.35
700	81.43	23	7.63	84.53	26	12.05	-3.1	104.4	8.1	2.8	1.09	1.96	H_0 acc.	-5.6	5.6	-0.90	0.18	0.82	0.30
800	80.93	19	7.37	84.24	26	11.53	-3.3	100.0	8.1	2.8	1.17	1.96	H_0 acc.	-5.5	5.5	-0.91	0.18	0.82	0.33
900	80.50	19	6.56	85.81	26	10.84	-5.3	86.4	8.1	2.6	2.04	1.96	H_0 ref.	-5.1	5.1	-1.13	0.13	0.87	0.57
1000	80.20	19	7.06	86.15	26	10.85	-6.0	89.3	8.0	2.7	2.23	1.96	H_0 ref.	-5.2	5.2	-1.04	0.15	0.85	0.63
1100	78.87	19	7.06	84.65	26	12.92	-5.8	118.0	7.9	3.0	1.92	1.96	H_0 acc.	-5.9	5.9	-0.66	0.25	0.75	0.53
1200	78.54	19	7.01	84.37	26	12.75	-5.8	115.0	7.9	3.0	1.96	1.96	H_0 ref.	-5.8	5.8	-0.68	0.25	0.75	0.54
1300	80.21	19	6.09	85.75	26	13.15	-5.5	116.1	8.0	2.9	1.89	1.96	H_0 acc.	-5.7	5.7	-0.77	0.22	0.78	0.51
1400	82.32	21	5.76	88.01	26	13.16	-5.7	110.9	8.2	2.9	1.98	1.96	H_0 ref.	-5.6	5.6	-0.91	0.18	0.82	0.54
1500	84.02	21	6.37	90.17	26	12.62	-6.1	106.5	8.4	2.8	2.17	1.96	H_0 ref.	-5.6	5.6	-1.00	0.16	0.84	0.60
1600	84.47	20	6.21	91.29	26	13.00	-6.8	112.6	8.4	2.9	2.35	1.96	H_0 ref.	-5.7	5.7	-0.95	0.17	0.83	0.64
1700	83.63	20	6.18	90.80	26	13.81	-7.2	124.9	8.4	3.0	2.36	1.96	H_0 ref.	-6.0	6.0	-0.79	0.21	0.79	0.64
1800	82.78	20	6.47	89.92	26	12.97	-7.1	113.7	8.3	2.9	2.44	1.96	H_0 ref.	-5.7	5.7	-0.87	0.19	0.81	0.67
1900	82.27	20	6.65	88.91	26	12.57	-6.6	108.8	8.2	2.9	2.31	1.96	H_0 ref.	-5.6	5.6	-0.90	0.18	0.82	0.64
2000	82.19	20	6.53	85.87	26	11.85	-3.7	98.1	8.2	2.7	1.34	1.96	H_0 acc.	-5.4	5.4	-1.04	0.15	0.85	0.37
2100	82.15	17	7.33	85.51	26	11.08	-3.4	95.9	8.2	2.8	1.20	1.96	H_0 acc.	-5.5	5.5	-0.96	0.17	0.83	0.34
2200	81.75	17	7.02	87.93	26	10.76	-6.2	89.8	8.2	2.7	2.28	1.96	H_0 ref.	-5.3	5.3	-1.06	0.15	0.85	0.65
2300	81.76	17	6.97	90.93	26	10.64	-9.2	88.0	8.2	2.7	3.41	1.96	H_0 ref.	-5.3	5.3	-1.08	0.14	0.86	0.98
2400	82.11	17	7.31	92.76	26	10.95	-10.6	93.9	8.2	2.8	3.82	1.96	H_0 ref.	-5.5	5.5	-0.99	0.16	0.84	1.10
2500	81.74	17	6.97	90.07	26	11.57	-8.3	100.5	8.2	2.8	2.94	1.96	H_0 ref.	-5.5	5.5	-0.93	0.18	0.82	0.83
2600	81.66	17	6.71	88.17	26	12.09	-6.5	106.7	8.2	2.9	2.26	1.96	H_0 ref.	-5.6	5.6	-0.88	0.19	0.81	0.63
2700	82.41	17	7.87	89.07	26	11.85	-6.7	109.7	8.2	3.0	2.21	1.96	H_0 ref.	-5.9	5.9	-0.78	0.22	0.78	0.64
2800	83.43	16	8.79	89.51	26	11.85	-6.1	116.8	8.3	3.2	1.90	1.96	H_0 acc.	-6.3	6.3	-0.65	0.26	0.74	0.56
2900	84.59	16	9.35	90.37	26	11.72	-5.8	118.7	8.5	3.3	1.76	1.96	H_0 acc.	-6.4	6.4	-0.62	0.27	0.73	0.53
3000	85.91	16	9.96	91.88	26	11.78	-6.0	124.0	8.6	3.4	1.76	1.96	H_0 acc.	-6.7	6.7	-0.57	0.28	0.72	0.54
3100	85.86	16	9.70	93.30	26	12.49	-7.4	132.8	8.6	3.4	2.16	1.96	H_0 ref.	-6.8	6.8	-0.53	0.30	0.70	0.65
3200	84.27	16	9.50	91.35	26	13.17	-7.1	142.3	8.4	3.5	2.02	1.96	H_0 ref.	-6.9	6.9	-0.44	0.33	0.67	0.59
3300	81.83	16	7.90	89.44	26	14.13	-7.6	148.3	8.2	3.4	2.24	1.96	H_0 ref.	-6.7	6.7	-0.44	0.33	0.67	0.63
3400	76.77	16	6.73	84.75	26	15.96	-8.0	176.2	7.7	3.6	2.25	1.96	H_0 ref.	-7.0	7.0	-0.20	0.42	0.58	0.60
3500	65.46	16	5.51	72.67	26	17.32	-7.2	198.8	6.5	3.7	1.97	1.96	H_0 ref.	-7.2	7.2	0.17	0.57	0.43	0.51
3600	33.97	16	8.82	38.68	26	12.00	-4.7	119.1	3.4	3.2	1.46	1.96	H_0 acc.	-6.3	6.3	0.91	0.82	0.18	0.43

Segment #4

Station (m)	Field Mean speed S_F (km/h)	#	Standard deviation (km/h)	Simulation Mean speed S_S (km/h)	#	Standard deviation (km/h)	S_F-S_S (km/h)	σ^2_{comb} (km/h)²	Δ (km/h)	$\sigma(S_F$-$S_S)$ (km/h)	$|Z|$	$|Z_{crit}|$	Result of test	Confidence interval Lower limit	Upper limit	Z_β	β	Power (1-β)	Hedges's effect size, g
0	38.15	24	4.09	37.51	26	3.49	0.6	14.4	3.8	1.1	0.59	1.96	H_0 acc.	-2.1	2.1	-1.57	0.06	0.94	0.17
100	55.88	24	6.59	58.94	26	5.99	-3.1	39.5	5.6	1.8	1.71	1.96	H_0 acc.	-3.5	3.5	-1.17	0.12	0.88	0.49
200	63.35	24	7.99	68.10	26	8.50	-4.7	68.2	6.3	2.3	2.04	1.96	H_0 ref.	-4.6	4.6	-0.76	0.22	0.78	0.57
300	65.20	23	8.30	67.29	26	10.32	-2.1	88.9	6.5	2.7	0.79	1.96	H_0 acc.	-5.2	5.2	-0.49	0.31	0.69	0.22
400	64.31	23	7.32	56.86	26	13.08	7.5	116.1	6.4	3.0	2.50	1.96	H_0 ref.	-5.9	5.9	-0.19	0.42	0.58	0.69
500	64.55	23	7.76	64.52	26	12.29	0.0	108.6	6.5	2.9	0.01	1.96	H_0 acc.	-5.7	5.7	-0.26	0.40	0.60	0.003
600	67.36	21	8.00	72.78	26	11.71	-5.4	104.6	6.7	2.9	1.88	1.96	H_0 acc.	-5.7	5.7	-0.37	0.35	0.65	0.53
700	69.16	22	8.09	73.55	26	13.10	-4.4	123.2	6.9	3.1	1.42	1.96	H_0 acc.	-6.1	6.1	-0.27	0.39	0.61	0.40
800	63.36	23	6.44	63.06	26	12.34	0.3	100.4	6.3	2.8	0.11	1.96	H_0 acc.	-5.4	5.4	-0.33	0.37	0.63	0.03

Note: α = .05; Δ = 0.1 × S_F

Segment #5

Station (m)	Field Mean speed S_F (km/h)	#	Standard deviation (km/h)	Simulation Mean speed S_S (km/h)	#	Standard deviation (km/h)	S_F-S_S (km/h)	σ^2_{comb} (km/h)^2	Δ (km/h)	$\sigma(S_F$-$S_S)$ (km/h)	$\|Z\|$	$\|Z_{crit}\|$	Result of test	Confidence interval Lower limit	Upper limit	Z_β	β	Power (1-β)	Hedges's effect size, g
0	50.40	23	4.90	54.87	26	6.18	-4.5	31.6	5.0	1.6	2.81	1.96	H_0 ref.	-3.1	3.1	-1.22	0.11	0.89	0.79
100	61.51	23	4.18	63.80	26	8.60	-2.3	47.5	6.2	1.9	1.21	1.96	H_0 acc.	-3.7	3.7	-1.28	0.10	0.90	0.33
200	65.84	23	4.92	67.13	26	8.61	-1.3	50.7	6.6	2.0	0.65	1.96	H_0 acc.	-3.9	3.9	-1.37	0.08	0.92	0.18
300	69.97	23	6.24	70.24	26	10.25	-0.3	74.1	7.0	2.4	0.11	1.96	H_0 acc.	-4.7	4.7	-0.96	0.17	0.83	0.03
400	72.98	23	7.14	71.05	26	9.88	1.9	75.8	7.3	2.4	0.79	1.96	H_0 acc.	-4.8	4.8	-1.03	0.15	0.85	0.22
500	73.44	23	6.64	75.88	26	9.20	-2.4	65.7	7.3	2.3	1.08	1.96	H_0 acc.	-4.5	4.5	-1.27	0.10	0.90	0.30
600	74.16	21	6.50	79.12	26	9.49	-5.0	68.8	7.4	2.3	2.12	1.96	H_0 ref.	-4.6	4.6	-1.21	0.11	0.89	0.60
700	74.38	21	6.82	78.62	26	10.01	-4.2	76.3	7.4	2.5	1.72	1.96	H_0 acc.	-4.8	4.8	-1.06	0.14	0.86	0.48
800	75.79	19	7.09	78.82	26	10.99	-3.0	91.2	7.6	2.7	1.12	1.96	H_0 acc.	-5.3	5.3	-0.85	0.20	0.80	0.32
900	75.68	17	8.44	77.50	26	9.92	-1.8	87.7	7.6	2.8	0.65	1.96	H_0 acc.	-5.5	5.5	-0.72	0.24	0.76	0.19
1000	75.27	16	7.38	79.18	26	9.46	-3.9	76.3	7.5	2.6	1.49	1.96	H_0 acc.	-5.1	5.1	-0.92	0.18	0.82	0.45
1100	74.57	17	8.02	79.72	26	8.83	-5.1	72.6	7.5	2.6	1.97	1.96	H_0 ref.	-5.1	5.1	-0.90	0.18	0.82	0.60
1200	75.31	18	8.85	81.78	26	9.46	-6.5	85.0	7.5	2.8	2.32	1.96	H_0 ref.	-5.5	5.5	-0.74	0.23	0.77	0.70
1300	73.95	18	8.06	80.07	26	11.19	-6.1	100.8	7.4	2.9	2.11	1.96	H_0 ref.	-5.7	5.7	-0.59	0.28	0.72	0.61
1400	67.86	18	6.41	72.17	26	11.16	-4.3	90.8	6.8	2.7	1.62	1.96	H_0 acc.	-5.2	5.2	-0.59	0.28	0.72	0.45
1500	58.06	18	5.42	61.21	26	13.00	-3.1	112.5	5.8	2.9	1.10	1.96	H_0 acc.	-5.6	5.6	-0.08	0.47	0.53	0.30

Note: α = .05; Δ = 0.1 × S_F

Segment #6

Station (m)	Field Mean speed S_F (km/h)	#	Standard deviation (km/h)	Simulation Mean speed S_S (km/h)	#	Standard deviation (km/h)	S_F-S_S (km/h)	σ^2_{comb} (km/h)^2	Δ (km/h)	$\sigma(S_F$-$S_S)$ (km/h)	$|Z|$	$|Z_{crit}|$	Result of test	Confidence interval Lower limit	Upper limit	Z_β	β	Power (1-β)	Hedges's effect size, g
0	19.17	25	5.41	27.25	26	6.96	-8.1	39.1	1.9	1.7	4.64	1.96	H_0 ref.	-3.4	3.4	0.86	0.80	0.20	1.29
100	52.42	25	3.54	53.32	26	9.62	-0.9	53.3	5.2	2.0	0.45	1.96	H_0 acc.	-3.9	3.9	-0.64	0.26	0.74	0.12
200	65.32	25	5.52	66.14	26	11.64	-0.8	84.1	6.5	2.5	0.32	1.96	H_0 acc.	-5.0	5.0	-0.62	0.27	0.73	0.09
300	69.67	25	7.66	71.89	26	12.65	-2.2	110.4	7.0	2.9	0.76	1.96	H_0 acc.	-5.7	5.7	-0.43	0.33	0.67	0.21
400	70.86	24	9.15	76.55	26	14.07	-5.7	143.2	7.1	3.3	1.71	1.96	H_0 acc.	-6.5	6.5	-0.17	0.43	0.57	0.48
500	72.98	24	8.33	79.48	26	14.93	-6.5	149.4	7.3	3.4	1.92	1.96	H_0 acc.	-6.6	6.6	-0.19	0.42	0.58	0.53
600	73.37	24	7.52	78.49	26	13.39	-5.1	120.5	7.3	3.0	1.68	1.96	H_0 acc.	-6.0	6.0	-0.45	0.33	0.67	0.47
700	72.77	21	7.48	71.97	26	14.68	0.8	144.6	7.3	3.3	0.24	1.96	H_0 acc.	-6.5	6.5	-0.24	0.41	0.59	0.07
800	70.17	17	7.98	71.37	26	17.90	-1.2	220.3	7.0	4.0	0.30	1.96	H_0 acc.	-7.9	7.9	0.21	0.58	0.42	0.08
900	70.84	17	8.53	72.16	26	18.16	-1.3	229.5	7.1	4.1	0.32	1.96	H_0 acc.	-8.1	8.1	0.24	0.60	0.40	0.09
1000	70.37	17	7.86	74.95	26	16.69	-4.6	194.0	7.0	3.8	1.21	1.96	H_0 acc.	-7.4	7.4	0.10	0.54	0.46	0.33
1100	66.40	18	6.62	74.50	26	15.45	-8.1	159.8	6.6	3.4	2.37	1.96	H_0 ref.	-6.7	6.7	0.01	0.50	0.50	0.64
1200	61.23	17	6.14	64.77	26	14.40	-3.5	141.1	6.1	3.2	1.11	1.96	H_0 acc.	-6.3	6.3	0.04	0.52	0.48	0.30
1300	63.37	17	6.20	63.63	26	11.50	-0.3	95.6	6.3	2.7	0.10	1.96	H_0 acc.	-5.3	5.3	-0.38	0.35	0.65	0.03
1400	66.45	19	6.92	71.29	26	10.74	-4.8	87.2	6.6	2.6	1.83	1.96	H_0 acc.	-5.2	5.2	-0.56	0.29	0.71	0.52
1500	67.47	19	7.42	76.43	26	12.87	-9.0	119.3	6.7	3.0	2.95	1.96	H_0 ref.	-6.0	6.0	-0.26	0.40	0.60	0.82
1600	68.39	17	6.37	78.61	26	14.19	-10.2	138.6	6.8	3.2	3.21	1.96	H_0 ref.	-6.2	6.2	-0.19	0.43	0.57	0.87
1700	69.28	17	6.17	79.67	26	15.36	-10.4	158.8	6.9	3.4	3.09	1.96	H_0 ref.	-6.6	6.6	-0.10	0.46	0.54	0.82
1800	69.01	16	7.34	82.06	26	16.01	-13.1	180.4	6.9	3.6	3.59	1.96	H_0 ref.	-7.1	7.1	0.06	0.52	0.48	0.97
1900	70.10	18	7.32	83.35	26	15.27	-13.3	160.4	7.0	3.5	3.84	1.96	H_0 ref.	-6.8	6.8	-0.07	0.47	0.53	1.05
2000	70.56	18	7.87	85.48	26	13.94	-14.9	140.8	7.1	3.3	4.52	1.96	H_0 ref.	-6.5	6.5	-0.18	0.43	0.57	1.26
2100	71.05	18	7.89	86.04	26	14.56	-15.0	151.4	7.1	3.4	4.40	1.96	H_0 ref.	-6.7	6.7	-0.12	0.45	0.55	1.22
2200	70.77	18	6.88	86.02	26	13.82	-15.2	132.8	7.1	3.2	4.83	1.96	H_0 ref.	-6.2	6.2	-0.28	0.39	0.61	1.32
2300	68.56	18	7.12	79.97	26	13.49	-11.4	128.8	6.9	3.1	3.64	1.96	H_0 ref.	-6.1	6.1	-0.23	0.41	0.59	1.00

Note: α = .05; Δ = 0.1 × S_F

Segment #7

Station (m)	Field Mean speed S_F (km/h)	#	Standard deviation (km/h)	Simulation Mean speed S_S (km/h)	#	Standard deviation (km/h)	S_F-S_S (km/h)	σ^2_{comb} (km/h)^2	Δ (km/h)	$\sigma(S_F$-$S_S)$ (km/h)	$|Z|$	$|Z_{crit}|$	Result of test	Confidence interval Lower limit	Upper limit	Z_β	β	Power (1-β)	Hedges's effect size, g
0	33.73	27	10.29	32.86	26	5.50	0.9	68.8	3.4	2.3	0.38	1.96	H₀ acc.	-4.4	4.4	0.46	0.68	0.32	0.10
100	53.62	27	4.95	59.53	26	6.63	-5.9	34.1	5.4	1.6	3.67	1.96	H₀ ref.	-3.2	3.2	-1.37	0.09	0.91	1.01
200	61.68	27	4.85	67.49	26	9.57	-5.8	56.9	6.2	2.1	2.77	1.96	H₀ ref.	-4.1	4.1	-0.98	0.16	0.84	0.77
300	61.97	25	5.95	69.32	26	10.25	-7.4	71.0	6.2	2.3	3.15	1.96	H₀ ref.	-4.6	4.6	-0.69	0.24	0.76	0.87
400	62.95	25	6.33	69.74	26	9.89	-6.8	69.5	6.3	2.3	2.93	1.96	H₀ ref.	-4.5	4.5	-0.76	0.22	0.78	0.82
500	64.73	26	6.27	69.51	26	9.75	-4.8	67.2	6.5	2.3	2.10	1.96	H₀ ref.	-4.5	4.5	-0.89	0.19	0.81	0.58
600	63.26	27	6.47	67.47	26	8.43	-4.2	56.2	6.3	2.1	2.03	1.96	H₀ ref.	-4.1	4.1	-1.10	0.14	0.86	0.56
700	66.00	27	6.63	67.19	26	8.63	-1.2	58.9	6.6	2.1	0.56	1.96	H₀ acc.	-4.2	4.2	-1.15	0.12	0.88	0.16
800	64.53	27	5.89	66.18	26	7.71	-1.7	46.8	6.5	1.9	0.88	1.96	H₀ acc.	-3.7	3.7	-1.45	0.07	0.93	0.24
900	47.68	27	4.33	46.22	26	6.60	1.5	30.9	4.8	1.5	0.95	1.96	H₀ acc.	-3.0	3.0	-1.14	0.13	0.87	0.26
1000	55.75	27	6.89	60.22	26	7.21	-4.5	49.7	5.6	1.9	2.31	1.96	H₀ ref.	-3.8	3.8	-0.92	0.18	0.82	0.63
1100	55.94	25	6.41	63.05	26	8.30	-7.1	55.2	5.6	2.1	3.43	1.96	H₀ ref.	-4.1	4.1	-0.74	0.23	0.77	0.96
1200	50.37	23	4.51	52.43	26	8.65	-2.1	49.3	5.0	1.9	1.06	1.96	H₀ acc.	-3.8	3.8	-0.64	0.26	0.74	0.29
1300	46.49	23	4.57	47.29	26	9.64	-0.8	59.2	4.6	2.1	0.38	1.96	H₀ acc.	-4.2	4.2	-0.24	0.41	0.59	0.10

Note: α = .05; Δ = 0.1 × S_F

Trajectory data

Anticipatory distance

Meas. sites	Field			Simulation			$d_{a,F}-d_{a,S}$ (m)	σ^2_{comb} (m²)	Δ (m)	$\sigma(d_{a,F}-d_{a,S})$ (m)	|Z|	|Z_{crit}|	Result of test	Confidence interval		Z_β	β	Power (1-β)	Hedges's effect size, g
	Mean value $d_{a,F}$ (m)	#	Standard deviation (m)	Mean value $d_{a,S}$ (m)	#	Standard deviation (m)								Lower limit	Upper limit				
C1-out	23.59	23	6.97	36.36	26	5.91	-12.8	41.31	2.4	1.9	6.87	1.96	H$_0$ ref.	-3.6	3.6	0.69	0.76	0.24	1.99
C2-in	17.55	23	14.74	25.85	26	6.58	-8.3	124.74	1.8	3.3	2.49	1.96	H$_0$ ref.	-6.5	6.5	1.43	0.92	0.08	0.74
C2-out	25.01	23	15.16	43.32	26	19.38	-18.3	307.40	2.5	4.9	3.70	1.96	H$_0$ ref.	-9.7	9.7	1.45	0.93	0.07	1.04
C3-in	45.88	19	14.49	75.13	26	23.61	-29.2	411.94	4.6	5.7	5.13	1.96	H$_0$ ref.	-11.2	11.2	1.16	0.88	0.12	1.44
C3-out	36.68	19	17.86	56.47	26	15.64	-19.8	275.70	3.7	5.1	3.87	1.96	H$_0$ ref.	-10.0	10.0	1.24	0.89	0.11	1.19
C4-in	39.88	19	16.74	55.52	26	12.91	-15.6	214.14	4.0	4.6	3.40	1.96	H$_0$ ref.	-9.0	9.0	1.09	0.86	0.14	1.07
C4-out	35.71	19	19.70	51.50	26	13.51	-15.8	268.58	3.6	5.2	3.02	1.96	H$_0$ ref.	-10.3	10.3	1.28	0.90	0.10	0.96
C5-in	41.41	20	23.33	61.13	26	25.17	-19.7	595.10	4.1	7.2	2.75	1.96	H$_0$ ref.	-14.1	14.1	1.38	0.92	0.08	0.81
C5-out	19.51	17	24.38	74.60	26	20.28	-55.1	482.76	2.0	7.1	7.73	1.96	H$_0$ ref.	-14.0	14.0	1.69	0.95	0.05	2.51
R	19.21	17	11.56	35.38	26	5.84	-16.2	72.94	1.9	3.0	5.34	1.96	H$_0$ ref.	-5.9	5.9	1.33	0.91	0.09	1.89
C6-out	36.56	17	19.91	65.25	26	15.34	-28.7	298.28	3.7	5.7	5.04	1.96	H$_0$ ref.	-11.2	11.2	1.32	0.91	0.09	1.66
C7-in	21.20	16	11.84	64.09	26	20.45	-42.9	313.94	2.1	5.0	8.61	1.96	H$_0$ ref.	-9.8	9.8	1.53	0.94	0.06	2.42

Note: $\alpha = .05$; $\Delta = 0.1 \times d_{a,F}$

Meas. sites	Field			Simulation			$d_{a,F}-d_{a,S}$ (m)	σ^2_{comb} (m²)	Δ (m)	$\sigma(d_{a,F}-d_{a,S})$ (m)	|Z|	|Z_{crit}|	Result of test	Confidence interval		Z_β	β	Power (1-β)	Hedges's effect size, g
	Mean value $d_{a,F}$ (m)	#	Standard deviation (m)	Mean value $d_{a,S}$ (m)	#	Standard deviation (m)								Lower limit	Upper limit				
C2-C3-C4-in	33.33	61	19.64	52.16	78	25.78	-18.8	542.59	3.3	3.9	4.89	1.96	H0 ref.	-7.6	7.6	1.09	0.86	0.14	0.81
C5-in	41.41	20	23.33	61.13	26	25.17	-19.7	595.10	4.1	7.2	2.75	1.96	H0 ref.	-14.1	14.1	1.38	0.92	0.08	0.81
C2-C3-C4-out	31.98	61	18.07	50.43	78	17.04	-18.5	306.18	3.2	3.0	6.13	1.96	H0 ref.	-5.9	5.9	0.90	0.82	0.18	1.05
C6-out	36.56	17	19.91	65.25	26	15.34	-28.7	298.28	3.7	5.7	5.04	1.96	H0 ref.	-11.2	11.2	1.32	0.91	0.09	1.66

Note: $\alpha = .05$; $\Delta = 0.1 \times d_{a,F}$

Average curvature

Curve #	Field Mean value c_F (m^{-1})	#	Standard deviation (m^{-1})	Simulation Mean value c_S (m^{-1})	#	Standard deviation (m^{-1})	c_F-c_S (m^{-1})	σ^2_{comb} (m^{-2})	Δ (m^{-1})	$\sigma(c_F-c_S)$ (m^{-1})	$|Z|$	$|Z_{crit}|$	Result of test	Confidence interval Lower limit	Upper limit	Z_β	β	Power (1-β)	Hedges's effect size, g
C1	-0.01033	23	0.00063	-0.00958	26	0.00058	-7.52E-04	3.66E-07	1.55E-03	1.74E-04	4.32	1.96	H_0 ref.	-0.00034	0.00034	-6.94	0.00	1.00	1.24
C2	0.00150	23	0.00036	0.00142	26	0.00022	8.40E-05	8.52E-08	2.26E-04	8.59E-05	0.98	1.96	H_0 acc.	-0.00017	0.00017	-0.67	0.25	0.75	0.29
C3	-0.00175	19	0.00019	-0.00163	26	0.00019	-1.19E-04	3.58E-08	2.63E-04	5.76E-05	2.07	1.96	H_0 ref.	-0.00011	0.00011	-2.61	0.00	1.00	0.63
C4	0.00178	19	0.00023	0.00167	26	0.00009	1.12E-04	2.69E-08	2.67E-04	5.57E-05	2.01	1.96	H_0 ref.	-0.00011	0.00011	-2.83	0.00	1.00	0.68
C5	0.00180	17	0.00005	0.00182	26	0.00001	-2.29E-05	1.03E-09	2.70E-04	1.20E-05	1.91	1.96	H_0 acc.	-0.00002	0.00002	-20.46	0.00	1.00	0.71
C6	-0.00204	17	0.00028	-0.00193	26	0.00015	-1.03E-04	4.48E-08	3.06E-04	7.43E-05	1.38	1.96	H_0 acc.	-0.00015	0.00015	-2.15	0.02	0.98	0.49

Note: α = .05; Δ = 0.15 × c_F

Curvature change rate

Curve #	Field Mean value $c_{r,F}$ (m^{-2})	#	Standard deviation (m^{-2})	Simulation Mean value $c_{r,S}$ (m^{-2})	#	Standard deviation (m^{-2})	$c_{r,F}-c_{r,S}$ (m^{-2})	σ^2_{comb} (m^{-4})	Δ (m^{-2})	$\sigma(c_{r,F}-c_{r,S})$ (m^{-2})	$|Z|$	$|Z_{crit}|$	Result of test	Confidence interval Lower limit	Upper limit	Z_β	β	Power (1-β)	Hedges's effect size, g
C1-out	1.73E-04	23	3.92E-05	1.78E-04	26	3.39E-05	-4.73E-06	1.33E-09	5.19E-05	1.05E-05	0.45	1.96	H_0 acc.	-2.06E-05	2.06E-05	-2.97	0.00	1.00	0.13
C2-in	4.25E-05	23	1.73E-05	4.22E-05	26	1.50E-05	3.58E-07	2.60E-10	1.28E-05	4.66E-06	0.08	1.96	H_0 acc.	-9.13E-06	9.13E-06	-0.78	0.22	0.78	0.02
C2-out	2.58E-05	23	6.60E-06	3.07E-05	26	1.71E-05	-4.98E-06	1.75E-10	7.73E-06	3.62E-06	1.38	1.96	H_0 acc.	-7.09E-06	7.09E-06	-0.18	0.43	0.57	0.38
C3-in	2.59E-05	19	1.20E-05	1.77E-05	26	5.87E-06	8.25E-06	8.04E-11	7.77E-06	2.99E-06	2.76	1.96	H_0 ref.	-5.85E-06	5.85E-06	-0.64	0.26	0.74	0.92
C3-out	2.60E-05	19	1.02E-05	2.41E-05	26	1.02E-05	1.92E-06	1.04E-10	7.81E-06	3.08E-06	0.62	1.96	H_0 acc.	-6.04E-06	6.04E-06	-0.57	0.28	0.72	0.19
C4-in	2.89E-05	19	7.69E-06	2.13E-05	26	6.23E-06	7.65E-06	4.73E-11	8.68E-06	2.15E-06	3.57	1.96	H_0 ref.	-4.21E-06	4.21E-06	-2.09	0.02	0.98	1.11
C4-out	2.55E-05	19	1.05E-05	2.15E-05	26	9.10E-06	3.98E-06	9.46E-11	7.65E-06	3.01E-06	1.32	1.96	H_0 acc.	-5.89E-06	5.89E-06	-0.59	0.28	0.72	0.41
C5-in	2.04E-05	20	7.93E-06	1.78E-05	26	5.87E-06	2.57E-06	4.67E-11	6.11E-06	2.11E-06	1.21	1.96	H_0 acc.	-4.14E-06	4.14E-06	-0.93	0.18	0.82	0.38
R	2.70E-05	17	4.67E-06	1.92E-05	26	2.70E-06	7.86E-06	1.30E-11	8.11E-06	1.25E-06	6.29	1.96	H_0 ref.	-2.45E-06	2.45E-06	-4.53	0.00	1.00	2.18
C6-out	2.15E-05	17	6.91E-06	2.49E-05	26	1.09E-05	-3.42E-06	9.11E-11	6.44E-06	2.72E-06	1.26	1.96	H_0 acc.	-5.32E-06	5.32E-06	-0.41	0.34	0.66	0.36
C7-in	4.23E-05	16	1.78E-05	2.28E-05	26	8.65E-06	1.96E-05	1.65E-10	1.27E-05	4.76E-06	4.11	1.96	H_0 ref.	-9.33E-06	9.33E-06	-0.71	0.24	0.76	1.52

Note: α = .05; Δ = 0.3 × $c_{r,F}$

A.3 Lane gap profiles along curves of Experiment #1

C17A-ccw

C12B-ccw

C8A-cw

C7B-cw

C11A-cw

C5B-cw

C17A-mod-ccw

C7A-mod-ccw

C1B-ccw

C6A-ccw

C10B-ccw

C13A-ccw

C9B-cw

C5A-ccw